Earthquake Recurrence, Clustering, and Persistent Segmentation near the Southern End of the 2004 Sunda Megathrust Rupture

Thesis by

Aron Jeffrey Meltzner

In Partial Fulfillment of the Requirements
for the Degree of
Doctor of Philosophy

California Institute of Technology
Pasadena, California

2010
(Defended 11 December 2009)

DEDICATION

to Nick
to Mom and Dad
with gratitude
for your unending love, support, and patience;
you each are my rock

in memory of
Adi Rahman Putra
who gave his life
in the pursuit of knowledge
that might someday
save the lives of others

and in memory of
all those who lost their lives in 2004
because we didn't yet know
of the need to prepare

ACKNOWLEDGMENTS

A Ph.D. thesis involving geological field work in a foreign country is never a single-person task, and the research I have done over the past five years is no exception: there are many individuals without whom I could not have been nearly as productive or as successful.

I owe my deepest gratitude to my research advisor, Kerry Sieh, for giving me the opportunity, guidance, and financial support to work on this exciting research in Sumatra. I first met Kerry in April 1997 as an undergraduate freshman who was already fascinated by and interested in studying earthquakes in California; from Day One, Kerry encouraged me to get involved in geological research, to branch out, to collaborate with others, and to grow as a scientist. For that early advice, I am greatly indebted.

My field work in Sumatra would not have been possible without tremendous logistical support from our Indonesian collaborators—in particular, Bambang Suwargadi and Danny Hilman Natawidjaja at the Indonesian Institute of Sciences (LIPI). Both Bambang and Danny worked tirelessly to pave the way for our field missions, both of them solved any unexpected problem that arose (no matter how complicated or dire), and both were proactive in trying to improve our team's efficiency and overall success. I am also grateful to John Galetzka (Caltech) and Dudi Prayudi (LIPI)—whose strong arms and skilled hands cut the slabs that I spent five years studying—and to Imam Suprihanto, Belle Philibosian (Caltech), and Rich Briggs (Caltech/USGS)—whose meticulous, reliable surveying on the total station allowed me to focus without distraction on the most important tasks, making observations and taking notes. Belle, Rich, and Danny also contributed to numerous helpful and stimulating discussions in the field and in the office over the years.

Many others contributed in vital ways to the results in my thesis. I thank Hong-Wei Chiang and Chuan-Chou (River) Shen at National Taiwan University, who performed the U-Th dating analyses of our coral samples and helped me understand both the meaning and the limitations of the results. My gratitude is also due to Duncan Agnew at Scripps Institution of Oceanography, who first taught me about the intricacies of tides and tide modeling; without his assistance, none of the critical improvements I've made to the modeling of water levels—and hence to the precision of our uplift and subsidence calculations—would have been possible. I also owe many thanks to Carl Wunsch (Massachusetts Institute of Technology) and Victor Zlotnicki (Jet Propulsion Laboratory) for conversations that helped me understand aspects of non-tidal sea level fluctuations and how to correct for them.

I am fortunate to have had support from many extraordinary people at Caltech. My academic advisor, Jean-Philippe Avouac, guided me through coursework, always had an open door, reliably had insightful and constructive advice, and offered valuable feedback on early drafts of my thesis. My two other committee members—Mark Simons and Don Helmberger—were immensely helpful also, offering their own perspectives and valuable suggestions as my thesis progressed. Although not on my committee, Joann Stock was always supportive and eager to offer helpful advice, for which I am grateful. Jeff Genrich provided processed SuGAr GPS data on numerous occasions, and our geology librarian, Jim O'Donnell, was always happy to help, whether by tracking down an obscure map or by getting a scanner to work. I benefited greatly from (and perhaps survived because of) the administrative support of Heather Steele, Sheri Garcia, Dian Buchness, Julie Schoen, Marcia Hudson, Carolyn Porter, and many others. Finally, I owe many thanks to fellow students Belle Philibosian and Wang Yu for offering feedback and keeping me sane, no matter which part of the world we were in at any given time.

In addition to the administrative support I received at Caltech, I am very thankful to Linda Chua of the Earth Observatory of Singapore, who frequently assisted with logistics in Singapore.

Early versions of Chapters 3 and 4 were reviewed by Katrin Monecke (University of Pittsburgh at Johnstown), Anthony Crone (USGS), Gavin Hayes (USGS), and Brian Atwater (USGS), and by my co-authors and committee members. Their comments led to a substantially improved final manuscript, and I am truly grateful for those contributions.

Although mentioned in the Dedication, I again wish to thank my parents and my husband, Nick, for all their loving support over the years. They have been selfless, they have put up (and continue to put up) with my crazy geologist's travel schedule, and I know I can always count on them for anything I need. Words cannot express my sincere love and deep gratitude to them.

ABSTRACT

The December 2004 moment magnitude (M_W) 9.2 earthquake was the largest in the world in four decades. Rupture of the Sunda megathrust in that event produced broad regions of uplift and subsidence. We defined the pivot line separating these regions as a first step in defining the extent of the rupture, relying on the interpretation of satellite imagery and modeled water levels as well as on field measurements of emerged coral microatolls. Uplift in 2004 extended from the middle of Simeulue island, Sumatra, at ~2.5°N, to Preparis island, Myanmar (Burma), at ~14.9°N; thus the 2004 rupture was ~1600 km long.

The Sunda megathrust ruptured again in March 2005 in an M_W 8.6 earthquake. We focused our efforts on Simeulue, which straddles the boundary of these two ruptures and behaved as a barrier to both. We extracted records of relative sea-level change from coral microatolls on fringing reefs directly above the southern end of the 2004 rupture and the northern end of the 2005 rupture. These records provide a detailed history of tectonic strain accumulation and release.

Along the coast of northern Simeulue, coral records reveal that predecessors of the 2004 earthquake occurred in the 10th and 14th–15th centuries AD. In the 14th–15th centuries, northern Simeulue experienced a cluster of large megathrust ruptures, associated with total uplift that was considerably more than in 2004. The strain released in 2004 under northern Simeulue took less than 250 years to accumulate if strain accumulation rates since 1948 can be extrapolated back in time. These observations suggest that re-rupture of at least the southernmost 100–200 km of the 2004 patch is possible in the coming decades.

The records from central-southern Simeulue indicate that none of the major uplifts known or inferred on northern Simeulue in the past 1100 years extended to southern Simeulue. In addition, the largest uplifts in the modern or paleogeodetic record in central-southern Simeulue apparently produced little or no uplift in northern Simeulue. These observations suggest that central Simeulue has behaved as a persistent barrier to rupture over at least the past 1100 years.

TABLE OF CONTENTS

LIST OF FIGURES

Chapter 5

LIST OF TABLES

Chapter 1

Introduction and Synthesis

Motivation: inadequacy of data for understanding earthquake cycles

Understanding the behavior of active faults over multiple seismic cycles has been an elusive goal of earthquake science. The extent to which fault behavior—including both strain accumulation and relief—varies over centennial to millennial time scales remains poorly resolved. Outstanding questions concern the regularity of fault rupture, the repeatability of the pattern of slip on a fault, and the roles of geologic structure and rheology in governing ruptures and their terminations. Instrumental records of earthquakes and ground deformation are commonly far too short to observe faults over more than a fraction of the cycle of interplate strain accumulation and release—which can last hundreds to more than hundreds of thousands of years—let alone over multiple earthquake cycles. Consequences of this inadequacy of observations include an inability to rigorously test many models of fault behavior and, in many parts of the world, an under-appreciation of seismic hazards. Probably the most devastating and tragic example of this is along the northern Sunda megathrust, where the magnitude 9.2 earthquake of 26 December 2004 and its associated tsunami caused widespread destruction and nearly 230,000 fatalities along coastlines of the Indian Ocean. In general, no significant threat had been perceived along this section of the megathrust, because no instrumental or historical record suggested earthquakes like this had occurred in the past [*Bilham*, 2005; *Bilham et al.*, 2005; *Subarya et al.*, 2006], and because the accepted models of megathrust potential productivity [*Ruff and Kanamori*, 1980; *Kanamori*, 1983] lacked sufficient data to be adequately tested.

The instrumental and historical records can be extended back in time in many places by careful examination of the geological record. Paleoseismology has contributed to understanding serial fault ruptures. This is a slow process, however, because relevant data bearing on how past strains have accumulated and been released along faults are difficult to obtain. Progress has been hampered by imprecision and incompleteness of most records, the difficulty to find suitable sites, and the long periods of time required to develop good sites once they are identified. The biggest obstacles in conventional trenching paleoseismology—both along continental faults and above subduction zones—have been the distance between well-developed sites with good records (often tens of kilometers or more) and limitations in the precision of dating (seldom better than ±30 years) afforded by radiocarbon techniques. The large uncertainties in the timing of past earthquakes and the long distances between sites have made the correlation of events along a fault ambiguous and subjective [*Weldon et al.*, 2005; *Biasi and Weldon*, 2009]. Furthermore, even in places where long records exist or precise details of past earthquakes are known—for example, along parts of the San Andreas [*Sieh et al.*, 1989; *Liu et al.*, 2004; *Weldon et al.*, 2004; *Scharer et al.*, 2007] and North Anatolian [*Stein et al.*, 1997] faults, and above the Cascadia [*Atwater and Hemphill-Haley*, 1997; *Atwater et al.*, 2005; *Kelsey et al.*, 2002, 2005; *Witter et al.*, 2003] and Nankai [*Ando*, 1975; *Sugiyama*, 1994] megathrusts—paleogeodetic data for interseismic periods are sparse or lacking.

Off the west coast of mainland Sumatra and on the Nicobar and Andaman Islands, there is an opportunity to address many of the outstanding questions of fault behavior over multiple earthquake deformation cycles. During Earth's two largest earthquakes of the past 44 years (1966–2009)—the M_W 9.2 Sumatra-Andaman earthquake of 2004 and the M_W 8.6 Nias-Simeulue earthquake of 2005—adjacent segments of the Sunda megathrust ruptured from the Equator to 15° N, with nearly 20 m of slip in 2004 [*Chlieh et al.*, 2007] and more than 11 m of slip in 2005 [*Briggs et al.*, 2006]. Like typical megathrust ruptures, these earthquakes produced regions of uplift above the elongated rupture patches, with troughs of subsidence immediately landward (away from the trench). The presence of outer-arc islands directly above the seismogenic regions of the Sunda megathrust—and within the uplift regions of these earthquakes—allowed for unprecedented documentation of the surface deformation associated with these megathrust earthquakes [*Meltzner et al.*, 2006; *Subarya et al.*, 2006; *Briggs et al.*, 2006]. In addition, coral microatolls on fringing reefs of the tropical archipelago record past vertical deformation, allowing us to examine details of past behavior of the Sunda megathrust.

Coral microatoll paleogeodesy, with its ability to provide continuous century-long or multi-century records of high precision paleo-elevation data with remarkably precise ages, yields unparalleled resolution in the reconstruction of both the pattern of interseismic strain accumulation and the timing and extent of past megathrust ruptures. The abundance and high precision of the data allow us to correlate events with high confidence, or to distinguish distinct events separated by a few decades or sometimes less. This, in turn, permits us to begin addressing questions about the timing and similarity of past ruptures, about earthquake recurrence models, about the persistence of barriers to rupture, and about the variability of strain accumulation over the seismic cycle and over multiple seismic cycles. The availability of such data is restricted to portions of the outer arc with islands, but, fortunately, suitable sites can commonly be found at spacings of less than 20 km on these islands and can be developed in a matter of a few days or less.

Over the course of four seasons of field work between May 2005 and February 2009, I, along with my advisor (K. Sieh) and field assistants, developed 27 paleogeodetic sites on the Sumatran outer arc islands between 0.5° and 3.0°N, many of which consist of two or three subsites separated by ~1 km or less. We sampled a total of 34 modern microatolls (microatolls that were living at the time of the 2004 earthquake) and 82 fossil microatolls and coral heads (those that died long ago, presumably in past uplift events), which combine to provide a rich archive of past deformation above this section of the Sunda megathrust. Results from 8 sites (comprising 9 modern and 28 fossil corals) are presented in this thesis, most of which will be submitted for publication soon after the defense; analyses of the remaining heads are still too preliminary to be presented at this time, but will be submitted for publication subsequently.

Content and organization of this thesis

This work is divided into five chapters. Chapter 2 contains the results of a study I led using satellite imagery and a handful of *in situ* measurements on coral microatolls to constrain the along-strike and downdip limits of the 2004 rupture of the Sunda megathrust. This chapter was published in the *Journal of Geophysical Research* [*Meltzner et al.*, 2006] and is reproduced here in its entirety without modification, except for changes to values in the "2sigma" column in Supplementary Table 1 (discussed in the next section) and for general reformatting of the auxiliary material. In addition to the changes in Supplementary Table 1, some of the measurements reported by *Meltzner et al.* [2006] that were derived from coral microatolls on northern Simeulue have since been revised slightly; however, rather than modify the content of the original paper, I discuss the revisions and corrections in detail, and I report revised values, in Chapters 3 and 4. None of the conclusions of *Meltzner et al.* [2006] are affected by these minor changes.

Chapters 3–5 contain results from paleogeodetic investigations above the Sunda megathrust. They focus on the region near the boundary of the 2004 M_W 9.2 rupture and the 2005 M_W 8.6 rupture to the south. The first two of these chapters focus on seven sites above the southern end of the 2004 rupture (see Chapter 3, Fig. 1): Chapter 3 is the main text, and Chapter 4 is the auxiliary material, of a manuscript that is in press in the *Journal of Geophysical Research*. Chapter 5 focuses on one site at the northern end of the 2005 rupture (see Chapter 5, Fig. 1) and contrasts the record found at that site with those from sites farther north. Chapters 4 and 5 both have appendices available as electronic supplements to this thesis. The electronic supplement for Chapter 4 contains high-resolution x-ray mosaics of the coral slabs and field photographs of the sites discussed in Chapters 3 and 4; the supplement for Chapter 5 contains high-resolution x-ray mosaics and field photographs for the site discussed in Chapter 5.

Uplift and subsidence associated with the 2004 earthquake

The primary objective of our work on the 2004 earthquake was to determine the limits of the region of uplift, and by extension, the downdip and along-strike extent of the rupture. While the most direct goal of paleoseismology and paleogeodesy is to extend the modern record of strain accumulation and relief into the past, it is important to document modern ruptures in as much detail as possible, in order to calibrate observations of deformation during past earthquakes. Furthermore, if we are to assess the earthquake hazard at present, we need to know not only what a fault is capable of over long periods of time, but also how it has behaved in the recent past, so that we may identify asperities or regions where substantial strain is accumulated at present.

Because the 2004 rupture was so long in length and duration, seismic inversions for the event were particularly non-unique and proved to be limited in their ability to resolve many details of slip, especially along the later, northern portion of the rupture. Moreover, because slip north of ~9°N generated little or no seismic radiation, the seismic inversions provide only a minimum constraint on the extent and amount of slip. Inversions of geodetic data (and joint inversions of both seismic and geodetic data) were critical to resolving the details of slip in the 2004 earthquake. Until the imagery-based geodetic observations in Chapter 2 were available, however, the sparse geodetic data obtained from a handful of campaign Global Positioning System (GPS) stations scattered above the 1600-km long rupture provided only limited constraints on the amount and distribution of slip [e.g., *Subarya et al.*, 2006]. Indeed, the observations of *Meltzner et al.* [2006] are still the most compelling evidence that the 2004 rupture was 1600 km long, extending northward to ~14.9°N.

Part of these efforts involved the development of a technique to combine information about tides with satellite images, in order to differentiate regions of coseismic uplift and coseismic subsidence. This method has since been used to study earthquakes along subduction zones elsewhere, such as the 2007 earthquake in the Solomon Islands [*Taylor et al.*, 2008].

Subsequent to the publication of the work on the 2004 rupture in the *Journal of Geophysical Research*, however, I became aware of certain phenomena, beyond tides, that influence sea surface heights; I also became aware of efforts by groups such as AVISO to extract from satellite altimetry data a near-global time series of sea level anomalies (available at http://www.aviso.oceanobs.com/en/data/products/sea-surface-height-products/global/msla/). Chapter 3 presents an improved methodology for determining water levels, and Chapters 3 and 4 both include revised estimates of the 2004 uplifts on Simeulue island.

The imagery-based constraints on land-level changes in the Andaman and Nicobar Islands in 2004, published by *Meltzner et al.* [2006], did not account for non-tidal sea level anomalies, and have not been recalculated. Fortunately, however, sea level anomalies in the Andaman and Nicobar Islands tend to be small: the standard deviation of those anomalies from 2000 to 2005 ranges from 5 to 7 cm over the Andaman–Nicobar region. These sea level anomalies, which are dominated by seasonal variability, should be effectively independent of the 5-cm standard deviation reported by *Meltzner et al.* [2006], which was determined based on 8 consecutive days of tide gauge data collected in January 2005. If the two independent errors are added in quadrature, the resulting 1σ error for the sea surface heights provided by the tide model would be 7–9 cm. The 2σ error for the difference in sea surface heights at the acquisition times of any pair of images, which was originally reported by *Meltzner et al.* [2006] as 14 cm for each pair of images, is corrected in Table S1 of Chapter 2 to be 24 cm for each pair of images. This larger error accounts for the fact that non-tidal sea level anomalies were not considered in the imagery-based uplift and subsidence calculations of *Meltzner et al.* [2006].

Imagery-based constraints on uplift or subsidence in the 2007 Solomon Islands earthquake also did not strictly account for non-tidal sea level anomalies, but the error bars provided by *Taylor et al.* [2008] implicitly accounted for those anomalies, just as the revised, larger error bars do in Table S1 of Chapter 2 of this thesis.

Paleogeodesy and paleoseismology of the Sunda megathrust

My research on the paleogeodesy and paleoseismology of the Sumatran outer arc from 0.5° to 3.0°N has yielded findings that can be divided into three geographical regions, based upon the regions' discrete rupture histories and the questions that are resolved in each region. The northern region of my field area is the southern part of the 2004 rupture: northern Simeulue and the Salaut islands to the northwest. Our foremost findings in this region involve documentation of evidence for a cluster of earthquakes in the 14th–15th centuries and an earlier event in the 10th century. If no great earthquakes are missing from the record, this suggests a 400- to 600-year recurrence interval for megathrust earthquakes or earthquake clusters at the southern end of the 2004 patch. The southern region corresponds roughly to the 2005 rupture—southern Simeulue, the Banyak Islands, and Nias—where we have solid evidence for an earthquake in 1861 and for several earlier ruptures. Central Simeulue, where cumulative uplift in the 2004 and 2005 earthquakes was half a meter or less, cooperates at times with the 2005 patch, but may also behave independently. We consider central Simeulue as a distinct region because of a complicated history of strain accumulation and relief along this section of the fault, and because the prehistoric record from this region, when contrasted with overlapping records from northern Simeulue, provides compelling evidence for a persistent barrier to rupture. The latter three chapters of this thesis include results from the northern region and from one particularly informative site in central Simeulue.

Chapters 3 and 4 are essentially two parts of a whole, both covering the six sites of northern Simeulue and the single site on Salaut Besar island to the northwest. Chapter 3 provides detailed analyses of the observations at our primary northern Simeulue site, an overview of the findings from northern Simeulue in general, and a discussion of potential implications; Chapter 4 is written as auxiliary material to Chapter 3, providing detailed results from the additional northern Simeulue sites. Chapter 3 also contains a thorough explanation of the methods employed and of assumptions that have been made in this study; while I have generally built upon methods developed by my advisor and previous graduate students [*Zachariasen*, 1998; *Zachariasen et al.*, 1999, 2000; *Natawidjaja et al.*, 2004, 2006, 2007], I have made fundamental advances and modified certain techniques. An interpreted line drawing of each coral slab cross-section in this study is included among the figures in Chapters 3 and 4; alternate versions of these cross-sections with high-resolution x-ray mosaics appear in the appendix (electronic supplement) to Chapter 4. Also in the electronic supplement to Chapter 4 are aerial photos of some of the sites, taken by helicopter in 2005 soon after the uplift, and field photos of some of the microatolls that were slabbed for analysis.

Chapter 5 contains detailed analyses of coral slabs from one site on the west coast of central Simeulue. This chapter is less polished than the preceding three chapters, and it is not structured to be submitted for publication in its present form, but it is sufficient to demonstrate that neither northern Simeulue ruptures nor central-southern Simeulue ruptures propagate far into each other's domain: during the times for which simultaneous records exist from both regions, all ruptures observed as significant uplifts in one region had little effect in the other. Ultimately, these results will be combined with observations from other central Simeulue sites that augment the evidence in Chapter 5, and all of this will be published together. Speculation and discussion are minimal at this early stage of the work in Chapter 5, but a thorough discussion of possible implications of the results will be presented in the eventual manuscript prepared for publication. Chapter 5 also has an appendix that is available as an electronic supplement. As with Chapter 4, this appendix includes versions of the cross-sections containing high-resolution x-ray mosaics, as well as field photos of some of the microatolls that were slabbed for analysis.

Altogether, the results from paleogeodetic investigations presented in this thesis provide a rich data set that sheds light on the rupture history of the southern end of the 2004 Sunda megathrust rupture patch and that constitutes compelling evidence that central Simeulue has acted as a persistent barrier to megathrust ruptures over, at least, the past 700 years.

References

Ando, M. (1975), Source mechanisms and tectonic significance of historical earthquakes along the Nankai Trough, Japan, *Tectonophysics*, 27, 119-140, doi:10.1016/0040-1951(75)90102-X.

Atwater, B. F., and E. Hemphill-Haley (1997), *Recurrence Intervals for Great Earthquakes of the Past 3,500 Years at Northeastern Willapa Bay, Washington*, 108 pp.

Atwater, B. F., S. Musumi-Rokkaku, K. Satake, Y. Tsuji, K. Ueda, and D. K. Yamaguchi (2005), *The Orphan Tsunami of 1700: Japanese Clues to a Parent Earthquake in North America*, 144 pp.

Biasi, G. P., and R. J. Weldon (2009), San Andreas fault rupture scenarios from multiple paleoseismic records: stringing pearls, *Bull. Seismol. Soc. Am.*, 99, 471-498, doi:10.1785/0120080287.

Bilham, R. (2005), A flying start, then a slow slip, *Science*, 308, 1126-1127, doi:10.1126/science.1113363.

Bilham, R., R. Engdahl, N. Feldl, and S. P. Satyabala (2005), Partial and complete rupture of the Indo-Andaman plate boundary 1847-2004, *Seismol. Res. Lett.*, 76, 299-311, doi:10.1785/gssrl.76.3.299.

Briggs, R. W., K. Sieh, A. J. Meltzner, D. Natawidjaja, J. Galetzka, B. Suwargadi, Y.-j. Hsu, M. Simons, N. Hananto, I. Suprihanto, D. Prayudi, J.-P. Avouac, L. Prawirodirdjo, and Y. Bock (2006), Deformation and slip along the Sunda megathrust in the great 2005 Nias–Simeulue earthquake, *Science*, 311, 1897-1901, doi:10.1126/science.1122602.

Chlieh, M., J.-P. Avouac, V. Hjorleifsdottir, T.-R. A. Song, C. Ji, K. Sieh, A. Sladen, H. Hebert, L. Prawirodirdjo, Y. Bock, and J. Galetzka (2007), Coseismic slip and afterslip of the great M_W 9.15 Sumatra–Andaman earthquake of 2004, *Bull. Seismol. Soc. Am.*, 97, S152-S173, doi:10.1785/0120050631.

Kanamori, H. (1983), Global Seismicity, in *Earthquakes: Observation, Theory and Interpretation* by H. Kanamori and E. Boschi, pp. 596-608, North-Holland, Amsterdam.

Kelsey, H. M., R. C. Witter, and E. Hemphill-Haley (2002), Plate-boundary earthquakes and tsunamis of the past 5500 yr, Sixes River estuary, southern Oregon, *Geol. Soc. Am. Bull.*, 114, 298-314, doi:10.1130/0016-7606(2002)114<0298:PBEATO>2.0.CO;2.

Kelsey, H. M., A. R. Nelson, E. Hemphill-Haley, and R. C. Witter (2005), Tsunami history of an Oregon coastal lake reveals a 4600 yr record of great earthquakes on the Cascadia subduction zone, *Geol. Soc. Am. Bull.*, 117, 1009-1032, doi:10.1130/B25452.1.

Liu, J., Y. Klinger, K. Sieh, and C. Rubin (2004), Six similar sequential ruptures of the San Andreas fault, Carrizo Plain, California, *Geology*, 32, 649-652, doi:10.1130/G20478.1.

Meltzner, A. J., K. Sieh, M. Abrams, D. C. Agnew, K. W. Hudnut, J.-P. Avouac, and D. H. Natawidjaja (2006), Uplift and subsidence associated with the great Aceh–Andaman earthquake of 2004, *J. Geophys. Res.*, 111, B02407, doi:10.1029/2005JB003891.

Natawidjaja, D. H., K. Sieh, S. N. Ward, H. Cheng, R. L. Edwards, J. Galetzka, and B. W. Suwargadi (2004), Paleogeodetic records of seismic and aseismic subduction from central Sumatran microatolls, Indonesia, *J. Geophys. Res.*, 109, B04306, doi:10.1029/2003JB002398.

Natawidjaja, D. H., K. Sieh, M. Chlieh, J. Galetzka, B. W. Suwargadi, H. Cheng, R. L. Edwards, J.-P. Avouac, and S. N. Ward (2006), Source parameters of the great Sumatran megathrust earthquakes of 1797 and 1833 inferred from coral microatolls, *J. Geophys. Res.*, 111, B06403, doi:10.1029/2005JB004025.

Natawidjaja, D. H., K. Sieh, J. Galetzka, B. W. Suwargadi, H. Cheng, R. L. Edwards, and M. Chlieh (2007), Interseismic deformation above the Sunda megathrust recorded in coral microatolls of the Mentawai islands, West Sumatra, *J. Geophys. Res.*, 112, B02404, doi:10.1029/2006JB004450.

Ruff, L., and H. Kanamori (1980), Seismicity and the subduction process, *Phys. Earth Planet. Inter.*, 23, 240-252, doi:10.1016/0031-9201(80)90117-X.

Scharer, K. M., R. J. Weldon, T. E. Fumal, and G. P. Biasi (2007), Paleoearthquakes on the southern San Andreas fault, Wrightwood, California, 3000 to 1500 B.C.: a new method for evaluating paleoseismic evidence and earthquake horizons, *Bull. Seismol. Soc. Am.*, 97, 1054-1093, doi:10.1785/0120060137.

Sieh, K., M. Stuiver, and D. Brillinger (1989), A more precise chronology of earthquakes produced by the San Andreas fault in southern California, *J. Geophys. Res.*, 94, 603-623, doi:10.1029/JB094iB01p00603.

Stein, R. S., A. A. Barka, and J. H. Dieterich (1997), Progressive failure on the North Anatolian fault since 1939 by earthquake stress triggering, *Geophys. J. Int.*, 128, 594-604, doi:10.1111/j.1365-246X.1997.tb05321.x.

Subarya, C., M. Chlieh, L. Prawirodirdjo, J.-P. Avouac, Y. Bock, K. Sieh, A. J. Meltzner, D. H. Natawidjaja, and R. McCaffrey (2006), Plate-boundary deformation associated with the great Sumatra–Andaman earthquake, *Nature*, 440, 46-51, doi:10.1038/nature04522.

Sugiyama, Y. (1994), Neotectonics of southwest Japan due to the right-oblique subduction of the Philippine Sea plate, *Geofis. Int.*, 33, 53-76.

Taylor, F. W., R. W. Briggs, C. Frohlich, A. Brown, M. Hornbach, A. K. Papabatu, A. J. Meltzner, and D. Billy (2008), Rupture across arc segment and plate boundaries in the 1 April 2007 Solomons earthquake, *Nature Geosci.*, 1, 253-257, doi:10.1038/ngeo159.

Weldon, R., K. Scharer, T. Fumal, and G. Biasi (2004), Wrightwood and the earthquake cycle: what a long recurrence record tells us about how faults work, *GSA Today*, 14 (9), 4-10, doi:10.1130/1052-5173(2004)014<4:WATECW>2.0.CO;2.

Weldon, R. J., T. E. Fumal, G. P. Biasi, and K. M. Scharer (2005), Past and future earthquakes on the San Andreas fault, *Science*, 308, 966-967, doi:10.1126/science.1111707.

Witter, R. C., H. M. Kelsey, and E. Hemphill-Haley (2003), Great Cascadia earthquakes and tsunamis of the past 6700 years, Coquille River estuary, southern coastal Oregon, *Geol. Soc. Am. Bull.*, 115, 1289-1306, doi:10.1130/B25189.1.

Zachariasen, J. (1998), Paleoseismology and paleogeodesy of the Sumatran subduction zone: a study of vertical deformation using coral microatolls, Ph.D. thesis, 418 pp., California Institute of Technology, Pasadena, CA.

Zachariasen, J., K. Sieh, F. W. Taylor, R. L. Edwards, and W. S. Hantoro (1999), Submergence and uplift associated with the giant 1833 Sumatran subduction earthquake: evidence from coral microatolls, *J. Geophys. Res.*, 104, 895-919, doi:10.1029/1998JB900050.

Zachariasen, J., K. Sieh, F. W. Taylor, and W. S. Hantoro (2000), Modem vertical deformation above the Sumatran subduction zone: paleogeodetic insights from coral microatolls, *Bull. Seismol. Soc. Am.*, 90, 897-913, doi:10.1785/0119980016.

Chapter 2

Uplift and subsidence associated with the great Aceh–Andaman earthquake of 2004

Aron J. Meltzner, Kerry Sieh, Michael Abrams, Duncan C. Agnew,

Kenneth W. Hudnut, Jean-Philippe Avouac, and Danny H. Natawidjaja

Reprinted from the *Journal of Geophysical Research*

Volume 111, B02407, doi:10.1029/2005JB003891

February 2006

with modifications to the Supplementary Files

Uplift and subsidence associated with the great Aceh-Andaman earthquake of 2004

Aron J. Meltzner,[1] Kerry Sieh,[1] Michael Abrams,[2] Duncan C. Agnew,[3] Kenneth W. Hudnut,[4] Jean-Philippe Avouac,[1] and Danny H. Natawidjaja[5]

Received 20 June 2005; revised 5 October 2005; accepted 22 November 2005; published 15 February 2006.

[1] Rupture of the Sunda megathrust on 26 December 2004 produced broad regions of uplift and subsidence. We define the pivot line separating these regions as a first step in defining the lateral extent and the downdip limit of rupture during that great $M_w \approx 9.2$ earthquake. In the region of the Andaman and Nicobar islands we rely exclusively on the interpretation of satellite imagery and a tidal model. At the southern limit of the great rupture we rely principally on field measurements of emerged coral microatolls. Uplift extends from the middle of Simeulue Island, Sumatra, at ~2.5°N, to Preparis Island, Myanmar (Burma), at ~14.9°N. Thus the rupture is ~1600 km long. The distance from the pivot line to the trench varies appreciably. The northern and western Andaman Islands rose, whereas the southern and eastern portion of the islands subsided. The Nicobar Islands and the west coast of Aceh province, Sumatra, subsided. Tilt at the southern end of the rupture is steep; the distance from 1.5 m of uplift to the pivot line is just 60 km. Our method of using satellite imagery to recognize changes in elevation relative to sea surface height and of using a tidal model to place quantitative bounds on coseismic uplift or subsidence is a novel approach that can be adapted to other forms of remote sensing and can be applied to other subduction zones in tropical regions.

Citation: Meltzner, A. J., K. Sieh, M. Abrams, D. C. Agnew, K. W. Hudnut, J.-P. Avouac, and D. H. Natawidjaja (2006), Uplift and subsidence associated with the great Aceh-Andaman earthquake of 2004, *J. Geophys. Res.*, *111*, B02407, doi:10.1029/2005JB003891.

1. Introduction

[2] The 26 December 2004 $M_w \approx 9.2$ Aceh-Andaman earthquake resulted from slip on the subduction interface between the Indo-Australian plate and the Burma microplate below the Andaman and Nicobar islands and Aceh province, Sumatra (Figure 1). The distribution of aftershocks (e.g., from U.S. Geological Survey, available at http://neic.usgs.gov/neis/poster/2004/20041226.html) suggests that the rupture extended over a distance of 1500 km (measured parallel to the arc), but seismic inversions for this event are nonunique and cannot resolve many details of slip, especially along the northern portion of the rupture [e.g., *Ammon et al.*, 2005]. Furthermore, considering that slip north of ~9°N appears to have generated little or no seismic radiation [*Lay et al.*, 2005; *Ammon et al.*, 2005], seismic inversions will only provide a minimum constraint on the extent and amount of slip, and geodetic inversions will be required to provide a maximum (and perhaps more accurate) constraint. However, inversions of the sparse geodetic data that were available prior to this study provided only limited constraints on the amount and distribution of slip [e.g., *Subarya et al.*, 2006].

[3] In this paper, we combine satellite imagery and ground observations to map the extent of coseismic uplift and for some locations to constrain or estimate the magnitude of uplift or subsidence. In general, for a subduction megathrust earthquake, coseismic deformation of the upper plate can be modeled using an elastic slip dislocation model [e.g., *Plafker and Savage*, 1970; *Plafker*, 1972; *Natawidjaja et al.*, 2004]; one simple model is shown in Figure 2. To a first order approximation, during the interseismic period the portion of the upper plate overlying the locked subduction interface is gradually depressed, while the region landward of the locked fault zone bows upward slightly; then, during the earthquake the region above the updip portion of the rupture recovers the elastic strain stored during the interseismic period and experiences sudden coseismic uplift, whereas the downdip end of the rupture and adjacent regions subside. A small fraction of the coseismic uplift may reflect permanent strain accumulation in the forearc region. Although no modeling is presented in this paper, the region of coseismic uplift approximates the north-to-south rupture extent and demarcates a minimum downdip width of faulting. Resolution of the pattern of uplift, using a dense

[1]Tectonics Observatory, Division of Geological and Planetary Sciences, California Institute of Technology, Pasadena, California, USA.
[2]Jet Propulsion Laboratory, California Institute of Technology, Pasadena, California, USA.
[3]Scripps Institution of Oceanography, University of California, San Diego, La Jolla, California, USA.
[4]U.S. Geological Survey, Pasadena, California, USA.
[5]Research Center for Geotechnology, Indonesian Institute of Sciences, Bandung, Indonesia.

0148-0227/06/2005JB003891$09.00

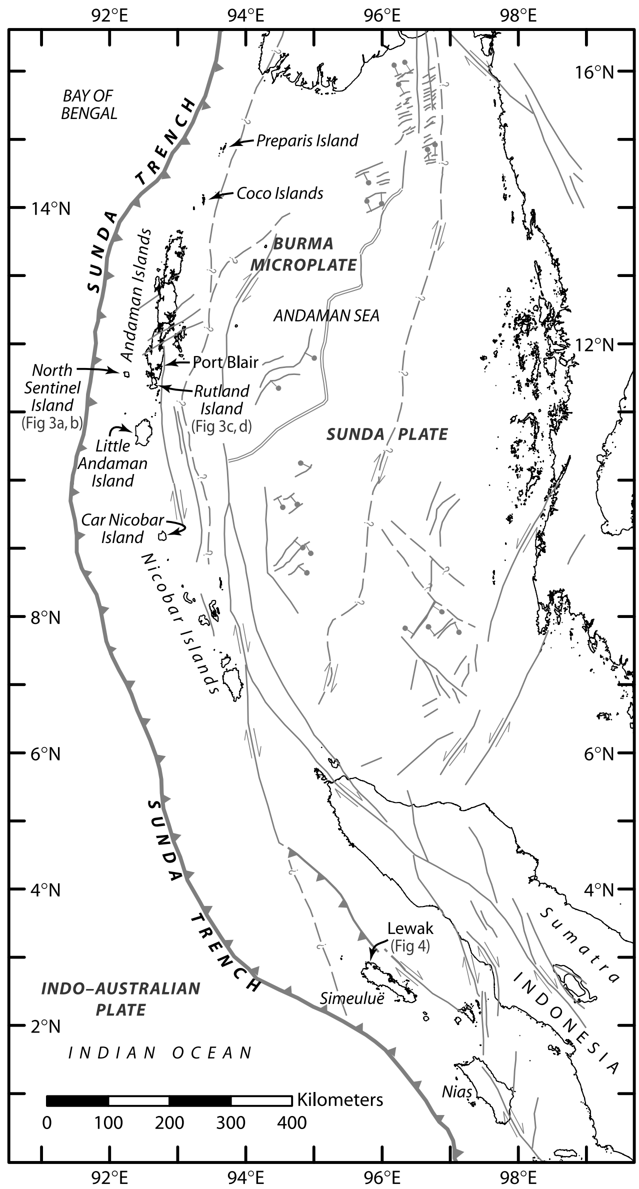

Figure 1. Overview map showing faults and plate boundaries from *Curray* [2005], places named in the text, and the general locations of Figures 3 and 4.

array of geodetic data points, can provide robust constraints on the coseismic slip distribution.

2. Procedure

2.1. Coral Background

[4] Our work combines two types of observations to arrive at a comprehensive map of uplift and subsidence associated with the 2004 earthquake and, in particular, of the "pivot line" separating the regions of uplift and subsidence. Fundamental to these techniques is the presence of coral heads and reefs surrounding many of the Andaman and Nicobar islands and much of the Indonesian archipelago. Each coral head or microatoll grows up to a certain elevation with respect to the annual lowest tides at a given locality. Above this maximum elevation, called the highest level of survival (HLS), a coral cannot survive and grow [*Taylor et al.*, 1987]. Corals living beneath the HLS grow both outward and upward (typically at rates on the order of 1 cm/yr) until the tops of the coral heads reach the HLS; subsequently, their tops die, and they are limited to horizontal growth. Although the elevation of the HLS of a coral relative to sea level is not strictly defined and varies according to genus or species, it nevertheless appears that HLS "tracks" lowest low-water levels with a sensitivity of a few centimeters [*Zachariasen et al.*, 2000]. A coral that is stable relative to the annual lowest tides should have a remarkably flat top. Thus coral microatolls can record tectonic uplift or subsidence. In addition, satellite imagery of coral reefs is useful for assessing differences in relative sea level, as the color and brightness of a reef in an image is strongly dependent upon the depth of water above the reef.

2.2. Analysis of Satellite Imagery

[5] Because many species of coral grow upward to near the annual low-tide level, they are sensitive to relative sea level changes of several centimeters or more. The water penetration depths for satellite images are typically tens of centimeters to a few meters [*Miller et al.*, 2005]. In standard analyses of false color satellite images, coral reefs appear to grade from a deep bluish color when submerged in comparatively deep water to a lighter, brighter blue when submerged under very shallow water to a pinkish or reddish white when exposed subaerially. (In these false color images, vegetation appears red; algae, which also appears red in false color, will not grow on living coral but will grow in the intertidal zone on coral heads that have been exposed and died; we interpret the reddish color on the coral reefs to result from algae growing on uplifted and exposed coral.)

[6] We examined Advanced Spaceborne Thermal Emission and Reflection Radiometer (ASTER), SPOT, IKONOS, QuickBird, and Landsat images of the region around the December 2004 rupture, identifying areas with different amounts of reef or land exposure in the different images. We compared satellite images acquired prior to the earth-

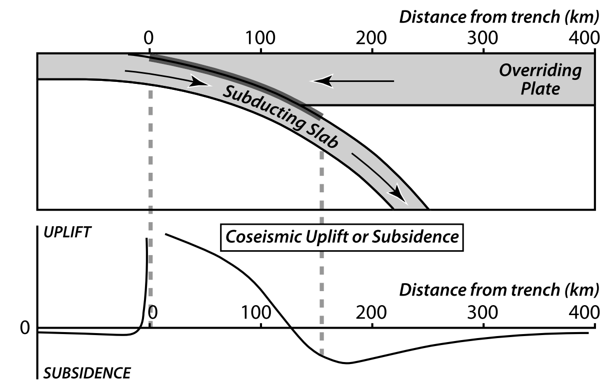

Figure 2. Generic elastic slip dislocation model. (top) Cross-section view across the subduction zone with the shaded parts corresponding to the lithosphere. The thick line represents the locked interface, which slips during the giant megathrust earthquakes. (bottom) Hypothetical pattern of coseismic uplift and subsidence and its geometrical relationship to slip on the locked interface. In a real case, factors including fault dip angle and slip distribution affect the actual pattern of uplift and subsidence.

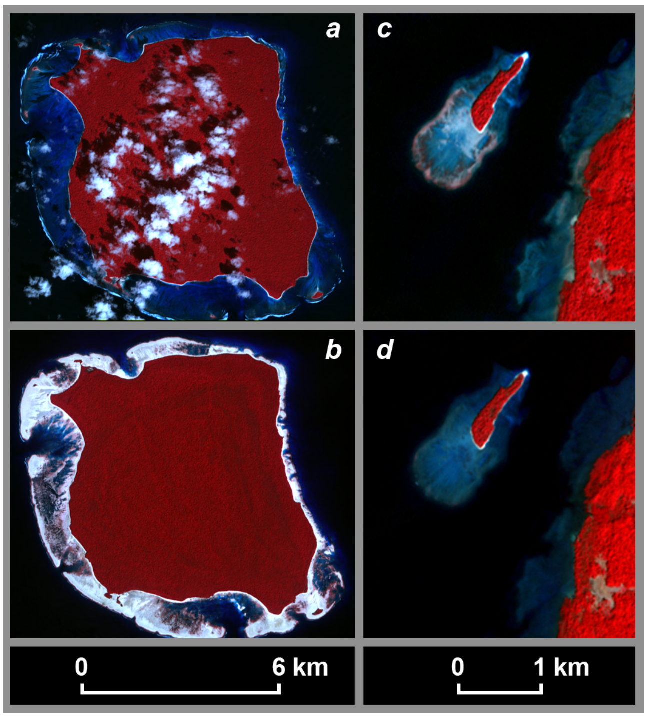

Figure 3. (a) Preearthquake and (b) postearthquake Advanced Spaceborne Thermal Emission and Reflection Radiometer (ASTER) images of North Sentinel Island, showing emergence of the coral reef surrounding the island. The tide was 30 ± 14 cm lower in the preearthquake image (acquired 21 November 2000) than in the postearthquake image (acquired 20 February 2005), requiring a minimum of 30 cm of uplift at this locality. Observations from an Indian Coast Guard helicopter on the northwest coast of the island suggest that the actual uplift is on the order of 1–2 m at this site [*Bilham et al.*, 2005]. (c) Preearthquake and (d) postearthquake ASTER images of a small island off the northwest coast of Rutland Island, 38 km east of North Sentinel Island, showing submergence of the coral reef surrounding the island. The tide was higher in the preearthquake image (acquired 1 January 2004) than in the postearthquake image (acquired 4 February 2005), requiring subsidence at this locality. The pivot line must run between North Sentinel and Rutland islands. Note that the scale for the North Sentinel Island images differs from that for the Rutland Island images.

quake with images acquired between 28 December 2004 and 26 March 2005 (we looked at images acquired as late as 15 August 2005 for Car Nicobar). After stretching and normalizing the color distribution in each image we relied on changes in the color and brightness of the reefs among the images to assess the relative levels of reef exposure. Fortunately, in most cases these differences in color and brightness were pronounced enough to be fairly insensitive to small variations in the overall color representations of the images. We then used a tidal model (discussed in Appendix A) to determine the relative sea surface height (SSH) at each location at the acquisition time of each image. The 2σ uncertainty of the tidal model is roughly ±10 cm, so the calculated difference between two SSHs for a given location should be accurate to ~14 cm or better. However, a ±14 cm (2σ) uncertainty associated with the overall satellite imagery method would be conservative; because we have only used image comparisons in which the difference in color or brightness is unambiguous, this effectively places a "buffer" of at least a few centimeters on our stated maximum or minimum bounds. Hence an appropriate 2σ uncertainty for a stated bound should be significantly less than 14 cm. Nonetheless, because we cannot quantify the aforementioned "buffer," we will retain the conservative 14 cm (2σ) uncertainty for use in this paper.

[7] The sensitivities of the satellite imagery method and of the tidal model were verified by comparing the apparent relative exposures among preearthquake images in numerous locations where multiple images were acquired prior to the earthquake. In looking only at images acquired between 2000 and 2004, we could neglect both interseismic vertical deformation and potential growth of the corals, which should be well within the uncertainty of the tidal model. Presumably, any differences in reef color or brightness among these images should be due solely to differences in the tides. In support of both the method and the tidal model, SSH differences as small as 5–10 cm (less than the stated 2σ uncertainty) were commonly recognizable among the images of a particular location, with lower SSHs corresponding to more brightly colored reefs.

[8] In order to document uplift of a reef we looked for a postearthquake image with more reef exposure than a preearthquake image of the same area taken at a lower tide; in that case, the difference in SSH between the two images can be taken as a minimum constraint on the amount of uplift. Similarly, to document subsidence, we looked for a preearthquake image with more reef exposure than a postearthquake image at a lower tide; in this case, the difference in SSH is a minimum constraint on the amount of subsidence. An example of each exercise is presented in Figure 3. In addition, we were also able to demonstrate subsidence in well-drained coastal areas that were not regularly flooded prior to December 2004 but which have been submerged since the earthquake.

2.3. In Situ Analysis of Coral Microatolls

[9] In addition to the satellite-based observations a set of field measurements of uplift was made on emerged coral heads around Simeulue Island, off the coast of Sumatra, by K. Sieh, D. H. Natawidjaja, J. Galetzka, and others (e.g., see Figure 4). Prior to the 26 December 2004 earthquake each of these corals was living, and the tops of each coral head coincided with the preearthquake HLS. During the earthquake these corals were uplifted, and the portions of each coral head now exposed to air would have been killed. Over the following days and weeks each time a new low tide was reached, an additional lower portion of the microatoll was exposed and died. For each microatoll a measurement was made of the vertical distance between the (now dead) top of the coral head and the present HLS, which was readily identifiable in the field by the pattern of algae growth; algae will not grow on living corals, but it was observed in many places to grow immediately above the coral HLS, extending as much as a half meter above the coral HLS. If the annual lowest tide (in the year preceding the earthquake) was equal to the lowest low tide that happened to occur in the time between the earthquake and

Figure 4. A *Porites* coral microatoll that died because of emergence on 26 December 2004 at Lewak, on Simeulue. The flat top of the coral head marks the preearthquake highest level of survival (HLS), and the new HLS is near the base of the coral (there is still living tissue on the coral, just at the water line). The pronounced horizontal line 10–15 cm below the top of the coral is the uppermost limit of algae growth; this level is not used for our measurement. The difference in elevation between the preearthquake HLS and the new HLS is 44 cm. Actual uplift at this site, which includes the 44 cm measured in the field plus a tidal correction of 2 cm (discussed in the text), is 46 cm. Photo courtesy of J. Galetzka, taken at very low tide.

the field measurement (most of the measurements were made on 17 or 18 January 2005), then the vertical distance between the preearthquake HLS and the HLS at the time of the measurement would equal the amount of uplift at the location. However, because the lowest tide between 26 December 2004 and the time of measurement was slightly higher than the annual lowest tide, a small correction needed to be made. For each location the tidal model (discussed in Appendix A) was used to calculate the difference between (1) the lowest low tide in the year preceding the earthquake and (2) the lowest low tide in the period between the earthquake and the time of the measurement; this difference was added to the in situ measurement of uplift. In general, this difference was less than 5 cm.

3. Results and Discussion

[10] We were able to apply the satellite imagery technique throughout the rupture area where there was available coverage both before and after the earthquake and where there were markers that were clearly exposed to different extents in the various images (any before-and-after image pair for which the relative extents of reef exposure could not be determined without ambiguity was discarded). We have near-complete coverage of the Andaman Islands, partial coverage of the Nicobar Islands, and spotty coverage in Sumatra. Because the climate in January to March is relatively dry in the Andamans but is wetter closer to the equator, it was increasingly difficult toward the south to acquire cloud-free images between 26 December 2004 and 28 March 2005. We supplemented the satellite-based work with the in situ measurements of uplift on the coral heads in northwestern Simeulue, where it was especially difficult to acquire clear postearthquake images prior to the subsequent 28 March 2005 Simeulue-Nias earthquake.

[11] Our results are summarized in Figure 5 and auxiliary material[1] Tables S1–S3. Broadly, the northern and western Andaman Islands were uplifted, whereas the southern and eastern portion of the islands subsided. The pivot line separating uplift from subsidence is nearest the Sunda Trench at about 11.4°N, but it trends obliquely away from the trench to the north and south. Farther south, all of the Nicobar Islands and northwestern mainland Sumatra subsided, so the location of the pivot line between 10°N and just north of 3°N is bounded only to the east. As seen from the field measurements of coral microatolls, there is a sharp uplift gradient across Simeulue, with the western tip of the island up 1.5 m and the southeastern 30 km of the 100 km long island having subsided. The pivot line is most tightly constrained in the Andaman Islands and on Simeulue.

[1] Auxiliary material is available at ftp://ftp.agu.org/apend/jb/2005JB003891.

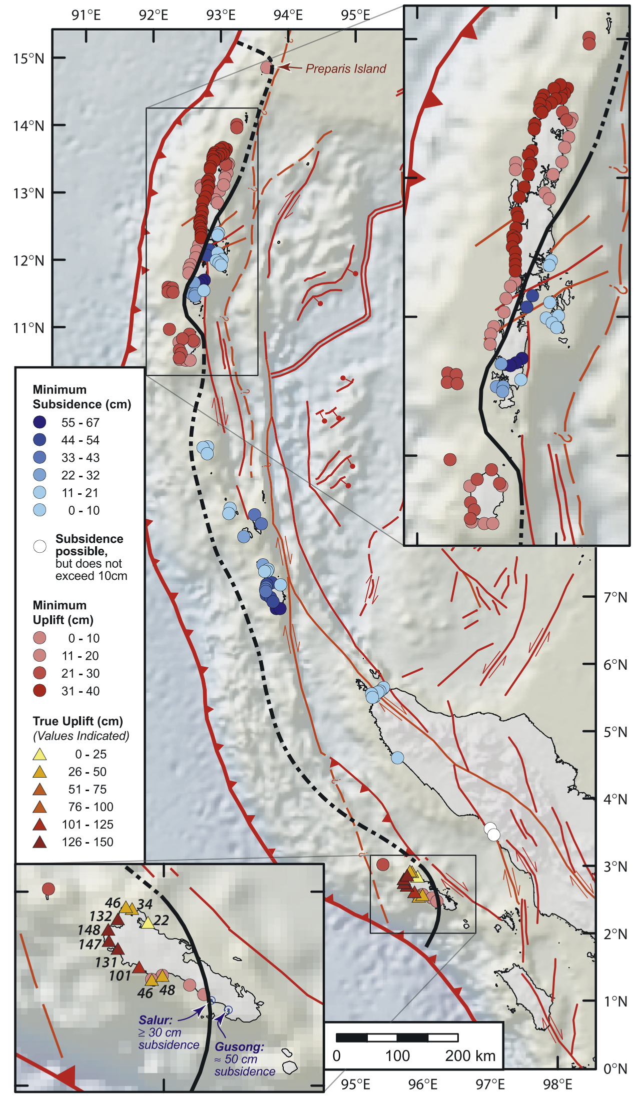

Figure 5. Summary map showing minimum constraints on uplift or subsidence from satellite imagery, as well as field measurements of uplift and subsidence on Simeulue. Also shown are faults from *Curray* [2005] and our best estimate of the location of the pivot line. The pivot line is shown as a solid thick black line where its location is more tightly constrained and as a dashed line where it is more poorly constrained. Estimate of subsidence at Busung, Gusong Bay, Simeulue, is from R. Peters (http://walrus.wr.usgs.gov/news/reportsleg1.html). The four imagery-based uplift constraints on Simeulue (pink circles) span both the 2002 and 2004 earthquakes and thus represent minimum net uplift for the two events. See text and Table S1 for more details.

[12] Resolution of slip at the northernmost end of the rupture is based upon a single datum at Preparis Island (Figure 5). Unfortunately, the only preearthquake ASTER image of Preparis Island is marred by high atmospheric water content, which affects the color of the image. While we do not feel this warrants discarding the datum, and while analysis of a (lower resolution) Landsat image of the region acquired on 11 January 2002 also supports minor (20–30 cm) uplift, we concede that this datum is not as robust as the majority of our imagery-based observations. Attempts to perform a comparable analysis using Envisat synthetic aperture radar (SAR) images were inconclusive (E. Fielding, personal communication, 2005; M. Tobita, personal communication, 2005).

[13] Concerns about the northernmost data point aside, our observations suggest that the 26 December 2004 rupture extended from under Simeulue Island northward to Preparis Island of Myanmar (Burma), near latitude 15°N. Although different authors have measured the length of the rupture differently, measured parallel to the arc (as opposed to along a straight line connecting the rupture endpoints), the rupture is ~1500 km long if it extends from northern Simeulue to latitude 14°N, and it is ~1600 km long if it extends to 15°N. Our preferred northern limit (15°N) is at least 100 km north of the northern extent of rupture suggested by aftershock locations (e.g., from the U.S. Geological Survey) and by inversions of seismic data [e.g., *Ammon et al.*, 2005]. However, in addition to the uplift directly over the rupture patch, minor uplift would be expected on the updip edge as well as beyond the northern and southern edges of the rupture (V. Gahalaut, personal communication, 2005). If real, the small amount of uplift at Preparis Island does not require that slip along the underlying fault plane propagated that far north, only nearly so.

[14] We must also consider the possibility of interseismic and postseismic slip being included in our observations. While the amount of interseismic slip that may have occurred within the period of our observations (less than 5 years) is probably a negligible fraction of the coseismic slip, postseismic slip may be significant. For example, continuous GPS data from the SAMP (Sampali) site near Medan along the northeast coast of Sumatra reveal a clear record of coseismic slip and postseismic relaxation: The daily time series from SAMP shows a coseismic horizontal displacement of 13.8 cm which increased logarithmically by about 15% over 15 days and by about 25% over 60 days following the earthquake [*Subarya et al.*, 2006]. Similarly, *Vigny et al.* [2005] report that Phuket, Thailand, moved 1.25 times the initial coseismic displacement there during the first 50 days after the earthquake, and *Gahalaut et al.* [2006] observed that during the period 11–22 January 2005, Port Blair moved horizontally by 3.5 cm in the same direction as that of the coseismic displacement. Hence our result at each location may be dependent upon the date of the postearthquake observation. Instead of attempting to model the separate contributions of coseismic and postseismic slip to each of our observations, we simply present the dates of each observation along with the respective datum (Tables S1–S3), and we leave it to the discretion of any users of our data to model the data as they see fit.

[15] In addition to postseismic slip following the 2004 earthquake, coseismic slip from an additional earthquake may have been captured by our imagery observations on Simeulue island. While we did not examine images of Simeulue captured after the 28 March 2005 earthquake, an earthquake of M_w 7.3 occurred in central Simeulue on 2 November 2002 [*DeShon et al.*, 2005]. At the four sites on Simeulue where we determined from imagery that there was

uplift (pink circles on Simeulue in Figure 5), the preearthquake images were all acquired prior to the November 2002 earthquake. (More details are provided in Table S1.) Hence the minimum uplift we report at those four sites is actually minimum net uplift that occurred during and between the 2002 and 2004 earthquakes. Uplift values determined from in situ microatoll measurements (Table S2), however, are clearly attributable to the 2004 earthquake. At a few sites in central Simeulue the coral microatolls record multiple uplift events. In those cases, the earlier uplift is on the order of $\sim$20 cm or less, and we tentatively attribute it to the 2002 earthquake.

[16] We should note that only at a few localities were we able to provide both maximum and minimum constraints on the amount of uplift or subsidence; in most cases we were able to provide only minimum constraints on uplift or subsidence. This is because the remote sensing method is limited by the tidal range and, in particular, by the range of SSH among the satellite images that were acquired; in the Andaman and Nicobar islands this range is typically 1 m or less, and in Sumatra this range is typically less than 0.5 m. In any case where the amount of uplift or subsidence exceeded the SSH range, this method can only provide a minimum bound on the amount of tectonic elevation change. Information from other sources [e.g., *Bilham et al.*, 2005] suggests that elevation changes (uplift or subsidence) of several meters were widespread throughout the affected region. Hence any minimum bounds on uplift or subsidence stated in this paper should not be construed to represent or approximate the actual uplift or subsidence at that location; only the sign of the elevation change (up or down) at a location, and hence the constraints on the pivot line, should be considered robust. We must also caution against attempts to interpret any trends among the uplift (red) points or among the subsidence (blue) points in Figure 5. That a stated minimum uplift at one point might be greater than a stated minimum uplift at a second point does not imply that the uplift at the first point is greater than the uplift at the second point.

[17] In an attempt to provide some ground truth to the satellite imagery method and to our results we compared the results presented in Table S1 with recently released campaign GPS vertical vectors from 16 sites in the Andaman and Nicobar islands [*Jade et al.*, 2005; *Gahalaut et al.*, 2006] and a handful of sites in Sumatra [*Subarya et al.*, 2006]. For each of the GPS data located within roughly 50 km of at least one satellite imagery observation (i.e., for all of the GPS data from the Andaman and Nicobars but for only a few of the Sumatra data), we compared the GPS vertical vector to the closest imagery-based data. Our observations and inferences using satellite imagery and the tidal model were almost without exception consistent with the GPS data. At only two sites were the campaign GPS vertical vectors beyond the maximum or minimum bounds derived from our work.

[18] At one of the sites with discrepancy, HAVE on Havelock Island, Andaman Islands (12.03°N, 92.99°E), *Jade et al.* [2005] calculate an uplift of 0.6 ± 2.5 cm that they infer represents the coseismic displacement and postseismic movement through February 2005. They subtracted 15 months of inferred interseismic motion (which had a negligible vertical component) from the record, as the last preearthquake site occupation occurred in September 2003. The result, 0.6 ± 2.5 cm, is barely beyond the minimum subsidence of 3 to 4 cm allowed at the nearest sites, 4 to 9 km away, based on images acquired on 1 January 2004 and 4 February 2005 (Table S1). However, the reported value of *Jade et al.* [2005] may be suspect. *Gahalaut et al.* [2006] occupied station GG (Govindgarh; 12.036°N, 92.983°E), only $\sim$1 km from HAVE, in March 2004 and January 2005, covering a shorter period of time and thereby allowing a more robust determination of the coseismic displacement vector. Their result, -18 ± 2 cm, is consistent with the imagery-based observations. The reason for the discrepancy between *Gahalaut et al.* [2006] and *Jade et al.* [2005] is unclear, but we note that our results for that vicinity are entirely consistent with the former and they are consistent with the latter within the stated (albeit conservative) ±14 cm (2σ) uncertainty resulting from the tide model.

[19] At the other site with discrepancy, Hut Bay (HB) on Little Andaman Island (10.696°N, 92.569°E), *Gahalaut et al.* [2006] report a coseismic elevation change of -26 ± 2 cm (i.e., 26 cm of subsidence), with successive site occupations in March 2004 and January 2005. In contrast, satellite images acquired on 1 January 2004 and 3 January 2005 (Table S1) indicate that the entire island of Little Andaman rose, with the eastern part (including Hut Bay) up at least 18 cm, although the nearest imagery-based datum to Hut Bay is more than 10 km away. Again, however, the GPS value may be suspect. Also using campaign GPS measurements, *Earnest et al.* [2005] determined that there was 36 cm of uplift at Hut Bay between August 2004 and early 2005, although the dates of their site occupations are not specified. Their result appears to be in conflict with that of *Gahalaut et al.* [2006] but is in complete agreement with our constraints. The reason for the discrepancy between *Gahalaut et al.* [2006] and *Earnest et al.* [2005] is unclear, but in further support of the imagery-based observations over the GPS observations of *Gahalaut et al.* [2006], *Bilham et al.* [2005] cite eyewitness reports of substantial (1–2 m, though this may be exaggerated) coseismic uplift at Hut Bay.

4. Conclusions

[20] We combine satellite imagery and ground observations of emerged and submerged coral reefs and microatolls and invoke a tidal model to resolve geodetic deformation associated with the 26 December 2004 Aceh-Andaman earthquake. We constrain the location of the pivot line separating regions of uplift and subsidence. Most of the rupture of the underlying megathrust must be west of this line. This line implies a rupture width that varies from slightly greater than 80 km to slightly greater than 120 km and a rupture length of $\sim$1600 km, at least 100 km longer than that suggested by aftershock locations and by seismic inversions to date. Our method of using satellite imagery to recognize apparent color differences in coral reefs, of correlating these color differences with differences in elevation relative to SSH, and of using a tidal model to place quantitative bounds on coseismic uplift or subsidence is a novel approach that can be adapted to other forms of remote sensing and can be applied to other

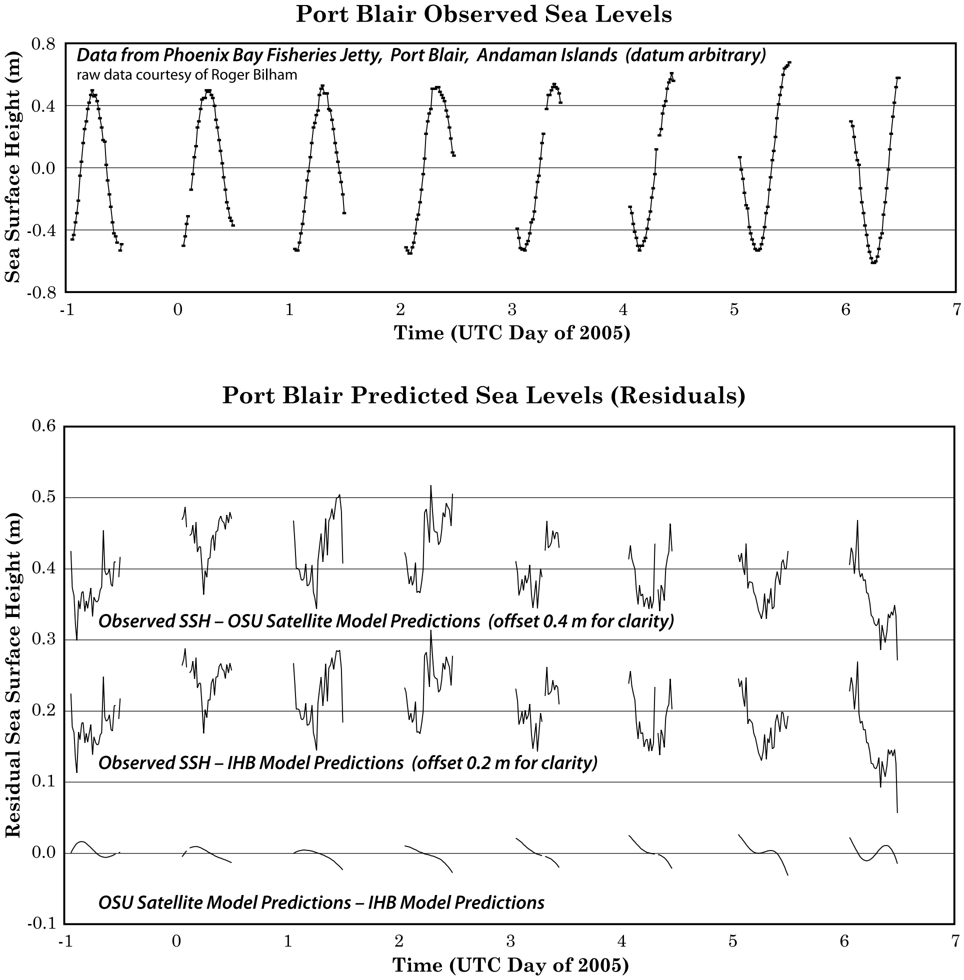

Figure A1. (top) Plot of the observed tides at Phoenix Bay Fisheries Jetty (PBFJ), Port Blair, Andaman Islands, for the period 31 December 2004 to 7 January 2005. (Day 0.0 corresponds to 1 January 2005, 0000:00 UTC.) (bottom) Residuals of the differences between the observations and the predictions of the Oregon State University (OSU) Bay of Bengal model, between the observations and the predictions of the International Hydrographic Bureau (IHB) model, and between the respective predictions of the OSU Bay of Bengal and IHB models. Each plot of residuals is offset vertically for clarity; also note the difference in the scale of the residual plots (Figure A1, bottom) in comparison to that of the observations (Figure A1, top). A significant portion of the residuals may be due to measurement errors or to imprecision in the tide gauge at PBFJ; still, the residuals fall within a 2σ uncertainty of $\pm$10 cm or less.

subduction zones in the tropics and perhaps elsewhere in the world.

Appendix A: Determination of Tide Heights

[21] In a comparison of preearthquake and postearthquake satellite imagery of reefs or coastal areas, in order to ascertain with certainty whether a particular area experienced uplift or subsidence, any variation in SSH due to tidal influences must be considered. In addition, as described in the body of this paper, if differences in the extent of reef exposure can be identified among the images of a location, then the difference in SSH between the images can be used to constrain the amount of uplift or subsidence.

[22] In order to determine the tidal height at each location of interest at the acquisition time of each satellite image we used the software package NLOADF [*Agnew*, 1997], along with harmonic tidal constituents extracted from the Oregon State University Regional Tidal Solutions (regional models based on satellite observations) for the Bay of Bengal and for Indonesia [*Egbert and Erofeeva*, 2002] (available at http://www.coas.oregonstate.edu/research/po/research/tide/region.html; hereinafter referred to as the Bay of Bengal and Indonesia models, respectively). The Bay of Bengal model covers the Andaman and Nicobar islands, and the Indonesia model covers Sumatra and its offshore islands, so these two models are sufficient for our study. The regional inverse solutions (including the Bay of Bengal and Indonesia models) have about the same residual magnitudes as the global solution TPXO.6 for the open ocean, but the regional solutions fit the data significantly better for areas with complex coastlines and bathymetry and are consequently preferred.

[23] To verify the harmonic tidal constituents extracted from the Bay of Bengal model, we compared the predictions of these constituents for Port Blair (in the Andaman Islands) for several arbitrary time periods with direct tide observations at the Phoenix Bay Fisheries Jetty (PBFJ) in Port Blair (Figure A1) and with the predictions from three ground-based sources: the Indian Tide Tables (ITT), the International Hydrographic Bureau (IHB), and the Admiralty Tide Tables (ATT). (See *Pugh* [2004, chapter 3] for a discussion of harmonic tidal constituents.) The ITT are published by the Survey of India and consist of predictions of times and heights of high and low tides at Port Blair, based on their (unknown to us) harmonic constituents, which are in turn based on tide gauge data; the predictions for January 1965 were read directly from the tables. The harmonic constituents of the IHB for Port Blair were derived from harmonic analysis of 41 years of tide gauge data (1880–1920) from the ITT; they are taken from *International Hydrographic Bureau* [1953, sheet 159]. The ATT are published by the British Admiralty and consist of harmonic constituents for Port Blair, also based on tide gauge data; the constituents for 1996 were chosen for this comparison. Note that the applicability of the ITT, the IHB, and the ATT predictions is limited to Port Blair and the few other locations for which tide gauge data exist; to assess the behavior of tides elsewhere in the Andaman and Nicobar islands and in Sumatra, a model based on satellite observations is more robust.

[24] Overall, the ITT and the IHB predictions should provide the closest approach to "ground truth" for the actual tidal heights, and the predictions for Port Blair of the ITT, the IHB, and the Bay of Bengal model are remarkably consistent with one another, lending credibility to the Bay of Bengal model. The standard deviation of the differences between the tidal observations at PBFJ and the predictions of the Bay of Bengal model is on the order of ±5 cm; likewise, for the year 2004 the standard deviation of the difference between the respective predictions of the Bay of Bengal model and the IHB constituents is roughly ±5 cm, and the maximum difference is under 20 cm. These values should provide a sense of the maximum likely errors in the Bay of Bengal model's predictions, at least for Port Blair. The ATT predictions differ somewhat from the others, so they will not be considered further. The Bay of Bengal model appears to be the best for use throughout the Andaman and Nicobar islands; the only location for which we did not use this model is for Port Blair itself, where the IHB tidal constituents should be most reliable. By extension of the foregoing discussion we considered the Indonesia regional model to be better than any ground-based local predictions for use throughout Sumatra.

[25] **Acknowledgments.** We thank Mohamed Chlieh, Chen Ji, Rich Briggs, and Rob McCaffrey for assistance and many insightful discussions. We are grateful to John Galetzka, Imam Suprihanto, and Bambang Suwargadi for data collection and invaluable field support in Indonesia and to Hidayat and Samsir of Derazona Air Services, our helicopter pilot and mechanic. We are very appreciative of Chris Goldfinger for collecting and sharing satellite imagery and of Roger Bilham for sharing data and making his manuscripts available to us, which benefited us tremendously. We thank JoAnne Giberson and Shaun Healy for ongoing GIS support. We also thank Vineet Gahalaut, Roger Bilham, and an anonymous reviewer for helpful reviews that led to substantial improvements in the paper. We acknowledge the use of QuickBird imagery made freely available by DigitalGlobe, and the use of IKONOS and SPOT 5 images acquired, processed, and made freely available by CRISP, National University of Singapore. This research was supported in part by the Gordon and Betty Moore Foundation and by NASA grant NAG5-10406. This is Caltech Tectonic Observatory contribution 23.

References

Agnew, D. C. (1997), NLOADF: A program for computing ocean-tide loading, *J. Geophys. Res.*, *102*, 5109–5110.
Ammon, C. J., et al. (2005), Rupture process of the 2004 Sumatra-Andaman earthquake, *Science*, *308*, 1133–1139.
Bilham, R., E .R. Engdahl, N. Feldl, and S. P. Satyabala (2005), Partial and complete rupture of the Indo-Andaman plate boundary 1847–2004, *Seismol. Res. Lett.*, *76*, 299–311.
Curray, J. R. (2005), Tectonics and history of the Andaman Sea region, *J. Asian Earth Sci.*, *25*, 187–228.
DeShon, H. R., E. R. Engdahl, C. H. Thurber, and M. Brudzinski (2005), Constraining the boundary between the Sunda and Andaman subduction systems: Evidence from the 2002 M_w 7.3 Northern Sumatra earthquake and aftershock relocations of the 2004 and 2005 great earthquakes, *Geophys. Res. Lett.*, *32*, L24307, doi:10.1029/2005GL024188.
Earnest, A., C .P. Rajendran, K. Rajendran, R. Anu, G. M. Arun, and P. M. Mohan (2005), Near-field observations on the co-seismic deformation associated with the 26 December 2004 Andaman-Sumatra earthquake, *Curr. Sci.*, *89*, 1237–1244.
Egbert, G. D., and S. Y. Erofeeva (2002), Efficient inverse modeling of barotropic ocean tides, *J. Atmos. Oceanic Technol.*, *19*, 183–204.
Gahalaut, V. K., B. Nagarajan, J. K. Catherine, and S. Kumar (2006), Constraints on 2004 Sumatra earthquake rupture from GPS measurements in Andaman-Nicobar islands, *Earth Planet. Sci. Lett.*, doi:10.1016/j.epsl.2005.11.051, in press.
International Hydrographic Bureau (1953), *Tides: Harmonic Constants*, *Int. Hydrogr. Bur. Spec. Publ., 26*, 121 pp., sheets 1–3055.
Jade, S., M. B. Ananda, P. D. Kumar, and S. Banerjee (2005), Co-seismic and post-seismic displacements in Andaman and Nicobar islands from GPS measurements, *Curr. Sci.*, *88*, 1980–1984.
Lay, T., et al. (2005), The great Sumatra-Andaman earthquake of 26 December 2004, *Science*, *308*, 1127–1133.
Miller, R. L., C. E. Del Castillo, and B. A. McKee (Eds.) (2005), *Remote Sensing of Coastal Aquatic Environments: Technologies, Techniques and Applications*, *Remote Sens. Digital Image Process.*, vol. 7, 347 pp., Springer, New York.
Natawidjaja, D. H., K. Sieh, S. N. Ward, H. Cheng, R. L. Edwards, J. Galetzka, and B. W. Suwargadi (2004), Paleogeodetic records of seismic and aseismic subduction from central Sumatran microatolls, Indonesia, *J. Geophys. Res.*, *109*, B04306, doi:10.1029/2003JB002398.
Plafker, G. (1972), Alaskan earthquake of 1964 and Chilean earthquake of 1960: Implications for arc tectonics, *J. Geophys. Res.*, *77*, 901–925.
Plafker, G., and J. C. Savage (1970), Mechanism of the Chilean earthquakes of May 21 and 22, 1960, *Geol. Soc. Am. Bull.*, *81*, 1001–1030.
Pugh, D. (2004), *Changing Sea Levels: Effects of Tides, Weather and Climate*, 280 pp., Cambridge Univ. Press, New York.
Subarya, C., M. Chlieh, L. Prawirodirdjo, J.-P. Avouac, R. McCaffrey, Y. Bock, K. Sieh, A. J. Meltzner, and D. H. Natawidjaja (2006), Static deformation of the great Aceh-Andaman earthquake, *Nature*, doi:10.1038/nature04522, in press.
Taylor, F. W., C. Frohlich, J. Lecolle, and M. Strecker (1987), Analysis of partially emerged corals and reef terraces in the central Vanuatu Arc: Comparison of contemporary coseismic and nonseismic with Quaternary vertical movements, *J. Geophys. Res.*, *92*, 4905–4933.
Vigny, C., et al. (2005), Insight into the 2004 Sumatra-Andaman earthquake from GPS measurements in southeast Asia, *Nature*, *436*, 201–206, doi:10.1038/nature03937.
Zachariasen, J., K. Sieh, F. W. Taylor, and W. S. Hantoro (2000), Modern vertical deformation above the Sumatran subduction zone: Paleogeodetic insights from coral microatolls, *Bull. Seismol. Soc. Am.*, *90*, 897–913.

M. Abrams, Jet Propulsion Laboratory 183-501, California Institute of Technology, 4800 Oak Grove Drive, Pasadena, CA 91109, USA.
D. C. Agnew, Scripps Institution of Oceanography 0225, University of California, San Diego, 9500 Gillman Drive, La Jolla, CA 92093, USA.
J.-P. Avouac, A. J. Meltzner, and K. Sieh, Tectonics Observatory, Division of Geological and Planetary Sciences, California Institute of Technology, Pasadena, CA 91125, USA. (meltzner@gps.caltech.edu; sieh@gps.caltech.edu)
K. W. Hudnut, U.S. Geological Survey, Pasadena Field Office, 525 South Wilson Avenue, Pasadena, CA 91106, USA.
D. H. Natawidjaja, Research Center for Geotechnology, Indonesian Institute of Sciences, Komplek LIPI Gd. 70, J1, Bandung 40135, Indonesia.

Auxiliary Material for Paper 2005JB003891

Uplift and subsidence associated with the great Aceh–Andaman earthquake of 2004

Aron J. Meltzner and **Kerry Sieh**
Tectonics Observatory, Division of Geological and Planetary Sciences,
California Institute of Technology,
Pasadena, California, USA

Michael Abrams
Jet Propulsion Laboratory,
California Institute of Technology,
Pasadena, California, USA

Duncan C. Agnew
Scripps Institution of Oceanography,
University of California, San Diego,
La Jolla, California, USA

Kenneth W. Hudnut
U.S. Geological Survey,
Pasadena, California, USA

Jean-Philippe Avouac
Tectonics Observatory, Division of Geological and Planetary Sciences,
California Institute of Technology,
Pasadena, California, USA

and **Danny H. Natawidjaja**
Research Center for Geotechnology,
Indonesian Institute of Sciences,
Bandung, Indonesia

Meltzner, A. J., K. Sieh, M. Abrams, D. C. Agnew, K. W. Hudnut, J.-P. Avouac, and D. H. Natawidjaja (2006), Uplift and subsidence associated with the great Aceh–Andaman earthquake of 2004, *J. Geophys. Res.*, 111, B02407, doi:10.1029/2005JB003891.

Introduction

This supplement consists of three tables that collectively constitute our data. Table S1 lists the constraints on vertical deformation that can be made from satellite imagery and the tidal model. Table S2 lists the estimates of vertical deformation on Simeulue that could be made from field observations in 2005, using uplifted coral microatolls in conjunction with the tidal model. Table S3 lists less quantitative information on coseismic subsidence on Simeulue, for two locations. Only some of the data listed in Tables S1–S3 are shown in map view on Fig. 5, whereas Tables S1–S3, collectively, are comprehensive.

1. **Table S1:** Vertical changes determined from satellite imagery.

1.1 Column "Latitude", degrees, latitude of the observation point, north of Equator.

1.2 Column "Longitude", degrees, longitude of the observation point, east of Greenwich.

1.3 Column "MinDeltaZ", minimum uplift (if positive) or maximum subsidence (if negative), in cm; "null" indicates that a given datum does not provide such constraint.

1.4 Column "MaxDeltaZ", maximum uplift (if positive) or minimum subsidence (if negative), in cm; "null" indicates that a given datum does not provide such constraint.

1.5 Column "2sigma", CONSERVATIVE (see text) 2-sigma uncertainty associated with both the minimum and maximum elevation changes, in cm. When stated as ± 14 cm, it is the uncertainty associated with the tidal model. When the uncertainty is listed as "0", the observation for that point is of submergence, i.e., of water connected to the ocean in a location where it would never have been previously; for these observations (all of which are in Aceh), the tidal model was not used.

Note added for Chapter 2 of AJM's thesis: Some values in this column have been changed. Values previously stated as ± 14 cm are now stated as ± 24 cm. These larger errors account for the fact that non-tidal sea level anomalies were not considered in the original imagery-based uplift and subsidence calculations. For more information, see Chapter 1 of this thesis.

1.6 Column "PreDate", acquisition date (yyyy/mm/dd, UTC) of the pre-earthquake image used for the final calculation of elevation change (additional pre-earthquake images may have been viewed for the study).

1.7 Column "PostDate", acquisition date (yyyy/mm/dd, UTC) of the post-earthquake image used for the final calculation of elevation change (additional post-earthquake images may have been viewed for the study).

1.8 Column "PreType", type of imagery of the pre-earthquake image used for the final calculation of elevation change (A: ASTER; I: IKONOS; Q: QuickBird; S: SPOT).

1.9 Column "PostType", type of imagery of the post-earthquake image used for the final calculation of elevation change (A: ASTER; I: IKONOS; Q: QuickBird; S: SPOT).

Points for which a minimum constraint on uplift or a minimum constraint on subsidence was determined are shown in map view on Fig. 5.

The following discussion might be useful for understanding Table S1:

a) If there is a positive number, say X, in column "MinDeltaZ", then any {uplift} greater than X is allowed.

b) If there is a negative number X in column "MinDeltaZ", then any {uplift} greater than X is allowed [this includes subsidence for which the absolute value of {elevation change} is less than abs(X), e.g., if X = –20 then 10 cm of subsidence is allowed; zero change or any positive uplift value would also be allowed].

c) If there is a number in column "MaxDeltaZ", call it Y, in addition to X in column "MinDeltaZ", then X < {elevation change} < Y.

d) If there is only a column "MaxDeltaZ" entry (only Y, no X) then {elevation change} < Y.

2. **Table S2:** Uplift on Simeulue determined from field measurements of coral microatolls.

2.1 Column "Latitude", degrees, latitude of the observation point, north of Equator.

2.2 Column "Longitude", degrees, longitude of the observation point, east of Greenwich.

2.3 Column "DeltaZ", uplift, in cm (none of these measurements were of subsidence).

2.4 Column "2sigma", estimated 2-sigma uncertainty associated with the calculation, in cm; sources of uncertainty include imprecision in the coral record, in the measurement technique, and in the tidal model.

2.5 Column "Date", date of measurement (yyyy/mm/dd).

These points are shown in map view on Fig. 5.

3. **Table S3:** Subsidence on Simeulue determined from field observations.

3.1 Column "Latitude", degrees, latitude of the observation point, north of Equator.

3.2 Column "Longitude", degrees, longitude of the observation point, east of Greenwich.

3.3 Column "DeltaZ", change in elevation, in cm.

(In Salur, we measured the depth of flooding of a well-drained locality where residents said water had never stood before, which effectively provides a minimum constraint on subsidence there; the uncertainty on this minimum constraint is difficult to assess.

In Busung, Gusong Bay, there is a rough estimate of subsidence from R. Peters, http://walrus.wr.usgs.gov/news/reportsleg1.html; no estimate of the uncertainty is available for this point, but it may be considerable.)

3.4 Column "Date", date of observation (yyyy/mm/dd).

3.5 Column "Location", name of location.

3.6 Column "Note", note on whether the value given in column "DeltaZ" is an estimate or a one-sided (minimum or maximum) constraint of the elevation change.

These points are shown in map view on Fig. 5.

Table S1: Vertical changes determined from satellite imagery

Latitude	Longitude	MinDeltaZ	MaxDeltaZ	2sigma*	PreDate	PostDate	PreType	PostType
14.862	93.682	20	null	*24*	2000/06/30	2005/01/10	A	I
14.015	93.236	23	null	*24*	2004/01/01	2005/01/03	A	A
13.967	93.237	23	null	*24*	2004/01/01	2005/01/03	A	A
13.648	93.081	38	null	*24*	2000/11/21	2005/01/03	A	A
13.611	93.060	38	null	*24*	2000/11/21	2005/01/03	A	A
13.619	93.033	38	null	*24*	2000/11/21	2005/01/03	A	A
13.674	93.029	38	null	*24*	2000/11/21	2005/01/03	A	A
13.647	92.984	38	null	*24*	2000/11/21	2005/01/03	A	A
13.599	92.909	39	null	*24*	2000/11/21	2005/01/03	A	A
13.568	92.895	39	null	*24*	2000/11/21	2005/01/03	A	A
13.575	93.038	35	null	*24*	2000/11/21	2005/01/03	A	A
13.571	92.996	35	null	*24*	2000/11/21	2005/01/03	A	A
13.541	92.964	35	null	*24*	2000/11/21	2005/01/03	A	A
13.516	92.922	35	null	*24*	2000/11/21	2005/01/03	A	A
13.537	92.882	38	null	*24*	2000/11/21	2005/01/03	A	A
13.493	92.879	38	null	*24*	2000/11/21	2005/01/03	A	A
13.473	92.898	38	null	*24*	2000/11/21	2005/01/03	A	A
13.389	92.846	38	null	*24*	2000/11/21	2005/01/03	A	A
13.354	92.841	37	null	*24*	2000/11/21	2005/01/03	A	A
13.199	92.825	36	null	*24*	2000/11/21	2005/01/03	A	A
13.167	92.800	36	null	*24*	2000/11/21	2005/01/03	A	A
13.108	92.819	36	null	*24*	2000/11/21	2005/01/03	A	A
13.092	92.808	37	null	*24*	2000/11/21	2005/01/03	A	A
13.025	92.799	37	null	*24*	2000/11/21	2005/01/03	A	A
13.478	93.045	21	null	*24*	2000/11/21	2005/01/03	A	A
13.419	93.074	21	null	*24*	2000/11/21	2005/01/03	A	A
13.431	93.113	17	null	*24*	2004/01/01	2005/01/03	A	A
13.400	93.099	17	null	*24*	2004/01/01	2005/01/03	A	A
13.296	93.090	17	null	*24*	2004/01/01	2005/01/03	A	A
13.222	93.061	17	null	*24*	2004/01/01	2005/01/03	A	A
13.117	93.041	17	null	*24*	2004/01/01	2005/01/03	A	A
13.027	92.978	1	null	*24*	2000/11/21	2005/02/04	A	A
12.894	92.919	1	null	*24*	2000/11/21	2005/02/04	A	A
12.894	92.919	null	17	*24*	2004/01/01	2005/01/03	A	A
13.111	92.709	10	null	*24*	2000/11/21	2005/02/04	A	A
13.062	92.707	10	null	*24*	2000/11/21	2005/02/04	A	A
12.936	92.770	40	null	*24*	2000/11/21	2005/01/03	A	A
12.864	92.734	40	null	*24*	2000/11/21	2005/01/03	A	A
12.752	92.718	40	null	*24*	2000/11/21	2005/01/03	A	A
12.717	92.726	39	null	*24*	2000/11/21	2005/01/03	A	A
12.641	92.710	39	null	*24*	2000/11/21	2005/01/03	A	A
12.583	92.688	39	null	*24*	2000/11/21	2005/01/03	A	A
12.569	92.710	39	null	*24*	2000/11/21	2005/01/03	A	A
12.557	92.690	39	null	*24*	2000/11/21	2005/01/03	A	A
12.504	92.684	39	null	*24*	2000/11/21	2005/01/03	A	A
12.467	92.705	38	null	*24*	2000/11/21	2005/01/03	A	A

Table S1: Vertical changes determined from satellite imagery

Latitude	Longitude	MinDeltaZ	MaxDeltaZ	2sigma*	PreDate	PostDate	PreType	PostType
12.413	92.705	38	null	*24*	2000/11/21	2005/01/03	A	A
12.378	92.706	37	null	*24*	2000/11/21	2005/01/03	A	A
12.331	92.705	37	null	*24*	2000/11/21	2005/01/03	A	A
12.852	92.950	1	null	*24*	2000/11/21	2005/02/04	A	A
12.852	92.950	null	17	*24*	2004/01/01	2005/01/03	A	A
12.405	92.964	null	-4	*24*	2004/01/01	2005/02/04	A	A
12.371	92.950	null	-4	*24*	2004/01/01	2005/02/04	A	A
12.257	92.704	8	null	*24*	2000/11/21	2005/02/04	A	A
12.257	92.704	null	36	*24*	2000/11/21	2005/01/03	A	A
12.221	92.671	9	null	*24*	2000/11/21	2005/02/04	A	A
12.221	92.671	null	37	*24*	2000/11/21	2005/01/03	A	A
12.133	92.639	9	null	*24*	2000/11/21	2005/02/04	A	A
12.035	92.625	9	null	*24*	2000/11/21	2005/02/04	A	A
11.930	92.551	10	null	*24*	2000/11/21	2005/02/04	A	A
11.877	92.529	10	null	*24*	2000/11/21	2005/02/04	A	A
11.804	92.525	10	null	*24*	2000/11/21	2005/02/04	A	A
11.662	92.603	null	-30	*24*	2004/12/02	2005/01/03	A	A
11.497	92.570	null	-30	*24*	2004/12/02	2005/01/03	A	A
12.153	92.830	null	-46	*24*	2004/12/02	2005/01/03	A	A
12.071	92.789	null	-45	*24*	2002/01/11	2005/02/04	A	A
11.702	92.754	null	-63	*24*	2004/12/02	2005/02/04	A	A
11.669	92.710	null	-66	*24*	2004/12/02	2005/02/04	A	A
11.649	92.670	null	-66	*24*	2004/12/02	2005/02/04	A	A
11.548	92.746	null	-3	*24*	2004/01/01	2005/02/04	A	A
12.105	92.954	null	-3	*24*	2004/01/01	2005/02/04	A	A
12.009	93.016	null	-4	*24*	2004/01/01	2005/02/04	A	A
11.992	92.929	null	-4	*24*	2004/01/01	2005/02/04	A	A
11.957	92.971	null	-4	*24*	2004/01/01	2005/02/04	A	A
11.924	93.003	null	-4	*24*	2004/01/01	2005/02/04	A	A
11.498	92.619	null	-23	*24*	2002/01/11	2005/02/04	A	A
11.463	92.614	null	-23	*24*	2002/01/11	2005/02/04	A	A
11.388	92.564	null	21	*24*	2004/01/01	2005/01/03	A	A
11.305	92.720	null	16	*24*	2004/01/01	2005/01/03	A	A
10.982	92.670	null	18	*24*	2004/01/01	2005/01/03	A	A
11.596	92.219	30	null	*24*	2000/11/21	2005/02/20	A	A
11.585	92.280	30	null	*24*	2000/11/21	2005/02/20	A	A
11.528	92.216	30	null	*24*	2000/11/21	2005/02/20	A	A
11.520	92.288	30	null	*24*	2000/11/21	2005/02/20	A	A
10.972	92.236	29	null	*24*	2000/11/21	2005/02/20	A	A
10.899	92.535	21	null	*24*	2004/01/01	2005/01/03	A	A
10.801	92.592	21	null	*24*	2004/01/01	2005/01/03	A	A
10.830	92.431	21	null	*24*	2004/01/01	2005/01/03	A	A
10.781	92.378	7	null	*24*	2002/01/11	2005/01/03	A	A
10.662	92.384	22	null	*24*	2004/01/01	2005/01/03	A	A
10.609	92.410	22	null	*24*	2004/01/01	2005/01/03	A	A

Table S1: Vertical changes determined from satellite imagery

Latitude	Longitude	MinDeltaZ	MaxDeltaZ	2sigma*	PreDate	PostDate	PreType	PostType
10.546	92.382	22	null	*24*	2004/01/01	2005/01/03	A	A
10.523	92.391	18	null	*24*	2004/01/01	2005/01/03	A	A
10.511	92.481	18	null	*24*	2004/01/01	2005/01/03	A	A
10.511	92.543	18	null	*24*	2004/01/01	2005/01/03	A	A
10.783	92.608	18	null	*24*	2004/01/01	2005/01/03	A	A
9.211	92.720	null	-9	*24*	2003/11/30	2005/08/15	A	A
9.118	92.798	null	-7	*24*	2003/11/30	2005/08/15	A	A
9.166	92.830	null	-7	*24*	2003/11/30	2005/08/15	A	A
8.460	93.068	null	3	*24*	2002/01/04	2005/03/24	A	A
8.311	93.137	null	-0.4	*24*	2002/01/04	2005/03/24	A	A
8.232	93.117	null	-8	*24*	2002/01/04	2005/03/24	A	A
8.232	93.232	null	22	*24*	2002/01/04	2005/02/13	A	A
8.002	93.328	null	3	*24*	2002/01/04	2004/12/28	A	S
7.890	93.339	null	-32	*24*	2001/07/21	2004/12/28	A	S
8.214	93.500	null	-39	*24*	2001/07/21	2004/12/28	A	S
8.080	93.601	null	-43	*24*	2001/07/21	2004/12/28	A	S
7.470	93.623	null	-22	*24*	2001/07/21	2005/01/28	A	A
7.401	93.701	null	-21	*24*	2001/07/21	2005/01/28	A	A
7.373	93.686	null	-21	*24*	2001/07/21	2005/01/28	A	A
7.371	93.648	null	-21	*24*	2001/07/21	2005/01/28	A	A
7.204	93.757	null	-46	*24*	2000/10/29	2005/02/06	A	A
7.180	93.680	null	-46	*24*	2000/10/29	2005/02/06	A	A
7.136	93.673	null	-38	*24*	2000/10/29	2005/02/06	A	A
7.104	93.663	null	-42	*24*	2000/10/29	2005/01/05	A	A
7.074	93.667	null	-42	*24*	2000/10/29	2005/01/05	A	A
7.026	93.674	null	-44	*24*	2000/10/29	2005/01/05	A	A
6.985	93.735	null	-44	*24*	2000/10/29	2005/01/05	A	A
6.920	93.774	null	-44	*24*	2000/10/29	2005/01/05	A	A
6.821	93.823	null	-67	*24*	2000/10/29	2005/01/05	A	A
6.820	93.877	null	-67	*24*	2000/10/29	2005/01/05	A	A
7.173	93.885	null	-10	*24*	2000/10/29	2005/01/28	A	A
3.014	95.406	28	null	*24*	2001/11/19	2005/03/03	A	A
2.548	95.937	13	null	*24*	2002/10/30	2005/01/30	A	A
2.569	95.992	8	null	*24*	2001/11/28	2004/12/29	A	A
2.519	96.133	5	null	*24*	2001/11/28	2005/02/24	A	A
2.470	96.206	4	null	*24*	2001/11/28	2005/01/23	A	A
2.415	96.225	-17	null	*24*	2003/10/17	2005/01/23	A	A
2.333	96.445	-28	null	*24*	2003/03/07	2005/02/24	A	A
2.405	96.487	-29	null	*24*	2003/03/07	2005/01/23	A	A
2.405	96.487	null	6	*24*	2003/01/18	2005/01/23	A	A
2.025	97.117	-13	null	*24*	2000/08/30	2005/02/08	A	A
2.108	97.087	-14	null	*24*	2000/08/30	2005/02/08	A	A
2.227	97.117	-14	null	*24*	2000/08/30	2005/02/08	A	A
2.253	97.198	-14	null	*24*	2000/08/30	2005/02/08	A	A
2.320	97.213	-15	null	*24*	2000/08/30	2005/02/08	A	A

Table S1: Vertical changes determined from satellite imagery

Latitude	Longitude	MinDeltaZ	MaxDeltaZ	2sigma*	PreDate	PostDate	PreType	PostType
5.646	95.414	null	0	0	null	2004/12/30	null	Q
5.626	95.400	null	0	0	null	2004/12/30	null	Q
5.592	95.360	null	0	0	null	2004/12/30	null	Q
5.577	95.333	null	0	0	null	2004/12/30	null	Q
5.560	95.300	null	0	0	null	2004/12/30	null	Q
5.548	95.270	null	0	0	null	2004/12/30	null	Q
5.542	95.252	null	0	0	null	2004/12/30	null	Q
5.552	95.235	null	0	0	null	2004/12/30	null	Q
5.508	95.277	null	0	0	null	2004/12/30	null	Q
5.498	95.249	null	0	0	null	2004/12/30	null	Q
4.600	95.622	null	0	0	2002/01/06	2005/03/19	A	A
3.547	97.000	-9	null	*24*	2003/03/07	2005/03/12	A	A
3.455	97.052	-9	null	*24*	2003/03/07	2005/03/12	A	A
3.338	97.125	-22	null	*24*	2002/01/31	2005/02/08	A	A
3.257	97.192	-22	null	*24*	2002/01/31	2005/02/08	A	A
2.907	97.441	null	10	*24*	2002/01/31	2005/03/05	A	A
2.871	97.515	null	1	*24*	2002/02/16	2005/03/05	A	A
2.254	97.935	null	42	*24*	2000/07/13	2005/02/01	A	A
2.188	98.038	null	42	*24*	2000/07/13	2005/02/01	A	A
2.146	98.125	null	42	*24*	2000/07/13	2005/02/01	A	A
2.096	98.176	null	42	*24*	2000/07/13	2005/02/01	A	A
2.027	98.266	null	43	*24*	2000/07/13	2005/02/01	A	A
2.010	98.373	null	44	*24*	2000/07/13	2005/02/01	A	A
1.972	98.348	null	43	*24*	2000/07/13	2005/02/01	A	A

* *Values in the '2sigma' column in italics (i.e., those entries listed as '24') have been modified from the original table published by Meltzner et al. [2006].*

These larger errors account for the fact that non-tidal sea level anomalies were not considered in the imagery-based uplift and subsidence calculations of Meltzner et al. [2006].

For more information, see Chapter 1 of this thesis.

Table S2: Uplift on Simeulue from field measurements of coral microatolls

Latitude	Longitude	DeltaZ*	2sigma*	Date
2.84368	95.91775	*22*	*23*	2005/01/18
2.91409	95.83584	*34*	*18*	2005/01/17
2.92359	95.80408	*46*	*23*	2005/02/05
2.86137	95.76308	*132*	*23*	2005/01/18
2.80665	95.71368	*148*	*18*	2005/01/17
2.74940	95.71628	*147*	*18*	2005/01/17
2.70852	95.76263	*131*	*18*	2005/01/17
2.61317	95.87225	*101*	*23*	2005/01/18
2.56913	95.99237	*48*	*23*	2005/01/18
2.54773	95.93723	*46*	*23*	2005/01/18

* *Values in the 'DeltaZ' and '2sigma' columns in this table are no longer considered the best estimates of uplift at these locations; they have since been modified slightly, and the errors have been reduced.*

Revised estimates of 2004 uplift on northern Simeulue are provided in Chapters 3 and 4 of this thesis; a detailed discussion of the revisions is provided in Chapter 4.

Table S3: Subsidence on Simeulue determined from field observations

Latitude	Longitude	DeltaZ	Date	Location	Note
2.443	96.241	-30	2005/01/18	Salur	minimum subsidence
2.392	96.332	-50	2005/04/08	Gusong	estimated subsidence

Chapter 3

Coral evidence for earthquake recurrence and an AD 1390–1455 cluster at the south end of the 2004 Aceh–Andaman rupture

Aron J. Meltzner, Kerry Sieh, Hong-Wei Chiang, Chuan-Chou Shen,

Bambang W. Suwargadi, Danny H. Natawidjaja, Belle E. Philibosian,

Richard W. Briggs, John Galetzka

in press in the *Journal of Geophysical Research*

doi:10.1029/2010JB007499

Abstract

Coral records of relative sea-level change provide a history of vertical interseismic and coseismic deformation along the coast of northern Simeulue Island, Sumatra, and reveal details about earthquakes in the 10th and 14th–15th centuries AD along the southern end of the December 2004 M_W 9.2 Sunda megathrust rupture. Over a 56-year period between AD 1390 and 1455, northern Simeulue experienced a cluster of megathrust ruptures, associated with total uplift that was considerably more than in 2004. Uplifted corals at two sites constrain the first event of the cluster to AD 1393 ± 3 and 1394 ± 2 (2σ). A smaller but well substantiated uplift occurred in northern Simeulue in 1430 ± 3. An inferred third uplift, in 1450 ± 3, killed all corals on the reef flats of northern Simeulue. The amount of uplift during this third event, though confirmed only to have exceeded 28 and 41 cm at two sites, probably surpassed the 100 and 44 cm that occurred respectively at those sites in 2004, and it was likely more than in 2004 over all of northern Simeulue. The evidence for past earthquake clustering combined with the inference of considerably greater uplift in 1390–1455 than in 2004 suggests that strain may still be stored along the southernmost part of the 2004 rupture. Interseismic subsidence rates recorded by northern Simeulue coral microatolls have varied by up to a factor of four at some sites from one earthquake cycle to another.

1. Introduction

The Sumatra–Andaman earthquake of 26 December 2004 ruptured 1600 km of the Sunda megathrust [*Meltzner et al.*, 2006], with slip that locally approached or exceeded 20 m [*Subarya et al.*, 2006; *Chlieh et al.*, 2007] (Figure 1). The associated tsunami had run ups of more than 30 m in Aceh [*Borrero et al.*, 2006; *Lavigne et al.*, 2009] and devastated coastlines around the Indian Ocean. Both the earthquake and tsunami were unexpected because no precedents existed in the short historical record, but both could have been foreseen had the paleoseismic record been known. Farther south along the Mentawai section of the megathrust, paleogeodetic records derived from coral microatolls have revealed evidence for past earthquake clustering at nearly regular intervals and suggest that section of the megathrust could potentially produce a great rupture in the coming decades [*Sieh et al.*, 2008]; in the region of the 2004 earthquake, however, little was known about the past behavior of the fault.

Most of what is known from the historical record about earthquakes in Sumatra was compiled by *Newcomb and McCann* [1987]. The only potentially M ~7.5 or greater historical (pre-21st century) earthquakes known to have affected Aceh occurred in 1861 and 1907. The 1861 earthquake was similar to that in 2005, involving a portion of the Sunda megathrust southeast of the 2004 rupture (Figure 1). The source of the 1907 earthquake is more enigmatic, but it was felt strongly on Nias and generated a tsunami that extended over 950 km of the mainland Sumatra coast and devastated Simeulue in particular [*Newcomb and McCann*, 1987]. Prior to 1861, essentially nothing is known historically about earthquakes in Aceh (A. Reid, personal communication, 2009).

Since the 2004 earthquake, considerable geological work has been done. Sequential uplifts of coral platforms and evidence for past subsidence have been identified in the Andaman Islands [*Rajendran et al.*, 2008] (Figure 1); sediment cores have exposed a 7200-year record of past shaking-induced turbidites (inferred to be proxies for earthquakes) off the coast of Sumatra

[*Patton et al.*, 2010]; and sedimentological evidence of predecessors of the 2004 tsunami have been uncovered along coastlines inundated in 2004 [*Jankaew et al.*, 2008; *Monecke et al.*, 2008]. On the coast of mainland Aceh (Figure 1), *Monecke et al.* [2008] found evidence in sediment cores for at least three inferred paleotsunamis: two older extensive sand sheets were deposited soon after AD 780–990 and AD 1290–1400, and an additional sand sheet of limited extent, which dated to younger than AD 1640–1950, might correlate with the historical tsunami in 1907. In Thailand (Figure 1), *Jankaew et al.* [2008] found evidence in hand-dug pits for several inferred paleotsunamis less than 2800 years old, the youngest of which was deposited soon after AD 1300–1450.

Yet in spite of this new wealth of knowledge, questions linger about details of the causative ruptures, about the current state of accumulated strain along the 2004 patch, and about whether earthquake clustering (as seen on the Mentawai section of the fault) tends to occur along portions of the 2004 rupture. The results we present here elucidate details of past Sunda megathrust ruptures and provide dates for these past events with sufficient precision to allow for an assessment of clustering.

We extracted records of relative sea-level change from coral microatolls on fringing reefs directly above the southern end of the 2004 rupture. Six paleogeodetic sites on northern Simeulue and one auxiliary site 40 km to the northwest on Salaut Besar Island (Figure 1)—all of which were uplifted in 2004—provide a repeated history of gradual interseismic subsidence followed by sudden coseismic uplift. We present evidence for a 14th–15th century cluster of earthquakes at these sites, and for an earlier event in the 10th century. Although somewhat speculative, the most reasonable estimates of cumulative uplift in the 14th–15th centuries are substantially higher than uplift in 2004 near the rupture's southern terminus; if similar amounts of strain had accumulated prior to the 14th–15th century sequence and prior to 2004 (as in a time-predictable model), this suggests significant unreleased strain is still stored along that part of the megathrust. Separately, however, we document evidence that interseismic strain accumulation rates are not uniform from one earthquake cycle to another.

This paper is divided into a main section and auxiliary material. In Section 2 of the main text, we introduce and explain refinements to techniques used in previous studies—e.g., by *Meltzner et al.* [2006], *Briggs et al.* [2006], and *Sieh et al.* [2008]—to determine coseismic changes. As we will demonstrate in later sections, these refinements improve both the accuracy and precision of estimates of vertical deformation since 1992. In particular, they lay groundwork for revising the estimates of coseismic uplift and subsidence in 2004 and 2005 reported by *Meltzner et al.* [2006] and *Briggs et al.* [2006]. The improvement to the precision of the estimates is appreciable, although most of the revised estimates fall within the uncertainties originally stated by *Meltzner et al.* [2006] and *Briggs et al.* [2006].

Results are presented in Sections 3–9. Section 3 includes a detailed examination of Lhok Pauh, the most comprehensive and central site on northern Simeulue; a discussion of the immediate implications of the results from this site; and an explanation of refinements to methods used in previous studies for determining interseismic subsidence rates. Sections 4–8 outline the main observations at other northern Simeulue sites and link to additional text and figures in the auxiliary material. From Lhok Pauh (Section 3), we build a case for three uplift events between AD 1390 and 1455; the other northern Simeulue sites support this interpretation and add information about the spatial extent of these uplifts. Evidence for the 10th-century uplift comes primarily from Ujung Salang (Section 6). Section 9 and accompanying auxiliary material present results from Salaut Besar Island, including observations of a possible upper-plate fault that we infer was reactivated during the 2004 earthquake. Following the results sections is a brief section discussing the relative sea level and land level histories (Section 10) and then a summary of the results (Section 11).

We begin to wrap up in Section 12 with a comparison between our results, results from other geological studies in the region, and relevant historical information. This is followed my more far-reaching discussion about general observations and their broad implications in Section 13, and eventually conclusions in Section 14.

2. Measuring Vertical Change: Geological Techniques

We derive uplift and subsidence data from massive coral microatolls of the genera *Porites* and *Goniastrea*. Because these are sensitive natural recorders of lowest tide levels [*Scoffin and Stoddart*, 1978; *Taylor et al.*, 1987; *Zachariasen et al.*, 2000; *Briggs et al.*, 2006], they are ideal natural instruments for measuring emergence or submergence relative to a tidal datum. Massive *Porites* and *Goniastrea* coral heads grow radially upward and outward until they reach an elevation that exposes their highest corallites to the atmosphere during lowest tides. This subaerial exposure kills the uppermost corallites in the colony, thus restricting future upward growth. The highest level to which a coral can grow is termed the highest level of survival (HLS) [*Taylor et al.*, 1987]. If a coral microatoll then rises or subsides, its morphology preserves information about relative water level prior to the land level change [*Taylor et al.*, 1987; *Briggs et al.*, 2006].

When coseismic uplift occurs, as was documented throughout northern Simeulue in 2004, those portions of the microatoll colony raised above lowest tides die, but if lower parts of the coral head are still below lowest tides, its uppermost living tissues demarcate a new, post-earthquake HLS [*Taylor et al.*, 1987]. When coseismic subsidence occurs, as has been documented elsewhere, a microatoll does not experience a sudden, dramatic change, but comparisons of the pre-subsidence HLS with low tide levels will bring to light the microatoll's subsidence. Following such subsidence, the microatoll will grow radially upward and outward, with its upward growth unchecked until the head again reaches the lowest tide levels, years to decades later.

For microatolls that are presently alive or whose timing of death is known (e.g., following the December 2004 uplift), the relative sea level time series recorded by the microatoll can be dated to within fractions of a year by counting back the coral's annual growth bands. For corals that died at an unknown point in the past, past uplift or subsidence events in their records can be dated using ^{230}Th techniques, which can optimally define the age of a coral sample to within a few years [*Shen et al.*, 2002; *Shen et al.*, 2008; *Frohlich et al.*, 2009].

2.1. Determination of coseismic vertical displacements from microatolls

Throughout our study area, we utilized two methods for determining 2004 coseismic uplift and postseismic uplift or subsidence. The two methods are complementary but yield slightly different information. The most straightforward technique involves measuring the difference between pre-earthquake and post-earthquake HLS at a site. This method can be used only in cases of uplift, and only where both pre-earthquake and post-earthquake HLS can be found. As was documented by *Briggs et al.* [2006], two uplift events only three months apart (as was the case with the 2004 and 2005 earthquakes) can be readily distinguished on a microatoll, provided that the lower part of the microatoll remains alive following the initial uplift, and provided that field observations are made sufficiently quickly after the later event that the coral surface is mostly unweathered. In contrast, if subsidence occurs subsequent to the uplift (as either postseismic, interseismic, or subsequent coseismic subsidence), this method will record only the initial uplift, and it may underestimate that initial uplift if the subsequent subsidence occurs before the lowest low tides occur.

The second method we employed involves comparing the pre-earthquake HLS with post-earthquake extreme low water (ELW, the extreme lowest water level over a fixed period of time, typically a year) and applying a correction based on the difference between HLS and ELW on living corals. To determine the post-earthquake ELW, we surveyed the water level at each site during our visit. Using the latitude, longitude, and exact time of our water level measurement as inputs, we used (*a*) a computational tide model, (*b*) satellite altimetry-based estimates of sea level anomalies, and (*c*) barometric measurements (each discussed in Section 2.3 or 2.4) to determine how much lower ELW should be at each survey site relative to the water level at the time of measurement. After the correction for the difference between post-earthquake HLS and ELW is applied, the difference between pre-earthquake HLS and post-earthquake ELW provides the net vertical change that occurred at the site from the time of the pre-earthquake HLS until the time of the measurement. It can be used in the case of net uplift or net subsidence, and it can be used whether or not the post-event HLS can be recognized, but it does not allow for the distinction of coseismic and subsequent changes.

2.2. The relationship between HLS and ELW

Although coral microatolls have been shown to track low water levels with an accuracy of a few centimeters [*Zachariasen et al.*, 2000], the actual difference between HLS and ELW has not previously been well determined. We reported [*Briggs et al.*, 2006] that *Porites* coral HLS appeared to lie about 4 cm above the annual extreme low tide off the west coast of Sumatra; however, at the time of that publication, we had a limited data set and were unaware of the magnitude of sea level anomalies (misfits between the tide model and observed sea surface heights) in the region. We have now determined the difference between HLS and ELW using a larger data set, an improved tide model, and appropriate sea level anomaly (SLA) estimates (see Section 2.3). We find that *Porites* coral HLS lies 19 ± 8 cm (2σ) above ELW off the west coast of Sumatra, where the overall annual extreme tidal range varies from 0.8 to 1.0 m. This difference should not be blindly applied elsewhere: it is expected that the difference between HLS and ELW is strongly dependent upon the overall tidal range at a location, as the duration spent out of water must play a role. Moreover, this difference is not appropriate for genera other than *Porites*: HLS of *Goniastrea* appears to be ~10 cm higher than that of *Porites* [*Natawidjaja et al.*, 2006], and HLS of other genera appear to be at other relative elevations.

2.3. Determination of ELW and of the difference between ELW and HLS

The determination of ELW at any site involves measuring the water level at a chosen time relative to "fixed" objects at the site (such as HLS on a microatoll), tying in the water level at the chosen time to the tidal cycle by way of a predictive tide model, and applying appropriate corrections retroactively based on documented SLAs and barometric variations not accounted for by the tide model.

2.3.1. Predictive tide model

The tide model we use is an updated version of that employed by *Meltzner et al.* [2006] and *Briggs et al.* [2006], based on the Oregon State University (OSU) regional inverse tidal solution for Indonesia [*Egbert and Erofeeva*, 2002] (available at http://www.coas.oregonstate.edu/research/po/research/tide/ind.html) using the software package NLOADF [*Agnew*, 1997]. The tidal solution incorporates the harmonic constituents $\mathbf{M_2}$, $\mathbf{S_2}$, $\mathbf{N_2}$, $\mathbf{K_2}$, $\mathbf{K_1}$, $\mathbf{O_1}$, $\mathbf{P_1}$, and $\mathbf{Q_1}$. It is a predictive model, based on the harmonic constituents extracted from 364 ten-day repeat cycles, or 10 years of TOPEX/Poseidon data. While this solution does a good job of predicting ocean tides, it does not consider any effects of the pole tide or non-harmonic influences on sea surface heights, such as the inverted barometer effect, drag caused by winds, or longer-term variations associated with the Indian Ocean Dipole (IOD) or El Niño–Southern Oscillation (ENSO).

2.3.2. Retroactive corrections

The SLA corrections we apply are based on those published online by AVISO (sea level anomalies and geostrophic velocity anomalies; available at http://www.aviso.oceanobs.com/en/data/products/sea-surface-height-products/global/msla/). These anomalies are determined retroactively by fitting altimetry data from multiple satellites and are available from late 1992 onwards. In order to compute the anomalies, AVISO first uses a harmonic tide model (GOT00, comparable to the OSU model used in our calculations) to remove the ocean tide signal from the direct altimetry observations. They also remove signals associated with the pole tide, the earth tide, the inverted barometer effect, and high-frequency dynamic barotropic sea surface variability induced by wind and surface pressure variations. It is thus valid to combine the OSU tidal predictions with the AVISO SLA estimates, but some potential contributions to sea surface height are still not incorporated into that result.

We now briefly assess the four signals, aside from the ocean tide signal, that are removed by AVISO before their calculation of SLA values, in order to determine whether any of the signals warrant being added back in. First, the pole tide signal is small, with an amplitude commonly ~0.5 cm [*Wunsch et al.*, 1997; *Pugh*, 2004]; it can be ignored for our purposes since it is well within the noise of our measurements. Second, the earth tide influences satellite altimetry readings, but it is not observable by a tide gauge or a geologist standing at the shoreline on the earth's surface because the tide gauge, geologist, island, and ocean are all moving up and down together [*Pugh*, 2004]; thus it is desirable to remove any earth tide signal observed by the satellites. Third, the effects of wind and surface pressure variability can be large in broad areas of shallow water, and winds parallel to shore can have a significant effect at mid-to-high latitudes due to the Ekman transport effect [*Pugh*, 2004], but because our study areas (Simeulue and surrounding islands) are surrounded by fairly deep water and are close to the Equator (and because we were never surveying in strong winds), both effects are mitigated; we assume they are within the noise of our measurements. Fourth, the inverted barometer effect may be the largest source of variability, and although the overall amplitudes of this effect tend to be lower in the tropics than elsewhere [*Wunsch and Stammer*, 1997; *Pugh*, 2004], we will attempt to correct for it; we discuss this further in Section 2.4.

2.3.3. Determination of ELW

At each site where we made a water level measurement, we use the tide model to compute the tide level (relative to mean sea level) at the location and exact time of the measurement. To compare the post-earthquake ELW with pre-earthquake HLS (to determine uplift or subsidence), we also compute the tide levels at that location every 30 minutes over the course of the year preceding the earthquake. To compare the post-earthquake ELW with post-earthquake HLS (as part of our general effort to determine that relationship), we compute the tide levels at that location every 30 minutes for the time period between the earthquake and the time of the measurement. For every time that we compute the tide elevation, we also determine the SLA. AVISO provides SLA values on a fixed grid of locations at 7-day intervals; for each site, we use the nearest node and apply a temporal linear interpolation to estimate the SLA at a particular time. We then add together the tide level and SLA at the time of measurement and at each 30-minute increment to obtain the best estimate of water level at each of those times. Finally, we determine the minimum water level over the chosen period of time, and we compare that to the water level at the time of the measurement. That difference is subtracted from the water level measured in the field, in order to determine how the ELW compares to the pre-earthquake or post-earthquake HLS.

2.3.4. The difference between ELW and HLS near Simeulue

An analysis of all sites for which we have reliable estimates of post-earthquake ELW and post-earthquake HLS suggests that *Porites* coral HLS lies 19 ± 8 cm above ELW, at least in the region off the west coast of Sumatra, as stated earlier. This offset is substantially larger than that reported by *Briggs et al.* [2006], primarily because Briggs et al. did not consider SLAs either at the time of their measurements (SLAs were around +12 cm at the time of most of their measurements in May–June 2005) or at the time of ELW (for areas uplifted in 2004, SLAs were around +1 cm during the spring tide on 12 January 2005 and –14 cm during the spring tide on 10 March 2005; for areas uplifted in 2005, SLAs were around –6 cm on 28 March 2005, about a day after spring tide and a few hours after the earthquake). Most of the uplift and subsidence values reported by *Briggs et al.* [2006] are not significantly affected, because of internally consistent assumptions.

2.3.5. Improved precision and accuracy in ELW determinations

The improved precision in the determination of the difference between ELW and *Porites* coral HLS off Sumatra is worth discussing. Much of this improved precision arises from the incorporation of SLA estimates in the calculations. If SLAs are ignored and assumed to be insignificant (as was done by *Meltzner et al.* [2006], *Briggs et al.* [2006], and *Sieh et al.* [2008]), then—using the same field measurements of HLS and water level as above—*Porites* HLS is calculated to be 7 ± 17 cm (2σ) above the annual lowest tide. Aside from the fact that this value (7 ± 17 cm), like the value reported by *Briggs et al.* [2006], is biased because SLAs are ignored (and hence the stated errors may be too small), the fact that the inclusion of SLAs in the calculation yields a relationship between ELW and *Porites* HLS with much less scatter (± 8 cm, instead of ± 17 cm) implies the inclusion of SLA corrections directly improves the accuracy of the ELW estimates, and hence of measurements of vertical deformation.

2.4. Correction for the inverted barometer effect

The inverted barometer effect may be described as follows: for sea-level atmospheric pressure P_{SL} at location (x, y) and time t, and for the instantaneous global over-ocean spatially averaged sea-level pressure $\overline{P_{SL}}$ at time t, the sea level change $\Delta\zeta$ will be given by

$$\Delta\zeta(x,y,t) = -\frac{P_{SL}(x,y,t) - \overline{P_{SL}}(t)}{\rho g} ,$$

where seawater density $\rho = 1.026$ g/cm^3 and $g = 980$ cm/s^2. For $\Delta\zeta$ in centimeters and P_{SL} in millibars, $\Delta\zeta = -0.995\,(P_{SL} - \overline{P_{SL}})$, so that a relative increase in local pressure of 1 mbar yields a decrease in sea level of ~1 cm. The term for the global over-ocean mean pressure, which is the average of all sea-level pressures at a given time at locations directly above the ocean, appears in the equation because water is nearly incompressible, and hence there is no oceanic response to changes in the global over-ocean atmospheric load [*Wunsch and Stammer*, 1997].

To determine the local atmospheric load, we obtained meteorological records, including sea-level-adjusted atmospheric pressure readings, from the National Oceanic and Atmospheric Administration (NOAA) / National Climatic Data Center (NCDC) Online Climate Data Directory (available at http://www.ncdc.noaa.gov/oa/climate/climatedata.html#hourly). We examined "hourly" records from eight weather stations in the vicinity of Simeulue: Sabang, Banda Aceh, Meulaboh, Lhokseumawe, Medan (Belawan), Medan (Polonia), Gunung Sitoli, and Sibolga. The Polonia record includes sea level pressure readings once every 1–3 hours, whereas the other stations have readings typically every 3–6 hours; Meulaboh is missing sea level pressure data from 26 December 2004 until March 2007, and Gunung Sitoli is missing sea level pressure data from April 2005 until January 2006. Where data are available, we determined the sea level pressure at the time of each of our field measurements. Across the eight regional stations, the range of barometric readings at any given time is typically 2–4 mbar, and if the two outlying stations (Sabang and Sibolga) are excluded, the range of readings rarely exceeds ~1 mbar. As is typical of sea level pressures in the tropics, the overall variation is low: at each weather station, the standard deviation (1σ) of the readings at the times of our measurements is 2 mbar or less, despite the fact that measurements were made at various times of the year. For the global atmospheric load, we interpolate from values determined at 6-hour intervals by Centre National d'Études Spatiales (CNES) / Collecte Localisation Satellites (CLS) (global spatial average sea-level pressure; available at ftp://ftp.cls.fr/pub/oceano/calval/pression/moy_globale_spatiale.txt). We apply the combined local and global correction for the inverted barometer effect (generally ±6 cm or less) as the final step in the uplift calculation.

3. Results from the Lhok Pauh (LKP) Sites

The Lhok Pauh site, along the northern northwest coast of Simeulue Island (Figure 2), consists of three subsites: LKP-A in the south, LKP-B ~1.8 km to the north, and LKP-C roughly half-way between the two (Figures 2–3). The sites were named after the nearby village of Lhok Pauh or Lokupau. Each subsite sits on or near a reef promontory, and the three subsites are separated from one another by small bays with sandy beaches. All three subsites have abundant modern heads (i.e., coral heads that were living at the time of the 2004 earthquake), as well as one or more generation of fossil heads (i.e., coral heads that died long before 2004, possibly in prior uplift events) from the 14th–15th centuries AD. Not a single head could be found dating to any time between the mid 15th and early 20th century. A total of two modern and eight fossil corals were sampled from the LKP sites (Figures 4–13).

In multiple respects, LKP is our most complete and informative site on northern Simeulue. The modern *Porites* microatoll (LKP-1) sampled at LKP-A records the longest sea-level history of any modern head found on Simeulue, going back to AD 1945. One well-preserved fossil *Porites* microatoll (LKP-2) was also sampled from that site. LKP-B provided the most heads and the most compelling fossil record on northern Simeulue. Four fossil *Porites* microatolls (LKP-3, LKP-4, LKP-5, and LKP-8), two fossil *Goniastrea* heads (LKP-6 and LKP-7), and one modern *Porites* microatoll (LKP-9) were sampled from LKP-B. In addition to the continuous modern sea-level history from AD 1945 to present obtained at LKP-A, LKP-B provides a separate continuous record from ~ AD 1345 (or earlier) to ~ AD 1450, with evidence for at least three uplift events during that period. A single fossil *Porites* microatoll (LKP-10) was sampled at LKP-C, which adds important data to the 15th-century record.

3.1. 2004 and subsequent uplift at the Lhok Pauh (LKP) sites

3.1.1. 2004 coseismic uplift

Coseismic uplift attributed to the 2004 earthquake at locations near the LKP sites, which was documented by *Briggs et al.* [2006], highlights some primary features of megathrust behavior and serves as a benchmark against which to compare past uplifts and patterns of interseismic subsidence. At their site KS05-70, which coincides with our site LKP-A, Briggs et al. reported 126 ± 21 cm of uplift (uncertainties herein will always be reported at 2σ). This amount was determined in January 2005 by comparing the pre-uplift HLS on *Porites* microatolls with ELW. As explained in Sections 2.2 and 2.3, they did not consider SLAs in their calculation; redoing the calculation with the original field measurements, an updated tide model, documented SLAs, the revised correction for the difference between HLS and ELW, and an appropriate inverted barometer correction results in the slightly lower (statistically indistinguishable) estimate of 123 ± 15 cm; this value includes the 2004 coseismic uplift and any postseismic vertical changes that had occurred by 18 January 2005.

As predicted by simple elastic dislocation modeling [*Plafker and Savage*, 1970; *Plafker*, 1972; *Savage*, 1983], sites farther from the trench experienced less coseismic uplift. At their nearby site RND05-D, which coincides with our site LKP-C, *Briggs et al.* [2006] reported 105 ± 6 cm of uplift in 2004, determined by directly comparing pre-uplift HLS with post-uplift

HLS. The Briggs et al. field team also surveyed water level at the time of their visit; although neither their surveyed water level nor the resulting calculated uplift were published, we use their field notes and surveyed water level to determine ELW and calculate a net uplift of 100 ± 9 cm as of the date of their site visit, 1 June 2005. Although the two values determined by different methods at the same site have overlapping errors, the fact that the net uplift estimate (determined from the surveyed water level and calculated ELW) is smaller is consistent with postseismic subsidence of ~5 cm or more occurring prior to June 2005. The LKP-B site was not visited prior to July 2007, but, by interpolating from nearby observations [*Briggs et al.*, 2006], we estimate 2004 uplift there to be ~100 cm.

2004 uplift values (observed or estimated in 2005) are listed in Table S1. The exact vertical change at the LKP sites during the March 2005 Southern Simeulue–Nias earthquake is unknown, but the fact that no outer "lip"—which would have indicated an additional diedown event after the initial 2004 uplift [e.g., *Briggs et al.*, 2006]—was observed in June 2005 on any of the still-living microatolls at RND05-D or nearby sites suggests there was either subsidence or little change in March 2005 at the LKP sites.

3.1.2. Postseismic subsidence and 2008 coseismic uplift

In the course of our field work, we documented ongoing uplift and subsidence that continued after mid-2005, in an attempt to better constrain postseismic behavior of the fault and to place observations of past displacements in better context. Uplift measurements were repeated at LKP-A in June 2006, at LKP-B in July 2007 and February 2009, and at LKP-C in February 2009. At all three sites, the water level was surveyed relative to pre-uplift HLS and tied to ELW, to determine the net vertical change at the site since immediately before the 2004 earthquake. The difference between the value determined in 2005 and one measured subsequently in the same location provides a measure of the net postseismic vertical displacement that occurred between those measurements, albeit with a comparatively large uncertainty. At LKP-A, net uplift as of

June 2006 was 91 ± 9 cm, suggesting 32 ± 17 cm of postseismic subsidence occurred between January 2005 and June 2006. At LKP-C, net uplift as of February 2009 was determined from the water level measurement to be 106 ± 9 cm, suggesting 6 ± 13 cm of net uplift between June 2005 and February 2009. In addition, a still-living *Porites* microatoll was found at LKP-C in 2009. Most of the head had died down in 2004, but it had a new outer living rim that had been growing radially upward and outward from below its post-2004 HLS. The uppermost part of this outer rim had experienced a still more recent diedown; based on this outer rim's morphology, we estimate that the most recent diedown occurred some time during the first half of 2008, possibly coincident with or soon after the 20 February 2008 M_W 7.3 Simeulue earthquake. The most recent HLS was 102 cm lower than the pre-2004 HLS, and the combined tide model and SLA calculations indicate that the ELW for the period from February 2008 until February 2009 was 6 cm higher than the ELW in 2004; hence, comparing pre-2004 HLS with post-2008 HLS indicates ~108 cm of net uplift (2004 to 2008), consistent with the value determined from the water level measurement. At LKP-B, net uplift was determined to be 88 ± 9 cm as of July 2007, and 102 ± 9 cm as of February 2009; 14 ± 12 cm of net uplift occurred between July 2007 and February 2009. We note that all our observations at the LKP sites are consistent with a history of substantial (centimeters to decimeters) but decreasing postseismic subsidence in the months following the 2004 earthquake, as well as uplift (presumably coseismic) in early 2008 (Figure 14a). The postseismic subsidence is similar to, although perhaps larger than, that observed by continuous GPS observations over the Nias rupture patch following the March 2005 Southern Simeulue–Nias earthquake [*Hsu et al.*, 2006].

3.2. Modern paleogeodetic record at the Lhok Pauh (LKP) sites

The LKP-1 and LKP-9 *Porites* microatolls were selected for slabbing because of the numerous concentric growth rings on their dead upper surfaces and especially well-preserved morphology. As with other heads in this study, we placed screws in the part of each head to be slabbed, and we surveyed those screws along with other critical points on the head, in order to enable establishment of a horizontal datum on the slab and to document and correct for any tilting that may have occurred. We then used a hydraulically driven chainsaw to extract a slab typically 7–8 cm thick containing the surveyed screws [*Zachariasen*, 1998]. Samples for ^{230}Th analysis were drilled from the slab, and a line of holes marking original horizontality was drilled into the slab. The coral slab was then set in concrete and taken to a marble factory, where a diamond blade saw was used to cut the slab into several slices typically 8–10 mm thick. The best slice from each head was then x-rayed and analyzed. Although none of the samples drilled from LKP-1 or LKP-9 for ^{230}Th dating were analyzed, samples from a modern head at another site (LWK-1) were used to test the validity of the technique. Details of that test are reported in the auxiliary material.

Interpreted x-ray mosaics of slabs LKP-1 and LKP-9 (Figures 4a and 5a, respectively) highlight features of the corals' growth histories. Because *Porites* (and *Goniastrea*) corals are annually banded [*Scoffin and Stoddart*, 1978; *Stoddart and Scoffin*, 1979; *Taylor et al.*, 1987], and because these heads died as a result of the 2004 uplift, the bands evident in the x-rays can be counted backwards to determine, commonly to the nearest fraction of a year, when any particular part of the coral head grew. From this, one can determine how high a coral happened to grow in any particular year (the highest level of growth, or HLG), when diedowns occurred, and the coral's HLS following each diedown.

3.2.1. HLG and HLS

At this point, it is important to clarify the distinction between HLG and HLS. HLG is the highest level up to which a coral head happened to grow in any given year; often, the upward growth of *Porites* heads is limited only by their radial growth rate of ~ 8–20 mm/yr. HLS is the theoretical—and in some years real—limit above which any living coral would have died due to exposure; in some years, HLS is not attained because the coral was not living high enough to experience a diedown. We have used the term HLS to refer to the highest corallites living in the year before the 2004 uplift, in the year after that event, and in the year after the 2008 diedown. At the LKP site, the HLG for the year beginning January 2004 was also its HLS, as many microatolls at the site experienced a small diedown of their uppermost few millimeters in late 2003 or early 2004. Following diedowns such as this one and those in 2004 and 2008, it is appropriate to use “HLS”; for years not immediately following a diedown, we use the term “HLG” to emphasize that a coral’s upward growth in those years may be limited only by its growth rate, and that its HLG is an unknown amount below its theoretical HLS.

3.2.2. Head LKP-1

LKP-1 began growing sometime prior to AD 1945. Because the lowest part of the interior of the slab could not be recovered (Figure 4a), the record prior to 1945 is missing, but we can infer from the slab’s morphology that a total of ~10 annual bands are missing. After the head began growing in ~ AD 1935, LKP-1 grew radially upward and outward until it first experienced a diedown (or “hit”) around late 1945. Again because the interior of the slab is missing, the exact timing and the amount of the diedown cannot be determined. Nonetheless, the morphology of the head—in particular, the observation that the coral’s growth bands from the years 1948, 1947, and presumably 1946 are “curling over” in their uppermost few centimeters—indicates that the uppermost part of the head died down some time around late 1945. The highest level at which the coral remained alive in the aftermath of that diedown is that year’s HLS, and following the diedown, the coral continued to grow radially upward and outward from below the HLS. This continued until the highest points on the coral once again experienced a “hit” and died down in early 1949. This time, the coral’s “growth unconformity” is preserved in the x-rayed slab; we can determine exactly when and how much the coral died down; and the uppermost few centimeters of subsequent growth bands can be seen clearly “curling over.” The process repeated multiple times, with subsequent diedowns occurring in late 1956, late 1961, early 1980, late 1982, late 1986, late 1991, late 1997, late 2003, and ultimately late 2004, when the diedown (this time caused by the earthquake) was so large that the entire coral head died.

3.2.3. Head LKP-9

LKP-9 also began growing some time (perhaps 10 years) before AD 1945, but apparently it was farther below low tide than LKP-1, and it did not grow high enough to be “hit” until late 1982. LKP-9 had subsequent “hits” in late 1986 and late 1991 (in both cases, the growth unconformity has been eroded away and the timing of the diedown cannot be determined precisely from the x-ray mosaic alone, but clear concentric rings on the microatoll observed *in situ* require that a diedown occurred at or within a fraction of a year of each of those times), and it died down again in late 1997, before being uplifted and killed completely in late 2004.

3.2.4. Comparison of LKP-1 and LKP-9 diedowns

It is notable that, for the period beginning in 1982, the diedowns occurred at the same times on both LKP-1 and LKP-9—with the exception of only the 2003 diedown seen on LKP-1—even though the two heads are 1.6 km apart. This suggests that the diedowns—or at least the majority of them—are responding to regionally significant phenomena, as opposed to local peculiarities that might affect only individual heads or a limited area. Indeed, we will show that diedowns on modern microatolls across northern Simeulue are mostly restricted to this limited set of years, and diedowns occur in those particular years on numerous heads across northern Simeulue (Figure S1). The LKP-9 head is not a useful record of sea-level history prior to 1982 because, without independent information, we cannot know how far below low tide a coral was before its first diedown.

3.2.5. Causes of diedowns

While any number of local peculiarities can cause diedowns on individual heads, we are more interested in those diedowns that occur simultaneously on multiple heads at multiple sites. Even if a diedown is widespread, the cause of the diedown is not necessarily clear. In particular, phenomena including (*a*) tectonic (seismic or aseismic) uplift [*Taylor et al.*, 1987; *Zachariasen et al.*, 1999; *Zachariasen et al.*, 2000; *Natawidjaja et al.*, 2004; *Briggs et al.*, 2006; *Natawidjaja et al.*, 2006; *Natawidjaja et al.*, 2007; *Sieh et al.*, 2008]; (*b*) regional oceanographic lowerings, such as those that occur off the coast of Sumatra during positive IOD events [*Taylor et al.*, 1987; *Woodroffe and McLean*, 1990; *Brown et al.*, 2002; *van Woesik*, 2004]; and even (*c*) extreme red tides [*Abram et al.*, 2003; *Natawidjaja et al.*, 2004; *Natawidjaja et al.*, 2007] have been proposed as potential causes of broad regional coral diedowns. For our purposes, it would be helpful if those diedowns that are tectonic in origin could be distinguished from those that are not.

3.2.6. The 1997–1998 diedown: non-tectonic

Fortunately, for the period since 1992, satellites have been collecting data that allow for calculations of SLAs nearly anywhere on the globe [e.g., AVISO (sea level anomalies and geostrophic velocity anomalies; available at http://www.aviso.oceanobs.com/en/data/products/sea-surface-height-products/global/msla/)]. Satellite altimetry data reveal that SLAs off the coast of northern Simeulue reached –23 cm during the late 1997–early 1998 positive IOD event, or ~5 cm lower than at any other time since 1992 (Figure S2); when tides are factored in, sea levels in 1997 and 1998 reached elevations ~4 cm lower than in September 1994, the next lowest incident of sea surface heights during the period 1993–2004. This alone can explain the 7–8 cm diedowns seen on LKP-1 and LKP-9 in late 1997, when one also considers that these microatolls had grown upward by ~5 cm (relative to the rest of the coral head) between late 1994 and late 1997; no tectonic explanation need be invoked for the 1997 diedown. [Between late 1994 and late 1997, the site presumably experienced ~2 cm of gradual interseismic subsidence as a result of steady strain accumulation, but the upward growth of the coral still would have outpaced tectonic subsidence by several centimeters over that time period.]

3.2.7. The 2003–2004 diedown: possibly tectonic

The cause of the late 2003–early 2004 ~1-cm diedown on LKP-1 (and on numerous other heads at the site, but not on LKP-9) is less clear. SLAs were as low as –12 cm in early 2004 (Figure S2), and with tides factored in, sea levels at that time reached as low as ~10 cm higher than their 1997–1998 minimum values. HLS on LKP-1 following the late 2003–early 2004 diedown was 9 cm higher (in the reference frame of the coral head) than after the late 1997–early 1998 diedown, but if the island (and hence the coral head) were gradually sinking interseismically between late 1997 and late 2003 at a rate of a half centimeter per year, then in terms of absolute elevation, the early 2004 HLS would be only ~6 cm higher than the early 1998 HLS. Assuming that the sea-level minima (from one year to the next) have relative errors that are small enough to be ignored for this purpose, then SLAs cannot by themselves explain the diedown in late 2003–early 2004. One possible explanation for the diedowns would be a lack of net tectonic subsidence during those years. While it is unlikely that strain accumulation simply stopped from 1998 to 2003, it is plausible that the 2 November 2002 M_W 7.2 Simeulue earthquake played a role here: interseismic subsidence during that time period may have been balanced at the LKP sites by several centimeters of coseismic or postseismic uplift associated with the 2002 earthquake.

3.2.8. Interpreting earlier diedowns, prior to satellite-derived SLA data

Unfortunately, satellite altimetry data do not extend back beyond 1992, and no regional tide gauge data are available to extend the local sea level history back in time. As with the late 1997 diedown, the dates of certain other widespread coral diedowns (late 1961, late 1982) also correspond to known positive IOD events [*Rao et al.*, 2002], which suggests that those diedowns were also likely caused by regional oceanographic lowerings. Indeed, the overarching correlation between positive IOD events and upwelling, lower sea surface temperature (SST), and lower sea surface height (SSH) in the southeastern tropical Indian Ocean suggests that the Indian Ocean dipole mode index (DMI, a measure of the severity of the IOD) or local negative SST anomalies (for which data extend back further) might be useful proxies for past SSH histories, but the correlation is complicated and far from perfect [e.g., *Rao et al.*, 2002], and in practice such proxies would have limited utility.

A more practical technique for distinguishing minor tectonic uplift from other diedowns is suggested by the pattern of growth on LKP-1 following the 1961 diedown. In late 1961, the LKP-1 microatoll died down by ~8 cm, making it the largest diedown other than that caused by the 2004 earthquake and ~1 cm larger than the late 1997 diedown. If a diedown results solely from an extreme temporary oceanographic lowering (lasting days to months), then for some time after sea levels return to normal, the coral's upward growth should be limited only by its growth rate, and not by sea levels, unless another extreme oceanographic lowering occurs soon after the first. For a considerable duration after a large non-tectonic diedown, we would anticipate that the coral would have unrestricted upward growth without additional diedowns. Indeed, following 1961, LKP-1 grew upwards unimpeded by diedowns for more than 24 cm and at least 17 years—the largest climb and longest period without a diedown of the microatoll's life. In contrast, if a diedown is caused by tectonic uplift, then, relative to the coral, sea level becomes "permanently" lower, and the coral's HLG in the years that follow should be as close to the coral's theoretical HLS as in any other year. In the case of uplift, we would not expect an unusual delay preceding the coral's next diedown, and all subsequent diedowns would be at lower elevations than predicted by the trend of prior diedowns. This scenario is not seen on LKP-1; if the 1961 diedown on LKP-1 were caused by tectonic uplift, then the only way to explain the subsequent morphology of the head is if the uplift were followed by tectonic subsidence (over the following days to years) that equaled or slightly exceeded the magnitude of uplift. Whereas both explanations are reasonable, a non-tectonic diedown is a simpler explanation in any case where such morphology is observed, and in light of the knowledge that the 1961 diedown corresponds to a strong positive IOD event, a non-tectonic oceanographic lowering is our preferred explanation for that diedown.

3.3. Modern interseismic subsidence rates at the Lhok Pauh (LKP) sites

3.3.1. Methods for calculating interseismic rates from HLG and HLS data

We can also use the coral microatoll cross-sections to constrain interseismic subsidence rates. A time series of HLG and HLS is plotted on Figures 4b and 5b for LKP-1 and LKP-9, respectively. In each case, we attempt to fit lines to the data, but the best method for doing this is not well established. The problem arises because, ideally, we would want a least squares fit to each year's HLS, but the vast majority of the data are HLG—underestimates of HLS. In some years, HLG is a fairly good estimate of HLS, and the former's underestimate of the latter is inconsequential; in other years, however, such as those following 1961 or other large non-tectonic diedowns, the underestimate can be quite severe. It is thus problematic to fit the HLG data because each of those data points is unquantifiably biased, to differing degrees. On the other hand, it is even more problematic to strictly fit the HLS data following each diedown: as we have shown in the preceding discussion, the extent of each diedown and the absolute water level at the time of each diedown are highly variable. If we attempt to strictly fit the HLS data, any tectonic signal will be overwhelmed by noise reflecting the random variability in time of SLAs (e.g., Figure S2). If there were satellite altimetry or regional tide gauge data extending back to the beginning of our coral HLS record, it would be straightforward to remove the SLA variability from the HLS record, but because such data exist for only the most recent part of that record, such a method is not viable.

We attempt to circumvent the problems with two different approaches at least squares fits of the data. The first method involves fitting a selected subset of the HLG data and is used on both modern and fossil heads. It requires some subjective analysis, but a systematic set of criteria are defined and followed in every case. The second method involves fitting a subset of the HLS data by adding back in a specified "diedown amount" appropriate for each diedown; this method, however, can only be used on modern heads. This method is more objective, but it requires us to look at all the modern heads in the region and estimate an "average diedown" for northern Simeulue for each year. In the end, we hope both methods converge at similar results: best-fitting lines with similar slopes. If both methods yield lines with similar slopes, we can interpret those slopes with increased confidence; if the slopes vary considerably, we take that variation as an indication of the uncertainty in those results.

3.3.2. Method 1: using pre-diedown HLG data

Our first method for fitting data is based on the argument that, following any non-tectonic diedown, the HLG will be a particularly severe underestimate of HLS; as the coral grows back up with time, HLG will approach HLS. Eventually, even a minor negative SLA—a fluctuation that occurs almost every year—can induce a diedown. Thus, the HLG values in the year or years immediately preceding a diedown are the best estimates of HLS in non-diedown years. These values are also the least affected by sea level variability: they are unaffected by the severity of the diedown that immediately follows, and they are only minimally affected by the timing of that eventual diedown, as, even if the diedown were delayed by several years, the slope of the least squares line would not be significantly affected (e.g., Figure 4b). The principle underlying this method, then, is that we wish to fit the one or two HLG points immediately prior to each diedown. Two complications, however, require modifications to the technique. The first is that the upper parts of the band or bands immediately preceding a diedown are the most prone to erosion following the diedown, so often we can get only a minimum estimate of HLG (in other words, a minimum estimate of a minimum estimate) in the year or years before a diedown. Because of this, we choose to fit the highest points preceding each diedown, not necessarily those points immediately preceding the diedown; every coral and every diedown are different, so every head must be considered on an individual basis. The second complication is that, prior to the coral's first diedown, we cannot know how far below ELW the coral was; there is no reason to believe that the HLG prior to that diedown was anywhere close to the theoretical HLS. (To illustrate this point, we can consider a hypothetical scenario in which a coral head is sitting 95 cm below HLS, until an earthquake uplifts it 100 cm. The coral then experiences a 5 cm diedown—the first of its life—but the HLG in the preceding year was still 95 cm below HLS.) To account for this second complication, we simply do not fit any points prior to the coral's initial diedown.

3.3.3. Method 2: using post-diedown HLS data

The second method involves estimating the diedown on every slabbed head on northern Simeulue, for each year in which most or all of the heads experienced a diedown. We average all the diedowns in a given year, and then add that average value back to the post-diedown HLS on each head for the given year. The result is an estimate of HLG (and HLS) prior to each diedown that doesn't suffer the problem of erosion prior to each diedown—or, at least, the problem on any particularly eroded head is mitigated by averaging the estimated diedowns on all northern Simeulue heads. This capitalizes on the fact that the HLS following a diedown is rarely eroded, because it necessarily is recorded on a more protected part of the head. An additional advantage of this method over the first is that, in most cases, it allows us to use data from a microatoll's initial diedown. This method depends upon the assumption that the spatial variability in the magnitude of each diedown (at least at the scale of northern Simeulue) is small; while the actual data reveal some variability, it appears to be small enough that using the average of the diedowns should not incorporate substantial errors. Finally, we attempt a least squares fit to these "corrected" post-diedown HLS values.

3.3.4. Corrections for eustatic sea-level change

The linear least squares line for each method is shown on the graphs in Figures 4b and 5b for LKP-1 and LKP-9, respectively. As seen in Figure 4b, the first method yields a slope of 7.2 mm/yr on LKP-1, using pre-diedown HLG data spanning the years 1948–2003. This slope is the submergence rate: the rate relative to sea level at which the coral descends below the surface of the water.

In order to obtain the subsidence rate—the absolute (geodetic) rate at which the site is pulled downward interseismically—the submergence rate must be corrected for eustatic sea level changes. Defined in this way, the subsidence rate includes land-level changes that are purely tectonic and those that result from isostasy:

$$\text{net subsidence} = \text{subsidence}_{\textit{tectonic}} - \text{uplift}_{\textit{isostatic}} = \text{coral submergence} - \text{eustatic rise}\ ,$$

where subsidence and submergence are positive downward, and uplift and eustatic sea level rise are positive upward. In Sumatra, the isostatic contribution should be comparatively small.

A number of studies have documented eustatic sea level rise over the past century. *Church and White* [2006] estimate a rise in global mean sea level of 1.84 ± 0.19 mm/yr for the period 1936–2001. *Jevrejeva et al.* [2006] obtained a similar global curve using a different technique, but their analysis shows that the Indian Ocean trend has been nonlinear: they find that Indian Ocean sea levels, on average, were rising by ~4 mm/yr from ~1930 to ~1947, by ~3 mm/yr until ~1958, by ~2 mm/yr until ~1965, by ~1 mm/yr until ~1980, and by <0.5 mm/yr since 1980. Meanwhile, *Beckley et al.* [2007] used satellite altimetry data to estimate sea level trends over the period 1993–2007. They found that sea levels rose off the west coast of Sumatra over that period, with rates of sea level rise increasing from northwest to southeast: ~2.0 mm/yr just northwest of

Simeulue, ~2.5 mm/yr just southeast of Simeulue, and ~3.0 mm/yr just west of Nias. The extent to which the Indian Ocean basin-wide values [*Jevrejeva et al.*, 2006] apply to Simeulue is unclear; in an attempt to simplify our calculations, we assume an average rate of sea level rise of 2 mm/yr since at least 1948, bearing in mind that regional sea level rise was likely faster than that prior to the 1960s. (In Section 3.5.1, we will argue that it is valid to assume a 2 mm/yr eustatic sea-level rise since AD 1925.)

3.3.5. Interseismic subsidence recorded by LKP-1

Correcting for sea level rise, the average submergence rate of 7.2 mm/yr for LKP-1 corresponds to a subsidence rate of 5.2 mm/yr. If we ignore data from after 1997 (to avoid any bias that might be introduced by the inferred uplift in 2002), the average interseismic submergence rate increases marginally to 7.3 mm/yr (not shown), with a corresponding subsidence rate of 5.3 mm/yr. The second method, using corrected post-diedown HLS data spanning 1962–1998, yields an average submergence rate of 7.2 mm/yr, or a subsidence rate of 5.2 mm/yr. All of these values are essentially identical, suggesting they are robust and not biased by any assumption that any one of the calculations might be based upon. We adopt the value 5.3 mm/yr for the 1948–1997 average subsidence rate at LKP-A. If this rate can be extrapolated back in time, then it would take ~230 years of strain accumulation to store the 2004 uplift potential (123 cm) at the site. As we will discuss in Section 13.3, however, our own observations suggest that subsidence rates at a site can vary over time.

3.3.6. A nonlinear trend in sea-level rise superimposed on uniform subsidence?

It is worth noting that the nonlinear trend in sea level rise observed by *Jevrejeva et al.* [2006] appears to show up in the Sumatran microatoll records. A linear least squares fit to the LKP-1 pre-diedown HLG data spanning 1948–1960 yields a submergence rate of 8.2 mm/yr, whereas a fit to the pre-diedown HLG data spanning 1977–1997 yields a submergence rate of

5.9 mm/yr. The difference in these two submergence rates matches the difference in the rates of sea level rise in the Indian Ocean estimated over those two time periods [*Jevrejeva et al.*, 2006]. In other words, the relative sea level history at LKP-A is consistent with the varying rate of eustatic sea-level rise estimated by *Jevrejeva et al.* [2006] superimposed on a constant subsidence rate of ~5.3 mm/yr from 1948 to 1997.

3.3.7. Interseismic subsidence recorded by LKP-9

For LKP-9, the first method yields an average submergence rate of 3.1 mm/yr, using pre-diedown HLG data spanning 1986–1996; the second method yields an average submergence rate of 1.2 mm/yr, using corrected post-diedown HLS data spanning 1983–1998. In contrast to the indistinguishable rates calculated for LKP-1, those for LKP-9 vary considerably, suggesting at least one of the calculations is biased. Indeed, the shorter duration of useful data and the greater amount of erosion on LKP-9 both act to increase the uncertainty of the rates. As LKP-9 (at site LKP-B) is farther from the trench than LKP-1 (at site LKP-A), we would expect the interseismic subsidence rate to be lower on LKP-9, but only marginally so; it is unclear why the calculated interseismic rates are so low on LKP-9. Some of the difference appears to be attributable to the different time periods over which the rates are calculated on the two heads, and in light of the high uncertainties and inconsistent estimates of the rate on LKP-9, we discount both estimates for LKP-9; however, a comparison of the two heads' morphologies and growth histories since 1982 (Figures 4, 5, 14a) reveals that some of the difference must be real.

3.4. 14th–15th century record at the Lhok Pauh (LKP) sites

3.4.1. The LKP-3 population of heads (including LKP-6 and LKP-7)

The most complete and compelling fossil record from Lhok Pauh comes from the LKP-B site. Fossil *Porites* microatoll LKP-3 (Figure 6) was sampled from a population of microatolls that all have similar morphologies at similar elevations (Figure 3b). All the heads in this population were interpreted in the field to be of the same generation based on their characteristics and proximity to one another. We chose to slab LKP-3 because it appeared to have the longest record and best preservation of any *Porites* head in the population, and because it appeared to be in place, i.e., it appeared untilted and there was no evidence that it had been moved. Two adjacent slices of LKP-3 (~1 cm apart) were x-rayed and are shown in Figure 6 a–b. LKP-6 and LKP-7 (Figures 7 and 8, respectively) are fossil *Goniastrea* heads collected nearby (Figure 3b) that were also interpreted in the field to be of the same generation. LKP-7 is a *Goniastrea* microatoll with a somewhat irregular (radially asymmetric) morphology that nonetheless resembles the morphologies of the other heads in the population and is at a similar elevation. LKP-6 is a *Goniastrea* tsunami block that was buried upside down in the soil. Its buried crown had a nearly pristine, unweathered outer surface that suggested it was living at the time it was overturned, and which we anticipated would be useful for accurately determining the date of the uplift event (and likely tsunami) that killed it.

Two samples from LKP-3 and one sample each from LKP-6 and LKP-7 were ^{230}Th-dated (Tables S2–S3; Figures 6 a–b, 7, 8a). Based only upon the samples' ages and the number of growth bands preserved after each sample, the weighted-average date of the outermost band of LKP-3 is AD 1400 ± 7; the dates of the outermost bands of LKP-6 and LKP-7 are AD 1395 ± 3 and 1390 ± 4, respectively (Table S3). In the x-rays of each of the three slabs (including both x-rayed slices of LKP-3), the outermost band is remarkably well preserved, and the perimeter of the head is nearly parallel to banding, suggesting minimal erosion. There appears to be a few millimeters of erosion in many places, but there is no evidence to suggest any of these heads have had one or more bands entirely eroded. In particular, most of the outer band of LKP-6 appears unweathered. We thus infer that LKP-6 is not missing any bands, and LKP-3 and LKP-7 are each missing a trivial 0.5 ± 0.5 annual bands of growth. The extraordinarily precise sample ages yield dates of death for these three heads that overlap, confirming our initial suspicions that they belong to the same generation. [We note that either the corals are coeval and died simultaneously, or no part of their records overlap and their dates of death must be many decades apart. This dichotomy arises because any event with a diedown large enough to kill one of the heads would be expected to have killed or caused a significant diedown on every other coral living at that elevation at the site at that time. A difference of many decades in these heads' ages is not permitted by the analyzed samples; the dating analyses are much more consistent with coeval heads.] We further note that both LKP-3 and LKP-7—the two heads that were living near HLS at the time—experienced diedowns of a few centimeters exactly seven years before their outermost preserved corallites, providing compelling evidence that the two heads are missing exactly the same number of bands (earlier we estimated that number to be 0.5 ± 0.5 bands). The weighted-average date of death of all three heads is AD 1394.2 ± 2.4 (Table S4). The preferred banding ages shown on Figures 6–8 assume each head died around AD 1394.2 (March 1394) and is missing 0.0–0.5 years of growth.

3.4.2. (Preliminary) estimate of uplift in 1394

Although only the uppermost 14–26 cm of the outer perimeter of slab LKP-3 was living at the time of uplift (Figure 6 a–b), two taller (unslabbed) microatolls from that population appear to have been living as far down as 50–55 cm below the high point on the outer rim. That the entirety of every head in the population appears to have died in the 1394 event implies that uplift was at least 50–55 cm. We will adopt the more conservative 50 cm as our minimum estimate of 1394 coseismic uplift at LKP-B.

3.4.3. The LKP-4 population of heads

The perimeter of fossil *Porites* microatoll LKP-4 (Figure 9) is ~14 cm lower than that of LKP-3 (Table S3), and LKP-4 has a considerably different morphology than the heads of the

LKP-3 population. LKP-4 itself grew amidst a population of heads (Figure 3b)—each at the same elevation, all in close proximity to one another, and each characterized by a middle ring higher than the rest. U-Th analyses of three samples from LKP-4 (Tables S2–S3; Figure 9a) yielded a weighted-average date of AD 1443 ± 31 for the outermost edge.

If the morphologies and dates of the LKP-3 and LKP-4 populations are considered jointly, observations suggest AD 1443 is too old to be the date of the outer edge of LKP-4, but a slightly younger date of AD 1450—which is well within the error of the weighted average—is likely the true date. Banding on LKP-4 can be counted inward from the outermost band unambiguously for 53 annual bands, and although band-counting is somewhat ambiguous earlier than that, there are necessarily several additional years of growth prior to the start of clear banding. For ~55 years prior to the coral's outer preserved band, the coral's HLG was higher than where HLS was immediately following the 1394 diedown (i.e., higher than a point 50 cm below the outer rim of LKP-3 or 36 cm below the outer rim of LKP-4; see Figure 9a); during those 55 years, LKP-4 never died down to the 1394 post-uplift HLS. Hence, none of these outer 55 bands could be the 1394 band, and the oldest permissible date of the head's outer preserved band is ~1449. This date is consistent with the ^{230}Th date: the 2σ error on the weighted-mean date permits the outermost band to be as young as late 1473.

3.4.4. Precise age of LKP-4; (comprehensive) estimate of uplift in 1394

Based on an admittedly speculative interpretation of the innermost part of LKP-4, we argue that the uplift in AD 1394 was close to 50 cm (earlier we established 50 cm as only a conservative minimum estimate of the uplift), and that the LKP-4 head died exactly 56 ± 1 years after LKP-3. The basis for this interpretation is that the inner head (the inner part of the lowest 17 cm of the slab) appears to have grown sideways (to the right in Figure 9a) for >5 years, until it appears to have died down by several centimeters, at least in the plane of the slab. Following the diedown, a single lobe of the original coral head continued to grow toward the right, while, simultaneously above the original inner head, coral began growing into the plane of the slab from somewhere out of the slab, eventually growing radially upward and outward within the plane of the slab (and developing clear, consistent banding). Our preferred interpretation is that the innermost, lowest part of LKP-4 was a tsunami block that was rolled but which remained alive and barely below HLS following the tsunami (and uplift). The interpretation that the inner block was rolled explains the irregular diedown (in 3 dimensions) it seems to have experienced, as well as the apparent sideways growth early in its life. We infer that the innermost part of the head started growing in the late 1380s, and that it was transported by a tsunami associated with the 1394 earthquake. If the last partial band before the diedown on the inner block dates to AD 1394, then counting outward yields a date of 1449 for the head's outer preserved band, as determined earlier. If our interpretation is correct, the irregular diedown within the presumed 1394 band suggests that the HLS immediately following the 1394 earthquake was 32–38 cm below the outer rim of LKP-4, or 46–52 cm lower than the outer rim of LKP-3. This is consistent with our earlier (minimum) estimate of 50 cm of uplift at LKP-B in AD 1394.

Again because of good preservation of the outer part of the head and no evidence to the contrary, we infer the LKP-4 slab is missing only 0.5 ± 0.5 annual bands of growth, and we assign a date of death for the head of AD 1450. If our interpretation that the inner part of LKP-4 is a tsunami block that was rolled in 1394 is correct, then the error on the date of death of LKP-4 is determined by adding in quadrature the independent errors associated with (*a*) the date of the 1394 event (±2.4); (*b*) the number of preserved bands on LKP-4 after the 1394 diedown (±1); and (*c*) the inferred number of missing bands (±0.5). In that case, the appropriate date of death for LKP-4 would be AD 1450 ± 3. If our speculation is wrong, however, and the inner part of LKP-4 was not affected by the 1394 tsunami, then the most appropriate date for the death of LKP-4 would be AD 1450 (+23/–3), i.e. 1447–1473. Figure 9a shows preferred banding ages on LKP-4 assuming the head died in 1450 and is missing 0.5 annual bands.

3.4.5. The high middle ring of the LKP-4 population: evidence for uplift around 1430

The high middle ring observed on LKP-4 and other heads in this population is indicative of a minor uplift event midway though the coral's life. As can be seen on the cross-section (Figure 9a), LKP-4 experienced a diedown of 10–14 cm, ~19 years prior to its outermost band; assuming the assigned date of death of AD 1450, this would have occurred during the year 1430. Unlike the unrestricted upward growth for 17 years following the AD 1961 diedown on LKP-1 (described in the Section 3.2.8), the AD 1430 diedown on LKP-4 appears to have been followed by another diedown ~3 years later and was clearly followed by two subsequent diedowns within the first 15 years; all diedowns that followed 1430 were at a lower "baseline" level relative to the trend of the earlier diedowns on LKP-4. (The 1430 and subsequent diedowns are the reason that the outer rings are lower than the middle ring.) Collectively, these observations suggest that the 1430 diedown was not caused by a brief oceanographic lowering but was instead caused by a sudden "permanent" lowering of mean sea level relative to the coral. The only plausible cause of this phenomenon would be sudden tectonic uplift of 10–14 cm at site LKP-B in AD 1430.

3.4.6. Head LKP-10 (coeval with LKP-4): evidence for strong shaking around 1430?

The fossil *Porites* microatoll collected at site LKP-C, LKP-10 (Figure 10), is a complicated head that turns out to be of a similar age as LKP-4. This microatoll is situated on a sandy beach (Figure 3c). It is radially asymmetric, with about three-fourths of its perimeter having died completely mid-way through the coral's life, while the seaward-facing quadrant remained alive for ~20 years longer, growing upward and outward and forming several concentric rings that are present only in that quadrant. A detailed survey of the coral head reveals that the higher outer rings (those present only in the seaward quadrant) are essentially horizontal, whereas the lower inner rings (each of which forms a complete circle) slope markedly seaward. These observations collectively suggest that the coral experienced a seaward tilting event ~20 years prior to its ultimate death, and only that part of the head that tilted downward survived. Other banding irregularities on the head suggest it may have tilted in a separate, earlier event; the sandy substrate of this head may make the head prone to tilting and settling.

Two samples from LKP-10 were ^{230}Th-dated (Tables S2–S3; Figure 10a), yielding a weighted-average date of AD 1435 ± 21 for the outer edge; a comparison of the diedowns and morphologies of LKP-10 and LKP-4 suggest the outer band of LKP-10 is near the younger limit of the 2σ range of 1415–1456. Among other diedowns, LKP-4 experienced diedowns ~32, 28, and 5 years prior to its outer edge (in the years 1418, 1422, and 1445, respectively); LKP-10 died down ~31, ~27, and 4 years prior to its outermost preserved corallites. The uplift event in AD 1430 seen on LKP-4 is not seen on the LKP-10 slab, but it likely corresponds to the tilting event on LKP-10, ~20 years prior to the latter's ultimate death. (If this association is correct, it would imply that shaking and/or a tsunami accompanied the uplift in AD 1430, either of which would, in turn, indicate that the uplift was coseismic.) All of this implies that the outer preserved band on LKP-10 dates to AD 1448 (Figure 10a). While the outer band is evenly preserved and the perimeter of the head is once again mostly parallel to banding, the comparison of LKP-10 with LKP-4 requires that the former is missing exactly one more band than the latter. Hence, we infer that LKP-10 is missing 1.5 ± 0.5 annual bands.

3.4.7. Minimum bounds on inferred uplift in 1450

In addition to resolving the timing of the uplift event that killed LKP-4 and LKP-10, we wish to know the magnitude of that uplift. The diedowns on the LKP-4 population of heads and on LKP-10 provide minimum bounds on the uplift in 1450. Only the uppermost 12–18 cm of LKP-4 (relative to its outer rim, not its high middle ring) appears to have been alive just prior to the diedown that killed the head, and no clear evidence could be found indicating any of the other heads in the population were living at lower elevations at the time; hence, the heads at site LKP-B require a minimum of only 12–18 cm of uplift in AD 1450. At LKP-C, the uppermost 28–32 cm of LKP-10 was living at the time, requiring at least 28 cm of uplift there. Although it appears that nothing on any of the LKP reefs seems to have survived the AD 1450 event—as we found no evidence of corals living anywhere on the reef flats at any time between AD 1450 and the 20th century—we can definitively say little more about the 1450 uplift at LKP than that it was at least 28 cm. In Section 3.7, we will discuss the lack of corals from the centuries following 1450, and we will speculate on what this absence may imply about the size of the 1450 uplift.

3.4.8. Head LKP-5

Fossil *Porites* microatoll LKP-5 (Figure 11) sits among yet another cluster of heads at site LKP-B (Figure 3b). This cluster is much closer to the water and to the edge of the reef than are the LKP-3 and LKP-4 populations, and it sits at a lower elevation (Table S3). The heads in this population are much more eroded than the LKP-3 and LKP-4 populations; they also appeared in the field to have a different morphology than either of the previously described heads, but it is unclear how much of the difference was due to the considerable erosion of the LKP-5 population. An examination of the LKP-5 slab (Figure 11a) reveals a complicated history and geometry. The slab consists of several disconnected blocks, and the original location of the innermost block relative to the rest of the head is ambiguous. While we are confident that the slab is shown in Figure 11a the way it was sitting in the field when we collected it, we cannot preclude that the outer part of the head settled relative to the inner block some time between when it grew and when it was slabbed. Nonetheless, for the discussion that follows, we assume that there was no differential settling of one part of the head relative to another, and that our band counting from the inner part of the head to the outer preserved edge is correct, at least to within a generous counting uncertainty of ±8 years.

The LKP-5 record is somewhat puzzling. U-Th analyses of five samples from LKP-5, including two from the innermost block, yield a weighted-average date of AD 1381 ± 23 for the outermost edge (Tables S2–S3; Figure 11a). This date implies that the LKP-5 record overlaps with that of LKP-3. Comparing the diedown intervals and morphologies of LKP-3 and LKP-5, the only way to reconcile the two overlapping records is if LKP-5 settled and is entirely missing 22 outer bands that are present on LKP-3. If that is the case, then both heads experienced diedowns in late 1345 and early 1355 (Figures 6 a–b, 11a). That LKP-5 could have settled by nearly 30 cm is consistent with observations at sites such as Simanganya in the Mentawai Islands, where the outer parts of the reef have demonstrably slumped by similar amounts relative to the inner parts of the reef [*Sieh et al.*, 2008]. That LKP-5 could be missing 22 outer bands is not inconceivable considering the extensive erosion noted in the field, but it is also possible that the head died prematurely due to some localized effect that did not affect the LKP-3 population.

3.4.9. Heads LKP-2 and LKP-8

The two other fossil *Porites* microatolls slabbed at the LKP sites—LKP-2 (Figure 12) from site LKP-A, and LKP-8 (Figure 13) from site LKP-B—both have outer band ^{230}Th dates in the mid-14th century, with high uncertainties. Both are solitary heads in the sense that neither was found amidst a population of heads with similar morphologies.

LKP-2 is a well preserved microatoll that was picked up and transported by the tsunami in 2004. It is a radially symmetric 1.4-m diameter circular head that was slightly tilted and clearly not attached to the bedrock substrate when we found it in 2006. Only 5.5 m away, we found a 1.4-m diameter circle of whitish algal encrustations on the barren sandstone bedrock; outside the circle, the bedrock is typically darker and more pockmarked by erosion. The proximity of the LKP-2 head to the circle on the bedrock, the similarity of their respective dimensions, and the "fresh" appearance of the circle allow us to infer with confidence that the LKP-2 head was sitting at the location of the circle up until the 2004 tsunami, when it was picked up and transported 5.5 m to the northeast (Figure 3a). Assuming LKP-2 originally grew in the location of the circle, we can restore its original growth position and elevation (Table S3).

At site LKP-B, head LKP-8 has broken up into several pieces that have tilted and settled relative to one another, but there is no evidence that any of those pieces have been transported.

LKP-8 is much more eroded than LKP-2, LKP-3, or LKP-4; concentric rings are still discernable but have been considerably rounded, making it difficult to compare the morphology of LKP-8 to that of other heads.

Based on the U-Th analyses, the outer band of LKP-2 dates to 1347 ± 46, and that of LKP-8 dates to 1373 ± 45. In both cases, the date permits the head to have died in the AD 1394 event or in an earlier event. We can examine the interior of slab LKP-3 (Figure 6 a–b) to determine when earlier uplift events (with sufficient uplift to kill LKP-2 and/or LKP-8) might have occurred. None of the partial diedowns on LKP-3 after late 1345 are large enough to have killed LKP-2 or LKP-8, so any date between 1346 and 1393 can be ruled out. There is no evidence that the 1345 diedown was large, but because 1345 was the first diedown on LKP-3, we do not know where HLS was prior to 1345, and if the 1345 diedown was caused by tectonic uplift, we have no upper bound on the amount of uplift that is permitted by data. Hence, significant uplift *could* have happened during or prior to AD 1345, although there is no strong reason to believe such uplift did occur in 1345. Continuing our examination of LKP-3, we note that the innermost part of the LKP-3 slab is overturned; a plausible cause for any overturned head is a tsunami. By counting annual bands back, we estimate that the inner head of LKP-3 was overturned around late AD 1318. Although somewhat speculative, this may also be a prior uplift event.

Of course, the possibility or suggestion that uplift events might have happened in AD 1318 or 1345 does not indicate that such events necessarily occurred. Based on the morphology of the LKP-3 slab, HLS following the 1345 diedown was 20 cm lower than LKP-3's outer rim (18 cm higher than the pre-2004 HLS at the site); HLG following the 1318 overturning event was 34 cm lower than LKP-3's outer rim (4 cm higher than pre-2004 HLS); and HLG in every year following 1318, until 1394, was higher than in 1318. LKP-2, whose outer rim was 39 cm above pre-2004 HLS in its inferred growth position, was most likely living all or nearly all the way down to its base 2 cm below pre-2004 HLS just before it died, although several centimeters of lateral erosion on LKP-2's lower perimeter make this assessment ambiguous; still, it is probable that the head would have survived any diedown after 1318 and before 1394 if it were living during those diedowns. Hence, the most likely date of death for LKP-2 is either AD 1318 or 1394. For reasons that will be more apparent once we discuss the fossil heads from nearby site LDL-B, we prefer the interpretation that LKP-2 died in 1394. We do not know the original position of LKP-8, but because it appears to have tilted and may have also settled, it may have grown at an elevation slightly higher than that at which we found it in 2007. Consequently, we cannot preclude that LKP-8 may have died during diedowns in 1345 or earlier. Based on the date of its outer preserved band and the likelihood that several annual bands have been completely eroded away, we prefer an interpretation that LKP-8, too, died as a result of the 1394 uplift, although other interpretations are permitted.

3.5. Interseismic subsidence during the 14th–15th centuries at Lhok Pauh (LKP)

The mid-14th to mid-15th century HLG/HLS record from LKP is punctuated by emergence (uplift) events in AD 1394, 1430, and 1450, with gradual interseismic submergence (and subsidence) preceding each event (Figure 14b). Prior to the 1394 event, heads LKP-2 and LKP-3 record the submergence. Heads LKP-5 and LKP-8 also have information from this period, but because both likely tilted and settled (as is apparent when their elevations are compared with those of LKP-2 and LKP-3), we do not use them in the construction of the sea level curves. *Goniastrea* head LKP-7 also records information about sea level prior to 1394, but because of its irregular morphology and lower position (Figure 14b), we also discard this head in reconstructing the sea level history. For the period 1394–1450, LKP-4 records the sea level history. LKP-10 also recorded information during this time, but because it tilted at least once during that interval, and because its lower elevation (Figure 14b) suggests it settled (again) at the time of or after its final death in 1450, we do not use LKP-10 for anything other than the minimum coseismic uplift in 1450, which would not be affected by settling.

The interseismic submergence rate recorded by LKP-2 (for site LKP-A) is 4.0 mm/yr, using pre-diedown HLG data spanning the years AD 1365 to 1393 (Figure 12b); a similar but marginally lower rate of 3.6 mm/yr is obtained (for site LKP-B) from the record on LKP-3 over the period 1352–1392 (Figure 6c). LKP-4 records an average interseismic submergence rate of 4.4 mm/yr between AD 1409 and 1427, and a rate of 3.5 mm/yr from 1431 to 1448 (Figure 9b). Although formal errors are difficult to establish using this method, it is likely that all of the rates recorded on LKP-2, LKP-3, and LKP-4 would be statistically indistinguishable from one another if realistic uncertainties were considered. Still, the faster rate on LKP-4 between 1409 and 1427 may indicate that the average rate was still biased by a faster postseismic rate more than 15 years after the 1394 earthquake.

3.5.1. Sea-level change over the past ~1 kyr

Nominally, the submergence rates we observe must be corrected for eustatic sea level change and other changes in local relative sea level unrelated to tectonics. A limited number of data sets exist that provide constraints on Holocene relative sea levels at a handful of locations around the Sunda Shelf, and some models have attempted to predict relative sea levels over the Holocene, but the data and models must all be understood and placed in context.

Foremost, we must understand that dramatic regional relative sea level changes can occur—even in places far removed from glaciers—in the absence of tectonics or ongoing eustatic sea level changes. The Sunda Shelf and nearby islands, including Sumatra and Simeulue, are located in the far field [*Clark et al.*, 1978] of the major ice loads during the last glacial maximum and were subject to a mid-Holocene highstand of several meters or more. The highstand is observed clearly throughout the tropics, but details of the timing and magnitude of the highstand, and how these vary spatially, remain unclear [*Dickinson*, 2001; *Peltier*, 2002; *Horton et al.*, 2005;

Bird et al., 2007; *Briggs et al.*, 2008]. Indeed, some regional variations in sea level are predicted by the spatially variable influences of hydroisostasy [*Horton et al.*, 2005], namely by the effects of continental levering, a process that is particularly complicated near the Sunda Shelf [*Mitrovica and Milne*, 2002].

Most models suggest that tropical relative sea levels fell monotonically over the late Holocene from the mid-Holocene highstand through the 19th century AD [*Dickinson*, 2001; *Peltier*, 2002; *Horton et al.*, 2005; *Briggs et al.*, 2008]. The model of *Peltier* [2004] (reported by *Briggs et al.* [2008]) predicts a steady relative sea-level drop of ~ 0.4–0.5 mm/yr for Nias Island (just southeast of Simeulue) since 4 ka, whereas S. Bradley (unpublished model) predicts a variable drop since 3 ka off the west coast of Sumatra, with northern Simeulue experiencing a sea level fall of ~0.4 mm/yr since 1 ka. These are both forward models that assume no ice-equivalent meltwater input since at least 1 ka (and ignore any tectonic effects) and predict the spatially variable glacio- and hydro-isostatic response of the crust. Neither has been calibrated to data from the past few thousand years, though, and the validity of these models around the complicated Sunda Shelf region is questionable. Relative sea level data since ~2 ka from tectonically stable locations in this region are sparse and do not appear to be self-consistent.

Given these uncertainties, any attempt to distinguish the long-term tectonic and isostatic signals in Sumatra is problematic. Indeed, this can be challenging in many places in the world. We will thus make no attempt to remove long-term isostatic uplift from the rates we report, but we will now address the issue of long-term eustatic change. We note that this treatment of the pre-20th century rates is consistent with our treatment of the 20th century rates: in our analyses of modern interseismic rates (Section 3.3.4), we similarly do not attempt to separate the tectonic and isostatic signals.

Jevrejeva et al. [2006] and *Church and White* [2006] estimate eustatic sea level change since the 19th century. Both show a net global sea level rise of 15–16 cm from 1925 to 2005.

Jevrejeva et al. [2006] suggest that global sea levels in 1925 were about the same as in the early 19th century, although the standard errors are large prior to 1870. (Eustatic sea level may have fallen slightly during the first half of the 19th century and risen by an equivalent amount during the latter half of the century, but the amplitudes of these changes were small; we will ignore them.) The change (or lack thereof) in eustatic sea level over the past 2 kyr is arguably best constrained by *Lambeck et al.* [2004], who, after independently correcting for tectonic and isostatic effects at multiple sites, calculate from high-precision archaeological evidence in the central Mediterranean that eustatic sea level in the Roman Period (~ AD 1) was 13 ± 9 cm lower than today (~ AD 2000). Taken together, these estimates suggest there was little net change in eustatic sea level from 2 ka until ~ AD 1925.

We make the simplifying assumption that eustatic sea level has been rising at 2 mm/yr since ~1925 but was steady prior to that, since at least 2 ka. One outcome of this is that the subsidence rates should equal the submergence rates documented from the fossil microatolls in our study, although pre-1925 eustatic sea level was ~16 cm lower than in 2005. As with the modern rates, the fossil subsidence rates we calculate include both tectonic and isostatic effects.

3.6. Summary of paleogeodetic and geodetic observations at Lhok Pauh (LKP)

Continuous histories of relative sea level at the LKP sites for the periods AD 1345 to 1450 and, separately, AD 1945 to present have been obtained. Prior to 1345, we can speculate that a tsunami occurred in 1318 ± 3, based only on the observation that a miniscule *Porites* head was overturned at that time, but such an inference is tenuous.

The mid-14th to mid-15th century history is one of interseismic subsidence at an average rate of 3.6–4.0 mm/yr from at least AD 1345 to 1394, ~50 cm of coseismic uplift in 1394 followed by rapid decreasing postseismic subsidence, interseismic subsidence at 4.4 mm/yr from 1409 to 1430, ~12 cm of coseismic uplift in 1430, more interseismic subsidence at 3.5 mm/yr from 1430 to 1450, and finally coseismic uplift in 1450 that was at least 28 cm and likely considerably more than that. The record is interrupted by the AD 1450 diedown, after which there is a five-century gap in data.

The record picks up again around AD 1945. From some time before 1948 until at least 1997 (and likely 2002), site LKP-A was subsiding at an average rate of 5.3 mm/yr, with LKP-B subsiding at a lower rate. A few centimeters of coseismic or postseismic uplift may have occurred during or following the 2002 earthquake, and then all sites were uplifted a meter or more in the 2004 earthquake. The 2004 uplift was followed by rapid decreasing postseismic subsidence, but that subsidence appears to have been interrupted by uplift (again), on the order of 15–20 cm, associated with the February 2008 earthquake.

The biggest remaining mysteries—as highlighted in Section 3.7—are what happened tectonically between AD 1450 and the early 20th century, and why it appears that no corals were living on the LKP reef flats during that time.

3.7. Enigma of missing coral record (AD 1450 to 20th century) and implications

A surprising observation following four seasons of fieldwork is the absence of corals at LKP—and (as we will show in later sections) anywhere on northern Simeulue—that date between the late 15th and early 20th centuries; this absence occurs despite abundant older and younger microatolls. We searched extensively for fossil heads: in 2005, we reconnoitered by helicopter much of the nearly 80 km of coral reefs that line the coast of northern Simeulue and offshore islands between Ujung Salang (USL) and Ujung Sanggiran (USG) (Figure 2); subsequently, we explored ~25 km of that coastline by foot. That we found numerous populations of 14th–15th century corals at sites scattered across northern Simeulue renders it unlikely that the 2004 or 1907 tsunamis (or perhaps some unknown tsunami in the 16th–19th centuries) caused widespread denudation of the northern Simeulue reefs. Similarly, even if portions of the reefs were buried by peat or beach deposits, or if plants that colonized the emerged reef flats affected the preservation of some older coral heads, the abundant preserved 14th–15th century corals argue that we would have found at least a few late-15th to early-20th century corals had they grown there. Instead, it appears inescapable that the reason no such corals can be found today on the northern Simeulue reef flats is that no corals grew there during that period.

We entertain tectonic as well as biological explanations for the lack of corals growing on the reef flats during that period, but we prefer the former and discount the latter. We feel the most plausible hypothesis is that the reef flats of northern Simeulue were sitting above the subtidal zone for most of those five centuries. This would have prevented coral colonies from establishing themselves on the reef flats during that time. Another possibility is that, after the uplift of 1450, some unknown biological phenomenon prevented coral colonies from re-establishing on the reef flats for nearly five centuries. A biological explanation is unlikely, however, as populations of microatolls were growing at numerous sites along the southern Simeulue coast during much of this interval [*Meltzner et al.*, 2008]. Moreover, we have no reason to believe that coral colonies were not growing in deeper water, just beyond the steep reef edges, at northern Simeulue sites. A number of studies [e.g., *Loya*, 1976; *Pearson*, 1981], and our own observations of coral behavior following paleo-uplifts elsewhere in Sumatra [e.g., *Meltzner et al.*, 2008; *Sieh et al.*, 2008], suggest it should have taken decades, not centuries, for corals to begin repopulating the reef flats, once there was sufficient accommodation space.

If indeed the absence of corals from AD 1450 until the early 20th century was caused by the reef's elevation above the subtidal zone, then we argue conservatively that HLS for most of those five centuries must have been lower than the elevation at which LKP-1 was growing during the early part of its life (i.e., the 1940s; see Figure 4b). If the contrary hypothesis—that HLS was higher than this level for extended periods of time (perhaps half a century or more) between 1450 and the 1930s—were true, then living corals at the elevation of LKP-1 should have been widespread during that time. In fact, our nearly exhaustive search of the northern Simeulue reef flats found no such corals. This conservative "maximum" elevation for HLS between 1450 and 1930—about 40–50 cm below the pre-2004 HLG—is indicated by a blue double-dashed horizontal line on Figure 14c.

A bolder but less defensible argument is based upon the level down to which corals died after the 2004 uplift. Uplift of 100 cm in 2004 was not sufficient to kill all the corals on the LKP reefs: some living microatolls persist today (in the months to years after 2004) at low elevations near the reef's edges. Thus, if HLS after the 1450 diedown were at the same elevation as after the 2004 uplift, there would likely have been corals that survived the 1450 diedown and continued to grow. If HLS then gradually rose as the site subsided in the ensuing decades, any microatolls that survived should have grown upwards to higher elevations. That we did not find any corals dating to 1450–1930 suggests HLS after 1450 was even lower than after 2004. However, the pitfall of this argument is that microatolls that survived a diedown to post-2004 levels might have only inhabited the reef edge at the time, and those heads might be rare and difficult to find now. We indicate this bolder "maximum" elevation for HLS following the 1450 diedown—at 100 cm below the pre-2004 HLG for site LKP-B—by a black double-dashed horizontal line on Figure 14c.

Given these constraints, we consider three possible tectonic mechanisms that could have caused the reefs to remain sufficiently elevated for most of this time. One possibility is that uplift in 1450 was so large that it took nearly five centuries of strain accumulation to bring the reef flats back down into the subtidal zone. This possible history is depicted on Figure 14c by the light blue field: after an assumed initial period of rapid postseismic submergence, the blue field from ~1500 to 1925 is bounded by lines representing steady submergence at 3.5 and 5.3 mm/yr, the minimum and maximum subsidence rates documented at Lhok Pauh in fossil and modern corals. This first possible history requires at least 2.5 m of uplift in 1450.

A second possibility is that interseismic submergence for one or more centuries following the 1450 uplift was less than 3.5 mm/yr. This would imply a history from 1450 to 1925 somewhere above the light blue field on Figure 14c. Nonetheless, the maximum elevation constraints discussed earlier argue that HLS from 1450 until ~1930 must have remained below the blue double-dashed line (–45 cm) and probably below the black double-dashed line (–100 cm) for much of that period.

A third possibility is that one or more uplifts (earthquakes) are missing from the record since 1450. Additional uplifts could have kept the reef flats elevated above the subtidal zone (at least most of the time) without requiring the 1450 uplift to be so great. One such hypothetical history is depicted on Figure 14c by the red dash-dotted curve. Note that any such history is constrained by the maximum elevation lines on the figure. Unfortunately, the historical record is too short to help in assessing the viability of large earthquakes between 1450 and ~1900: the earliest historical earthquake to affect Aceh and its surroundings occurred in 1861, but even for that event, the historical record does not provide any information from Aceh itself.

Regardless of the details of the history, one robust observation is that HLS (and hence relative sea level) was 23 cm higher just prior to the 1450 diedown than it was prior to the 2004 diedown (Figure 14c). Thus, given the more conservative "maximum" elevation for HLS following 1450, the 1450 uplift must have been more than ~0.7 m. Considering the bolder "maximum" elevation for HLS, uplift in 1450 was probably more than 1.2 m.

It is difficult to explain the 450-year absence of corals on the LKP reef flats without positing that the 1450 uplift was nearly as large as or larger than the uplift of 2004. Moreover, it seems quite likely that the combined uplifts of 1394, 1430, and 1450 were considerably larger than the combined uplifts of 2002, 2004, and 2008.

3.7.1. Problems with the deeper microatoll record

While a good procedure to test the hypothesis that the reef flats remained elevated above the subtidal zone—and a good method to distinguish among the mechanisms proposed as causes of the reef's high elevation—might be to look farther out on the reef slope (beyond the reef flat) for microatolls at lower elevations, there are several challenges to and pitfalls associated with such an attempt. First, the reef slope—in contrast to a typically wide reef flat with ample area on which coral microatolls can develop—tends to be steep, resulting in a much narrower band around the reef edge on which corals might develop into microatolls at times of low relative sea level; thus, far fewer microatolls should develop during such times, and those microatolls might be harder to find. Second, searching for microatolls on the northern Simeulue reef slopes would be a daunting logistical challenge at many sites, at least at present: since the 2004 uplift, the surf zone tends to be near the reef slope; whether at high or low tide, strong currents make a search for microatolls there difficult at best, and dangerous at worst. Third, the reef slope tends to be unstable: along the reef edge at numerous sites following the 2004 and 2005 earthquakes, we observed living microatolls (that had been growing up to their HLS just prior to the earthquakes) that had recently settled or slumped—presumably a result of strong shaking. These microatolls were commonly observed to be at different elevations (decimeters apart) and in some cases fresh fissures cut across the reef slope. Hence, even if one were to find microatolls on the reef slope, their reliability as paleo-sea-level indicators would be suspect. In general, we have not searched the reef slopes for old microatolls.

4. Results from the Lhok Dalam (LDL) Sites

The Lhok Dalam site sits near the western tip of Simeulue and consists of two subsites: LDL-A to the east, and LDL-B ~1.5 km to the west (Figures 2, S3). The sites were named after the nearby village and small bay, both of the same name ("lhok" is the local word for *bay*;

"dalam" is Indonesian for *deep*). LDL-A sits on the west side of the Lhok Dalam bay, near its mouth; LDL-B is on a reef promontory adjacent to the Lhok Dalam village. LDL-A has abundant modern heads, but all of the larger ones tilted in 2004; there is also a population of large, highly eroded, tilted fossil microatolls, all with a similar morphology, presumably of a single generation. Perhaps because of the site's location near the bay, the site seems to have experienced widespread compaction and/or liquefaction during shaking in 2004. LDL-B is a mostly barren reef, with isolated small modern microatolls anchored to the substrate, and a few scattered fossil microatolls; many of the fossil heads appear to have been picked up and transported by a tsunami at some time in the past.

One modern and one fossil microatoll were sampled from LDL-A; three fossil heads were sampled from LDL-B. The fossil corals from LDL-B all date to the 14th–15th centuries AD: based on a weighted average of dates from the three morphologically similar microatolls at LDL-B, we estimate the timing of a 46 ± 4 cm diedown to be AD 1393.6 ± 2.7 (August 1393). This is indistinguishable from a similar date obtained independently at the LKP sites (Table S4). The fossil head from LDL-A is centuries older, but its age is poorly resolved: the event that killed it could have happened at any time between the early 6th and early 12th centuries AD (Table S3). Details of our observations and analysis at the LDL sites are provided in the auxiliary material, including Figures S3–S8.

5. Results from the Langi (LNG) Site

The Langi site (LNG-A) lies roughly halfway between the LKP and LDL sites, along the northwest coast of Simeulue (Figures 2, S9). The site was named after the nearby village of the same name. Like the LKP sites, LNG-A sits on a reef promontory and has abundant modern and multiple fossil heads. One modern and one fossil microatoll were sampled from the LNG-A site.

The fossil head dates to ~ AD 1400, and we attribute its death to the 1394 earthquake. Details of our observations at the LNG site are provided in the auxiliary material, including Figures S9–S11.

6. Results from the Ujung Salang (USL) Site

The Ujung Salang site (USL-A) lies 7 km southeast of LDL-A, along the southwest coast of Simeulue (Figures 2, S12). The site was named after the nearby village and promontory of the same name ("ujung" is an Indonesian word for *point*). USL-A sits on a reef on the protected side of the promontory. It has abundant modern heads and a small population of fossil microatolls. One modern and one fossil microatoll were sampled from the USL-A site. The fossil head died around AD 956 ± 16. This is presumably the date of an earlier uplift, and it may correspond to the death of the oldest (albeit imprecisely dated) coral sampled at Lhok Dalam. Details of our observations at the USL site are provided in the auxiliary material, including Figures S12–S14.

7. Results from the Lewak (LWK) Sites

The Lewak site sits at the northern tip of Simeulue and consists of two subsites: LWK-A to the east, and LWK-B ~1.2 km to the west (Figures 2, S15). The sites were named after the nearby village of the same name. LWK-A and LWK-B sit on adjacent reef promontories north and northwest of Lewak village, respectively. LWK-A has abundant pancake-shaped modern microatolls, but no fossil heads. LWK-B also has pancake-shaped modern microatolls, and it has at least two generations of scattered fossil microatolls. One modern microatoll was sampled from LWK-A; four fossil microatolls were sampled from LWK-B. The fossil heads all date to the 14th–15th centuries AD. The paleogeodetic record from the coral microatolls at Lewak is augmented by data from a continuous GPS (cGPS) station of the Sumatran GPS Array (SuGAr) network (Caltech Tectonics Observatory, daily SuGAr GPS data analysis; available at http://www.gps.caltech.edu/~jeff/sugar/); the cGPS station, LEWK, was installed in February

2005. Details of our observations at the LWK sites are provided in the auxiliary material, including Figures S15–S21.

8. Results from the Ujung Sanggiran (USG) Site

The Ujung Sanggiran site (USG-A) lies 7 km east-southeast of LWK-A, along the northeast coast of Simeulue (Figures 2, S22). USG-A sits on the west side of the Ujung Sanggiran promontory, just east of Sanggiran village. It has a modest population of modern *Porites* microatolls, but only two fossil microatolls were found. One modern and both fossil microatolls were sampled from the USG-A site. The fossil heads both date to the 14th–15th centuries AD. Details of our observations at the USG site are provided in the auxiliary material, including Figures S22–S25.

9. Results from the Pulau Salaut (PST) Site

We also visited Salaut Besar Island (Pulau Salaut Besar), a small islet ~40 km northwest of Simeulue's northwest coast (Figures 1, S26). One sample from a population of weathered microatolls at Salaut yielded a death date of AD 1372 ± 17, although the death could have occurred later if we underestimated the number of annual bands that were eroded off the head (Figure S27). This coral death most likely corresponds to the 1394 event on northern Simeulue and suggests the 1394 rupture extended over at least the southernmost 60–80 km of the 2004 rupture. Details are provided in the auxiliary material.

While reconnoitering Salaut Besar, we came across what we infer to be a tectonic upper-plate landward-vergent thrust fault cutting across the southern end of the islet (Figure S26). Walking along the reef, we observed a fresh scarp with nearly 2 m of relief, down to the east. The beach berm that would have been active up until the recent uplift appears to be offset across this feature. Standing at the scarp, it is not immediately clear whether the feature is the result of localized reef collapse or is a more substantial tectonic fault. Additional observations, outlined in the auxiliary material, support a tectonic interpretation and suggest the displacement occurred during the 2004 earthquake. If this interpretation is correct, it would imply that the slip vector calculated from the campaign GPS monument on Salaut is strongly influenced by the upper-plate motion. This, in turn, could seriously bias slip models' estimates of the amount of slip on the megathrust in that region; as a consequence, it may be prudent to revisit modeling of slip in the 2004 earthquake. Although logistical and time constraints precluded careful documentation of the fault, our observations and a more thorough discussion of potential implications are provided in the auxiliary material.

10. Depiction of the Relative Sea Level and Land Level Histories

Relative sea level histories for the 14th–15th centuries for Lhok Dalam, Lhok Pauh, and Lewak are plotted in Figure 15. As mentioned earlier, the relative sea level history from AD 1345 to present for Lhok Pauh—with speculation on reasonable histories that may have filled the post-1450 data gap—is presented in Figure 14c. The elevations of data plotted on these figures are those measured in the field. Slopes reflect submergence rates, and the differences in elevation between the modern heads and fossil heads result from a combination of changes in land level and eustatic sea level over time. In Figure 15, Lewak heads LWK-2, LWK-3, and LWK-5 are assumed to have died due to uplift in AD 1450, for reasons discussed in the auxiliary material.

Corresponding land level histories—which are inverted and corrected for 20th century eustatic sea level rise—appear in Figure 16 (14th–15th centuries for Lhok Dalam, Lhok Pauh, and Lewak) and Figure 17 (AD 1345 to present for Lhok Pauh). In these land level histories, slopes reflect subsidence rates, and the differences in elevation between the modern heads and fossil heads result solely from tectonic or isostatic changes in land level. To correct for eustatic effects in Figures 16 and 17, we assume an average sea level rise of 2 mm/yr since 1925, and we take sea level to have been steady prior to that; thus, the elevations of all pre-20th century corals have been shifted down by 16 cm on Figures 16 and 17.

11. Summary of Paleoseismic Results

Observations from seven sites spanning 50 km near the southern end of the 1600-km-long 2004 Aceh–Andaman rupture tell a consistent story. Time series of relative sea level at these sites indicate that all of northern Simeulue and Salaut rose during an earthquake in AD 1394; the maximum documented uplift was 50 cm (Figure 18A). Another earthquake occurred 36 years later, although uplift on northern Simeulue was small; at the Lhok Pauh site, where the timing is unambiguous, uplift was 12 cm (Figure 18B). Northern Simeulue was again uplifted in AD 1450; although the amount of uplift is not tightly constrained, it apparently was sufficient to raise the northern Simeulue reef flats far above the subtidal zone (Figure 18C).

All seven sites rose again in 2004, by up to ~1.5 m on Simeulue (Figure 18D) and up to ~2 m at the Pulau Salaut site; none, however, experienced significant uplift in the M_W 8.6 earthquake of 28 March 2005 to the south (Figure 1). Some of the northern Simeulue sites rose in the M_W 7.2 and M_W 7.3 Simeulue earthquakes of 2 November 2002 and 20 February 2008, respectively, but the combined uplift effected by the 2002 and 2008 earthquakes generally did not exceed ~20 cm at any site.

The Lhok Pauh site, along the northwest coast of Simeulue, is our most complete and informative site. Uplift in 2004 was 123 cm at the southernmost (most trenchward) subsite and ~100 cm at the northernmost subsite (Table S1). A modern microatoll at the southern Lhok Pauh subsite recorded an average subsidence rate (adjusted for eustatic sea level rise) of 5.3 mm/yr between 1948 and 1997. If this rate can be extrapolated back in time, the 123 cm of coseismic uplift there would have taken ~230 years to accumulate. The 2004 coseismic uplift was followed by substantial postseismic subsidence.

The earliest event for which we have solid evidence of uplift at Lhok Pauh occurred in AD 1394.2 (March 1394) ± 2.4. At that time, the upper 50 cm of all living microatolls at the site died, implying 50 cm of coseismic uplift (Figure 16B). Two small coral heads that overturned at the site in 1394 suggest there was at least a small tsunami.

A 12-cm diedown occurred on microatolls at the site 36 ± 1 years later, in AD 1430 ± 3. Although this diedown was small, it appears to have affected every microatoll living at the site at the time, and relative sea level remained lower after the diedown, indicating the diedown was the result of "permanent" tectonic uplift. One head growing on a sandy beach berm at Lhok Pauh tilted seaward at about this time, consistent with slumping or compaction of the underlying sediments during strong shaking in 1430.

A complete die-off of corals on the reef flats at Lhok Pauh occurred 56 ± 1 years after the 1394 diedown, in AD 1450 ± 3. Uplift was at least 28 cm and may have been much more.

After the AD 1450 die-off, corals did not begin to recolonize the reef flats at Lhok Pauh until the early 20th century. Indeed, no corals have been found on any of the northern Simeulue reef flats from that time period, although older and younger corals are abundant and widespread. It is unlikely that the northern Simeulue reef flats would have remained devoid of living corals for so long unless some physical reason prevented corals from recolonizing: many corals from this period have been found on southern Simeulue [*Meltzner et al.*, 2008].

The most plausible explanation for the 450-year absence of corals on the northern Simeulue reef flats following the AD 1450 uplift is that the reef flats were elevated above the subtidal zone for most of the period between then and the early 20th century. Conservatively, following the reasoning in Section 3.7, land levels for most of the period 1450–1930 must have been higher than where they were when LKP-1 started growing in the 1930s, adjusted for sea level rise since ~1925—i.e., above the blue double-dashed line on Figure 17. Arguably, land levels for most of 1450–1930 were probably also higher than where they were immediately after the 2004 uplift, again adjusted for sea level rise since ~1925—i.e., above the black double-dashed line on Figure 17.

This would have been the case if (*a*) 1450 uplift was so large (≥2.5 m) that it took nearly five centuries of strain accumulation to bring the reef flats back down into the subtidal zone (depicted on Figure 17 by the light blue curve and light blue shaded field); (*b*) interseismic subsidence for one or more centuries following the 1450 uplift was less than 3.5 mm/yr; or (*c*) one or more uplifts (earthquakes) that could have kept the reef flats elevated above the subtidal zone (at least most of the time) is missing from the record since 1450 (e.g., the red dash-dotted curve on Figure 17).

Regardless of the details, one robust observation is that HLS (and hence relative sea level) was 23 cm higher just prior to the 1450 diedown than it was prior to the 2004 uplift (Figure 14c). Assuming sea levels themselves were 16 cm lower in 1450, this requires that land levels were 39 cm lower just prior to the 1450 diedown than just prior to 2004 (Figure 17). Thus, given the more conservative "minimum" land levels following 1450, the 1450 uplift must have been more than ~0.7 m. Considering the bolder "minimum" land levels, uplift in 1450 was probably more than 1.2 m.

It is difficult to explain the 450-year absence of corals on the LKP reef flats without the 1450 uplift being nearly as large as or larger than that in 2004. The combined uplift in 1394, 1430, and 1450 must have been considerably larger than that in 2002, 2004, and 2008.

The unusually detailed record obtained at Lhok Pauh provides a paleoseismic uplift history that can be extended to other sites along the northern Simeulue coast. Microatolls at Lhok Dalam, 14 km southwest of Lhok Pauh near the western tip of Simeulue, tell a story strikingly similar to the one at Lhok Pauh. A population of heads at Lhok Dalam died down 46 cm in AD 1393.6 (August 1393) ± 2.7. This date is determined independently of the nearly identical date at Lhok Pauh. Taking a weighted average of the dates at Lhok Pauh and Lhok Dalam, the date of the event is AD 1393.9 (November 1393) ± 1.8 (Table S4).

At Lewak, near the northern tip of Simeulue 7 km north-northeast of Lhok Pauh, three morphologically similar microatolls died together around AD 1474 ± 26. This date and its associated uncertainty barely encompass AD 1450. Each of these microatolls has an HLS record extending back ~44 years. If the heads died after 1450 but prior to 1494, we would expect to see the 1450 uplift in their HLS records, considering Lewak's proximity to Lhok Pauh and the enormity of the uplift there. In contrast, no such uplift is seen in the middle of these microatolls' records, so the most plausible interpretation is that they all died due to at least 41 cm of uplift in 1450. As at Lhok Pauh, following this die-off, corals did not begin to recolonize the reef flats at Lewak until the early 20th century. This implies the reef flats at Lewak were also elevated above the subtidal zone for most of the mid-15th to early 20th centuries, and it suggests the 1450 uplift there was much more than 41 cm.

Direct evidence for uplift around AD 1394 is not preserved in the corals at Lewak, but one microatoll documents the HLS history and interseismic subsidence during the first half of the 14th century. The lack of colinearity between the 14th century time series and the beginning of the 15th century records suggests that an uplift event occurred at some time during the gap between the records (Figure 16C). If this non-colinearity is explained entirely by uplift in 1394, then we estimate the 1394 uplift at Lewak to be ~30 cm.

At Ujung Salang, 7 km southeast of Lhok Dalam, we did not find heads that dated from the 14th–15th centuries, but one sample from a population of microatolls yielded a death date of AD 956 ± 16. This may record an earlier megathrust rupture under northern Simeulue. It may be the same event as that which killed the oldest sampled coral at Lhok Dalam, but the imprecise date of the earliest diedown at Lhok Dalam precludes a definitive correlation.

12. Comparisons with Other Paleoseismic Sites

Results of paleotsunami studies in mainland Aceh and Thailand add to the findings presented here and may bear on some of our unanswered questions.

At Meulaboh on the coast of mainland Aceh (Figure 1), *Monecke et al.* [2008] found at least three paleotsunami sand deposits. Their middle deposit (which they call unit B) rests on detrital plant fragments dated to AD 1290–1400 but is probably older than 1510–1950 (Figure 17, bottom). It contains two depositional units separated locally by an organic-rich stratum. It is not clear whether these two depositional units represent two pulses of a single tsunami or two tsunamis separated, perhaps, by decades, because it was observed only in 2-cm-diameter cores and because lulls between waves can yield organic layers within the deposit of a single tsunami (K. Monecke, personal communication, 2009; B. Atwater, personal communication, 2010). Nonetheless, the Meulaboh results are consistent with at least one, and perhaps two tsunamigenic earthquake ruptures off the coast of Aceh between 1390 and 1455.

At Phra Thong Island in Thailand (Figure 1), *Jankaew et al.* [2008] found tsunami deposits that they inferred to be slightly younger than detrital bark high in the underlying soil, three pieces of which gave concordant ages in the range AD 1300–1450. In contrast to the ambiguity about the number of 14th- and 15th-century tsunamis recorded at Meulaboh in Aceh, Phra Thong's photogenic record for 14th- and 15th-century overwash is limited to a single sand sheet, even at sites where a centimeter of peat had capped the 2004 deposit by 2008, and where the soil beneath the 2004 deposit escaped obvious erosion by the 2004 tsunami (B. Atwater, personal communication, 2010).

The tsunami deposits at Phra Thong likely monitor several hundred kilometers of fault-rupture area entirely north of ~4° N, whereas the Meulaboh deposits likely monitor ruptures entirely south of ~6° N. Two closely timed tsunamis soon after a date in the range AD 1290–1400 along the Acehnese coast, with only one observed in Thailand, could be interpreted to suggest that one rupture extended at least as far north as the Nicobar Islands, while the other extended no farther north than ~4° N (Figure 1): if both ruptures extended well north of 4° N, it is likely that destructive tsunamis would have reached the Thai coastline in both cases. The Meulaboh observations also suggest that at least one of the 14th–15th century northern Simeulue uplifts was not associated with a tsunami large enough to leave a trace at Meulaboh.

In addition to the tsunami deposits at Meulaboh already mentioned (their unit B), *Monecke et al.* [2008] identified a tsunami sand (their unit A) that must be younger than a date within the range AD 1640–1950. This may have been from the historical tsunami of AD 1907, known to have devastated Simeulue and affected mainland Sumatra from Banda Aceh to Padang. *Jankaew et al.* [2008] did not find evidence for paleotsunamis younger than the post-1300 deposits already discussed. If *Monecke et al.*'s [2008] unit A was indeed deposited by the 1907 tsunami and if both the Meulaboh and Phra Thong records are complete, those records argue against the tectonic history cartooned by the red dash-dotted curve on Figures 14c and 17; in other words, if the paleotsunami records are complete, they argue that our history is not missing any large uplifts, either.

The oldest paleotsunami unit of Monecke et al. (their unit C) is younger than AD 780–990 but probably older than 1000–1170; we surmise that it may correspond to uplift on northern Simeulue around AD 956.

In addition to the paleotsunamis identified at Meulaboh and Phra Thong Island, some of the imprecisely dated inferred uplift or subsidence events in the Andaman Islands [*Rajendran et al.*, 2008] may correlate with the 10th–15th century northern Simeulue uplifts. If so, it would suggest that at least one of these paleo-ruptures extended over an area similar to the 2004 rupture. High-precision dates from microatolls in the Andaman and Nicobar Islands could test this hypothesis and help determine the northward extent of each northern Simeulue rupture. The northern Simeulue uplifts may also correlate with turbidites in the sedimentary record off the west coast of Sumatra [*Patton et al.*, 2010], and if so, improved dating resolution of the offshore turbidite record could be useful for determining the northward extent of the northern Simeulue ruptures.

12.1. Limited information from the historical record

An understanding of the written history of Aceh helps paint a picture of the uncertainty of the completeness of the earthquake catalog for Aceh, of why any 14th–15th century great earthquakes and tsunamis could be missing from the historical record, and of why similar events could be missing much later than that. The principal events of the Acehnese history are shown on a time line at the bottom of Figure 17.

Prior to ~ AD 1500, Aceh was of little consequence on the regional front, consisting of several completely distinct Muslim port-states or small coastal kingdoms, including those of Daya, south of modern-day Banda Aceh; Lambri (Lamreh), just east of Banda Aceh; Pidie, ~50 km farther east; and Samudra-Pasai, at present-day Lhokseumawe (Figure 1) [*Reid*, 2005; *Ricklefs*, 2008]. The northern coast of Aceh had been visited by a number of foreign explorers, and while those foreigners did not make note of any earthquakes or tsunamis or lingering damage therefrom, their visits were brief and in no way approach a continuous record: Marco Polo visited Pasai and Samudra (then distinct kingdoms), Pidie, Lambri, and two more southerly kingdoms around 1292 [*Polo*, 1993]; the Moroccan traveler Ibn Battuta passed through the port-state of Samudra in 1345 and 1346, on his way to and from China [*Dunn*, 2005; *Ricklefs*, 2008]; and Ming voyager Zheng He visited the ports of Samudra and Lambri on six trips between 1405 and 1422 and on a seventh trip in 1432–1433 [*Dreyer*, 2007].

Aceh began a transformation in the early 16th century AD, as a result of both internal and external political circumstances. A new sultanate formed around AD 1500 at the site of Lambri [*Reid*, 2005]. Shortly thereafter, in 1509, the Portuguese arrived, and in 1511 they conquered

Malacca, across the Straits in present-day Malaysia [*Reid*, 2005]. Around 1520, the first sultan of Aceh began a series of campaigns to drive the Portuguese out of northern Sumatra, conquering the northern coast and instigating a century of wars and bitter conflicts with the Portuguese and other neighboring states [*Reid*, 2005; *Ricklefs*, 2008]. Throughout the later 16th century, Aceh remained a significant military force in the Straits of Malacca and was a leading center of trade and Islamic study, but it was often plagued by internal dissension: assassinations, coups, and failed military adventures were common [*Ricklefs*, 2008].

In the early 17th century, Aceh reached its brief "golden age," with a series of military triumphs up until Aceh's expansionist campaigns were brought to a halt in 1629 by the Portuguese [*Ricklefs*, 2008]. After this, Aceh began to decline, both for political reasons and because Aceh had, at that point, grown too big too fast: it had become difficult to feed the non-agricultural population that was essential to its success in war and commerce. At this point, Aceh entered a long period of internal disunity and ceased to be a significant force outside the northern tip of Sumatra [*Ricklefs*, 2008]. Nonetheless, the Sultanate of Aceh persisted until the Aceh War (1873–1903) against the Dutch [*Reid*, 2005; *Ricklefs*, 2008].

Prior to the 20th century, record-keeping in Aceh was far from consistent. Notably, because Aceh resisted European colonization more than other parts of Sumatra, the preservation of written records from there is worse than elsewhere. Thus, although earthquakes are known historically to have hit Padang and Bengkulu south of the Equator at least as early as 1681 [*Newcomb and McCann*, 1987], large earthquakes could be missing from the Acehnese record as late as the 19th century. Even for the 1861 earthquake, which uplifted southern Simeulue [*Meltzner et al.*, 2009] and surely must have been felt throughout Aceh, historical information is available from Nias and mainland North Sumatra province (both south of Aceh), but not from Simeulue or mainland Aceh.

13. Discussion

13.1. Interpretation of uplifts: causative faults

Evidence for three coseismic uplifts on northern Simeulue between AD 1390 and 1455 is presented, and the uplifts are associated with earthquakes on the underlying megathrust. The 1394 and 1450 uplift patterns recorded in the corals are consistent with slip on the megathrust but are less consistent with slip along potential upper plate structures. In 1394, sites along both the southwest and northeast coasts of Simeulue appear to have been uplifted, and the gradient between the two coasts (and in particular between sites LDL and LKP) was very low (Figure 18A). The uplift in 1450 also likely stretched from the southwest to the northeast coast, and uplift was likely high over all of northwestern Simeulue, considering the 450-year absence of corals there after 1450. In both cases, upper plate faults onshore Simeulue striking roughly northwest to southeast cannot explain the uplift pattern, because at least some sites would be expected to subside. Although an unrecognized, hypothetical upper plate thrust off the coast of Simeulue might uplift the entire island, splay faults and backthrusts tend to be steeper than the megathrust and accordingly produce uplifts with higher gradients. The very low gradient in the uplift distribution in 1394, and the inferred large uplifts along both the southwest and northeast coasts in 1450, are more consistent with slip along the megathrust than with slip along any possible upper plate faults. The fault responsible for the 1430 uplift is less clear. While we cannot preclude the possibility that slip along the predominantly strike-slip Pagaja fault just southwest of Lewak [*Endharto and Sukido*, 1994; *Barber and Crow*, 2005] produced the small uplift at Lhok Pauh in 1430, the Pagaja fault is concealed where it projects across Holocene deposits—suggesting a lack of very recent activity—and there is no reason to prefer such an interpretation over one in which the 1430 uplift was, like the others, produced by slip along the megathrust.

13.2. Implications for future hazard

Along Sumatra, the relative plate motion is partitioned into nearly perpendicular thrusting on the megathrust at ~45 mm/yr and trench-parallel, right-lateral slip along the Sumatra fault. If no large earthquakes are missing from the record, and if the megathrust is fully locked (coupling factor = 1.0) and strain is accumulating at 45 mm/yr, then 25 m of strain would have accumulated between 1450 and 2004. Even with a coupling factor of 0.8—which characterizes significant portions of the megathrust where adequate data are available, between 2° N and 4° S [*Chlieh et al.*, 2008]—20 m of strain would have accumulated since 1450, double the amount that was relieved in 2004 under northern Simeulue and the Simeulue Basin. Indeed, much more slip occurred in 2004 farther to the northwest, around 4° N, than under northern Simeulue and the Simeulue Basin [*Subarya et al.*, 2006; *Chlieh et al.*, 2007] (Figure 1). This suggests that strain may still be stored along the southern end of the 2004 rupture patch.

The cluster of earthquakes over a 56-year period in the 14th–15th centuries at the southern end of the 2004 patch demonstrates that this part of the fault is capable of clustering; the inference that the combined uplift in the AD 1390–1455 cluster was considerably greater than during the recent sequence of events, argues that there is a precedent for anticipating additional slip during another earthquake under northern Simeulue in the coming decades. To the extent that cumulative slip in individual earthquake clusters tends toward slip-predictable and/or characteristic behavior, additional slip should be expected in the coming decades. We speculate that if an additional event occurs, its spatial extent will most likely be limited to a 100–200 km length beneath northern Simeulue and the Simeulue Basin, southeast of the southern region of >15 m of slip in 2004 (dark blue patch, Figure 20). Alternatively, although perhaps less likely, this rupture may extend northward to the larger patch of high slip in 2004 trenchward of the Nicobar Islands (light blue patch, Figure 20).

Along the Mentawai section of the Sunda megathrust, a similar study of microatolls recovered a record spanning the past 700 years that revealed a history of earthquake clustering there, with each failure sequence apparently culminating in the largest event of the cluster, and with a supercycle periodicity of ~200 years [*Sieh et al.*, 2008]. It is worth noting that available data suggest the supercycle period at the southern end of the 2004 patch has been longer, roughly 400–600 years, over the past millennium. The largest northern Simeulue event in AD 1390–1455 also appears to be the final event of the sequence, but additional data are not available with which to evaluate whether this is a typical mode of failure for this portion of the megathrust. It is unknown whether the inferred 10th-century uplift was also part of a cluster. Even though we posit an additional large rupture along the southern 100–200 km of the 2004 patch in the coming decades, there is no evidence to suggest the displacements will be larger than in 2004.

13.3. Interseismic subsidence

Finally, an examination of interseismic subsidence rates inferred in this study suggests that strain accumulation is complicated spatially over short distances and is non-uniform over time. At any given "snapshot" in time, there appears to be an overall tendency toward faster rates closer to the trench—as predicted by elastic dislocation models [*Savage*, 1983]—but commonly there are exceptions. Furthermore, at individual sites within our study area, the rate does not appear to be uniform from one earthquake cycle to the next.

In the 20th century, subsidence rates were highest at LDL-A and USL-A on the southwest coast of Simeulue and much lower at LWK-A and USG-A on the northeast coast, but rates were anomalously low at LNG-A and LKP-B in between (Figure 19). Uncertainties in each of the rates are difficult to assess due to irregularities in coral growth and erosion, and due to differences in the duration of each record (Figure S1), yet the observation that subsidence was faster at LKP-A than at either LNG-A or LKP-B is real and significant—at least for the portions of the records that overlap.

The most spectacular and compelling example of variability in the rate from one earthquake cycle to another is at Lewak, where the 14th-century subsidence rate appears to be a factor of four larger than the 15th-century rate, and at least twice as large as the 20th-century rate (Figures 16, 19). Both the 14th- and 20th-century heads at Lewak have a record that spans more than 40 years, and the 15th-century record includes two microatolls that span more than 30 years and provide nearly identical results, so none of the rates should be biased by averaging over too short a period. Additionally, both the 20th- and 14th-century heads (LWK-1, Figure S16a, and LWK-4, Figure S20a, respectively) were well preserved with multiple even concentric rings that precluded any tilting (in the case of LWK-1) or that allowed us to confidently correct for very minor tilting (1.0° in the case of LWK-4). Hence, all the rates determined at Lewak—and the unexpected variation among those rates—should be considered fairly robust.

Other sites also show evidence for rates that vary from one earthquake cycle to another. At Ujung Salang—another site with long records—the 20th-century subsidence rate is 7.1 mm/yr or more (Figure 19), compared to the 10th-century rate of 4.7 mm/yr (Figure S14b). At Lhok Pauh, most of the rates are in better agreement, except for the modern rate at LKP-B, which is anomalously low (Figures 16, 19). The 15th-century rate at Ujung Sanggiran (Figure S24b) is more than triple the 20th-century rate (Figure 19), but that earlier rate is based on a record that spans only 19 years, so the anomalously high rate may not have much significance.

The difference in rates over time might be explained in part if there were variations in eustatic sea level or in isostatic adjustments that we did not consider, but eustasy or isostasy cannot explain all of the differences. We note that, with the exceptions of the anomalously high rates on LWK-4 (Figure S20b) and USG-2 (Figure S24b) and the anomalously low rate on LKP-9 (Figure 5b), the subsidence rates determined on fossil microatolls are 0–3 mm/yr lower than the respective modern rates at each site. This apparent low bias in the fossil rates may belie our earlier assumption of steady eustatic sea level in the 10th–15th centuries and may hint instead at gradual eustatic sea level fall (at perhaps 1–2 mm/yr) over that period. Alternatively, regional isostatic uplift around Simeulue may have been 1–2 mm/yr faster during the 10th–15th centuries than in more recent times. While the glacial isostatic adjustment models [e.g., *Peltier*, 2004] do not predict such a pronounced change in rates of isostatic adjustment over the past millennium, the models have not been calibrated to data from that period.

The anomalously high rates on LWK-4 and USG-2, however, cannot be explained by eustasy or isostasy. Either of those processes would be expected to affect all sites on northern Simeulue simultaneously, given the sites' proximity to one another and the fact that isostasy and eustasy operate on regional to global scales. The USG-2 record (Figure S24b) overlaps with records at the nearby sites of Lewak and Lhok Pauh (Figure 16), neither of which were subsiding at abnormally fast rates at the time. Part of the LWK-4 record overlaps with records at Lhok Pauh and Lhok Dalam (Figures 15–16), and again, neither Lhok Pauh nor Lhok Dalam were subsiding anomalously rapidly at the time.

These observations suggest that the elastic dislocation model may be oversimplified; complications might arise from small-scale heterogeneities in the frictional properties along the fault. The anomalously rapid 14th-century rate at Lewak may suggest a period of increased coupling under the site and/or a period during which the locked zone extended farther downdip, to the northeast of the site. One explanation is suggested by *Bachmann et al.* [2009], who present evidence from an exhumed subduction zone for fluids circulating along the plate interface and for transient changes in pore pressure; they argue that these changes may give rise to variations in coupling over the seismic cycle. Although we may not yet fully understand the reasons or appreciate the implications, the observation of twofold to fourfold variations in the interseismic subsidence rate at a given site, from one earthquake cycle to another, appears to be robust.

14. Conclusions

Records of relative sea-level change extracted from coral microatolls on fringing reefs directly above the southern end of the December 2004 M_W 9.2 Sunda megathrust rupture provide a repeated history of gradual interseismic subsidence followed by sudden coseismic uplift. The coral records reveal details about a cluster of earthquakes over a 56-year period in the 14th and 15th centuries and suggest an earlier uplift in the 10th century AD. The 10th-century event is not well documented but is inferred based upon a population of microatolls that died around AD 956 ± 16. The first uplift of the 14th–15th century cluster is dated independently at two sites to have occurred in AD 1393 ± 3 or 1394 ± 2 (2σ); the maximum documented uplift was 50 cm. A smaller but well substantiated uplift occurred in northern Simeulue in 1430 ± 3; at the Lhok Pauh site, where the timing is unambiguous, uplift was 12 cm. A third event is inferred in 1450 ± 3, during which all corals on the reef flats of northern Simeulue died. Uplift of northern Simeulue in the third event is poorly resolved but was likely nearly as large as or larger than that in 2004. Results of paleotsunami studies in mainland Aceh and Thailand are compatible with our findings; the most straightforward interpretation of the paleotsunami results suggests the northern Simeulue coral record is not missing any great earthquakes, at least since the 12th century AD. These observations suggest that significant strain may still be stored along the southernmost part of the 2004 rupture. Subsidence rates recorded by the corals are not uniform over time, having varied by a factor of 2–4 at individual sites from one earthquake cycle to another.

Figure 1. Regional map of the 26 December 2004 rupture and other large ruptures of the northern Sunda megathrust. And, Andaman Islands; Nic, Nicobar Islands; Sim, Simeulue Island. The 2004 rupture shown is a hybrid of Model G-M9.22 of *Chlieh et al.* [2007] south of 14° N and Model B of *Subarya et al.* [2006] to the north; 10- and 15-m contours of slip from *Chlieh et al.* [2007] are dashed yellow and blue, respectively. Larger displacements, exceeding 20 m in places, are suggested by Model B [*Subarya et al.*, 2006]. Other rupture locations are from *Rivera et al.* [2002], *Bilham et al.* [2005], *Briggs et al.* [2006], and *Meltzner et al.* [2008]; the 1907 location is speculative. Australia to Sunda relative plate motion is from *Prawirodirdjo and Bock* [2004] and faults are generalized from *Curray* [2005]. Paleotsunami sites at Meulaboh, Aceh [*Monecke et al.*, 2008] and Phra Thong Island, Thailand [*Jankaew et al.*, 2008] are labeled Me and PT. Banda Aceh and Lhokseumawe are BA and Lh. (**Inset A**) My, Th, Si, and Ja are Myanmar, Thailand, Singapore, and Java; the red line is the Sunda megathrust. Blue box shows location of main figure. (**Inset B**) Simeulue and nearby islands, along with paleogeodesy sites discussed in this paper: USL (Ujung Salang), LDL (Lhok Dalam), LNG (Langi), LKP (Lhok Pauh), LWK (Lewak), USG (Ujung Sanggiran), PST (Pulau Salaut Besar). Location of Inset B is indicated by blue box marked 'B' on main map.

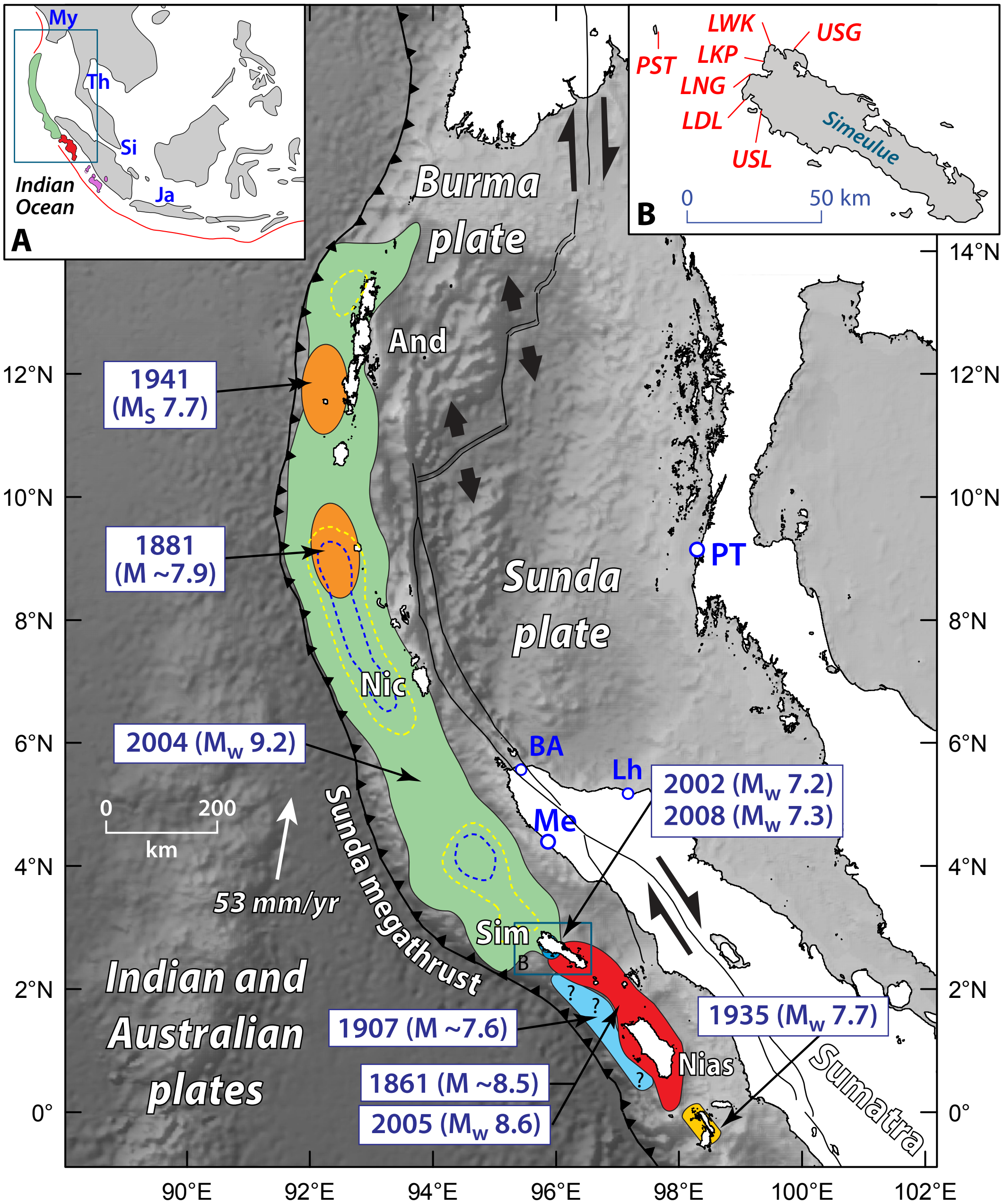

My
Th
Si
Ja
Indian Ocean
A
PST
LWK
LKP
LNG
LDL
USL
USG
Simeulue
0
50 km
B
Burma plate
Sunda plate
And
Nic
Sim
Nias
Sumatra
BA
Lh
Me
PT
1941 (M_S 7.7)
1881 (M ~7.9)
2004 (M_w 9.2)
2002 (M_w 7.2)
2008 (M_w 7.3)
1907 (M ~7.6)
1861 (M ~8.5)
2005 (M_w 8.6)
1935 (M_w 7.7)
0 200 km
53 mm/yr
Sunda megathrust
Indian and Australian plates
14°N
12°N
10°N
8°N
6°N
4°N
2°N
0°
90°E
92°E
94°E
96°E
98°E
100°E
102°E

Figure 1.

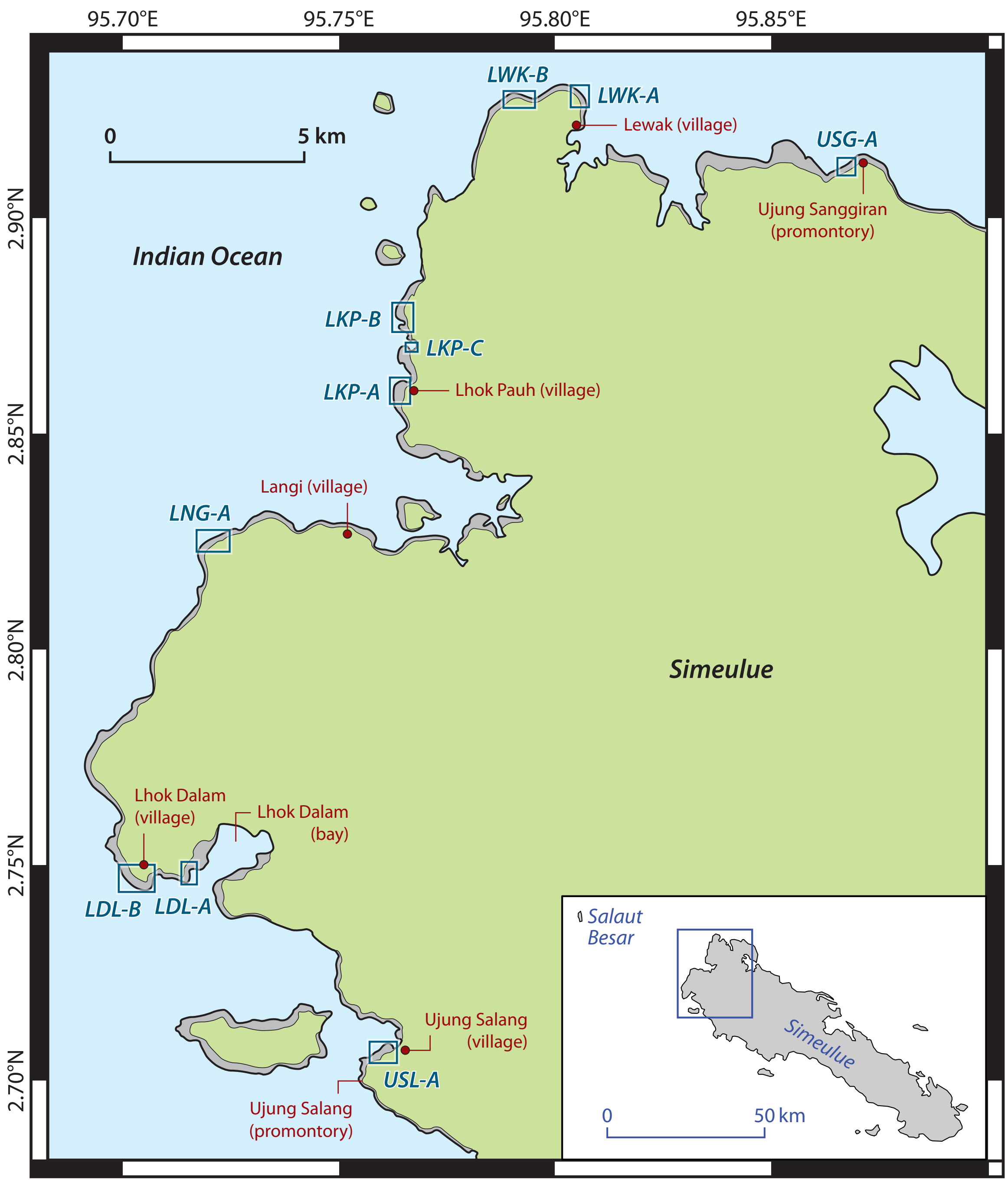

Figure 2. Paleogeodesy sites of northern Simeulue. Green regions were above high tide before the 2004 uplift; gray shading designates reef that was submerged prior to 2004 but which is now subaerially exposed at low tide. Inset shows locations relative to all of Simeulue and also shows relative location of Pulau Salaut Besar (Salaut Besar Island).

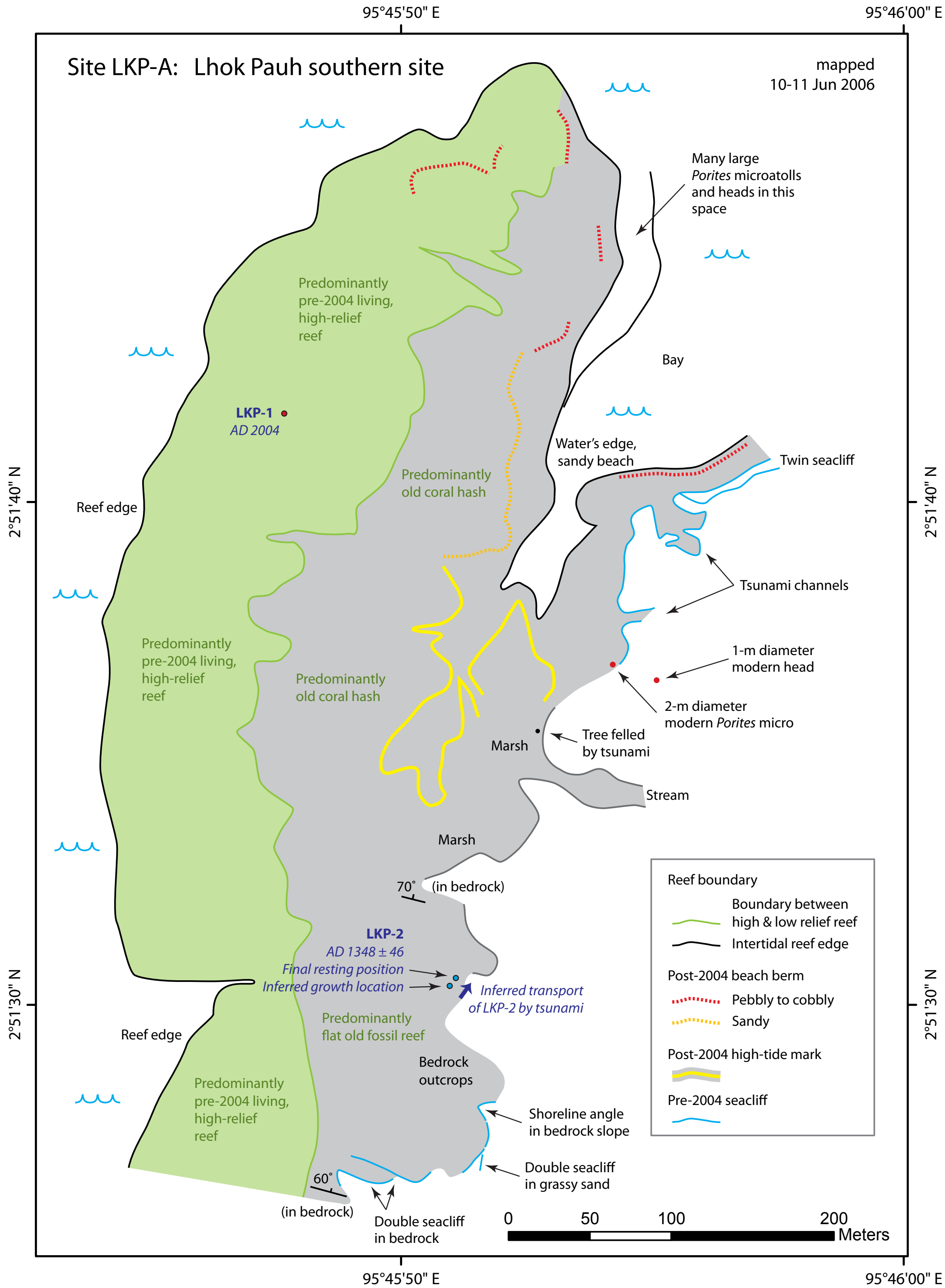

Figure 3a. Map of site LKP-A, northwest coast of Simeulue, showing sampled microatolls and their dates of death.

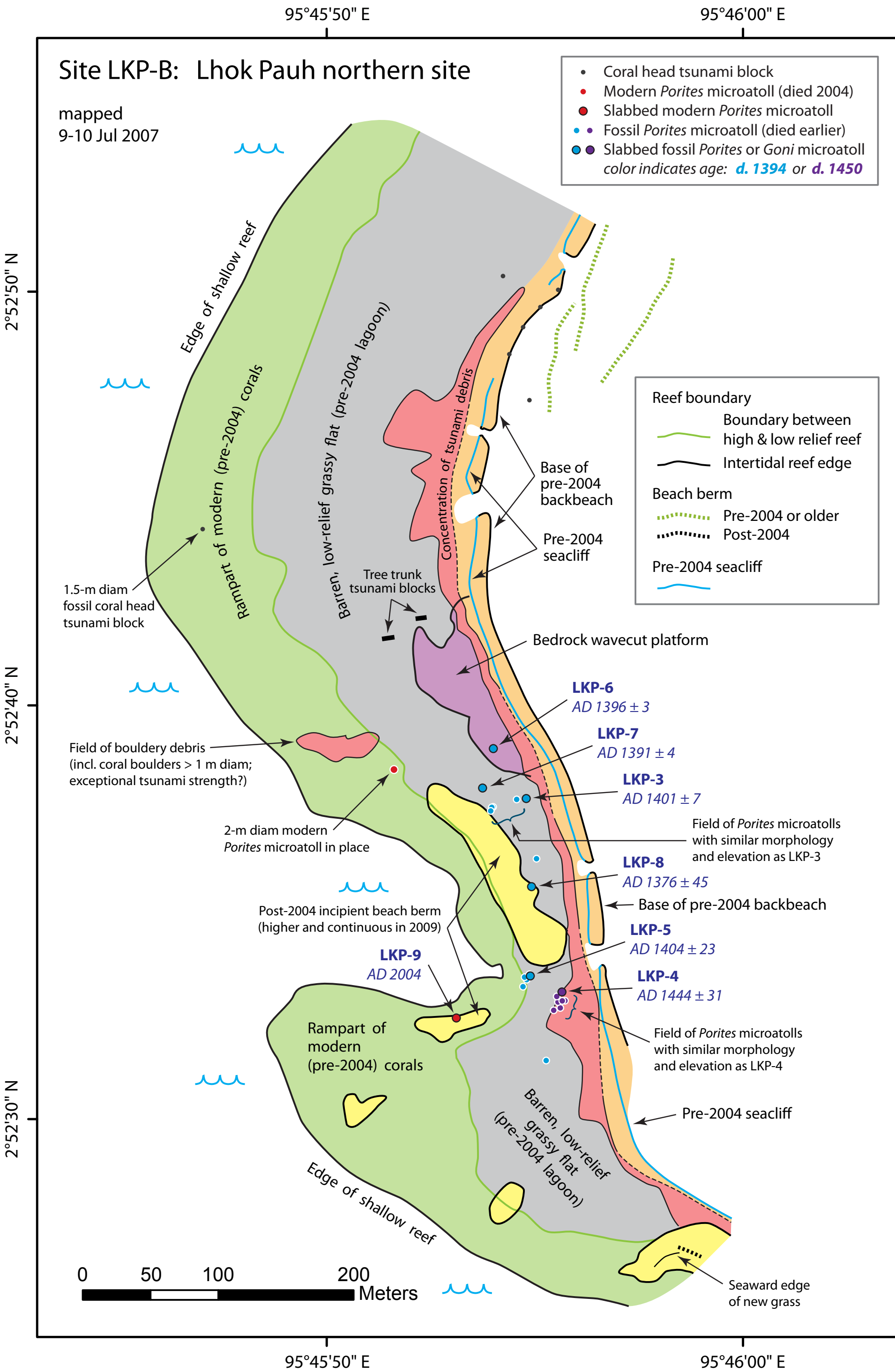

Figure 3b. Map of site LKP-B, northwest coast of Simeulue, showing sampled microatolls and their dates of death.

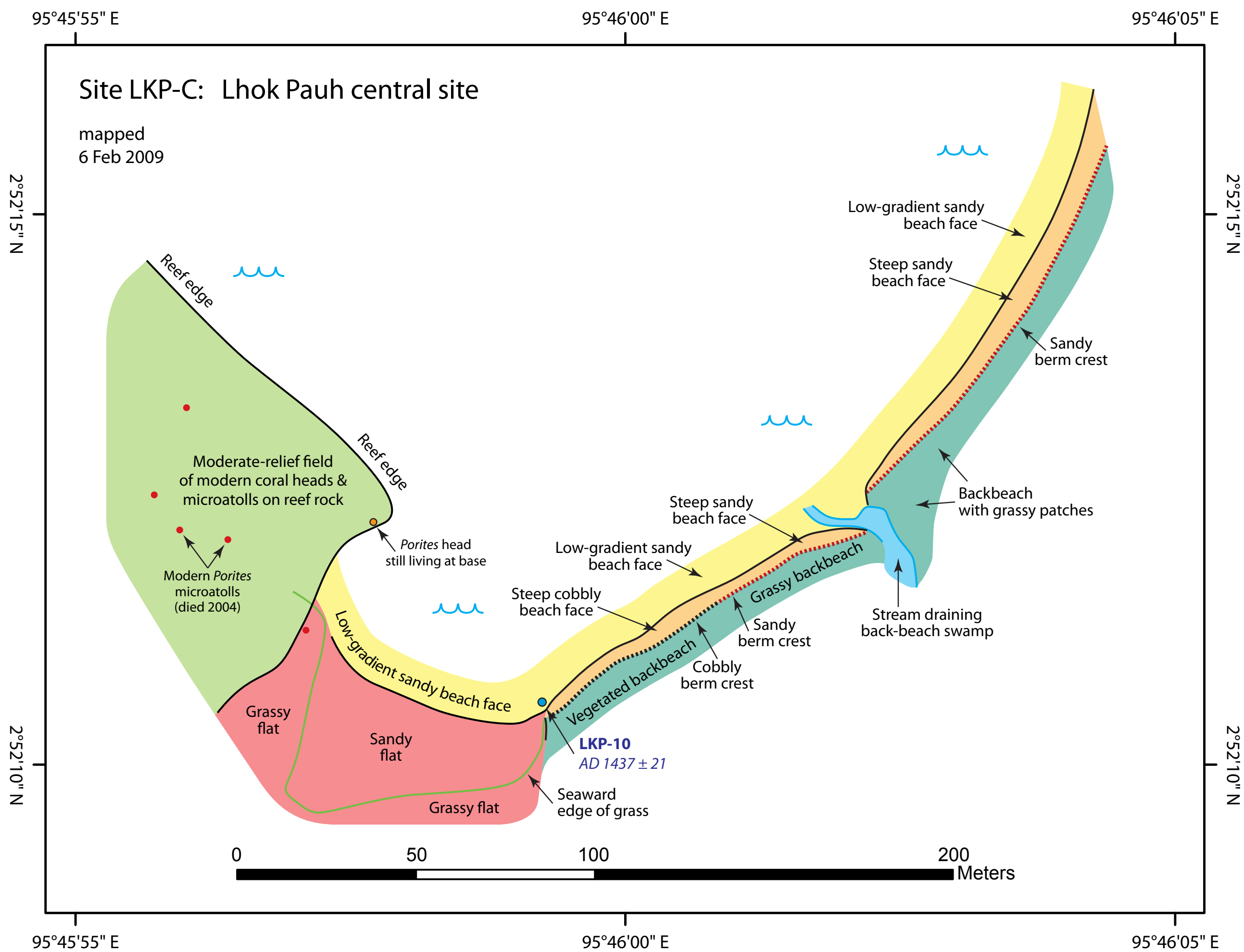

Figure 3c. Map of site LKP-C, northwest coast of Simeulue, showing the sampled microatoll and its date of death.

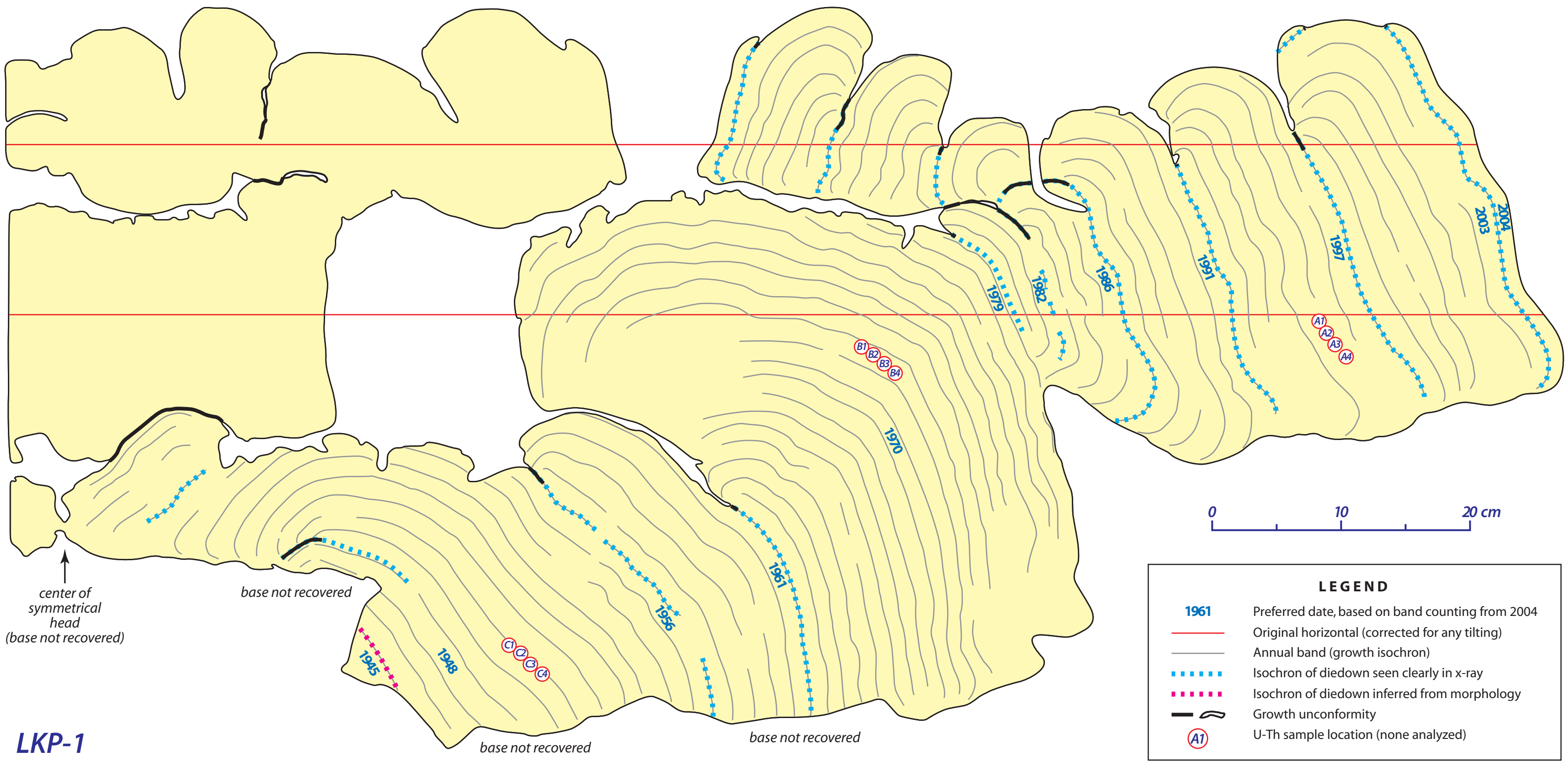

Figure 4a. Cross-section of slab LKP-1, from site LKP-A.

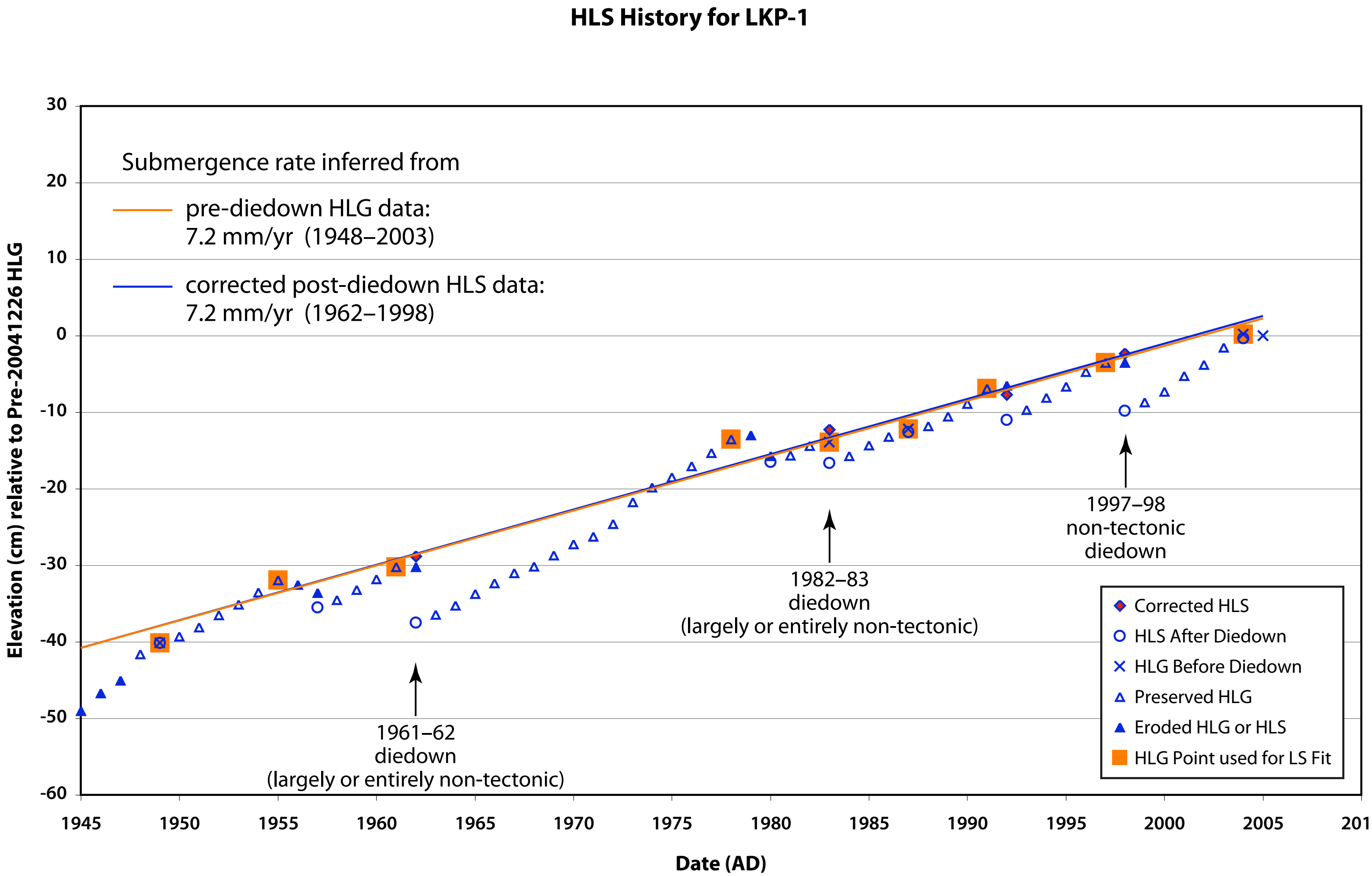

Figure 4b. Graph of relative sea level history derived from slab LKP-1.

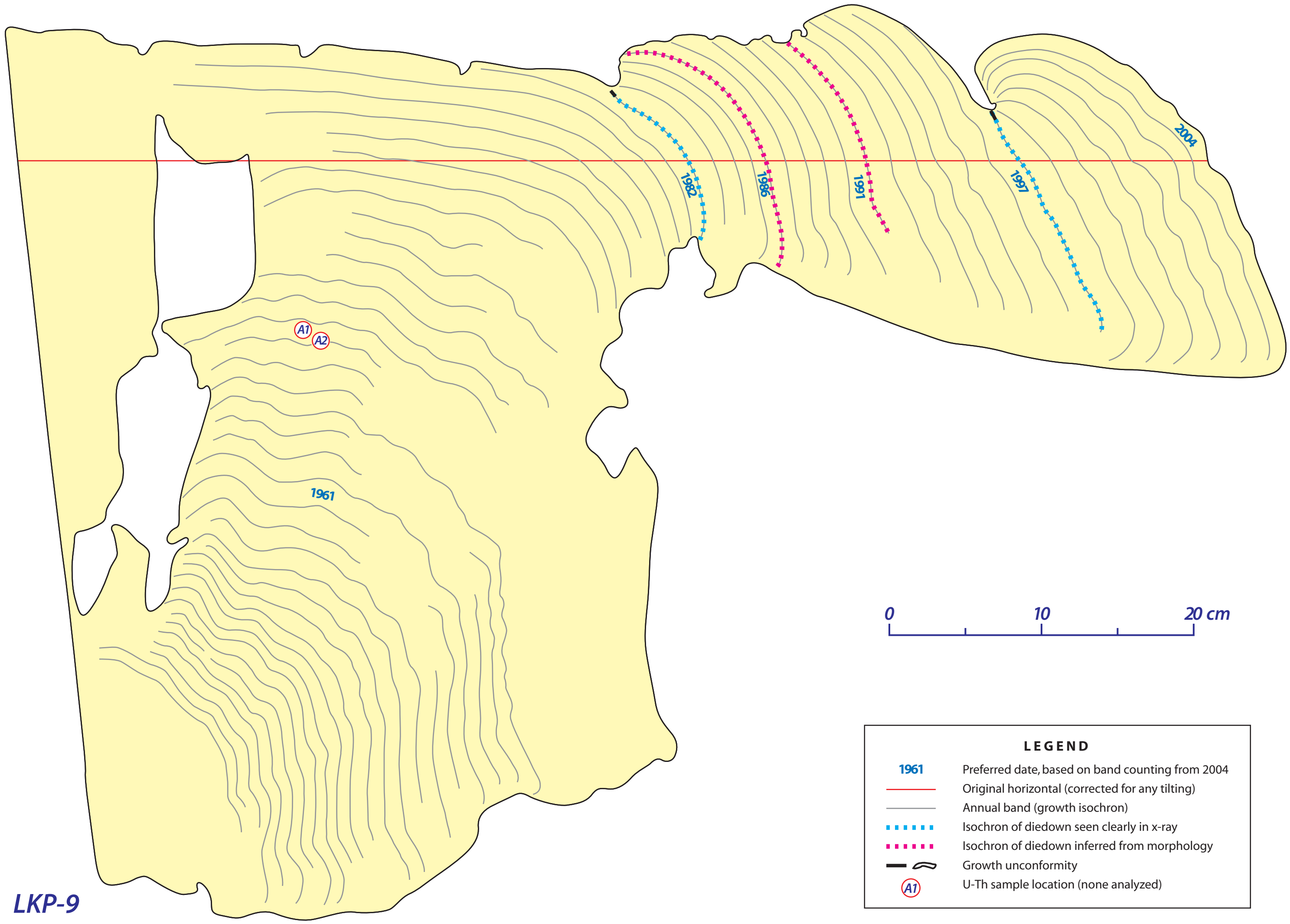

Figure 5a. Cross-section of slab LKP-9, from site LKP-B.

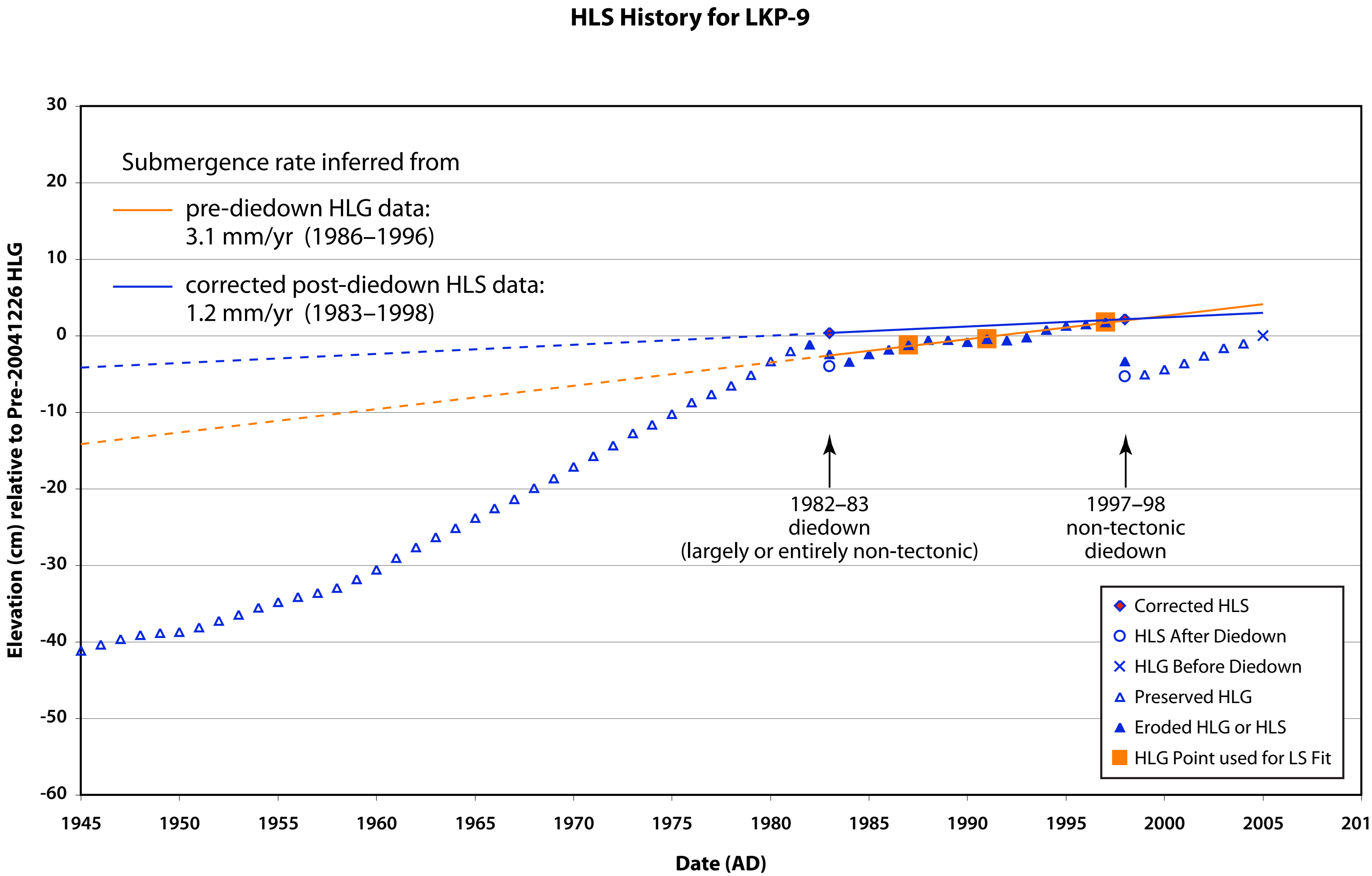

Figure 5b. Graph of relative sea level history derived from slab LKP-9.

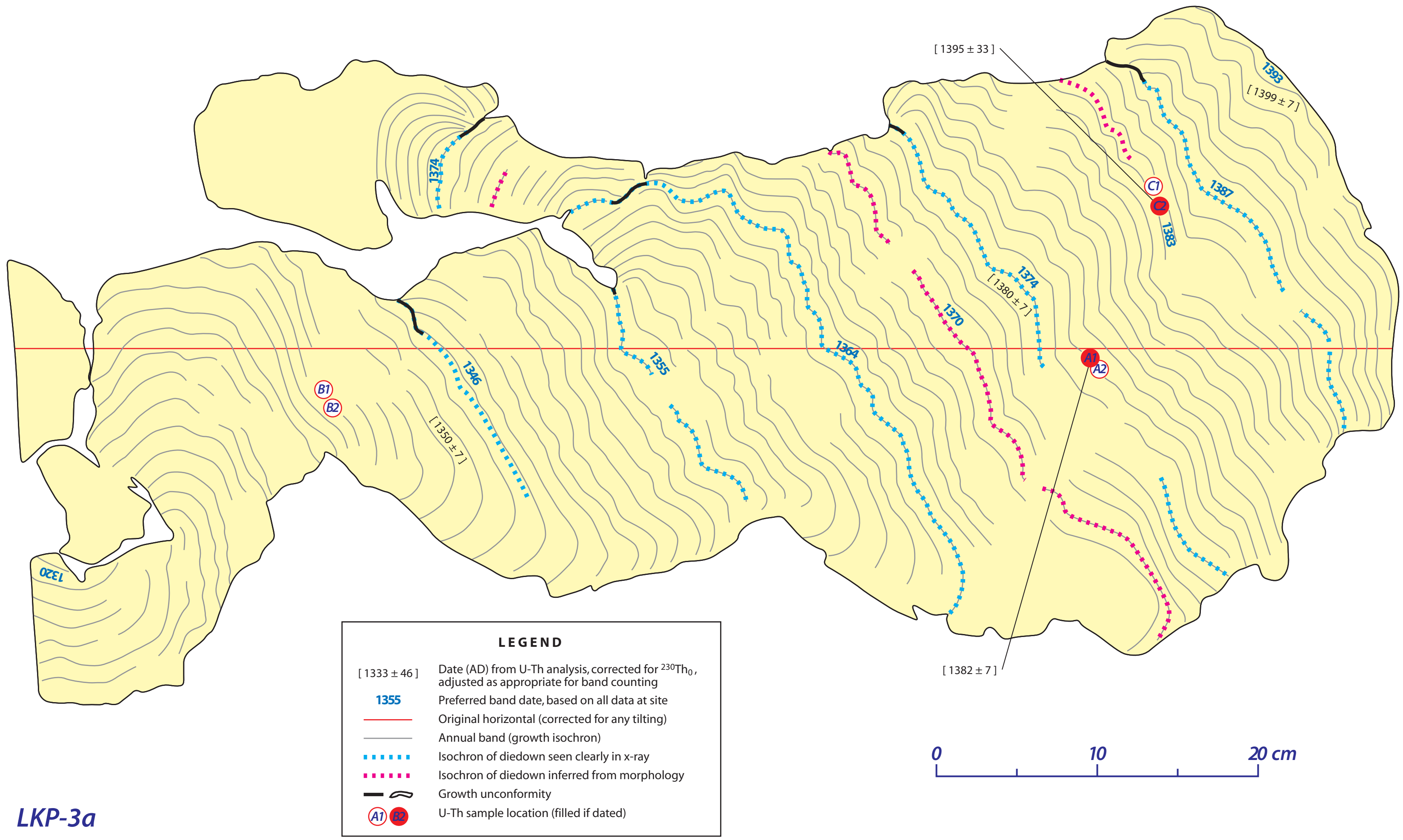

Figure 6a. Cross-section of slab LKP-3 (parallel slice a), from site LKP-B.

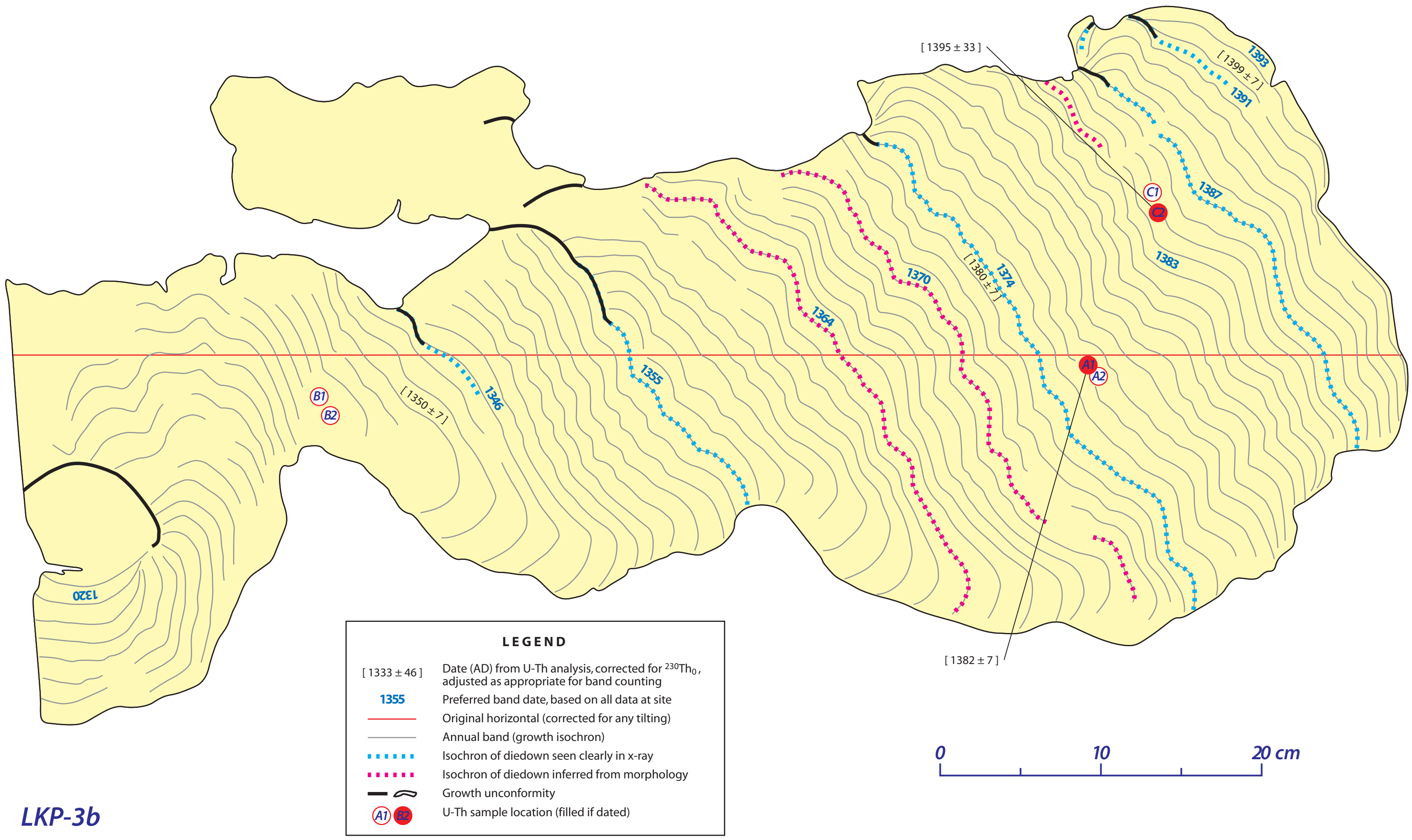

Figure 6b. Cross-section of slab LKP-3 (parallel slice b), from site LKP-B.

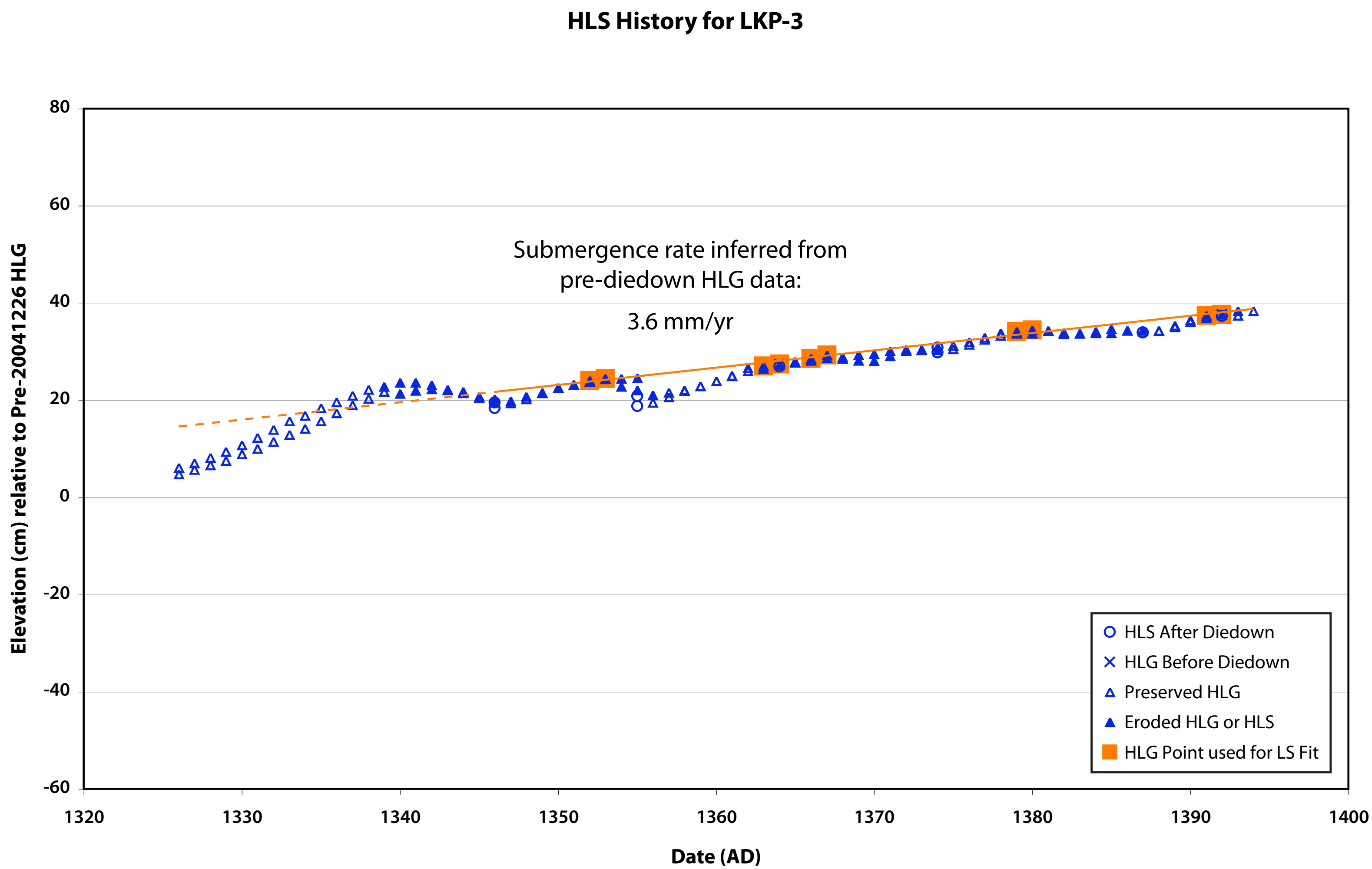

Figure 6c. Graph of relative sea level history derived from slab LKP-3.

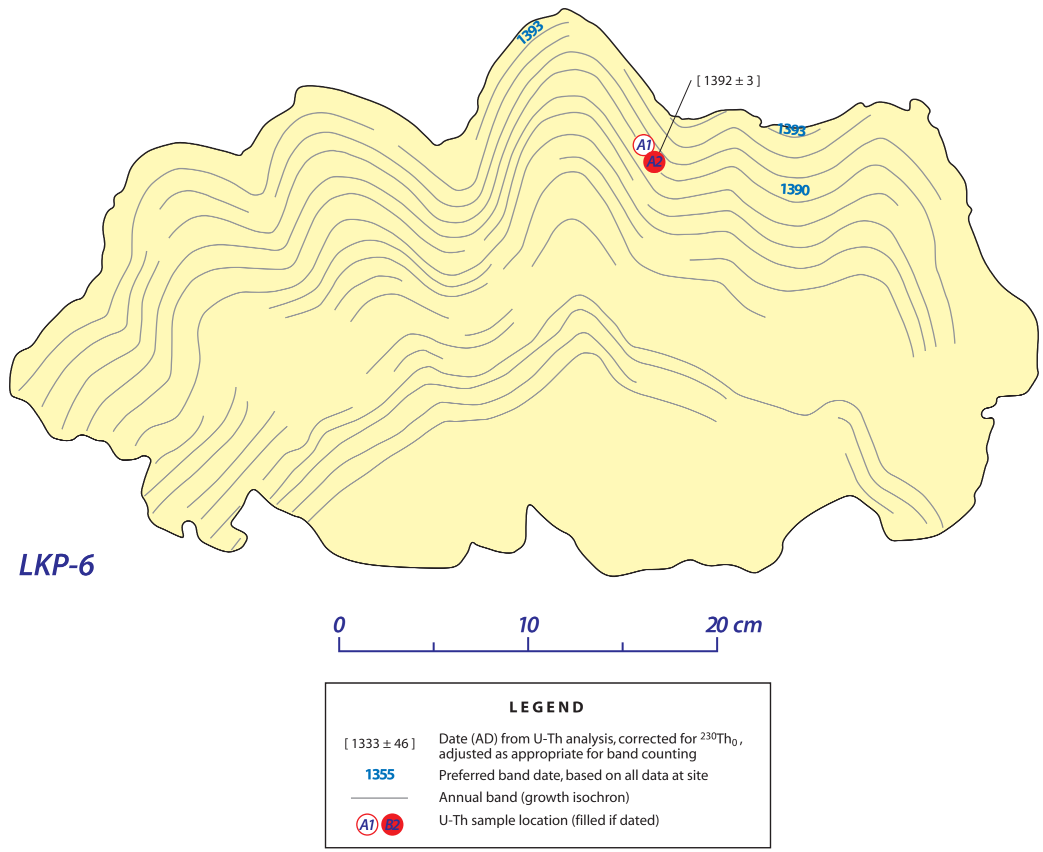

Figure 7. Cross-section of slab LKP-6, from site LKP-B.

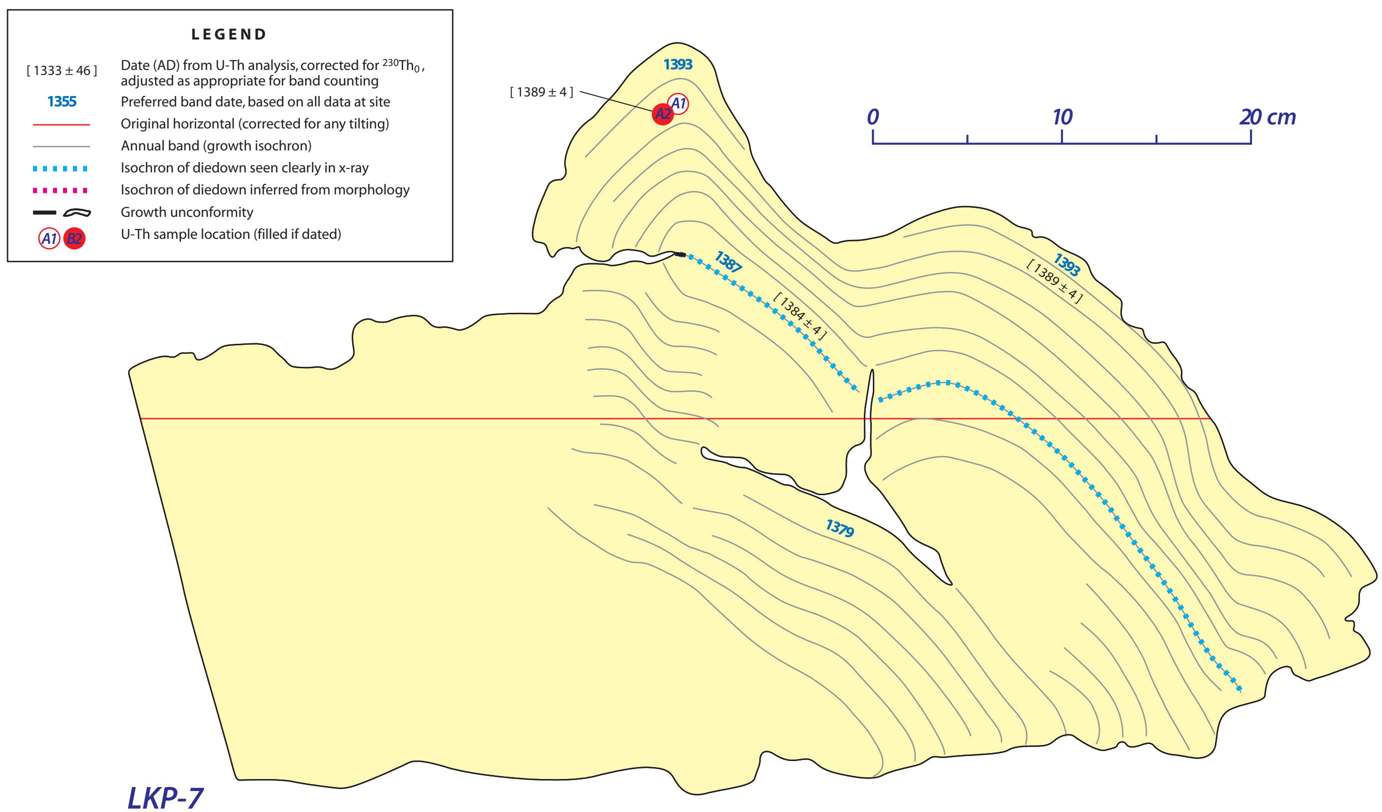

Figure 8a. Cross-section of slab LKP-7, from site LKP-B.

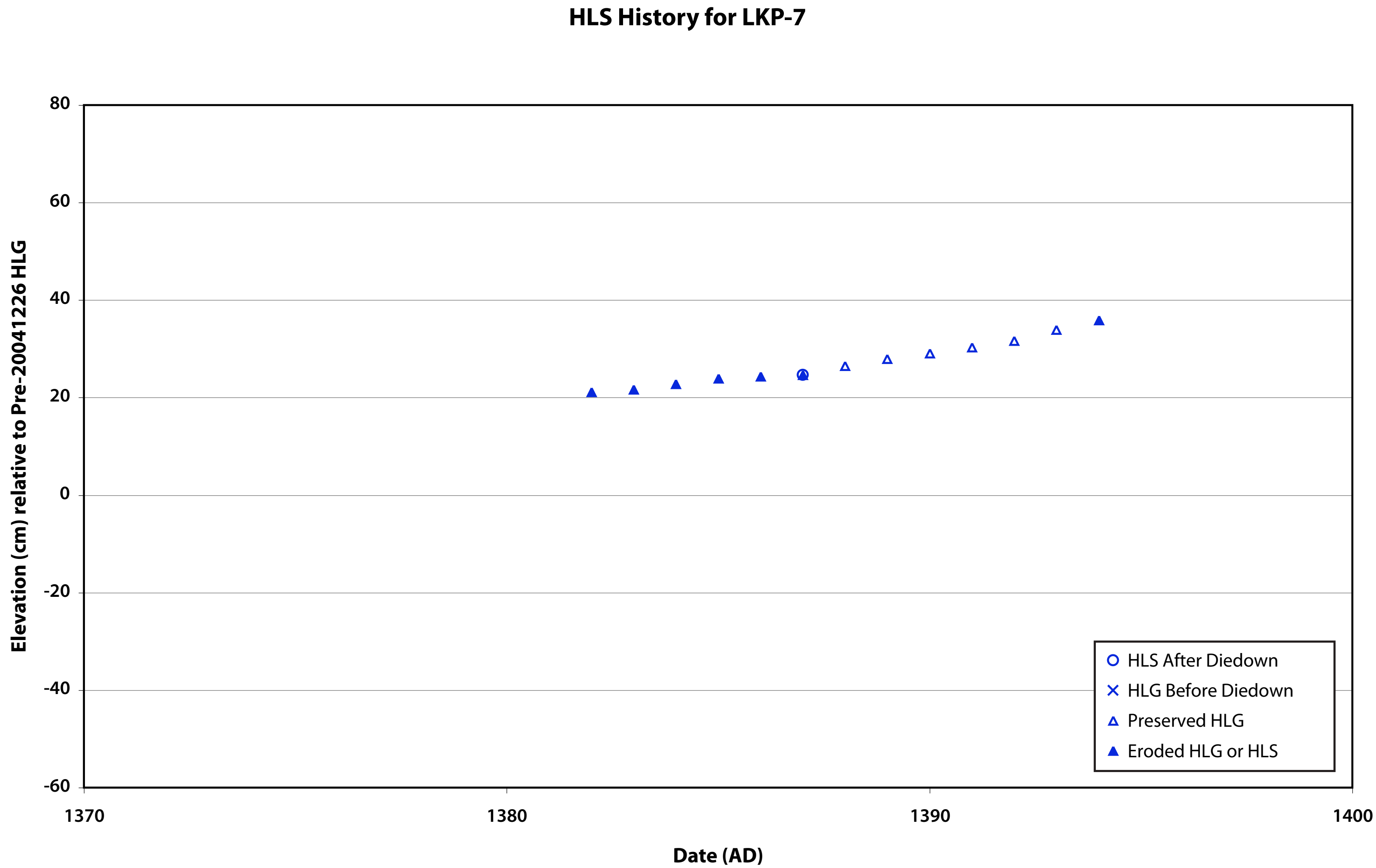

Figure 8b. Graph of relative sea level history derived from slab LKP-7.

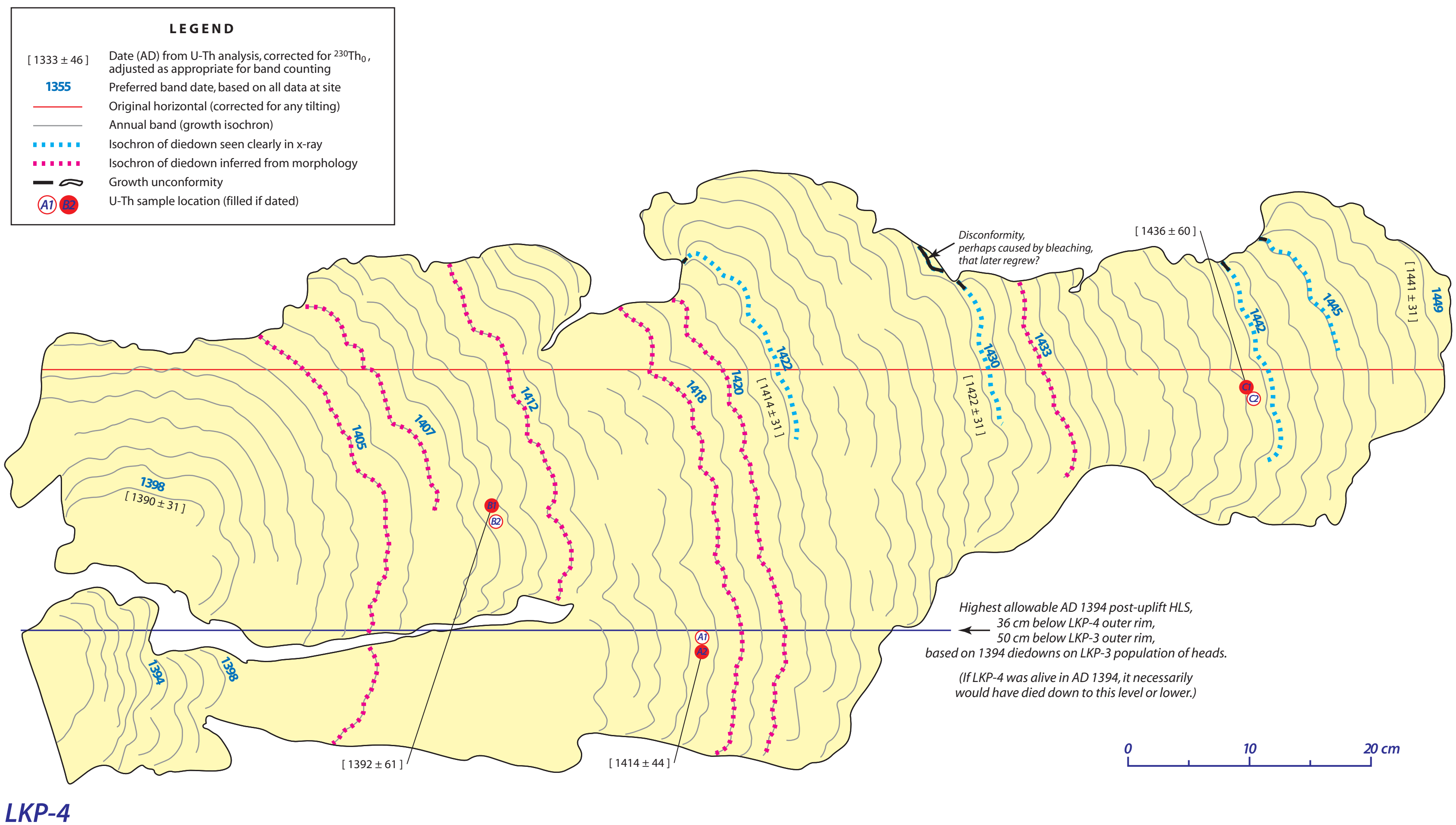

Figure 9a. Cross-section of slab LKP-4, from site LKP-B.

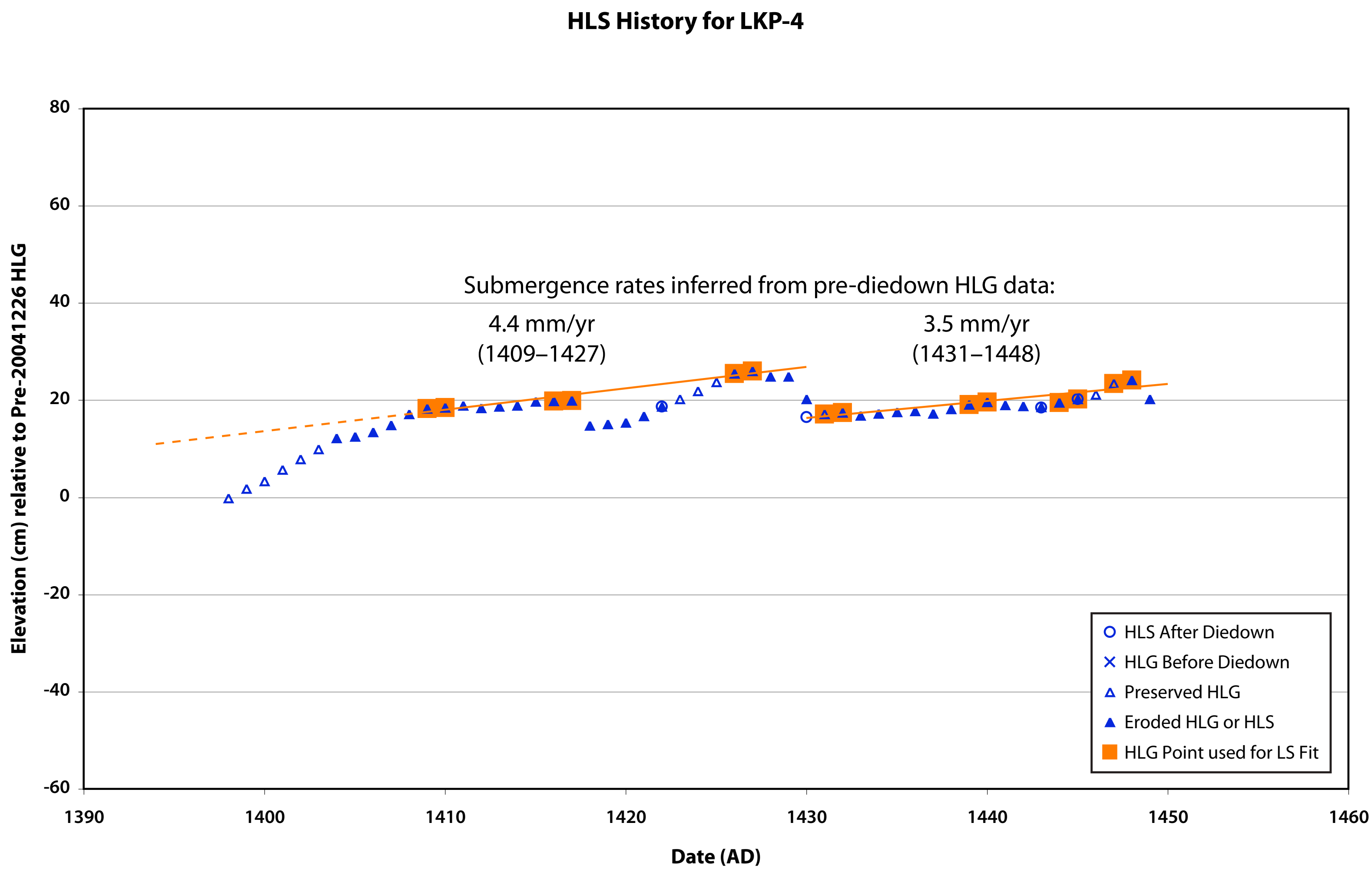

Figure 9b. Graph of relative sea level history derived from slab LKP-4.

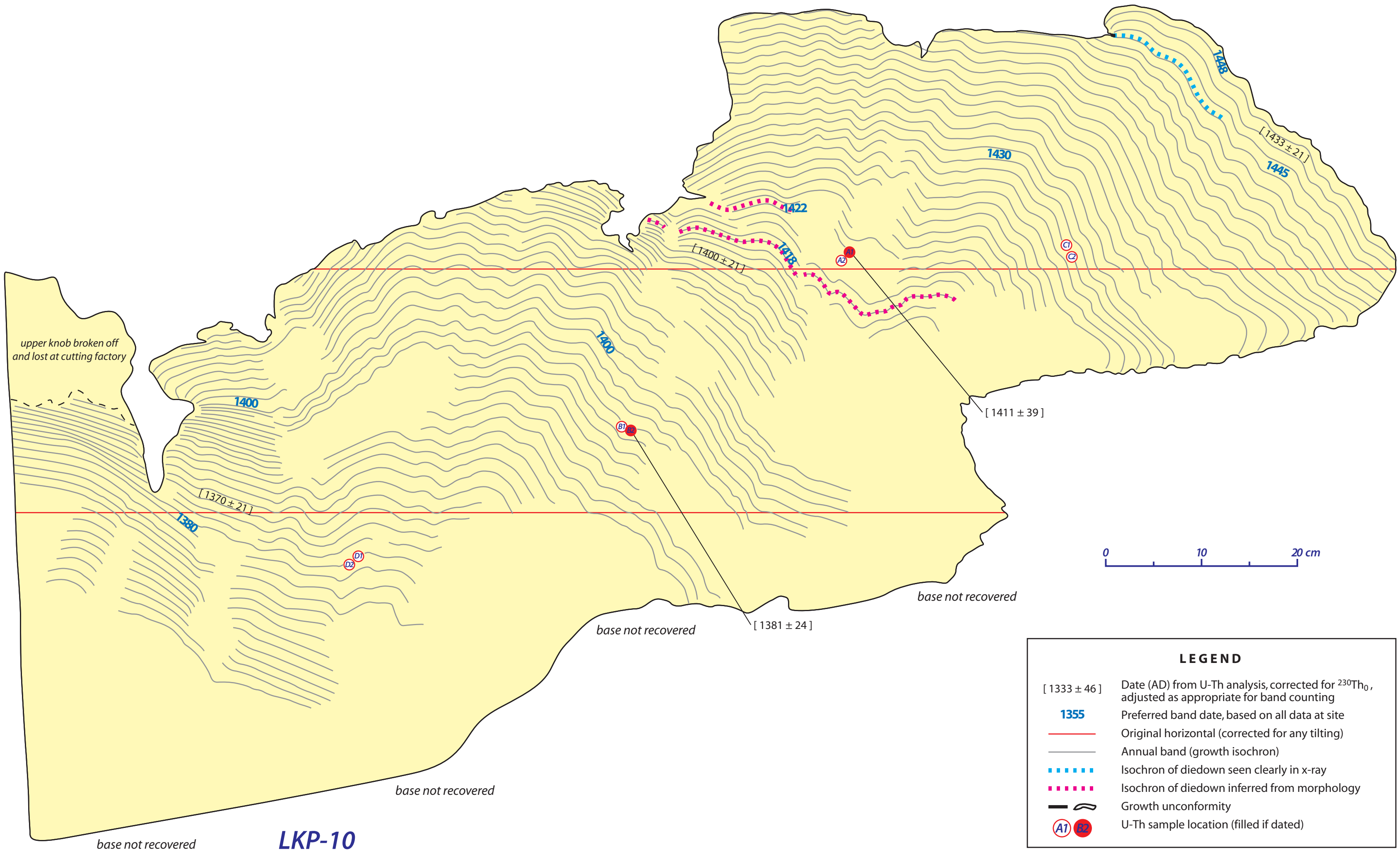

Figure 10a. Cross-section of slab LKP-10, from site LKP-C.

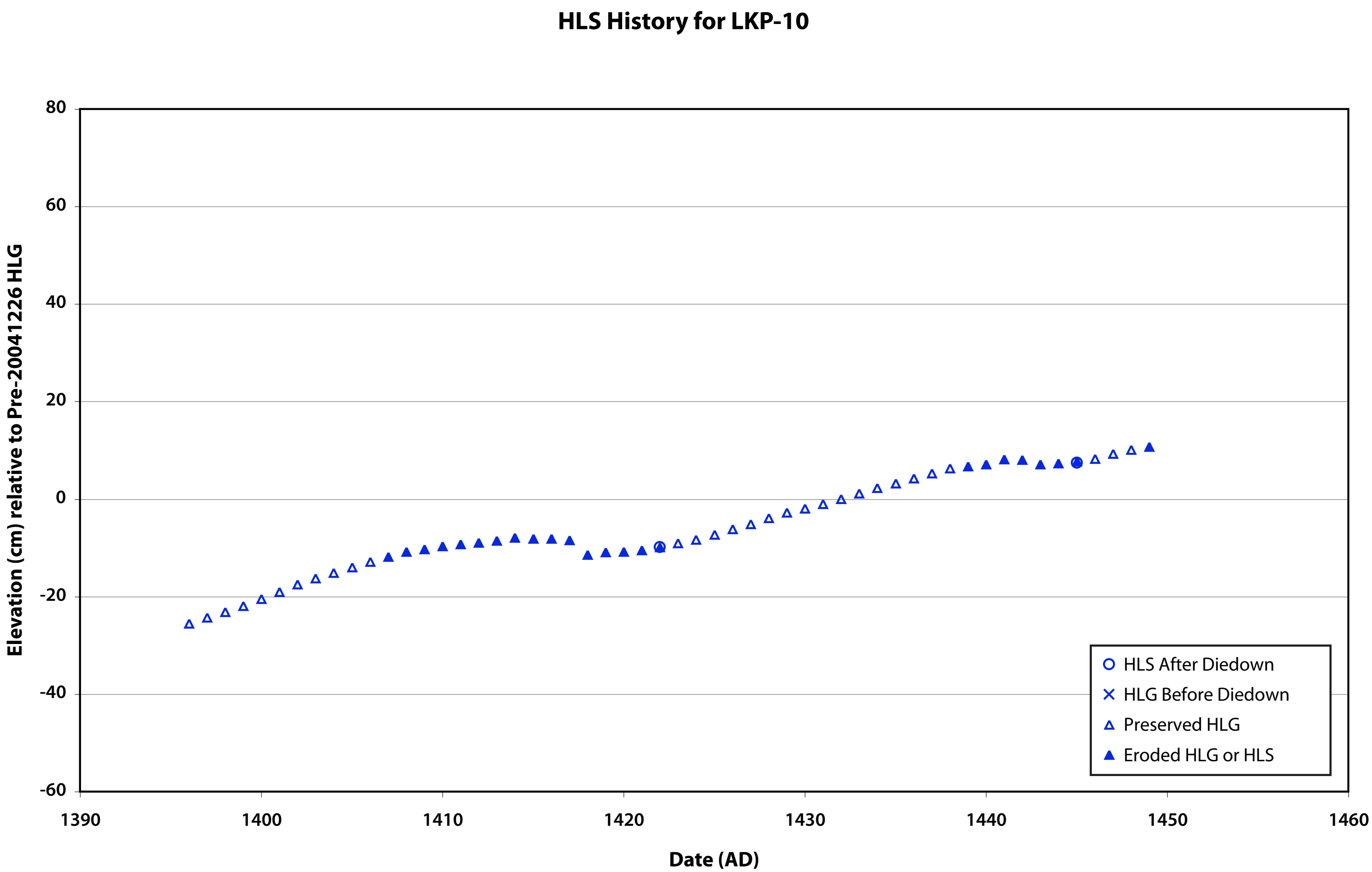

Figure 10b. Graph of relative sea level history derived from slab LKP-10.

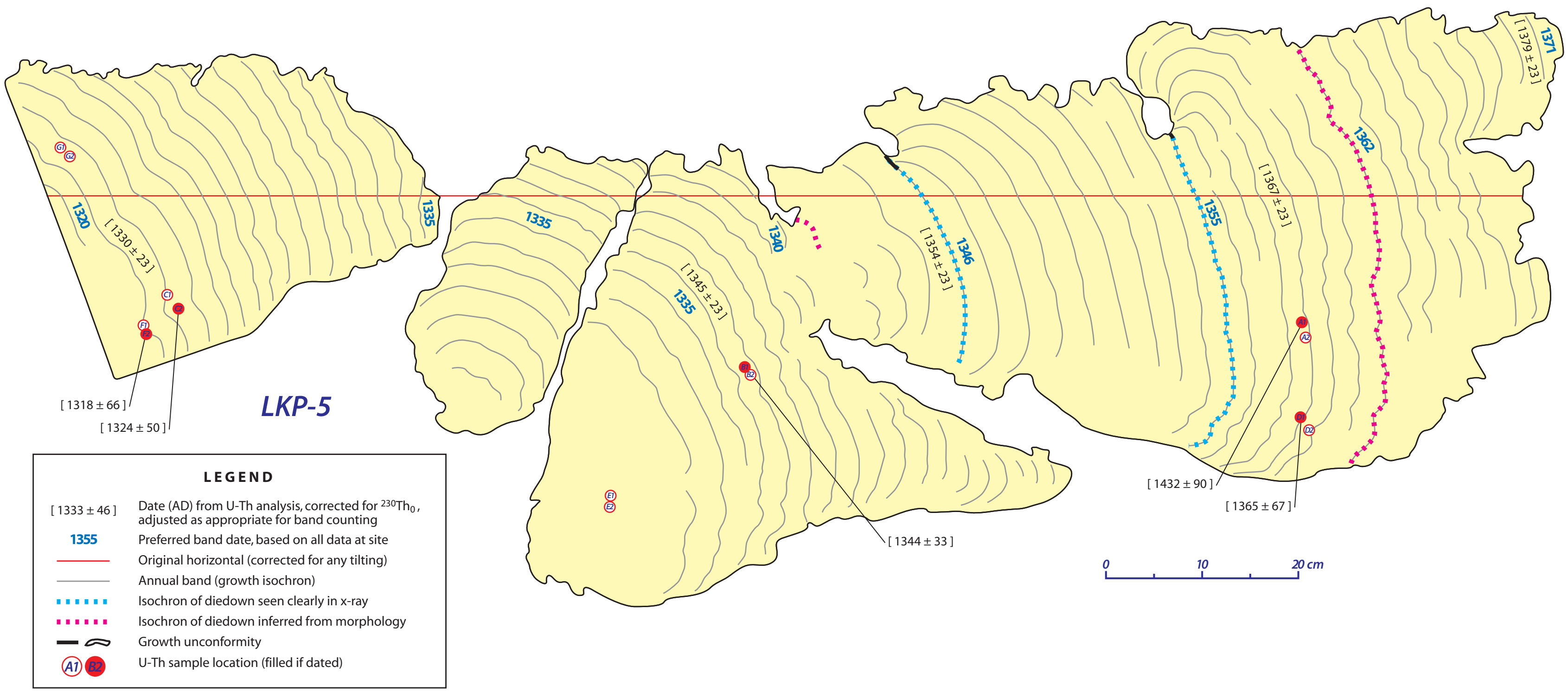

Figure 11a. Cross-section of slab LKP-5, from site LKP-B.

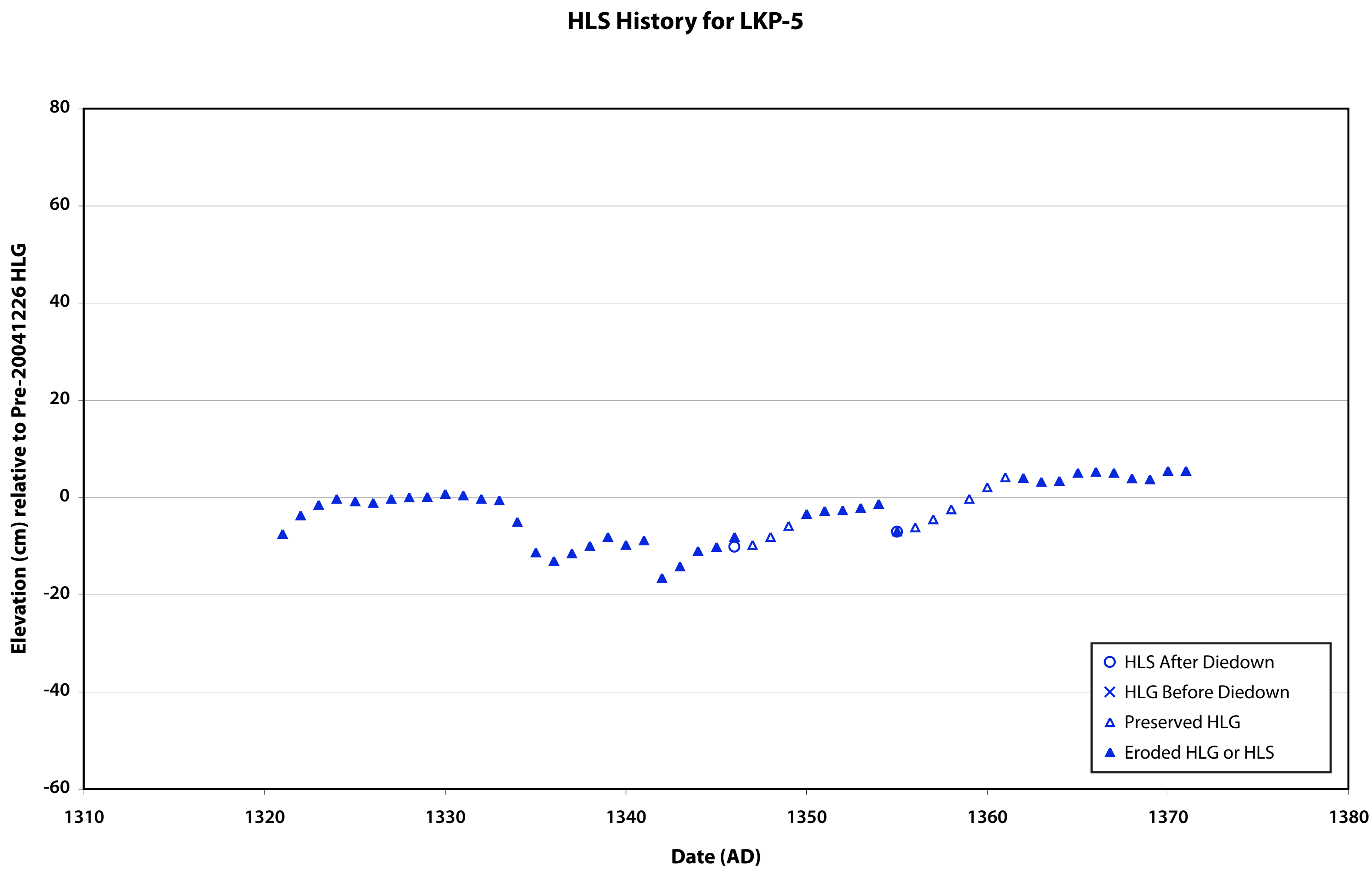

Figure 11b. Graph of relative sea level history derived from slab LKP-5.

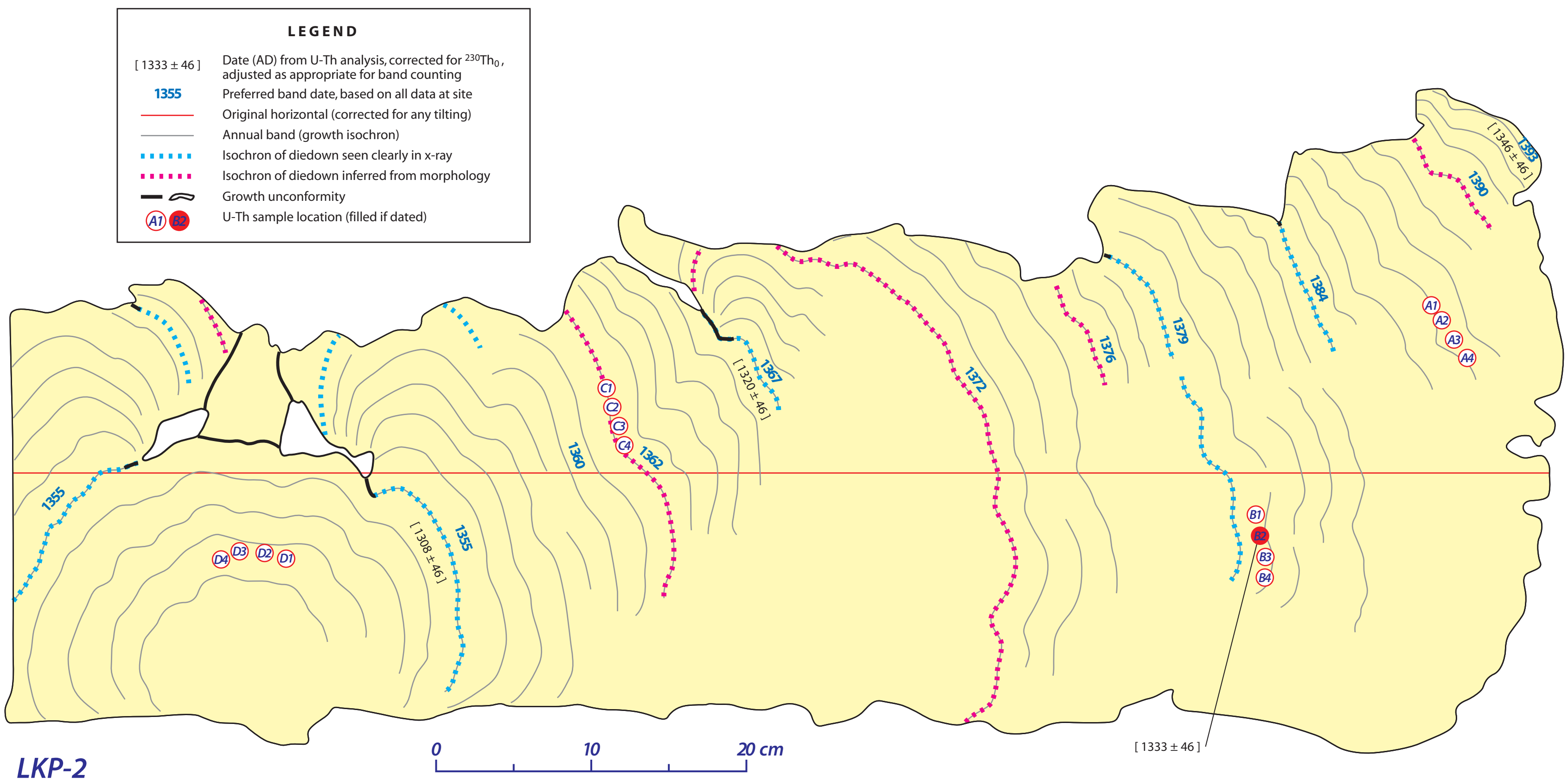

Figure 12a. Cross-section of slab LKP-2, from site LKP-A.

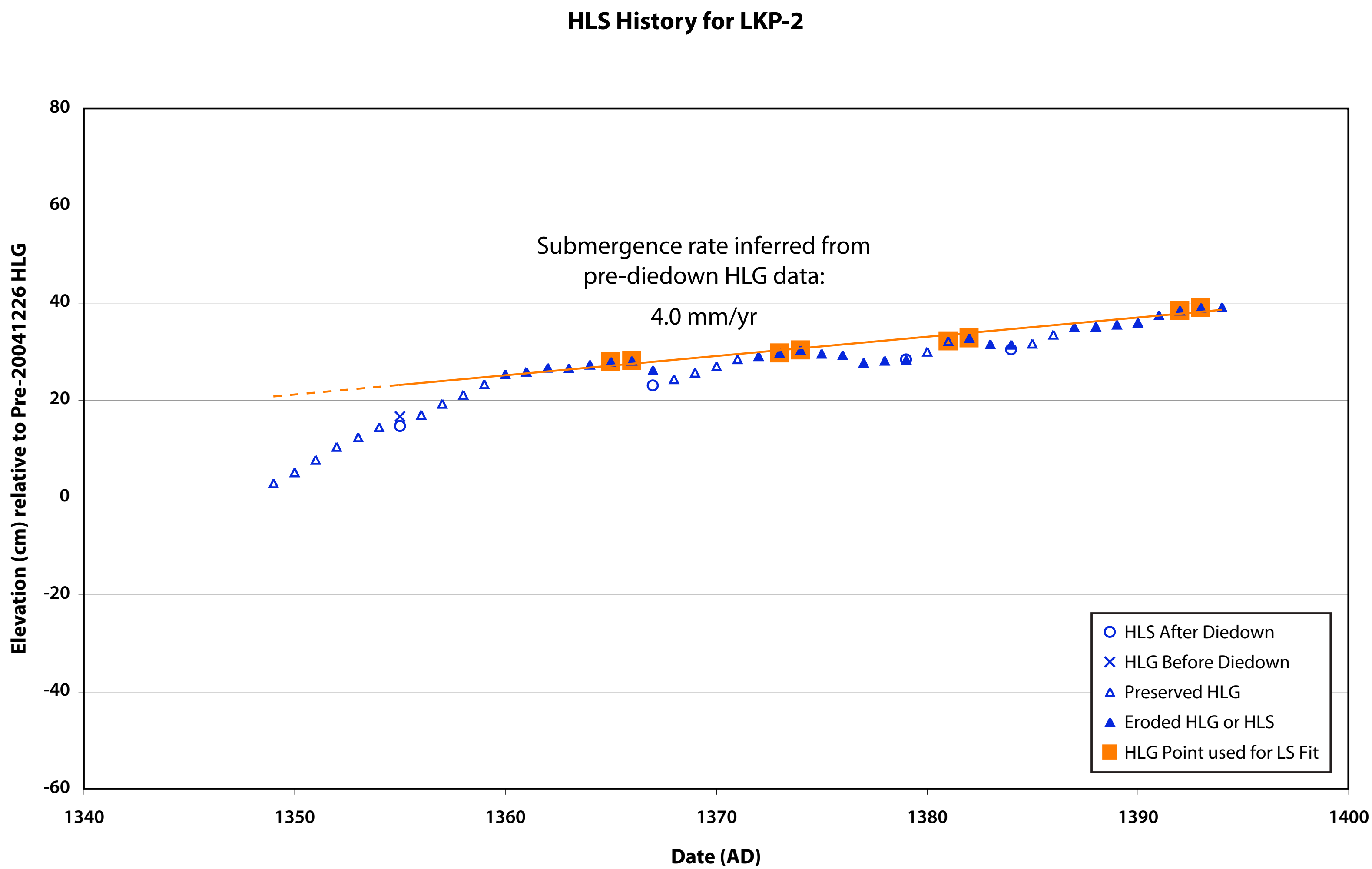

Figure 12b. Graph of relative sea level history derived from slab LKP-2.

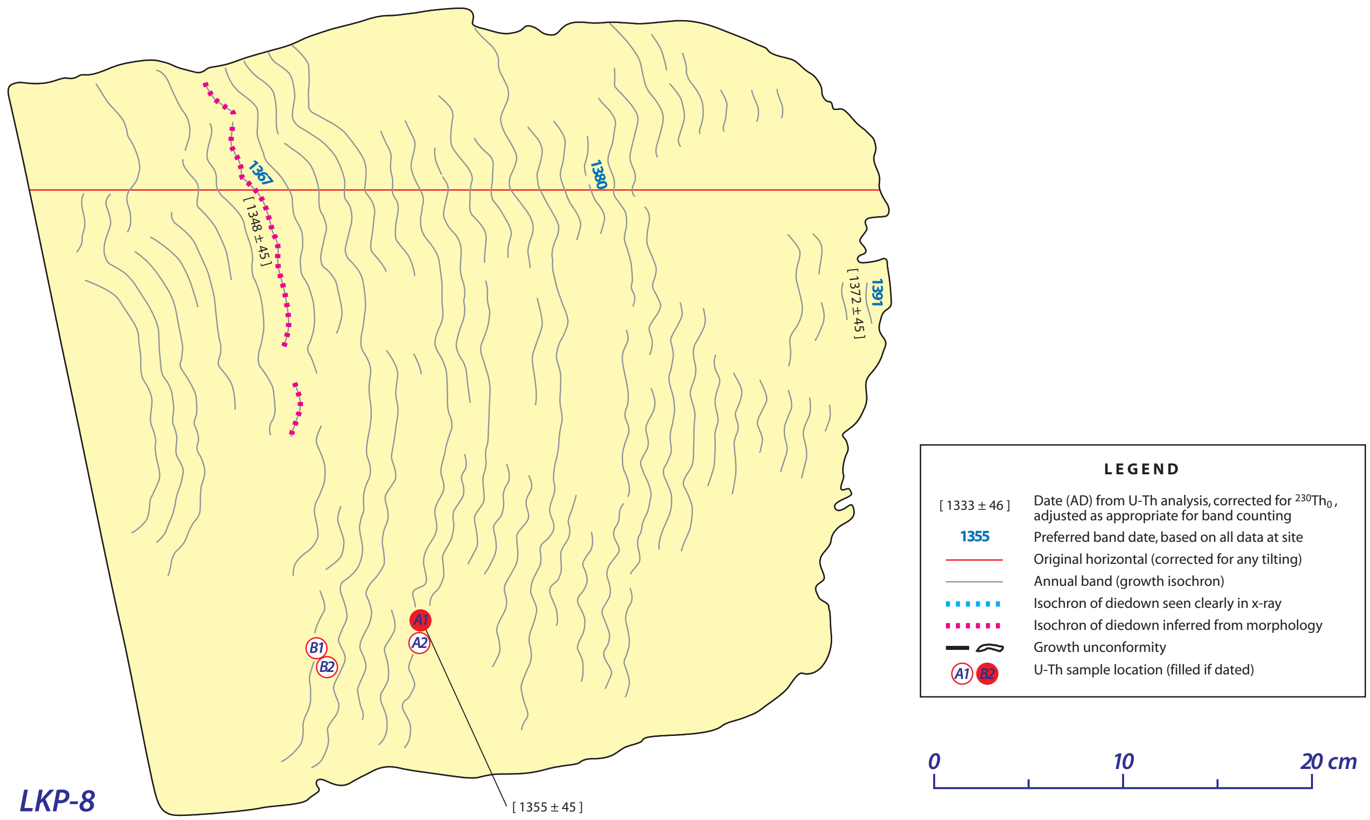

Figure 13a. Cross-section of slab LKP-8, from site LKP-B.

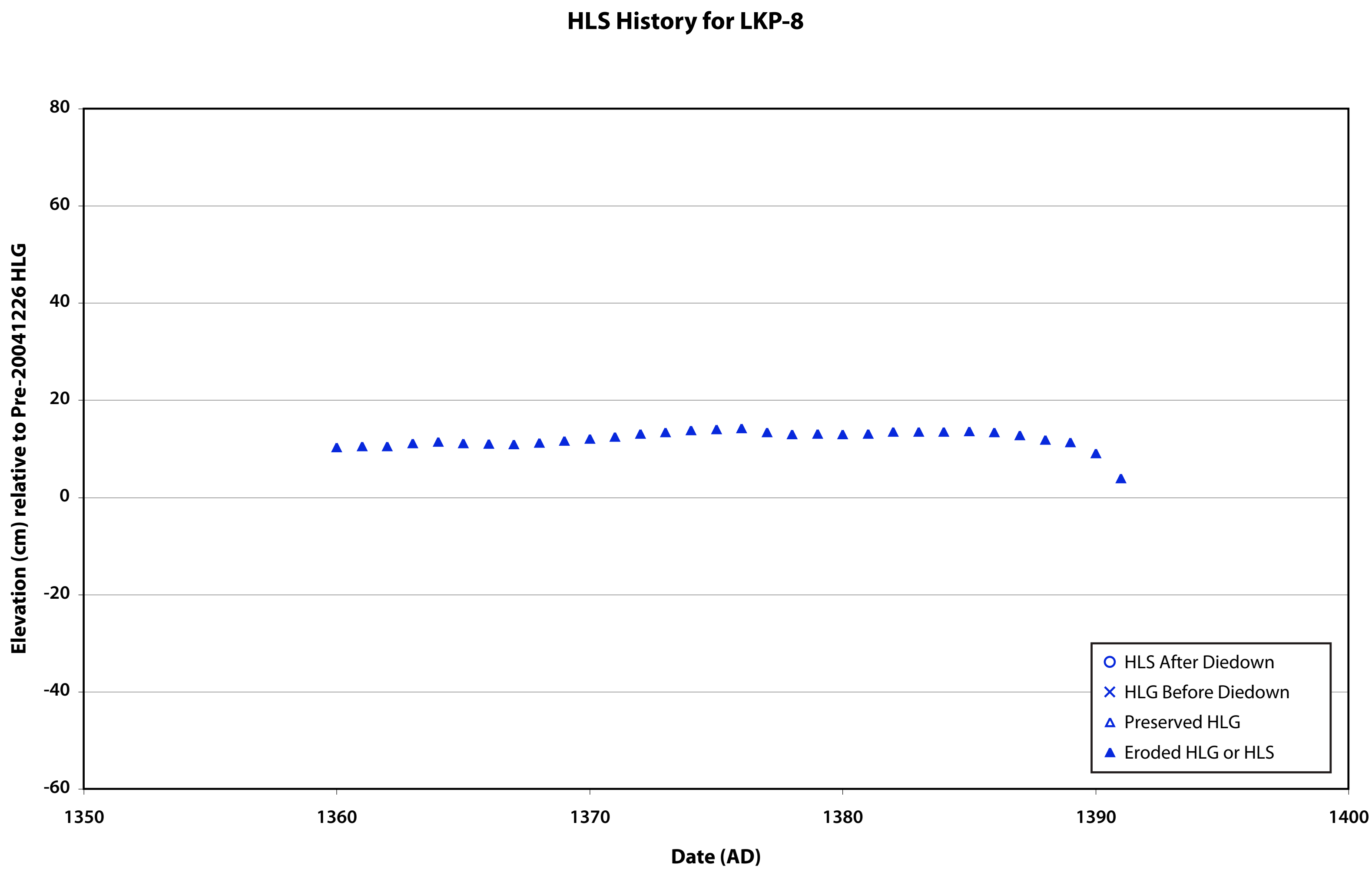

Figure 13b. Graph of relative sea level history derived from slab LKP-8.

Figure 14a. 20th-century relative sea level histories (through 2004) of the LKP-A and LKP-B sites, based respectively on slabs LKP-1 and LKP-9, and post-2004 histories at all LKP sites based on diedowns and/or water level measurements discussed in the text. The elevations of LKP-1 and LKP-9 in any given year are plotted relative to the outer band on the respective head; the elevations of the two heads are not known relative to one another. Plotted in this manner, LKP-9 appears to be 8–10 cm higher than LKP-1 for much of 1962–1998. Some of this difference is an artifact that arises from LKP-9's slower upward growth (compared to LKP-1) from 1998 to 2004; a portion of the difference appears to be real, however, and implies slower interseismic submergence at LKP-B from 1982 (or earlier) through 1997 (or later).

Figure 14b. Relative sea level histories for the 14th–15th centuries at the LKP sites. Interseismic submergence rates at LKP-B, shown in black, are based on LKP-3 and LKP-4; the pre-1394 rate at LKP-A, shown in gray, is based on LKP-2.

Figure 14c. LKP relative sea level history, AD 1320–2009. The relative elevations of microatolls on this plot are those observed in the field; no correction for eustatic sea level change has been made. Rates and elevations are well controlled by data where represented by solid black lines (see Figures 14 a–b for details); where they can be reasonably inferred (pre-1450), dashed black lines are shown. The light blue field represents possible relative sea level histories assuming no earthquakes are missing and submergence occurred steadily at a rate between the maximum and minimum subsidence rates documented at this site; a lower rate cannot be precluded. The red dash-dotted curve is schematic and represents one possible history if earthquakes are missing from the record. Relative sea levels could not have been much higher than the "maximum" elevation for extended periods between 1450 and ~1900 because, in that case, corals would have likely recolonized the reef flats within decades. See text for discussion.

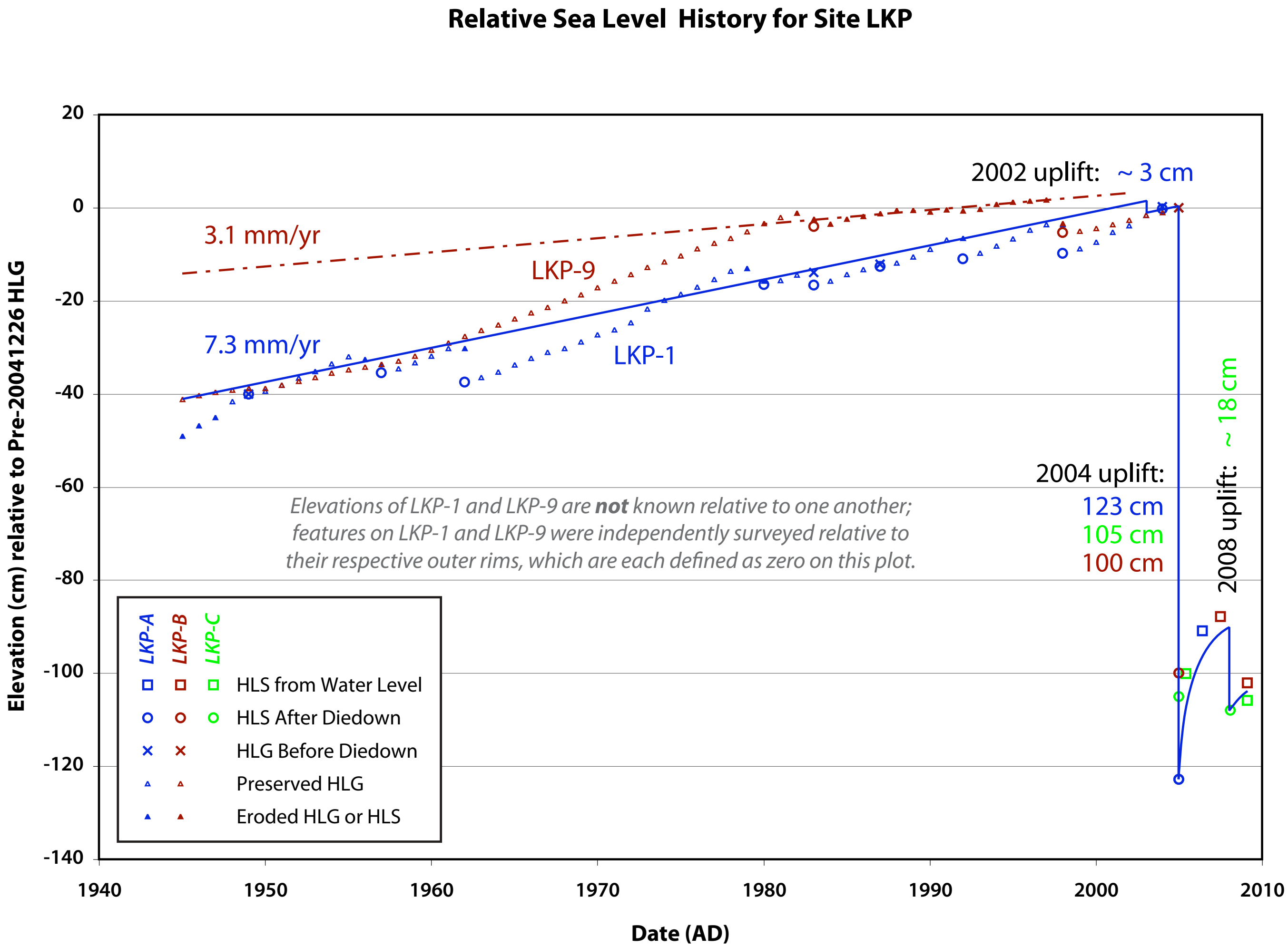
Relative Sea Level History for Site LKP
2002 uplift: ~ 3 cm
3.1 mm/yr
LKP-9
7.3 mm/yr
LKP-1
2004 uplift:
123 cm
105 cm
100 cm
2008 uplift: ~ 18 cm
Elevations of LKP-1 and LKP-9 are not known relative to one another; features on LKP-1 and LKP-9 were independently surveyed relative to their respective outer rims, which are each defined as zero on this plot.
LKP-A
LKP-B
LKP-C
HLS from Water Level
HLS After Diedown
HLG Before Diedown
Preserved HLG
Eroded HLG or HLS
Elevation (cm) relative to Pre-20041226 HLG
Date (AD)
20
0
-20
-40
-60
-80
-100
-120
-140
1940
1950
1960
1970
1980
1990
2000
2010

Figure 14a.

Relative Sea Level History for Site LKP

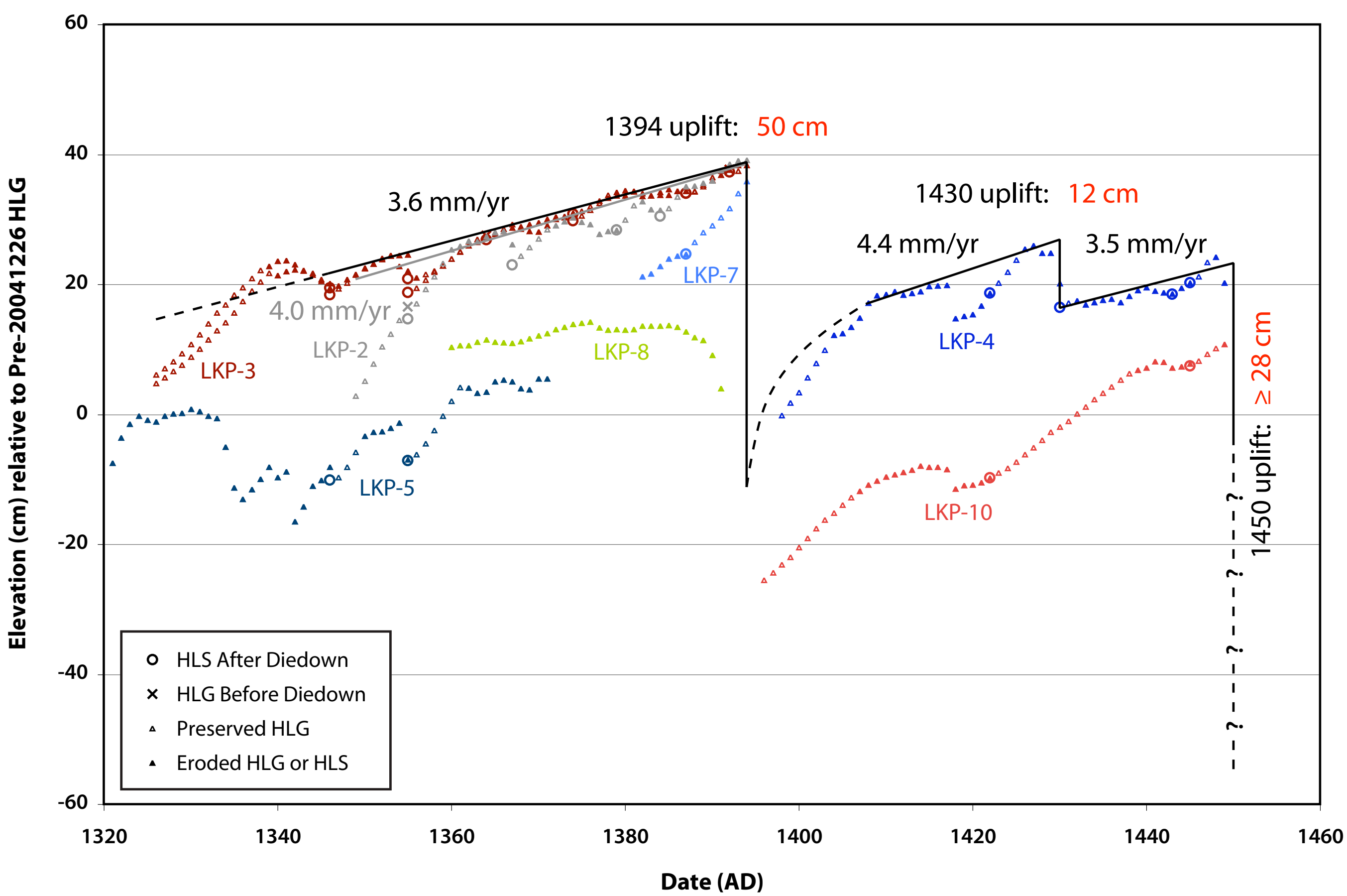

Figure 14b.

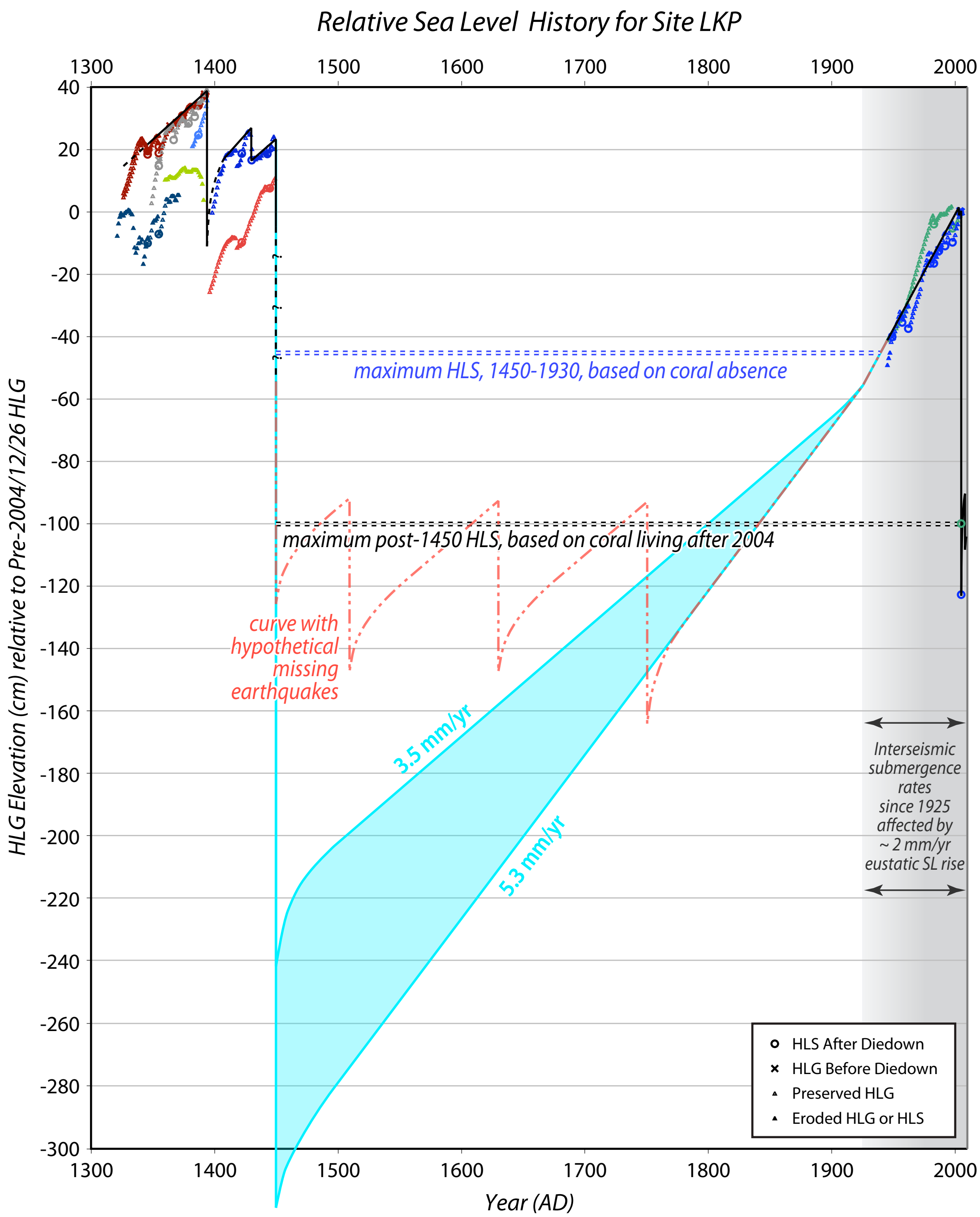
Relative Sea Level History for Site LKP
HLG Elevation (cm) relative to Pre-2004/12/26 HLG
Year (AD)
maximum HLS, 1450-1930, based on coral absence
maximum post-1450 HLS, based on coral living after 2004
curve with hypothetical missing earthquakes
3.5 mm/yr
5.3 mm/yr
Interseismic submergence rates since 1925 affected by ~ 2 mm/yr eustatic SL rise
HLS After Diedown
HLG Before Diedown
Preserved HLG
Eroded HLG or HLS

Figure 14c.

Figure 15. Preferred relative sea level histories through the 14th–15th centuries at sites (**A**) Lhok Dalam, (**B**) Lhok Pauh, and (**C**) Lewak. No corrections for eustatic sea level change have been made. Data from coral microatolls at these sites are shown. Where these data reasonably constrain the history of interseismic submergence and coseismic emergence, the black curve is solid; where the history is inferred, it is dashed. Uplift amounts (in cm) are labeled in red. Interseismic submergence rates (in mm/yr) are indicated in blue. Vertical gray lines mark dates of uplifts. Fourteenth-century microatoll elevations at Lhok Dalam are shown as we observed them in the field, but the 14th-century relative sea level history is not known relative to 2004 elevations because none of the 14th-century heads at the site were in place.

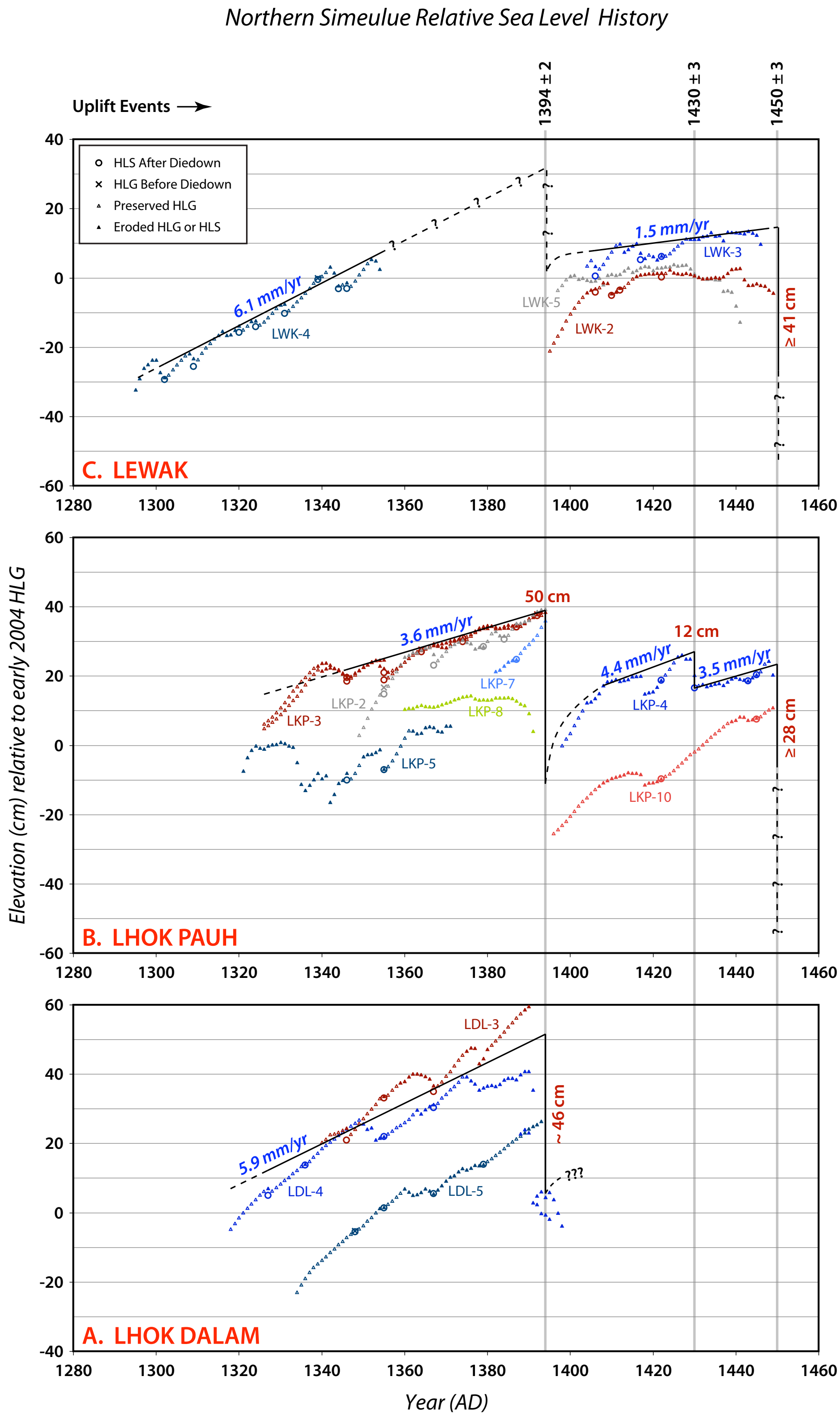
Northern Simeulue Relative Sea Level History
Uplift Events
1394 ± 2
1430 ± 3
1450 ± 3
HLS After Diedown
HLG Before Diedown
Preserved HLG
Eroded HLG or HLS
6.1 mm/yr
1.5 mm/yr
LWK-4
LWK-5
LWK-2
LWK-3
≥ 41 cm
C. LEWAK
50 cm
3.6 mm/yr
12 cm
4.4 mm/yr
3.5 mm/yr
LKP-2
LKP-3
LKP-5
LKP-7
LKP-8
LKP-4
LKP-10
≥ 28 cm
B. LHOK PAUH
LDL-3
5.9 mm/yr
LDL-4
LDL-5
~ 46 cm
???
A. LHOK DALAM
Elevation (cm) relative to early 2004 HLG
Year (AD)

Figure 15.

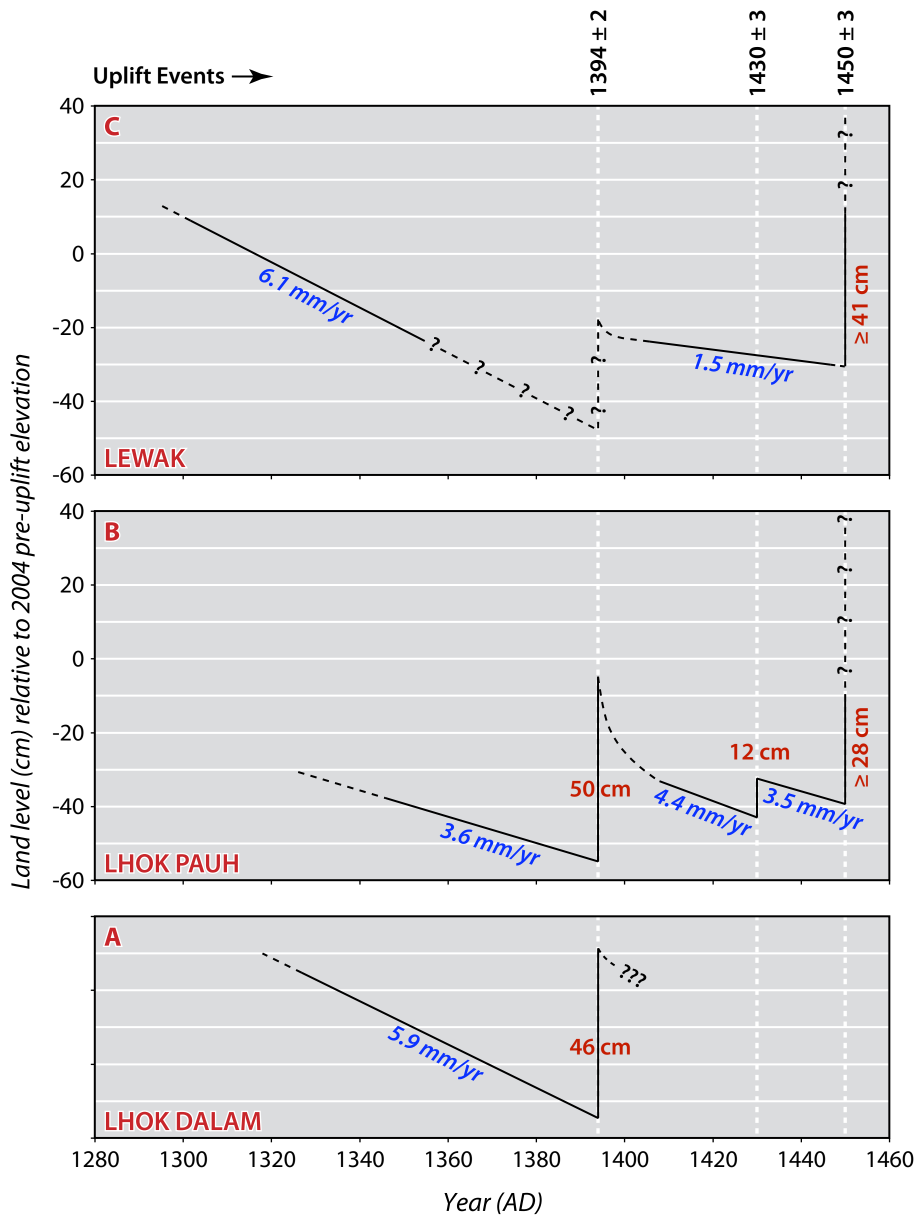

Figure 16. Histories of interseismic subsidence and coseismic uplift through the 14th–15th centuries at sites (**A**) Lhok Dalam, (**B**) Lhok Pauh, and (**C**) Lewak. Data constrain solid parts of the curves well (cf. Figure 15); dashed portions are inferred. Uplift amounts (in centimeters) are red. Interseismic subsidence rates (in millimeters per year) are blue. Vertical dotted white lines mark dates of uplifts. (**B–C**) The zero elevation datum at each site is the site's elevation immediately prior to the 2004 uplift, corrected as described in the text for eustatic sea-level rise since the 20th century. Fourteenth-century elevations at Lhok Dalam (**A**) are not known relative to 2004 elevations because none of the 14th-century heads at the site were in place.

Figure 17. (*Top*) History of interseismic subsidence and coseismic uplift for AD 1320–2009 at Lhok Pauh. The rates and elevations shown have been inverted from Figure 14c and corrected for eustatic sea-level rise as discussed in the text; for uncorrected elevations and original data, see Figure 14. Data constrain solid black parts of the curves well. The light blue field represents possible elevation histories assuming no earthquakes are missing and subsidence occurred steadily at a rate between the maximum and minimum rates documented at this site; a lower rate cannot be precluded. The red dash-dotted curve is schematic and represents one possible history if earthquakes are missing from the record. Land levels could not have been much lower than the "minimum" elevation for extended periods between 1450 and ~1900 because, in that case, corals would have likely recolonized the reef flats within decades. (*Bottom*) Time line summarizing paleotsunami and historical data discussed in the text. At Phra Thong and Meulaboh, bars indicate possible ages of identified tsunami deposits. Dates of voyagers' visits to Aceh indicated. MP: Marco Polo. IB: Ibn Battuta. ZH: Zheng He (Ming voyages). See text for details.

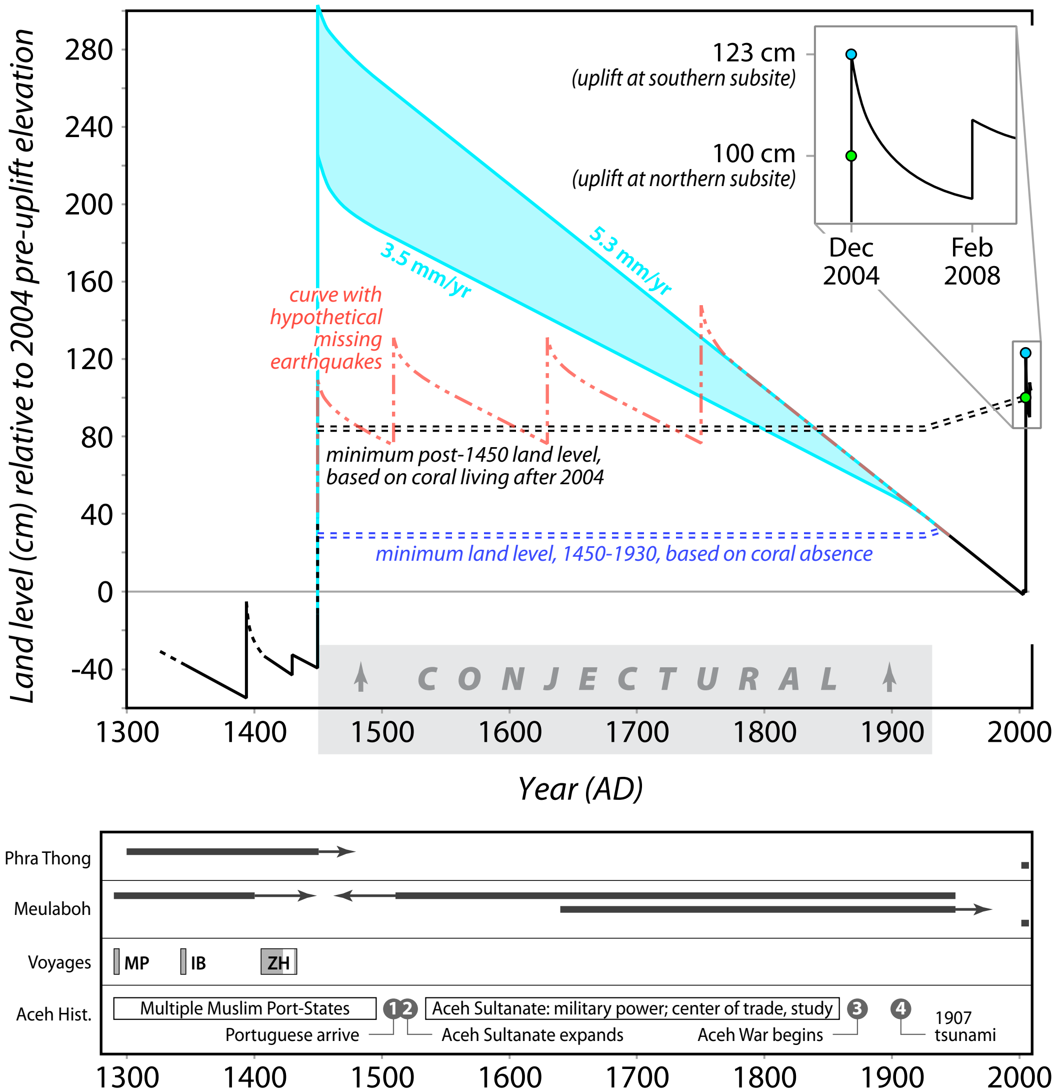

Land level (cm) relative to 2004 pre-uplift elevation
280
240
200
160
120
80
40
0
-40
123 cm
(uplift at southern subsite)
100 cm
(uplift at northern subsite)
Dec 2004
Feb 2008
5.3 mm/yr
3.5 mm/yr
curve with hypothetical missing earthquakes
minimum post-1450 land level, based on coral living after 2004
minimum land level, 1450-1930, based on coral absence
CONJECTURAL
1300
1400
1500
1600
1700
1800
1900
2000
Year (AD)
Phra Thong
Meulaboh
Voyages
MP
IB
ZH
Aceh Hist.
Multiple Muslim Port-States
Aceh Sultanate: military power; center of trade, study
1
2
3
4
Portuguese arrive
Aceh Sultanate expands
Aceh War begins
1907 tsunami

Figure 17.

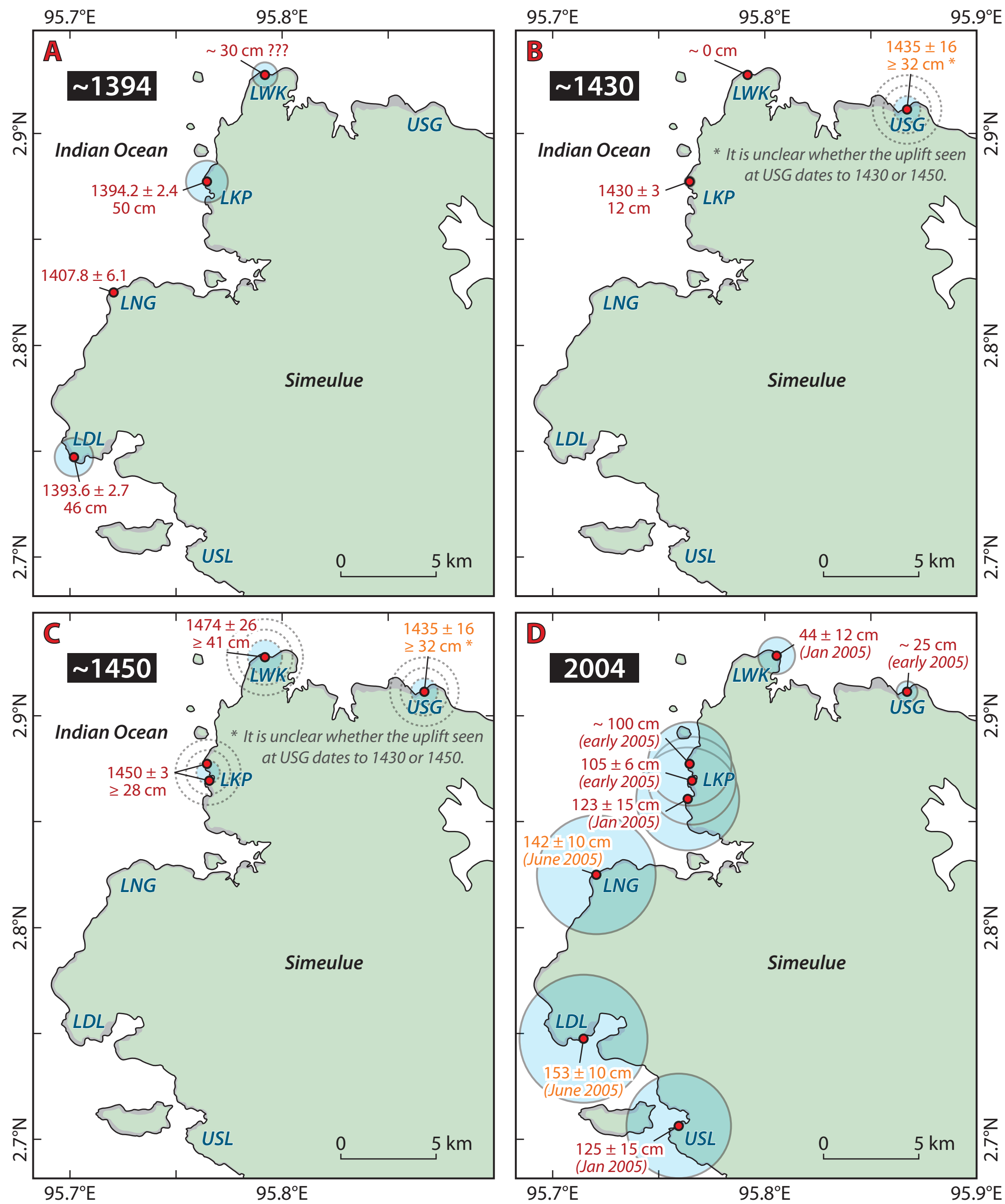

Figure 18.
Maps of coseismic uplift in the (**A**) 1394, (**B**) 1430, (**C**) 1450, and (**D**) 2004 events. (**A–C**) Uplift amounts are below the date of emergence (± 2σ) determined at each site. (**D**) Uplift attributed to the 2004 earthquake, plus any postseismic vertical motion that had occurred as of the date indicated; see text for details. (**A–D**) If no uplift amount is provided, then no data are available. Blue circle diameters are proportional to uplift. Concentric dotted circles emphasize cases where only a minimum bound on uplift is known; actual uplift may be considerably higher.

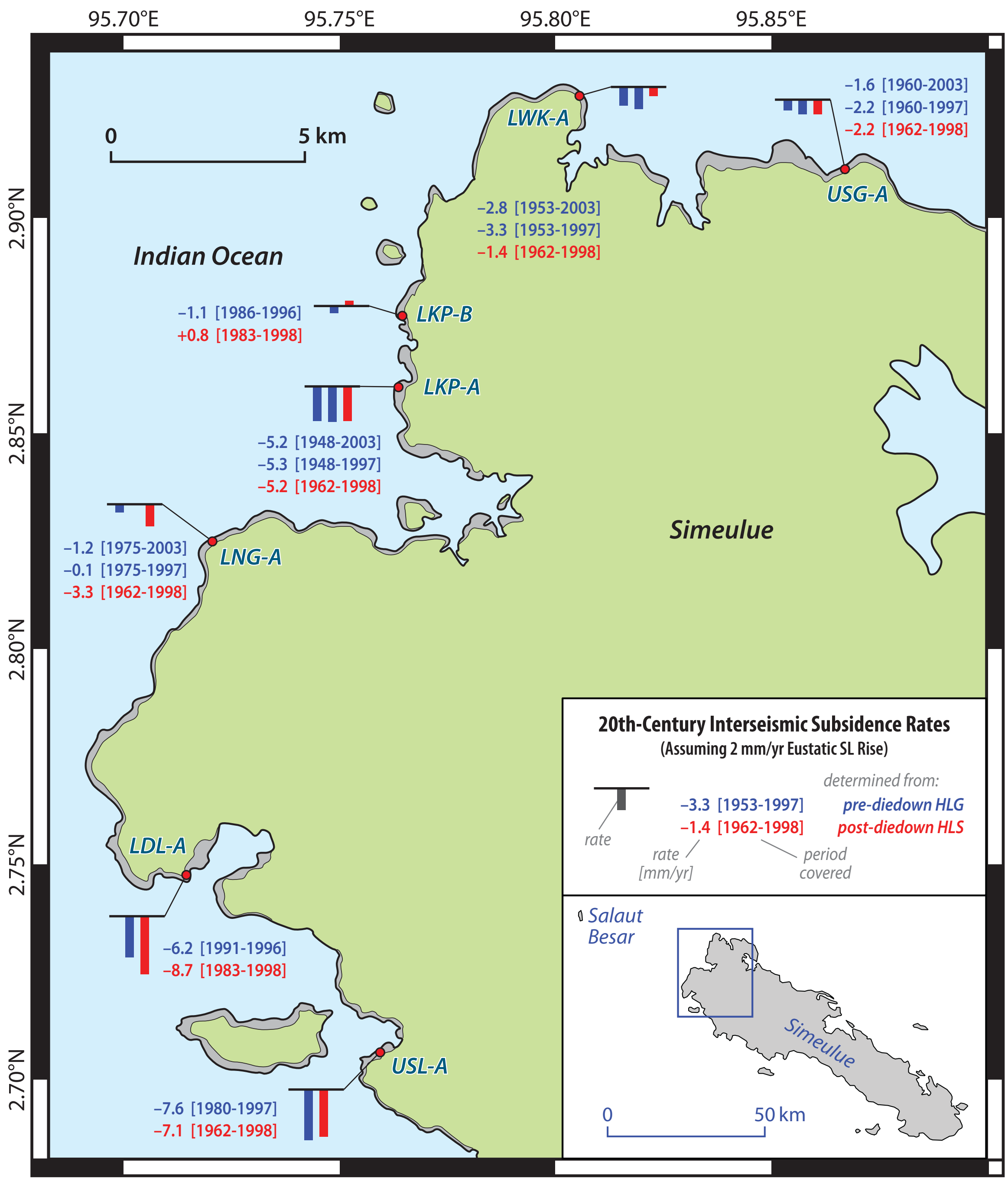

Figure 19. Pre-2004 interseismic subsidence rates at northern Simeulue paleogeodesy sites.

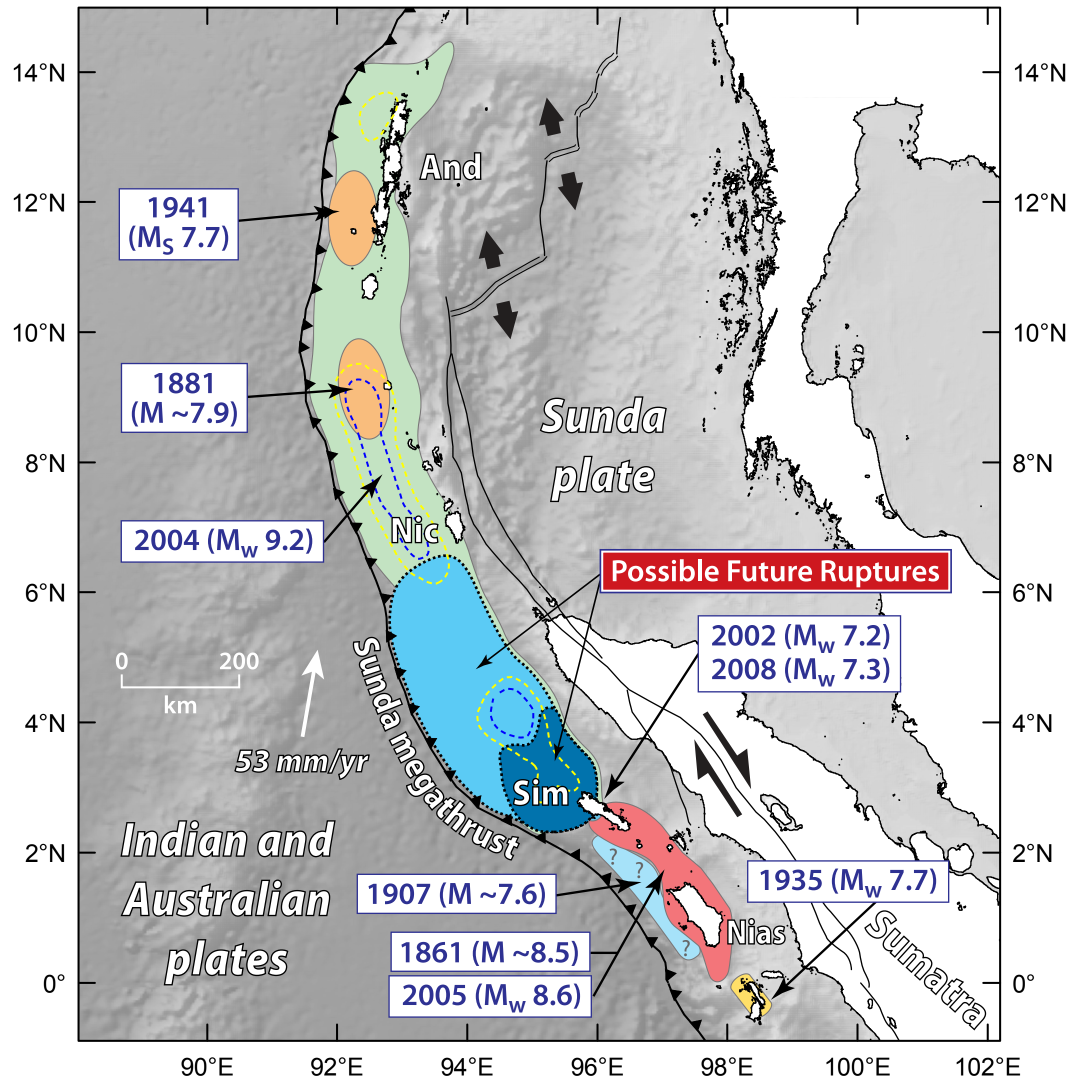

Figure 20. Regional map showing the 26 December 2004 rupture and plausible sources for future large Sunda megathrust ruptures discussed in the text. Compare to Figure 1.

References

Abram, N. J., M. K. Gagan, M. T. McCulloch, J. Chappell, and W. S. Hantoro (2003), Coral reef death during the 1997 Indian Ocean Dipole linked to Indonesian wildfires, *Science*, 301, 952-955, doi:10.1126/science.1083841.

Agnew, D. C. (1997), NLOADF: A program for computing ocean-tide loading, *J. Geophys. Res.*, 102, 5109-5110, doi:10.1029/96JB03458.

Bachmann, R., O. Oncken, J. Glodny, W. Seifert, V. Georgieva, and M. Sudo (2009), Exposed plate interface in the European Alps reveals fabric styles and gradients related to an ancient seismogenic coupling zone, *J. Geophys. Res.*, 114, B05402, doi:10.1029/2008JB005927.

Barber, A. J., and M. J. Crow (2005), Structure and structural history, in *Sumatra: Geology, Resources and Tectonic Evolution*, Geological Society Memoir No. 31, edited by A. J. Barber, et al., pp. 175-233, Geological Society, London.

Beckley, B. D., F. G. Lemoine, S. B. Luthcke, R. D. Ray, and N. P. Zelensky (2007), A reassessment of global and regional mean sea level trends from TOPEX and Jason-1 altimetry based on revised reference frame and orbits, *Geophys. Res. Lett.*, 34, L14608, doi:10.1029/2007GL030002.

Bilham, R., R. Engdahl, N. Feldl, and S. P. Satyabala (2005), Partial and complete rupture of the Indo-Andaman plate boundary 1847-2004, *Seismol. Res. Lett.*, 76, 299-311, doi:10.1785/gssrl.76.3.299.

Bird, M. I., L. K. Fifield, T. S. Teh, C. H. Chang, N. Shirlaw, and K. Lambeck (2007), An inflection in the rate of early mid-Holocene eustatic sea-level rise: a new sea-level curve from Singapore, *Estuar. Coast. Shelf Sci.*, 71, 523-536, doi:10.1016/j.ecss.2006.07.004.

Borrero, J. C., C. E. Synolakis, and H. Fritz (2006), Northern Sumatra field survey after the December 2004 great Sumatra earthquake and Indian Ocean tsunami, *Earthq. Spectra*, 22, S93-S104, doi:10.1193/1.2206793.

Briggs, R. W., K. Sieh, A. J. Meltzner, D. Natawidjaja, J. Galetzka, B. Suwargadi, Y.-j. Hsu, M. Simons, N. Hananto, I. Suprihanto, D. Prayudi, J.-P. Avouac, L. Prawirodirdjo, and Y. Bock (2006), Deformation and slip along the Sunda megathrust in the great 2005 Nias–Simeulue earthquake, *Science*, 311, 1897-1901, doi:10.1126/science.1122602.

Briggs, R. W., K. Sieh, W. H. Amidon, J. Galetzka, D. Prayudi, I. Suprihanto, N. Sastra, B. Suwargadi, D. Natawidjaja, and T. G. Farr (2008), Persistent elastic behavior above a megathrust rupture patch: Nias island, West Sumatra, *J. Geophys. Res.*, 113, B12406, doi:10.1029/2008JB005684.

Brown, B. E., K. R. Clarke, and R. M. Warwick (2002), Serial patterns of biodiversity change in corals across shallow reef flats in Ko Phuket, Thailand, due to the effects of local (sedimentation) and regional (climatic) perturbations, *Mar. Biol.*, 141, 21-29, doi:10.1007/s00227-002-0810-0.

Chlieh, M., J.-P. Avouac, V. Hjorleifsdottir, T.-R. A. Song, C. Ji, K. Sieh, A. Sladen, H. Hebert, L. Prawirodirdjo, Y. Bock, and J. Galetzka (2007), Coseismic slip and afterslip of the great M_W 9.15 Sumatra–Andaman earthquake of 2004, *Bull. Seismol. Soc. Am.*, 97, S152-S173, doi:10.1785/0120050631.

Chlieh, M., J.-P. Avouac, K. Sieh, D. H. Natawidjaja, and J. Galetzka (2008), Heterogeneous coupling of the Sumatran megathrust constrained by geodetic and paleogeodetic measurements, *J. Geophys. Res.*, 113, B05305, doi:10.1029/2007JB004981.

Church, J. A., and N. J. White (2006), A 20th century acceleration in global sea-level rise, *Geophys. Res. Lett.*, 33, L01602, doi:10.1029/2005GL024826.

Clark, J. A., W. E. Farrell, and W. R. Peltier (1978), Global changes in postglacial sea level: a numerical calculation, *Quat. Res.*, 9, 265-287, doi:10.1016/0033-5894(78)90033-9.

Curray, J. R. (2005), Tectonics and history of the Andaman Sea region, *J. Asian Earth Sci.*, 25, 187-228, doi:10.1016/j.jseaes.2004.09.001.

Dickinson, W. R. (2001), Paleoshoreline record of relative Holocene sea levels on Pacific islands, *Earth Sci. Rev.*, 55, 191-234, doi:10.1016/S0012-8252(01)00063-0.

Dreyer, E. L. (2007), *Zheng He: China and the Oceans in the Early Ming Dynasty: 1405–1433*, Pearson Longman, New York.

Dunn, R. E. (2005), *The Adventures of Ibn Battuta: A Muslim Traveler of the 14th Century*, Revised ed., 379 pp., University of California Press, Berkeley, CA.

Egbert, G. D., and S. Y. Erofeeva (2002), Efficient inverse modeling of barotropic ocean tides, *J. Atmos. Oceanic Technol.*, 19, 183-204, doi:10.1175/1520-0426(2002)019<0183:EIMOBO>2.0.CO;2.

Endharto, M., and Sukido (1994), Geological Map of the Sinabang Sheet, Sumatera, scale 1:250,000, Geological Research and Development Centre, Bandung, Indonesia.

Frohlich, C., M. J. Hornbach, F. W. Taylor, C.-C. Shen, A. Moala, A. E. Morton, and J. Kruger (2009), Huge erratic boulders in Tonga deposited by a prehistoric tsunami, *Geology*, 37, 131-134, doi:10.1130/G25277A.1.

Horton, B. P., P. L. Gibbard, G. M. Milne, R. J. Morley, C. Purintavaragul, and J. M. Stargardt (2005), Holocene sea levels and palaeoenvironments, Malay–Thai Peninsula, southeast Asia, *The Holocene*, 15, 1199-1213, doi:10.1191/0959683605hl891rp.

Hsu, Y.-J., M. Simons, J.-P. Avouac, J. Galetzka, K. Sieh, M. Chlieh, D. Natawidjaja, L. Prawirodirdjo, and Y. Bock (2006), Frictional afterslip following the 2005 Nias–Simeulue earthquake, Sumatra, *Science*, 312, 1921-1926, doi:10.1126/science.1126960.

Jankaew, K., B. F. Atwater, Y. Sawai, M. Choowong, T. Charoentitirat, M. E. Martin, and A. Prendergast (2008), Medieval forewarning of the 2004 Indian Ocean tsunami in Thailand, *Nature*, 455, 1228-1231, doi:10.1038/nature07373.

Jevrejeva, S., A. Grinsted, J. C. Moore, and S. Holgate (2006), Nonlinear trends and multiyear cycles in sea level records, *J. Geophys. Res.*, 111, C09012, doi:10.1029/2005JC003229.

Lambeck, K., M. Anzidei, F. Antonioli, A. Benini, and A. Esposito (2004), Sea level in Roman time in the central Mediterranean and implications for recent change, *Earth Planet. Sci. Lett.*, 224, 563-575, doi:10.1016/j.epsl.2004.05.031.

Lavigne, F., R. Paris, D. Grancher, P. Wassmer, D. Brunstein, F. Vautier, F. Leone, F. Flohic, B. De Coster, T. Gunawan, C. Gomez, A. Setiawan, R. Cahyadi, and Fachrizal (2009), Reconstruction of tsunami inland propagation on December 26, 2004 in Banda Aceh, Indonesia, through field investigations, *Pure Appl. Geophys.*, 166, 259-281, doi:10.1007/s00024-008-0431-8.

Loya, Y. (1976), Recolonization of Red Sea corals affected by natural catastrophes and man-made perturbations, *Ecology*, 57, 278-289, doi:10.2307/1934816.

Meltzner, A. J., K. Sieh, M. Abrams, D. C. Agnew, K. W. Hudnut, J.-P. Avouac, and D. H. Natawidjaja (2006), Uplift and subsidence associated with the great Aceh–Andaman earthquake of 2004, *J. Geophys. Res.*, 111, B02407, doi:10.1029/2005JB003891.

Meltzner, A. J., K. Sieh, B. E. Philibosian, H. Chiang, C. Shen, B. W. Suwargadi, and D. H. Natawidjaja (2008), Earthquake recurrence and long-term segmentation near the boundary of the 2004 and 2005 Sunda megathrust ruptures, *Eos Trans. AGU*, 89, Fall Meet. Suppl., Abstract T51C-08.

Meltzner, A. J., K. E. Sieh, H. Chiang, C. Shen, B. Philibosian, B. W. Suwargadi, and D. H. Natawidjaja (2009), Earthquake clusters and persistent segmentation near the boundary of the 2004 and 2005 Sunda megathrust ruptures, *Eos Trans. AGU*, 90, Fall Meet. Suppl., Abstract T11D-07.

Mitrovica, J. X., and G. A. Milne (2002), On the origin of late Holocene sea-level highstands within equatorial ocean basins, *Quat. Sci. Rev.*, 21, 2179-2190, doi:10.1016/S0277-3791(02)00080-X.

Monecke, K., W. Finger, D. Klarer, W. Kongko, B. G. McAdoo, A. L. Moore, and S. U. Sudrajat (2008), A 1,000-year sediment record of tsunami recurrence in northern Sumatra, *Nature*, 455, 1232-1234, doi:10.1038/nature07374.

Natawidjaja, D. H., K. Sieh, S. N. Ward, H. Cheng, R. L. Edwards, J. Galetzka, and B. W. Suwargadi (2004), Paleogeodetic records of seismic and aseismic subduction from central Sumatran microatolls, Indonesia, *J. Geophys. Res.*, 109, B04306, doi:10.1029/2003JB002398.

Natawidjaja, D. H., K. Sieh, M. Chlieh, J. Galetzka, B. W. Suwargadi, H. Cheng, R. L. Edwards, J.-P. Avouac, and S. N. Ward (2006), Source parameters of the great Sumatran megathrust earthquakes of 1797 and 1833 inferred from coral microatolls, *J. Geophys. Res.*, 111, B06403, doi:10.1029/2005JB004025.

Natawidjaja, D. H., K. Sieh, J. Galetzka, B. W. Suwargadi, H. Cheng, R. L. Edwards, and M. Chlieh (2007), Interseismic deformation above the Sunda megathrust recorded in coral microatolls of the Mentawai islands, West Sumatra, *J. Geophys. Res.*, 112, B02404, doi:10.1029/2006JB004450.

Newcomb, K. R., and W. R. McCann (1987), Seismic history and seismotectonics of the Sunda Arc, *J. Geophys. Res.*, 92, 421-439, doi:10.1029/JB092iB01p00421.

Patton, J. R., C. Goldfinger, A. E. Morey, M. Erhardt, B. Black, A. M. Garrett, Y. Djadjadihardja, and U. Hanifa (2010), Temporal clustering and recurrence of Holocene paleoearthquakes in the region of the 2004 Sumatra-Andaman earthquake, *Seismol. Res. Lett.*, 81, 290.

Pearson, R. G. (1981), Recovery and recolonization of coral reefs, *Mar. Ecol. Prog. Ser.*, 4, 105-122, doi:10.3354/meps004105.

Peltier, W. R. (2002), On eustatic sea level history: Last Glacial Maximum to Holocene, *Quat. Sci. Rev.*, 21, 377-396, doi:10.1016/S0277-3791(01)00084-1.

Peltier, W. R. (2004), Global glacial isostasy and the surface of the ice-age earth: the ICE-5G (VM2) model and GRACE, *Annu. Rev. Earth Planet. Sci.*, 32, 111-149, doi:10.1146/Annurev.Earth.32.082503.144359.

Plafker, G. (1972), Alaskan earthquake of 1964 and Chilean earthquake of 1960: implications for arc tectonics, *J. Geophys. Res.*, 77, 901-925, doi:10.1029/JB077i005p00901.

Plafker, G., and J. C. Savage (1970), Mechanism of the Chilean earthquakes of May 21 and 22, 1960, *Geol. Soc. Am. Bull.*, 81, 1001-1030, doi:10.1130/0016-7606(1970)81[1001:MOTCEO]2.0.CO;2.

Polo, M. (1993), *The Travels of Marco Polo: The Complete Yule-Cordier Edition (Vols. 1 & 2)*, Dover Publications.

Prawirodirdjo, L., and Y. Bock (2004), Instantaneous global plate motion model from 12 years of continuous GPS observations, *J. Geophys. Res.*, 109, B08405, doi:10.1029/2003JB002944.

Pugh, D. (2004), *Changing Sea Levels: Effects of Tides, Weather and Climate*, 280 pp., Cambridge Univ. Press, New York, doi:10.2277/0521532183.

Rajendran, K., C. P. Rajendran, A. Earnest, G. V. R. Prasad, K. Dutta, D. K. Ray, and R. Anu (2008), Age estimates of coastal terraces in the Andaman and Nicobar Islands and their tectonic implications, *Tectonophysics*, 455, 53-60, doi:10.1016/j.tecto.2008.05.004.

Rao, S. A., S. K. Behera, Y. Masumoto, and T. Yamagata (2002), Interannual subsurface variability in the tropical Indian Ocean with a special emphasis on the Indian Ocean Dipole, *Deep-Sea Res. II*, 49, 1549-1572, doi:10.1016/S0967-0645(01)00158-8.

Reid, A. (2005), *An Indonesian Frontier: Acehnese and Other Histories of Sumatra*, 439 pp., Singapore University Press, Singapore.

Ricklefs, M. C. (2008), *A History of Modern Indonesia Since c. 1200*, 4th ed., 496 pp., Stanford University Press, Stanford, CA.

Rivera, L., K. Sieh, D. Helmberger, and D. Natawidjaja (2002), A comparative study of the Sumatran subduction-zone earthquakes of 1935 and 1984, *Bull. Seismol. Soc. Am.*, 92, 1721-1736, doi:10.1785/0120010106.

Savage, J. C. (1983), A dislocation model of strain accumulation and release at a subduction zone, *J. Geophys. Res.*, 88, 4984-4996, doi:10.1029/JB088iB06p04984.

Scoffin, T. P., and D. R. Stoddart (1978), The nature and significance of microatolls, *Philos. Trans. R. Soc. London Ser. B*, 284, 99-122, doi:10.1098/rstb.1978.0055.

Shen, C.-C., R. L. Edwards, H. Cheng, J. A. Dorale, R. B. Thomas, S. B. Moran, S. E. Weinstein, and H. N. Edmonds (2002), Uranium and thorium isotopic and concentration measurements by magnetic sector inductively coupled plasma mass spectrometry, *Chem. Geol.*, 185, 165-178, doi:10.1016/S0009-2541(01)00404-1.

Shen, C.-C., K.-S. Li, K. Sieh, D. Natawidjaja, H. Cheng, X. Wang, R. L. Edwards, D. D. Lam, Y.-T. Hsieh, T.-Y. Fan, A. J. Meltzner, F. W. Taylor, T. M. Quinn, H.-W. Chiang, and K. H. Kilbourne (2008), Variation of initial ^{230}Th/^{232}Th and limits of high precision U-Th dating of shallow-water corals, *Geochim. Cosmochim. Acta*, 72, 4201-4223, doi:10.1016/j.gca.2008.06.011.

Sieh, K., D. H. Natawidjaja, A. J. Meltzner, C.-C. Shen, H. Cheng, K.-S. Li, B. W. Suwargadi, J. Galetzka, B. Philibosian, and R. L. Edwards (2008), Earthquake supercycles inferred from sea-level changes recorded in the corals of West Sumatra, *Science*, 322, 1674-1678, doi:10.1126/science.1163589.

Stoddart, D. R., and T. P. Scoffin (1979), Microatolls: review of form, origin and terminology, *Atoll Res. Bull.*, 224, 1-17.

Subarya, C., M. Chlieh, L. Prawirodirdjo, J.-P. Avouac, Y. Bock, K. Sieh, A. J. Meltzner, D. H. Natawidjaja, and R. McCaffrey (2006), Plate-boundary deformation associated with the great Sumatra–Andaman earthquake, *Nature*, 440, 46-51, doi:10.1038/nature04522.

Taylor, F. W., C. Frohlich, J. Lecolle, and M. Strecker (1987), Analysis of partially emerged corals and reef terraces in the central Vanuatu Arc: comparison of contemporary coseismic and nonseismic with Quaternary vertical movements, *J. Geophys. Res.*, 92, 4905-4933, doi:10.1029/JB092iB06p04905.

van Woesik, R. (2004), Comment on "Coral reef death during the 1997 Indian Ocean Dipole linked to Indonesian wildfires", *Science*, 303, 1297, doi:10.1126/science.1091983.

Woodroffe, C., and R. McLean (1990), Microatolls and recent sea level change on coral atolls, *Nature*, 344, 531-534, doi:10.1038/344531a0.

Wunsch, C., and D. Stammer (1997), Atmospheric loading and the oceanic "inverted barometer" effect, *Rev. Geophys.*, 35, 79-107, doi:10.1029/96RG03037.

Wunsch, C., D. B. Haidvogel, M. Iskandarani, and R. Hughes (1997), Dynamics of the long-period tides, *Prog. Oceanogr.*, 40, 81-108, doi:10.1016/S0079-6611(97)00024-4.

Zachariasen, J. (1998), Paleoseismology and paleogeodesy of the Sumatran subduction zone: a study of vertical deformation using coral microatolls, Ph.D. thesis, 418 pp., California Institute of Technology, Pasadena, CA.

Zachariasen, J., K. Sieh, F. W. Taylor, R. L. Edwards, and W. S. Hantoro (1999), Submergence and uplift associated with the giant 1833 Sumatran subduction earthquake: evidence from coral microatolls, *J. Geophys. Res.*, 104, 895-919, doi:10.1029/1998JB900050.

Zachariasen, J., K. Sieh, F. W. Taylor, and W. S. Hantoro (2000), Modem vertical deformation above the Sumatran subduction zone: paleogeodetic insights from coral microatolls, *Bull. Seismol. Soc. Am.*, 90, 897-913, doi:10.1785/0119980016.

Chapter 4

Coral evidence for earthquake recurrence and an AD 1390–1455 cluster at the south end of the 2004 Aceh–Andaman rupture

(Auxiliary Material)

Aron J. Meltzner, Kerry Sieh, Hong-Wei Chiang, Chuan-Chou Shen,

Bambang W. Suwargadi, Danny H. Natawidjaja, Belle E. Philibosian,

Richard W. Briggs, John Galetzka

in press in the *Journal of Geophysical Research*

doi:10.1029/2010JB007499

4.1. 2004 and subsequent uplift at the Lhok Dalam (LDL) sites

4.1.1. 2004 coseismic uplift

Coseismic uplift attributed to the 2004 earthquake at LDL-A was reported by both *Meltzner et al.* [2006] and *Briggs et al.* [2006]. The value reported by Meltzner et al., 147 ± 18 cm of uplift, is based on a field measurement made 17 January 2005. This value was determined by comparing the pre-uplift HLS on a single slightly tilted *Porites* microatoll with ELW, but the calculation did not consider SLAs. Redoing the calculation with the original field measurements, an updated tide model, documented SLAs, the revised correction for the difference between HLS and ELW, and an appropriate inverted barometer correction results in a nearly identical estimate of 146 ± 15 cm. This value includes the 2004 coseismic uplift and any postseismic vertical changes that had occurred by 17 January 2005, but it should be considered a minimum estimate of uplift because the microatoll may have settled an unknown amount. The value reported by Briggs et al. (at their site RND05-H), 151 ± 12 cm of uplift, is based on a field measurement made 1 June 2005. This amount was determined by comparing pre-uplift HLS with post-uplift HLS on the highest, least tilted *Porites* microatolls. The Briggs field team also surveyed water level at the time of their visit to the site; although neither their surveyed water level nor the resulting calculated uplift were published, we use their field notes and surveyed water level to determine ELW and calculate a net uplift of 153 ± 10 cm as of the date of their site visit, 1 June 2005. The two values determined in June 2005 by different methods are essentially identical; like the value based on the January 2005 measurement, these should be considered minimum estimates of uplift, but because in June 2005 pre-uplift HLS was surveyed on multiple microatolls and an effort was made to find the highest, least tilted microatolls, the June 2005 values are likely closer approximations to the true uplift than is the January 2005 value. We adopt 153 ± 10 cm as the best estimate of net uplift at LDL-A as of 1 June 2005.

4.1.2. Postseismic change

We returned to LDL-A in June 2006, at which time we re-determined the net uplift since immediately before the 2004 earthquake by comparing the pre-uplift HLS on the highest, least tilted *Porites* microatolls to ELW. Net uplift at LDL-A as of June 2006 was 154 ± 10 cm, suggesting there was no change between June 2005 and June 2006. Like the June 2005 values, the June 2006 value should be considered a minimum estimate of uplift, but it is likely a decent approximation to the true uplift.

The LDL-B site was visited only once, in July 2007, and we were unable to make any estimate of 2004 uplift there. No still-living microatolls were found at the site, and extremely high surf, with waves crashing at the steep edge of the reef, prevented us from estimating the water level there with any useful precision.

4.2. Modern paleogeodetic record at Lhok Dalam (LDL)

4.2.1. Head LDL-1

The LDL-1 *Porites* microatoll was selected for slabbing because it appeared to have the longest HLS record of any modern microatoll at the site. LDL-1 began growing some time in the late 1950s, but it did not reach HLS until late 1982 (Figure S4a). Subsequent diedowns occurred in late 1991, late 1997, and ultimately late 2004, when coseismic uplift killed the entire head. These all correspond to diedowns seen at the LKP sites.

4.2.2. Interseismic subsidence recorded by LDL-1

A time series of HLG and HLS for LDL-1 is plotted on Figure S4b; we attempt to fit the data using the two methods described in Section 3.3. Using pre-diedown HLG data spanning the very brief period AD 1991–1996, we obtain a submergence rate of 8.2 mm/yr, or a subsidence rate of 6.2 mm/yr. Alternatively, using corrected post-diedown HLS data spanning 1983–1998, we obtain an average submergence rate of 10.7 mm/yr, or a subsidence rate of 8.7 mm/yr. Simple elastic dislocation modeling predicts that sites nearer the trench should experience faster interseismic tectonic subsidence; indeed, both methods described in Section 3.3 yield a high rate of interseismic subsidence from microatoll LDL-1. We prefer the latter result because it is based upon a longer time series, and we adopt 8.7 mm/yr as the 1983–1998 average subsidence rate at LDL-A.

4.3. 14th–15th century record at Lhok Dalam (LDL)

Despite an extensive search of the reef around our eventual LDL-B site, we found fewer than ten fossil microatolls there. At least some of them—and perhaps all of them—were transported at some time in the past: many appear to have settled and come to rest in their present position, in that their shape does not conform to the substrate; some are clearly tilted, and a few even rock back and forth if leaned against; and none appear to be anchored to the substrate.

4.3.1. Heads LDL-3, LDL-4, and LDL-5

We slabbed the three most well preserved fossil microatolls at the site: LDL-3, LDL-4, and LDL-5 (Figures S5–S7, respectively). These three heads have similar but not identical morphologies, which made it impossible to determine in the field whether they are of a single generation. We anticipated at the time that at least two are of the same generation, but because different parts of the record seemed better preserved on different heads, we decided to sample all three. In particular, microatoll LDL-4 is unique in that it has a low outer concentric ring. This outer ring is considerably eroded, particularly on the side of the head where the higher inner rings are more well preserved. Because of this, we cut two slabs from head LDL-4: slab LDL-4A through an entire radius where the higher inner rings are best preserved (Figure S6a), and slab LDL-4B through the low outer ring where that ring is best preserved (Figure S6b).

One sample each from LDL-3, LDL-4A, and LDL-4B, and three samples from LDL-5, were dated by U-Th analysis (Tables S2–S3; Figures S5–S7). Based only upon the samples' ages and the number of growth bands preserved after each sample, the date of the outer edge of LDL-3 is late AD 1403 (± 7) (Figure S5a; Table S3), and the weighted-average date of the outer edge of LDL-5 is late AD 1392 (± 3) (Figure S7a; Table S3). For LDL-4, we estimate the date of the youngest preserved band *above the low outer ring*, i.e., for the discussion that follows, we ignore the low outer ring and focus on the upper part of the head. Based on sample LDL-4A-A2, the youngest preserved band on the upper part of LDL-4A dates to AD 1399 ± 17 (Figure S6a), whereas sample LDL-4B-A2 yields a date of AD 1370 ± 8 for the youngest preserved band on the upper part of LDL-4B (Figure S6b). From the morphology and level of preservation of LDL-4, we know that the youngest preserved band on the upper parts of LDL-4A and LDL-4B should be within a few years of one another, i.e., those parts of the two slabs appear to have sustained similar amounts of erosion. Hence, the two dates should be similar; the fact that they disagree at 2σ indicates that at least one of those dates is in error by more than 2σ.

The dates of the outer preserved bands on LDL-3, LDL-5, and the upper part of LDL-4 are close, but their 2σ errors do not overlap. When we estimate and account for the number of missing bands on each head, the discrepancies do not disappear and may get marginally worse. In order to estimate the number of missing bands, we first observe that all the slabbed microatolls are fairly well preserved: there is no indication that either LDL-3 or LDL-5 is missing more than a few bands, and, likewise, above the low outer ring, neither slab of LDL-4 appears to be missing more than a few bands. We can more precisely estimate the number of missing bands if we examine the intervals between diedowns on the microatolls. LDL-3 experienced significant diedowns 12, 24, and 36 years prior to its outer preserved edge (Figure S5a). LDL-4A also experienced diedowns 12, 24, and 36 years prior to the youngest preserved band on the upper part of the head (Figure S6a). Similarly, LDL-5 experienced significant diedowns 15, 27, and 39 years prior to its outer preserved edge (Figure S7a). These observations support the notion that all three heads are coeval, and they suggest (*a*) that the upper part of LDL-4A is missing the same number of bands as LDL-3, and (*b*) that both are missing exactly three more bands than LDL-5.

We assume that LDL-5 is missing 0.5 ± 0.5 annual bands of growth based on the good preservation of its outer rim, and we assume LDL-3 and the upper part of LDL-4A are both missing exactly three more bands, i.e., 3.5 ± 0.5 annual bands. The low outer ring of LDL-4 is less eroded near the LDL-4B slab than near the LDL-4A slab, but it is not obvious how that relates to the relative erosion (in the two slabs) of the outer bands of the upper part of the head. We estimate the upper part of LDL-4B is missing 3.0 ± 3.0 bands, with the larger error in this case reflecting the higher uncertainty in that estimate. Using these assumptions, we calculate that LDL-3 died in 1407 ± 7, LDL-5 died in 1393 ± 3, and the upper part of LDL-4 died in 1379 ± 7; the weighted average of these dates is AD 1393.6 ± 2.7 (August 1393), which is indistinguishable from the date obtained at the LKP sites (Table S4).

While it is troubling that none of the diedown dates on the LDL-B heads overlap at 2σ, we can make a compelling argument in support of the interpretation that those diedowns were synchronous. As is evident on Figures S5–S7, each of the three heads grew for ~50 years or more from the time of their earliest diedown until they experienced a diedown of several decimeters or more (for LDL-3 and LDL-5, this was their ultimate death). If the >30 cm diedowns on the three heads were not synchronous, they must have been separated by ~50 years or more. The dates (with 2σ errors) disagree much less if all three heads are coeval than if we assume otherwise. In other words, despite the disagreement in the dates, the dates are far more consistent with a scenario in which the three heads' large diedowns were all synchronous than they are with any other permissible scenario.

The lack of overlap in the diedown dates might raise speculation, however, that the stated errors from the U-Th analyses are underestimates of the true error. If we arbitrarily assume all stated errors are 50% too low and double them, the diedown dates on the three heads barely overlap, and the resulting weighted average date would be AD 1393.6 ± 5.3.

The preferred banding ages shown on Figures S5–S7 assume each head died around AD 1394.2 (the date determined from the LKP sites) and is missing the number of annual bands inferred earlier. This combination of assumptions produces the attractive result that LDL-3, LDL-4, and LDL-5 all experienced significant diedowns in early AD 1355, early 1367, and early 1379. We further note that diedowns are also seen at those times on LKP-2, if our earlier assumption about the age of LKP-2 is correct. This is the reason to which we alluded earlier (in Section 3.4.9) that we prefer a date of death of AD 1394 for LKP-2.

4.3.2. Uplift in 1394

We determine the coseismic uplift at LDL-B in AD 1394 from an examination of the morphologies of all three heads at the site. Of the three, apparently only LDL-4 was tall enough that its base survived the 1394 diedown and recorded the post-diedown HLS. The upper surface of LDL-4 is considerably eroded, though, such that it does not preserve the pre-diedown HLG. On both LDL-3 and LDL-5, the outer rim reaches 27 cm above the 1355 post-diedown HLS and 13 cm above the 1379 post-diedown HLS; assuming the 1394 pre-diedown HLG was a similar height above the respective features on LDL-4A, the 1394 diedown on LDL-4 was 42–50 cm. While it is perhaps a coincidence that the 1394 uplift was the same at LDL-B as at LKP-B, the fact that, at both places, it was half the uplift as in 2004, or less, indicates that the 1394 earthquake was not similar to the 2004 event, and it may have been substantially smaller.

4.3.3. 15th-century record

It is unclear why only a few annual bands are preserved on LDL-4 after the 1394 diedown. A second diedown soon after 1394 is possible, but it is just as likely that the head lived for decades after 1394, only to have the outer part not preserved. Given the head's morphology, it is reasonable to speculate that, if the head did indeed grow outward for many years after the 1394 diedown, then the outer part of the head might have broken off and fallen away from the interior, simply as a consequence of the outer rings' weight; we have seen examples of this elsewhere. If the head was subsequently transported by a tsunami, then the outer parts of the head might have been carried elsewhere. Regardless of the details, the lack of a long post-1394 record at the LDL sites precludes a comparison to that part of the history at the LKP sites.

4.3.4. Interseismic subsidence recorded by LDL-3, LDL-4, and LDL-5

The interseismic subsidence rates prior to 1394 at LDL-B appear to be high, but not as high as the late-20th century rate at LDL-A. LDL-3 and LDL-5 appear to have submerged at average rates of 7.2 and 6.1 mm/yr over the years 1354–1390 and 1354–1393, respectively. LDL-4 submerged at an average rate of 5.9 mm/yr over the years 1335–1375. As at LKP, we assume the subsidence rates equal the submergence rates for the 14th century microatolls.

4.4. Earlier record at Lhok Dalam (LDL)

4.4.1. Head LDL-2

The fossil microatoll from site LDL-A, head LDL-2 (Figure S8), is of limited utility. Because it was tilted and badly eroded, we knew prior to sampling it that it would not provide useful information about the head's original elevation, or about interseismic rates. We chose to remove only a short slab, which we hoped would provide an estimate of the timing of a past event. Unfortunately, the samples we selected for U-Th analysis were high in Th content, and thus provided a very imprecise date (Table S2). The event that killed LDL-2 could have happened at any time between the early 6th and early 12th centuries AD (Table S3).

5.1. 2004 and subsequent uplift at the Langi (LNG) site

5.1.1. 2004 coseismic uplift

Coseismic uplift in 2004 at LNG-A was determined by *Briggs et al.* [2006]. At their site RND05-G, which coincides with our site LNG-A, Briggs et al. reported 128 ± 16 cm of uplift, determined in June 2005 by comparing the pre-uplift HLS on *Porites* microatolls with ELW. As at other sites, however, they did not consider SLAs in their calculation; redoing the calculation with the original field measurements, an updated tide model, documented SLAs, the revised correction for the difference between HLS and ELW, and an appropriate inverted barometer correction results in a higher estimate of 142 ± 10 cm; this value includes the 2004 coseismic uplift and any postseismic vertical changes that had occurred by 1 June 2005. As predicted by simple elastic dislocation modeling [*Plafker and Savage*, 1970; *Plafker*, 1972], the uplift at LNG was greater than at LKP but less than at LDL (Table S1; Figure 18D).

5.1.2. Postseismic subsidence

In June 2006, we re-measured net uplift at LNG-A by surveying the water level relative to pre-uplift HLS (on some of the same heads measured by Briggs et al. a year earlier) and tying the water level to ELW. The net uplift as of June 2006 was 124 ± 9 cm, suggesting 18 ± 14 cm of postseismic subsidence occurred between June 2005 and June 2006. This is consistent with our observations at the LKP sites of substantial but decreasing postseismic subsidence following the 2004 earthquake.

5.2. Modern paleogeodetic record at Langi (LNG)

5.2.1. Head LNG-1

The LNG-1 *Porites* microatoll was selected for slabbing because of the numerous concentric growth rings on its dead upper surface and its well-preserved morphology. LNG-1 began growing some time in the late 1930s, but it did not reach HLS until 1961 (Figure S10a). Subsequent diedowns occurred around late 1975, late 1978, late 1979 (early 1980), late 1982, late 1986, late 1991, early 1993, late 1997, late 2003 (early 2004), and ultimately late 2004, when coseismic uplift killed the entire head. Many of these diedowns correspond to diedowns seen on LKP-1.

5.2.2. The 2003–2004 diedown: possibly tectonic

The HLS on LNG-1 following the late 2003–early 2004 diedown was 8 cm higher (in the reference frame of the coral head) than the HLS after the late 1997–early 1998 diedown; this is similar to the difference on LKP-1. Following the logic applied at the LKP sites, the diedown in late 2003–early 2004 on LNG-1 suggests that the LNG-A site experienced several centimeters of coseismic or postseismic uplift associated with the 2002 earthquake.

5.2.3. Interseismic subsidence recorded by LNG-1

A time series of HLG and HLS for LNG-1 is plotted on Figure S10b; we attempt to fit the data using the two methods discussed in Section 3.3. The first method, using pre-diedown HLG data spanning AD 1975–2003, yields a submergence rate of 3.2 mm/yr on LNG-1, or a subsidence rate of 1.2 mm/yr. If we ignore data from after 1997, the average submergence rate drops to 2.1 mm/yr (not shown), corresponding to essentially zero subsidence. The second method, using corrected post-diedown HLS data spanning 1962–1998, yields an average submergence rate of 5.3 mm/yr, or a subsidence rate of 3.3 mm/yr. There is considerable disagreement among these values, probably because the time period over which we can apply the first method is so short. We prefer the result of the second method because it is based upon a longer time series, and we adopt the value 3.3 mm/yr as the 1962–1998 average subsidence rate at LNG-A.

The elastic dislocation model predicts that the interseismic tectonic subsidence rate at LNG-A should be lower than at the LDL sites but higher than at the LKP sites. Comparing the rates at those sites in the decades prior to 2004, LDL-A appears to have been subsiding the fastest and LKP-B the slowest (as expected), but subsidence was faster at LKP-A than at LNG-A (contrary to expectations; see Figure 19). Even if we assume an average sea level rise of only 1 mm/yr over the period 1962–1998 (which might be justifiable based on the rates of sea level rise obtained by *Jevrejeva et al.* [2006]), the subsidence rate at LNG-A would be 4.3 mm/yr, which would not eliminate the irregularity. This suggests the 1-D elastic model is oversimplified, and strain accumulation may be complicated spatially, temporally, or both. Such complications may arise from small-scale heterogeneities and/or time-varying frictional properties along the plate interface.

5.3. 14th–15th century record at Langi (LNG)

5.3.1. Head LNG-2

We sampled one fossil *Porites* microatoll at the LNG-A site, but because the head was too far from water for us to use a hydraulic chainsaw to cut a slab from the head, we had to chisel off a piece of the microatoll's outer rim by hand instead. The chiseled sample, LNG-2 (Figure S11), allowed us to date the head's death, but provides no information about interseismic rates leading up to the head's death.

U-Th analysis of a sample from LNG-2 yielded a date for the head's outer preserved band of AD 1406 ± 6 (Tables S2–S3; Figure S11). There appears to be minor erosion of the outer preserved band, but there is no indication that more than a few annual bands are missing. The head's U-Th age and the proximity of LNG-A to the LKP and LDL sites suggest that LNG-2 was killed by the same event that caused the ~50-cm diedowns on the microatolls at LKP and LDL. If we assume that this head died in AD 1394—even though this is beyond the 2σ error of the U-Th analysis—and if we also assume there are 2 ± 2 missing annual bands, then a diedown seen several years prior to the outer preserved band on the LNG-2 slab (Figure S11) would correspond to a diedown in early AD 1387 seen on LKP-3 (Figure 6 a–b) and LKP-7 (Figure 8a). The preferred banding ages shown on Figure S11 are based on these assumptions.

6.1. 2004 and subsequent uplift at the Ujung Salang (USL) site

6.1.1. 2004 coseismic uplift

Coseismic uplift attributed to the 2004 earthquake at USL-A was reported by both *Meltzner et al.* [2006] and *Briggs et al.* [2006]. The value reported by Meltzner et al., 131 ± 18 cm, is based on a field measurement made 17 January 2005. This value was determined by comparing the pre-uplift HLS on a single slightly tilted *Porites* microatoll with ELW, but the calculation did not consider SLAs. Redoing the calculation with the original field measurements, an updated tide model, documented SLAs, the revised correction for the difference between HLS and ELW, and an appropriate inverted barometer correction results in a nearly identical estimate of 125 ± 15 cm. This value includes the 2004 coseismic uplift and any postseismic vertical changes that had occurred by 17 January 2005. The uplift reported by Briggs et al. (at their site USL05-A), 121 ± 23 cm, is based on a field measurement made 1 June 2005. This amount was determined by comparing pre-uplift HLS on an untilted *Porites* microatoll with post-uplift HLS on a different, still-living *Porites* microatoll. (Incidentally, the still-living microatoll surveyed in June 2005 was the same one used in January. We verified in June that this head had not settled, beyond the tilting it experienced during the shaking in 2004.) We adopt 125 ± 15 cm as the best estimate of 2004 coseismic uplift at USL-A.

6.1.2. Postseismic change

In June 2006, we re-determined net uplift at USL-A by comparing the pre-uplift HLS on untilted *Porites* microatolls to ELW. Net uplift at USL-A as of June 2006 was 117 ± 10 cm, suggesting there was little if any subsidence (8 ± 18 cm) between January 2005 and June 2006.

6.1.3. 2008 coseismic uplift

We returned to USL-A in February 2009 to document uplift associated with the 2008 earthquake. Net uplift, from prior to the 2004 earthquake until February 2009, was determined by comparing pre-uplift HLS to ELW to be 122 ± 10 cm; 5 ± 12 cm of net uplift occurred between June 2006 and February 2009. We also re-examined the same still-living microatoll surveyed in 2005. Most of the head had died down in 2004, but, as expected, it had a new outer living rim that had been growing radially upward and outward from below its post-2004 HLS. The uppermost part of this outer rim had experienced a still more recent diedown of ~3 cm; based on this outer rim's morphology, we estimate that the most recent diedown occurred some time during the first half of 2008, possibly coincident with or soon after the 20 February 2008 M_W 7.3 Simeulue earthquake. The most recent HLS, which was horizontal over most of the head, was 118 cm lower than the pre-2004 HLS on the untilted microatolls. The combined tide model and SLA calculations indicate that the ELW for the period from February 2008 until February 2009 was 5 cm higher than the ELW in 2004; hence, comparing pre-2004 HLS with post-2008 HLS indicates ~123 cm of net uplift (2004 to 2008), consistent with the value determined from the water level measurement in 2009. As at the LKP sites, our observations at USL-A are consistent with a history of postseismic subsidence in the year or so following the 2004 earthquake, as well as uplift (presumably coseismic) in early 2008.

6.2. Modern paleogeodetic record at Ujung Salang (USL)

6.2.1. Head USL-1

The USL-1 *Porites* microatoll was selected for slabbing because of the numerous concentric growth rings on its dead upper surface and its well-preserved morphology. USL-1 began growing some time in the first half of the 20th century, but it did not reach HLS until 1961 (Figure S13a). Subsequent diedowns occurred around late 1982, late 1997, and ultimately late 2004, when coseismic uplift killed the entire head. These all correspond to diedowns seen elsewhere.

6.2.2. Interseismic subsidence recorded by USL-1

A time series of HLG and HLS for USL-1 is plotted on Figure S13b. Using pre-diedown HLG data spanning AD 1980–1997, we obtain a submergence rate of 9.6 mm/yr, or a subsidence rate of 7.6 mm/yr. Alternatively, using corrected post-diedown HLS data spanning 1962–1998, we obtain an average submergence rate of 9.1 mm/yr, or a subsidence rate of 7.1 mm/yr. Both methods yield a high rate of interseismic subsidence, as expected for this site from elastic dislocation modeling. We prefer the latter result because it is based upon a longer time series, and we adopt 7.1 mm/yr as the 1962–1998 average subsidence rate at USL-A.

6.3. Earlier record at Ujung Salang (USL)

6.3.1. Head USL-2

We slabbed one fossil *Porites* microatoll at the USL-A site, from a small population of tilted heads with similar morphologies. The fossil microatoll, USL-2 (Figure S14), died around AD 956 ± 16 (Tables S2–S3). This is presumably the date of an earlier uplift event, and it may correlate with the date of death of LDL-2, but so far, these are the only two heads dated from northern Simeulue that are older than the 14th century AD. In general, our sampling strategy was to target the fossil heads at each site that appeared youngest (i.e., least eroded), in the hope that the record we obtained would be more complete over the past few centuries, at the expense of it extending farther back in time. It is likely that other microatolls exist on the northern Simeulue reefs of the vintage of USL-2 and LDL-2, but further work will be needed to locate, sample, and analyze those heads. Because USL-2 was tilted and badly eroded, it does not provide useful information about the head's original elevation or about interseismic rates prior to its death.

7.1. 2004 and subsequent uplift at the Lewak (LWK) sites

7.1.1. 2004 coseismic uplift

Coseismic uplift attributed to the 2004 earthquake at LWK-A was reported by both *Meltzner et al.* [2006] and *Briggs et al.* [2006], although there are problems with both reported values. The uplift reported by Meltzner et al., 46 ± 23 cm, is based on a field measurement made by J. Galetzka on 5 February 2005, the date that the nearby SuGAr station was installed. The problem with this value is the unfortunate result of a miscommunication between J.G. and the authors. Contrary to statements by *Meltzner et al.* [2006] in the caption of their figure 4, the diedown observed at LWK-A—i.e., the difference between the pre-earthquake HLS and the new HLS observed on 5 February 2005—was not 44 cm. Photos made available more recently to the authors by J.G. clearly and unmistakably show that the diedown was only 33 cm. Separately, the correction discussed by *Meltzner et al.* [2006] did not consider SLAs. The combined tide model and SLA calculations indicate that the ELW during the period 26 December 2004 to 5 February 2005 was 11 cm higher than the ELW in 2004; hence, an 11 cm correction must be added to the 33 cm diedown. The uplift observed at LWK-A therefore should have been reported as 44 ± 12 cm, with the formal error determined according to the procedure adopted by *Briggs et al.* [2006]. We adopt this value as the best estimate of coseismic uplift at LWK-A.

The uplift reported by Briggs et al. at their site RDD05-I (which corresponds to LWK-A), 47 ± 6 cm, is based on a field measurement made on 31 May 2005. This amount, determined by comparing pre-uplift HLS with post-uplift HLS on *Porites* microatolls, is suspect because of irregularities with the apparent post-uplift HLS. By the time of their site visit at the end of May, the corals had died down by an additional 12 cm or more, compared to their HLS in February 2005. (This was entirely the result of a significant negative SLA in March 2005: on 10 March 2005, water levels at LWK reached 6 cm lower than at any time in 2004.) When Briggs et al. visited the site in May 2005, they found only a single, small irregular patch of living corallites, on the lowest few centimeters of an otherwise dead *Porites* microatoll. This was the basis of the uplift value reported by *Briggs et al.* [2006]. We now believe that those still-living corallites were living above their theoretical HLS; this could have happened if the corallites were in a protected pool that did not fully drain at ELW [*Scoffin and Stoddart*, 1978; *Smithers and Woodroffe*, 2000]. While the uplift reported by Briggs et al. might be underestimated only slightly, the uncertainty is under-reported: by their own methodology, the 2σ uncertainty is ±23 cm. Factoring in the revised correction for the lower ELW on (and in the days around) 10 March 2005, our revision of the uplift reported by *Briggs et al.* [2006] is 39 ± 23 cm. The Briggs et al. field team also surveyed water level at the time of their visit to the site; although neither their surveyed water level nor the resulting calculated uplift were published, we use their field notes and surveyed water level to determine ELW and calculate a net uplift of 46 ± 15 cm as of the date of their site visit, 31 May 2005. This value is more precise, and we also consider it to be more reliable, than the value reported by *Briggs et al.* [2006].

7.1.2. Postseismic uplift and subsidence: early 2005

The daily time series from cGPS station LEWK allows us to check the net displacement at the site between 5 February and 31 May 2005, and it extends the record forward to the present. From 5 February to 28 March 2005, LEWK recorded a total of ~1.0 cm of gradual postseismic subsidence. Zero vertical displacement is seen at LEWK around the date of the M_W 8.6 Southern Simeulue–Nias earthquake (28 March), but the trend of the vertical displacement reverses at that time: in April and May, ~3.5 cm of gradually decreasing postseismic uplift is observed. The net change from 5 February to 31 May 2005 is up ~2.5 cm, perfectly consistent with our estimates from coral microatolls at LWK-A.

7.1.3. Later postseismic change and 2008 coseismic uplift

The LEWK record indicates that, unlike Lhok Pauh and Langi, Lewak experienced little vertical change from June 2005 through January 2008. LEWK's position just prior to the February 2008 earthquake was only ~1 cm higher than at the end of May 2005. LEWK was uplifted coseismically ~3 cm in February 2008, and it rose ~1 cm more in the following months.

7.1.4. Uplift at LWK-B site

The LWK-B site was visited only once, in July 2007. Comparing the pre-uplift HLS on several *Porites* microatolls to ELW, we determined the net uplift there, from just prior to the 2004 earthquake to the time of our site visit, to be 54 ± 9 cm. The slightly greater uplift at LWK-B is consistent with that site's location slightly closer to the trench, in comparison with LWK-A.

7.2. Modern paleogeodetic record at Lewak (LWK)

7.2.1. Head LWK-1

The LWK-1 *Porites* microatoll was selected for slabbing because it appeared to have the longest HLS record of any modern microatoll at the site. LWK-1 began growing some time in the 1940s, but it did not reach HLS until late 1951 (Figure S16a). LWK-1 experienced more diedowns than any other head slabbed on northern Simeulue, presumably because of its comparatively fast growth rate and the site's comparatively slow interseismic submergence rate. After its initial diedown in late 1951, subsequent diedowns occurred around late 1954, late 1956, early 1958, late 1961, late 1967, late 1971, late 1975, late 1978, late 1979 (early 1980), late 1982, late 1991, late 1997, late 2003 (early 2004), and ultimately late 2004, when coseismic uplift killed the entire head. Many of these diedowns coincide with diedowns seen at the other sites.

7.2.2. Interseismic subsidence recorded by LWK-1

A time series of HLG and HLS for LWK-1 is plotted on Figure S16b. Using pre-diedown HLG data spanning AD 1953–2003, we obtain a submergence rate of 4.8 mm/yr, or a subsidence rate of 2.8 mm/yr. If we ignore data from after 1997, the average submergence rate increases to 5.3 mm/yr (not shown), corresponding to a subsidence rate of 3.3 mm/yr. Alternatively, using corrected post-diedown HLS data spanning 1962–1998, we obtain an average submergence rate of 3.4 mm/yr, or a subsidence rate of 1.4 mm/yr. We prefer the result from the first method, because it is based upon a longer time series; thus, we adopt 3.3 mm/yr as the 1953–1997 average subsidence rate at LWK-A.

7.2.3. The 2003–2004 diedown: non-tectonic at LWK

The diedown in late 2003 or early 2004 is of interest because of its potential association with the 2002 earthquake. The HLS on LWK-1 following the late 2003–early 2004 diedown was 11 cm higher (in the coral head reference frame) than the HLS after the late 1997–early 1998 diedown (Figure S16b); if the site was gradually subsiding interseismically at 1.4–3.3 mm/yr between late 1997 and late 2003, then in terms of absolute elevation, the early 2004 HLS would be 9–10 cm higher than the early 1998 HLS. As at Lhok Pauh and Langi, ELW near Lewak in early 2004 was ~10 cm higher than in 1997–1998. Unlike at the LKP and LNG sites, however, SLAs alone can explain the diedown in early 2004 at Lewak; no uplift associated with the 2002 earthquake need be invoked there.

7.2.4. A test of the U-Th dating method

Samples from LWK-1 were used to test the validity of the U-Th dating technique. Details of that test are reported later in the auxiliary material.

7.3. 14th–15th century record at Lewak (LWK)

The four most well preserved fossil microatolls found at site LWK-B were slabbed for analysis. Three of those microatolls (LWK-2, LWK-3, and LWK-5; Figures S17–S19, respectively) date to the 15th century; the other (LWK-4; Figure S20) dates to the 14th century. Microatolls LWK-2, LWK-3, and LWK-5 have similar but not identical morphologies. We suspected in the field that they are of the same generation, but because different parts of the record seemed better preserved on different heads, we decided to sample all three. LWK-4 has a different morphology and was less eroded than the others. Because of its greater preservation, we anticipated that LWK-4 would be younger than the others; we were a little surprised, then, that it turned out to be older, based on U-Th analyses. We note, however, that LWK-4 was partly buried in the beach berm when we visited the site in 2007; its greater preservation could be explained if it had been protected in or landward of the beach berm for much of the previous 650 years.

7.3.1. Heads LWK-2, LWK-3, and LWK-5

Two samples each from LWK-2, LWK-3, and LWK-5 were dated by U-Th analyses (Tables S2–S3; Figures S17a, S18a, S19a). Based only upon the samples' ages and the number of growth bands preserved after each sample, we obtain weighted-average dates of 1467 ± 51, 1460 ± 46, and 1477 ± 38 for the outer preserved bands of LWK-2, LWK-3, and LWK-5, respectively. To verify that the records overlap and to help estimate the number of missing bands on each head, we compare the intervals between diedowns on the three microatolls. LWK-2 experienced diedowns 44, 38, 28, ~13, and ~6 years prior to its outer preserved edge (Figure S17a); likewise, LWK-3 experienced diedowns 41, 35, 25, ~10, and ~3 years prior to its outer preserved edge (Figure S18a); and LWK-5 is much more extensively eroded, but diedowns ~36, ~30, and ~20 years prior to its outer edge are still subtly preserved in the head's morphology (Figure S19a). [Although some of these diedowns are not obvious in the x-rayed cross-sections, their existence is substantiated by concentric rings that were observed in the field on the heads' upper surfaces. In the cases where the growth unconformities have been eroded away (thick pink dotted curves, Figures S17a, S18a, S19a), the concentric rings require that the indicated diedowns occurred, although the timing of any such diedown may be uncertain by ± 1–2 yr.] These observations support the argument that all three heads are coeval; LWK-3 appears to be missing exactly three more bands than LWK-2, and LWK-5 appears to be missing ~8 more bands than LWK-2.

We assume that LWK-2 is missing 0.5 ± 0.5 annual bands of growth, based on the lack of evidence that more bands than that are missing; we assume LWK-3 is missing 3.5 ± 0.5 annual bands; and we assume LWK-5 is missing 8.5 ± 2.0 annual bands. Using these assumptions, we calculate a weighted average date of death for these heads of AD 1474.4 ± 25.5 (Tables S3–S4). The 2σ error bars barely encompass AD 1450, the date of an event seen at the LKP sites.

7.3.2. Possible interpretations of the age of LWK-2, LWK-3, and LWK-5

We show two reasonable interpretations of banding ages on Figures S17a, S18a, and S19a. In one interpretation (red years), we assume each head died around AD 1474.4 (May 1474) and is missing the number of annual bands stated above. This combination of assumptions produces the attractive result that LWK-2, LWK-3, and LWK-5 all experienced significant diedowns in early AD 1430, early 1436, and early 1446; diedowns also occurred around early 1461 and early 1468 on LWK-2 and LWK-3, and presumably were recorded at those times on LWK-5 as well, before those parts of LWK-5 were eroded. The main complication with this interpretation is that no diedown is seen around 1450, when a very large uplift is interpreted to have occurred at Lhok Pauh, only 6.5 km to the south-southwest.

An alternate, perhaps more plausible, interpretation is that these three heads all died in AD 1450, in the same event that killed LKP-4 and LKP-10. We assume the same numbers of missing annual bands as above. In this case, the banding ages are shown in blue on Figures S17a, S18a, and S19a, and the respective diedowns occurred in AD 1406, 1412, 1422, ~1437, and ~1444.

7.3.3. Interseismic subsidence recorded by LWK-2, LWK-3, and LWK-5

Time series of HLG and HLS for LWK-2, LWK-3, and LWK-5 are plotted individually on Figures S17b, S18b, and S19b, and together on Figures S21 and 15. The heads show similar submergence (and subsidence) rates: averages of 1.4 and 1.5 mm/yr are obtained from LWK-2 and LWK-3, respectively. However, the observation that LWK-3 is consistently 8–10 cm higher than the two coeval heads suggests that either (*a*) LWK-3 was moved, or (*b*) LWK-2 and LWK-5 both settled. From our field observations, it is not clear which of those actually occurred, because, aside from some minor tilting of LWK-2 and LWK-3, none of the heads are obviously out of place. Fortunately, the difference in absolute elevations is small, and it is probable that at least one of the heads is in its original growth position; hence, for calculations in which an error of a decimeter can be tolerated, it is probably safe to assume the heads are at their original elevations.

7.3.4. Minimum bounds on inferred uplift in 1450

To determine a minimum bound on the coseismic uplift at LWK-B in AD 1450 (or AD 1474), we assume the HLSs following the respective diedowns in 1406 (1430) and 1422 (1446) were the same on all three heads, and we ignore the three heads' absolute elevations. The validity of such an assumption is supported by the observation that, on each of the three heads, HLS following the 1422 diedown was ~5 cm higher than after the 1406 diedown (Figures S17–S19). The upper part of the outer rim appears to be considerably eroded on LWK-2 and LWK-5, but it is much better preserved on LWK-3 (Figures S17–S19, S21). On the other hand, LWK-5, being the tallest of the three, provides the best constraint on the minimum diedown. From LWK-3, we determine that the HLG prior to the 1450 diedown was 12 cm higher than the 1406 post-diedown HLS and 7 cm higher than the 1422 post-diedown HLS; from LWK-5, we know that the HLS following the 1450 diedown was no higher than 29 cm below the 1406 post-diedown HLS or 34 cm below the 1422 post-diedown HLS. Hence, the minimum uplift in AD 1450 (AD 1474) was 41 cm. As with the 1450 uplift at the LKP sites, the absence of corals living on the LWK reef flats at any time after the 1450 (1474) diedown until the early 20th century suggests that the uplift in 1450 (1474) was considerably more than 41 cm.

7.3.5. Head LWK-4

Two samples from LWK-4 yielded a weighted-average date of 1353 ± 10 for the head's outer preserved edge (Tables S2–S3; Figure S20a). We assume LWK-4 is missing 0.5 ± 0.5 annual bands of growth, based on the head's excellent preservation. Hence, the head's inferred date of death is 1354 ± 10. It is difficult to relate this diedown to any of the uplifts identified at other sites. The preferred banding ages shown on Figure S20a assume the head died in early AD 1355 (the date of a large diedown seen at the LKP and LDL sites) and is missing 0.5 annual bands. This has the added attraction that the penultimate diedown on LWK-4 dates to AD 1346, the date of another diedown seen at the LKP and LDL sites. Different assumptions about the exact age of LWK-4 may be just as reasonable, however.

7.3.6. Interseismic subsidence recorded by LWK-4, and death of LWK-4

Because only the uppermost 11 cm of the outer edge of LWK-4 appears to have been living just prior to the head's ultimate death (Figure S20a), all we can say about that diedown is that it was at least 11 cm. Given that the head might have been killed by such a small diedown, it is entirely possible that the cause of the diedown was a transient oceanographic lowering, instead of tectonic uplift. The average subsidence rate recorded by LWK-4 was 6.1 mm/yr (Figure S20b), considerably higher than the 15th or 20th century rates.

8.1. 2004 and subsequent uplift at the Ujung Sanggiran (USG) site

8.1.1. 2004 and 2005 coseismic uplift, and postseismic change

Although observations made in 2005 at nearby sites [*Briggs et al.*, 2006] suggested that USG-A rose in both the 2004 and 2005 earthquakes, we did not visit USG-A until July 2007. Unfortunately, as a result of this delay and other complications, our inferences regarding individual uplifts in 2004 and 2005 are tenuous.

As discussed by *Briggs et al.* [2006], where microatolls rose during both the 2004 and 2005 earthquakes, it was possible (during our site visits in May and June 2005) to differentiate between the two uplifts, as long as the initial uplift was not sufficient to entirely kill all the microatolls at a site. Key to our ability to recognize the two uplifts was the fact that the lower parts of the microatolls—which survived the first uplift but not the second—still appeared "fresh" and unweathered as of June 2005. Unfortunately, by the time we first visited USG-A two years later, the recently dead corals were a bit more weathered, and it was difficult to distinguish the two uplifts. Further complicating this effort, the lower part of the slab from the modern microatoll (USG-1) died years before 2004, precluding identification of the post-2004, pre-2005 HLS in the slab x-ray (Figure S23a).

We surmise that the 2004 uplift at USG-A was ~25 cm, but that inference is debatable. We observed a horizontal lip running along the perimeter of one microatoll, ~25 cm below the pre-2004 HLS; we infer that lip to demarcate the post-2004 HLS. The lip and the surface below it appeared fresher than the surface above the lip. While it is tempting to associate the second diedown with presumed uplift in the March 2005 earthquake, we cannot ascertain with confidence the timing, and hence the cause, of that diedown. The inferred 2004 uplift, ~25 cm, is consistent with the nearest observations made in January 2005 [*Briggs et al.*, 2006].

In July 2007, we determined the net uplift that had occurred at USG-A since immediately prior to the 2004 earthquake by comparing the pre-uplift HLS on *Porites* microatolls to ELW. This value, 32 ± 9 cm, includes the 2004 and 2005 coseismic uplifts and any postseismic uplift or subsidence that had occurred up to July 2007.

8.1.2. 2008 coseismic uplift

We returned to USG-A in February 2009 to document uplift associated with the 2008 earthquake. Net uplift from prior to the 2004 earthquake until February 2009, again determined by comparing pre-uplift HLS to ELW, was 50 ± 10 cm; 18 ± 14 cm of net uplift occurred between July 2007 and February 2009. Presumably, most or all of this uplift occurred coseismically in February 2008.

8.2. Modern paleogeodetic record at Ujung Sanggiran (USG)

8.2.1. Head USG-1

The USG-1 *Porites* microatoll was selected for slabbing because of the numerous concentric growth rings on its dead upper surface and its well-preserved morphology. USG-1 began growing some time in the 1930s, but it does not appear to have reached HLS until early 1958 (Figure S23a). Subsequent diedowns occurred around late 1961, late 1971, late 1978, late 1982, late 1986, late 1991, late 1997, late 2003 (early 2004), and ultimately late 2004, when the head died entirely. These all correspond to diedowns seen elsewhere.

8.2.2. Interseismic subsidence recorded by USG-1

A time series of HLG and HLS for USG-1 is plotted on Figure S23b. Using pre-diedown HLG data spanning AD 1960–2003, we obtain a submergence rate of 3.6 mm/yr, or a subsidence rate of 1.6 mm/yr. If we ignore data from after 1997, the average submergence rate increases to 4.2 mm/yr (not shown), corresponding to a subsidence rate of 2.2 mm/yr. Using corrected post-diedown HLS data spanning 1962–1998, we also obtain an average submergence rate of 4.2 mm/yr, or a subsidence rate of 2.2 mm/yr. We adopt 2.2 mm/yr as the 1960–1997 average subsidence rate at USG-A. As at LWK-A, the interseismic subsidence rate here is low, as expected for this site from elastic dislocation modeling.

8.2.3. The 2003–2004 diedown: possibly tectonic

Again as at LWK-A, the diedown in late 2003 or early 2004 is of interest because of its potential association with the 2002 earthquake. The HLS on USG-1 following the late 2003–early 2004 diedown was 6 cm higher (in the coral head reference frame) than the HLS after the late 1997–early 1998 diedown (Figure S23b); if the site was gradually subsiding interseismically at ~2.2 mm/yr between late 1997 and late 2003 and there was no uplift in 2002, then in terms of absolute elevation, the early 2004 HLS would be ~5 cm higher than the early 1998 HLS. Considering that the ELW was ~10 cm higher in early 2004 than in 1997–1998, the early 2004 diedown can be best explained if ~5 cm of uplift at USG-A resulted from the 2002 earthquake.

8.3. 14th–15th century record at Ujung Sanggiran (USG)

8.3.1. Heads USG-2 and USG-3

The two fossil microatolls found at site USG-A were both slabbed for analysis. USG-2 (Figure S24) was fairly eroded, but at least one ring could still be identified in the field. USG-3

(Figure S25) was considerably more eroded, and its original microatoll morphology was barely discernable.

Two samples each from USG-2 and USG-3 were dated by U-Th analyses (Tables S2–S3; Figures S24a, S25). Based only upon the samples' ages and the number of growth bands preserved after each sample, we obtain weighted-average dates of late 1432 (± 15) and mid-1320 (± 29) for the outer preserved bands of USG-2 and USG-3, respectively. For reasons outlined in the next paragraph, we assume USG-2 is missing 2 ± 2 annual bands and USG-3 is missing 5 ± 5 bands, although each head's appearance would be equally consistent with more erosion than we assume. Using these assumptions, we calculate weighted-average dates of death of AD 1435 ± 16 and 1326 ± 29, respectively (Table S3). For USG-2, the 2σ error bars barely encompass AD 1450, although the mean date is closer to AD 1430, the year of another known uplift event on northern Simeulue.

The preferred banding ages on Figure S24a assume USG-2 died in early AD 1450 and is missing 2 bands. This produces the attractive result that the 1430 uplift event is also seen on the head. The preferred banding ages on Figure S25 assume the outer preserved band on USG-3 dates to AD 1328; in that case, a diedown in early 1309 seen on LWK-4 is also seen on USG-3.

8.3.2. Interseismic subsidence recorded by USG-2, and death of USG-2

Based on the morphology of USG-2, it appears the uplift that killed the head was at least 32 cm, and it could have been considerably more. The average subsidence rate recorded by USG-2 was ~7.2 mm/yr (Figure S24b). This is considerably higher than the modern rate, but it was determined based on only a 19-year record. Because of the extensive erosion on USG-3, it is not possible to estimate the size of the diedown that killed it or the interseismic rate it recorded during its lifetime.

9.1. Description of the Pulau Salaut (PST) site

Two small islets lie ~40 km northwest of the northwest coast of Simeulue: Pulau Salaut Besar and Pulau Salaut Kecil (*Big Salaut Island* and *Little Salaut Island*, respectively; Figures 2, S26). All of Salaut Kecil and most of Salaut Besar are surrounded by extremely rugged, steep-sided, uplifted reefs; the only exception is the northern northeast coast of Salaut Besar, which has a ~2-m high, steep sandy high-energy beach scarp, with reef rock at the base of the scarp.

Higher swells than those experienced along the coast of Simeulue persisted during our only visit to those islands, in February 2009. Indeed, high swells appear to be a regular feature in this area: high swells have been experienced by prior investigators in the area [U.S. Geological Survey (USGS) (2005), Notes from the field ... USGS scientists in Sumatra studying recent tsunamis; available at http://walrus.wr.usgs.gov/news/reportsleg1.html], and our own attempt in July 2007 to travel to those islands was aborted because of the high swells approaching the islands. The islands' coastal morphology (described above) also appears to be consistent with persistent high swells.

The combination of the high swells and the rugged coastline made landing our dinghy on either island a perilous proposition. After scouting both islands for landing sites, we determined our only safe option was to guide our dinghy toward the sandy beach, but to swim to shore for the final 8–10 m. This action precluded us from bringing ashore the total station for surveying or the cutting equipment for coral slabbing.

After swimming ashore, we explored 2.7 km of the eastern and southern coasts of Pulau Salaut Besar by foot (Figure S26). Much of the reef is barren, eroded reef rock, but small modern corals and microatolls, and a small population of larger fossil *Porites* microatolls were found on the southeast coast of the island. The reefs were littered with large coral head tsunami blocks, especially along the same part of the coast where heads were found in place.

Because we could not bring our surveying or cutting equipment ashore, we did not attempt to sample any modern microatolls. We did, however, chisel a piece off the outer edge of one of the fossil microatolls (PST-1), in order to estimate the date of the presumed uplift event that killed the head. Like many of the fossil heads on northern Simeulue, PST-1 appears to have died in the late 14th century AD.

In the course of our reconnaissance of the southern part of Salaut Besar, we came across what appears to be a tectonic fault scarp. Unfortunately, circumstances (including a lack of equipment and limited time) prevented us from fully documenting this feature, and we were not able to follow the feature far into the nearly impenetrable jungle; nonetheless, in the next section, we discuss our observations and present speculative evidence that the linear feature we observed is indeed a fault, and that it ruptured at the time of or soon after the 2004 earthquake. Field photos of the inferred scarp are provided in the electronic supplement.

9.2. A landward-vergent thrust fault on Pulau Salaut Besar

9.2.1. A tectonic scarp?

At the southern tip of Pulau Salaut Besar, we observed a fresh scarp cutting across the uplifted barren reef for at least 50 m (Figure S26). This scarp had nearly 2 m of relief, with the reef surface down to the east. Abundant reef-rock boulders of up to 1 m in diameter sat at the base of the scarp, apparently having collapsed off the scarp, forming an incipient colluvial wedge on top of the reef flat. We attempted to follow the scarp into the jungle, but it broadened and became more diffuse as it ran into the lush jungle. Where the scarp was abrupt on the reef flat, we looked for slickensides that would have been indicative of relative motion along a fault. However, any such signs had been buried or destroyed by four years of erosion and scarp retreat. Standing at the scarp, it was not immediately clear whether the feature was the result of localized reef collapse or was a more substantial tectonic fault. Additional observations, outlined below, support a tectonic interpretation.

9.2.2. Evidence for recent offset?

Walking along the southern coast of the island, we identified a sandy beach berm running more or less continuously along the outer edge of the dense jungle; this berm appears to have been offset across the proposed fault. When we visited the site in February 2009, this berm was covered by young coconut palms that ranged from a few decimeters up to 3 or 4 m high; based upon their heights and our observations at other recently uplifted sites, none of the coconut palms growing on this berm appeared to be more than ~4 years old. We consequently interpret this to be the pre-2004 beach berm, the active berm until the 2004 uplift. Only after it was uplifted and sequestered from wave action could coconut palm seedlings take root and begin to grow there. We identified this berm both west and east of the aforementioned escarpment, but west of the scarp it was ~2 m higher than to the east. The distance over which the berm's elevation appears to have been affected suggests a tectonic cause.

9.2.3. Evidence for cumulative offset?

Two other observations support a tectonic interpretation. First, an arcuate lineament exists on 15-m resolution satellite imagery (various ASTER and panchromatic Landsat images, from both before and after the 2004 mainshock) extending from the location of the scarp on the reef into the jungle for more than 300 m (Figure S26); the extension of the lineament farther to the northwest is not clear from imagery. Second, an elevated reef terrace juts into the ocean ~400 m northwest of the observed reef scarp, on the upthrown side of the scarp and lineament. We surmise that this elevated reef is mid-Holocene in age or older, and we crudely estimate (from a distance of ~100 m) its elevation to be ~10 m above mean sea level; its elevation is difficult to explain other than as the cumulative result of repeated uplift along an upper-plate thrust or reverse fault. The portion of the recent uplift attributable to slip on the megathrust is presumably elastic and will be recovered by interseismic subsidence, but uplift due to dip slip along the upper-plate fault may be permanent.

9.2.4. Possible continuation of the fault to the northwest

Klingelhoefer et al. [2010] and *Singh et al.* [2008] each acquired deep marine reflection data along trench-normal profiles ~18 km and ~24 km, respectively, northwest of Pulau Salaut Besar. At kilometer 43 of their profile BGR06-141, *Klingelhoefer et al.* [2010] mapped a shallow southwest-dipping thrust fault along the northeastern margin of the Simeulue plateau. If real, this feature is roughly along strike of Salaut Besar Island, intersecting the BGR06-141 profile 18 km northwest of Salaut. Although this feature would not necessarily connect with the structure we observed on Salaut, its presence in the BGR06-141 line would support the existence of either a single fault or a family of such faults along strike in that vicinity. *Singh et al.* [2008] did not image any shallow thrust faults near the Simeulue plateau that could correspond to the feature we observed on Salaut, which suggests that the feature does not extend to their line farther northwest.

9.2.5. Timing of slip along this inferred fault

If the abrupt step in elevation of the pre-2004 beach berm is a result of differential tectonic uplift, that uplift could not have happened much before the 2004 earthquake. Had any dip slip occurred along this fault more than a few months to a year before the 2004 earthquake, a new, lower beach berm should have formed west of the scarp (at the elevation of the berm to the east), and the higher berm west of the scarp would be populated by slightly older coconut palms than those found at present in the berm to the east; in contrast, no lower berm is observed to the west, and the age distribution of coconut palms in the berm appears to be similar on the two sides of the scarp.

We consider it most likely that slip on the fault occurred during the 2004 mainshock, but we also consider other possibilities. We searched both the Global CMT catalog [Global Centroid Moment Tensor (CMT) Project, catalog search; available at http://www.globalcmt.org/CMTsearch.html] and the EHB relocated hypocenter catalog [*Engdahl et al.*, 2007] for additional candidate earthquakes that could have produced the observed displacements.

9.2.6. Information from earthquake catalogs

A search of the Global CMT catalog from January 2003 to February 2009 reveals only two earthquakes of $M_W \geq 5.0$ within 15 km of the observed scarp: M_W 5.6 and M_W 5.7 events, both on 27 December 2004. One event of $M_W \geq 6.0$ is located within 25 km of the scarp: an M_W 6.7 event on 26 February 2005, 18 km away. An expanded search of all events within 60 km of the scarp with at least one magnitude (M_W, M_S, or m_b) above 6.5 in the Global CMT catalog yielded no additional candidate earthquakes.

The EHB catalog's locations are more accurate than those in the Global CMT catalog, but the EHB catalog provides hypocenters rather than moment centroids. The EHB catalog (through October 2007) contains four events of $M_W \geq 5.0$ within 15 km of our observed scarp: the M_W 5.6 event on 27 December 2004; M_W 6.3 and M_W 5.7 events on 30 March 2005; and an M_W 5.8 event on 29 September 2007. Of these, the M_W 6.3 event in March 2005 is a particularly likely candidate, with its hypocenter only 2.3 km from the observed scarp, a reported 1σ error of 2.5 km in its location [*Engdahl et al.*, 2007], and a moment tensor consistent with either slip on the megathrust or slip on a high-angle northwest-striking, southwest-dipping reverse fault (Global CMT catalog). Like the other events in the region, however, this earthquake was deep (hypocentral depth: 27.5 km) [*Engdahl et al.*, 2007], leading *Singh et al.* [2008] to interpret it as a lower-plate event. One additional event of $M_W \geq 6.0$ is located within 30 km of the scarp: the M_W 6.7 event on 26 February 2005, 17 km away according to the EHB catalog. Again, an expanded search of all events within 60 km of the scarp with at least one magnitude (M_W, M_S, or m_b) above 6.5 in the EHB catalog yielded no additional candidate events.

9.2.7. Our preferred interpretation

Based on our geomorphic observations at the site and our two catalog searches, the most plausible timing of displacement along the inferred upper-plate fault is either during the 2004 mainshock, or in the M_W 6.3 aftershock on 30 March 2005. Nonetheless, because the observed displacement is higher than would be expected for a M_W 6.3 earthquake, and because of the March 2005 event's depth, we prefer the explanation that the motion along the upper-plate fault occurred during the 2004 mainshock.

9.3. 2004 uplift at Pulau Salaut Besar (PST)

Uplift in 2004 at Pulau Salaut Besar was large—larger than at any other island in the earthquake—but details of the pattern of uplift are unclear. Several estimates of 2004 uplift on Pulau Salaut Besar have been published. *Subarya et al.* [2006] report 210 ± 9 cm of uplift (2σ) based on campaign GPS measurements at site R171, but the location they provide for the R171 monument is incorrect; the actual location is 2.97988 °N, 95.38773 °E (C. Subarya, personal communication, 2009; Figure S26). The reported uplift was corrected for interseismic deformation in the years prior to the 2004 uplift, but it includes any postseismic motion that had occurred prior to the monument reoccupation on 7 February 2005. *Jaffe et al.* [2006] estimate 2.4 and 1.7 m of uplift at locations 60 m apart from one another near the northern tip of the island, based on the "old high tide to new high tide" and an "uplifted berm and beach platform," respectively. Their measurements were made on 9 April 2005 [U.S. Geological Survey (USGS) (2005), Notes from the field ... USGS scientists in Sumatra studying recent tsunamis; available at http://walrus.wr.usgs.gov/news/reportsleg1.html]. Rather than being an indication of differential uplift at these two closely spaced points, we interpret the difference in the two estimates to reflect the estimates' uncertainties; we note that the average of Jaffe et al.'s estimates is indistinguishable from the R171 campaign GPS uplift [*Subarya et al.*, 2006].

The main difficulty in interpreting the campaign GPS measurement is the uncertainty in its location with respect to the proposed upper-plate reverse fault. It is unclear from our observations in the field and from imagery whether the structure (*a*) terminates or wraps offshore in the southern 0.5 km of the island and does not extend farther north, or (*b*) continues up the west coast of the island, parallel to shore. (A lineament appears in imagery running along the west coast of the island, but that lineament may simply be an old beach berm and swale.) In the former case, site R171 would be on the downdropped side of the inferred fault, but in the latter case, R171 might be on the upthrown side. Based on available imagery, we prefer the interpretation that the fault wraps offshore just north of the inferred uplifted mid-Holocene reef, which would place R171 on the downdropped block, but it is admittedly ambiguous.

If the upper-plate fault displacement occurred during the 2004 mainshock, then the slip vector calculated at site R171 (including the reported uplift of 210 ± 9 cm) [*Subarya et al.*, 2006] is biased by the upper-plate motion. If site R171 is on the downdropped side of that structure, then the 2004 coseismic uplift at the southwestern tip of Salaut Besar would have been ~4 m, which would be consistent with our observations in 2009. In that case, motion along the thrust would have increased the horizontal vector at site R171 and decreased the uplift. This might seriously impact slip models' estimates of the amount of slip on the megathrust in that region [e.g., *Subarya et al.*, 2006; *Banerjee et al.*, 2007; *Chlieh et al.*, 2007; *Rhie et al.*, 2007]; as a consequence, it may be prudent to revisit modeling of slip on the megathrust in the 2004 earthquake.

9.4. Paleogeodetic record at Pulau Salaut Besar (PST)

9.4.1. Head PST-1

Along the southeast coast of Pulau Salaut Besar, we found three clustered large fossil *Porites* microatolls that appeared to be in place and were considerably eroded. They had similar morphologies and were at about the same elevation; we inferred they were of the same generation. We chiseled off a sample for dating (PST-1; Figure S27) from the outer rim of the largest (2.5-m radius) and most preserved of the three microatolls. The outer preserved edge of PST-1 dates to late AD 1355 (± 7) (Tables S2–S3; Figure S27), but the head is likely missing many outer bands. We infer that the head died as a result of the AD 1394 uplift seen on northern Simeulue; if 16 annual bands have been eroded from the slab in Figure S27, then an earlier diedown on the outer part of PST-1 occurred in 1355, the year of an inferred transient oceanographic lowering on northern Simeulue. However, if we assume 16 ± 16 bands are missing and we count outward from the dated sample, then we calculate the head's date of death to be AD 1372 ± 17 (Table S3). This suggests that the age obtained for U-Th sample PST-1-B1 is slightly too old, that 32 or more bands are actually missing, or that the head died prior to 1394.

The outer rim of head PST-1 is ~46 cm higher than the center of the inner hemisphere of the head, suggesting ~46 cm of upward growth accompanied 2.5 m of outward growth. Assuming an average growth rate of 16.2 mm/yr (estimated from the chiseled slab in Figure S27), this corresponds to an average interseismic submergence rate of 3.0 mm/yr over the prior ~150 years. The outer rim of PST-1 is ~72 cm higher than our best estimate of 2004 pre-uplift HLG, although a lack of well-developed in-place modern microatolls near the PST-1 population makes our estimate of pre-2004 HLG questionable.

15. A Test of the U-Th Dating Method

LWK-1 was used to test the validity of the U-Th dating technique. Several samples were drilled and dated by the U-Th dating method (Figure S16a; Table S5). For subsamples C1 and C2, the initial thorium ratio, $[^{230}Th/^{232}Th]_0$, was determined by 3-D isochron techniques to be $3.01 \pm 0.47 \times 10^{-6}$ [*Shen et al.*, 2008]; for the remaining samples on this head, it remains an open question whether it is most appropriate to assume an initial thorium ratio of $3.01 \pm 0.47 \times 10^{-6}$, as suggested specifically for this head by *Shen et al.* [2008], or an initial ratio of $6.5 \pm 6.5 \times 10^{-6}$, as suggested by *Zachariasen et al.* [1999] for all Sumatran samples whose initial ratio has not been determined by isochron techniques. Although assuming an initial ratio of $3.01 \pm 0.47 \times 10^{-6}$ for all samples on LWK-1 clearly yields U-Th ages that are more consistent with the samples' true ages (Figure S16a), the initial ratio can vary considerably from one head to another at a given site (Table S2), and we also have an example (unpublished) of significant variation (i.e., ratios that are incompatible at 2σ) from two bands on the same head. Furthermore, we have assumed an initial ratio of $6.5 \pm 6.5 \times 10^{-6}$ for all fossil head samples whose initial ratio was not determined by isochrons; hence, for the purpose of testing the validity of those results, we should examine the results of the U-Th dating procedure on LWK-1 assuming the initial ratio is $6.5 \pm 6.5 \times 10^{-6}$ in all cases where it has not been determined to be otherwise (Table S5a; Figure S16a). Although the ages determined using the less precise initial ratio are less precise themselves, none are within 1σ of their true age, but all four are within 1.3 standard deviations of their true age (as determined by band counting).

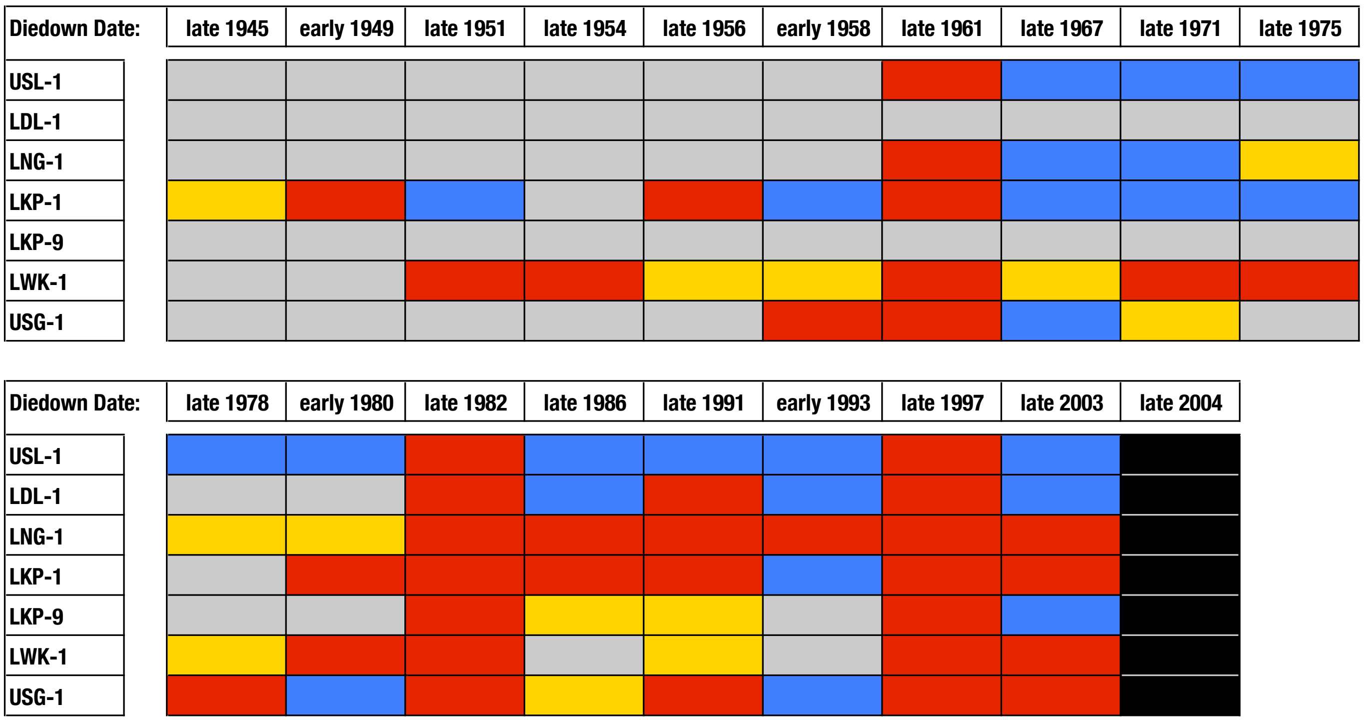

EVERY **date on which a slabbed coral experienced a diedown is represented in the table above, even if only a single microatoll was affected.**
The following colors in the boxes above indicate whether, within temporal resolution of the stated date, a diedown occurred on the microatoll:

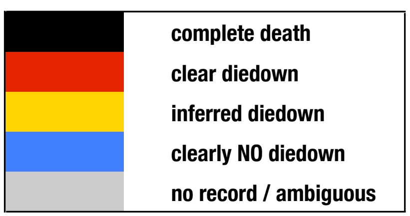

Figure S1. Dates of coral diedowns on 20th-century northern Simeulue microatolls.

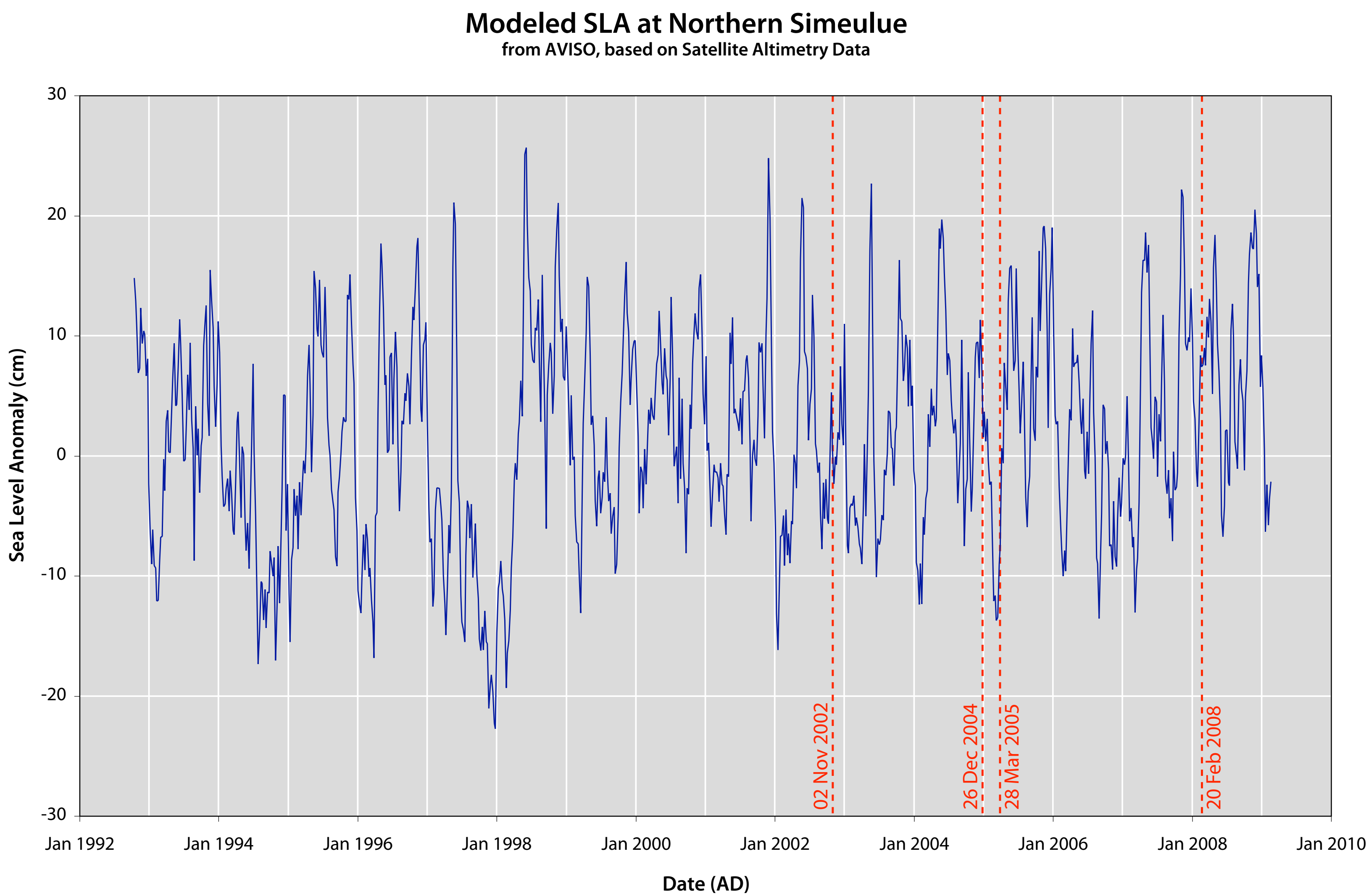

Figure S2. Modeled northern Simeulue SLAs from AVISO, based on satellite altimetry data.

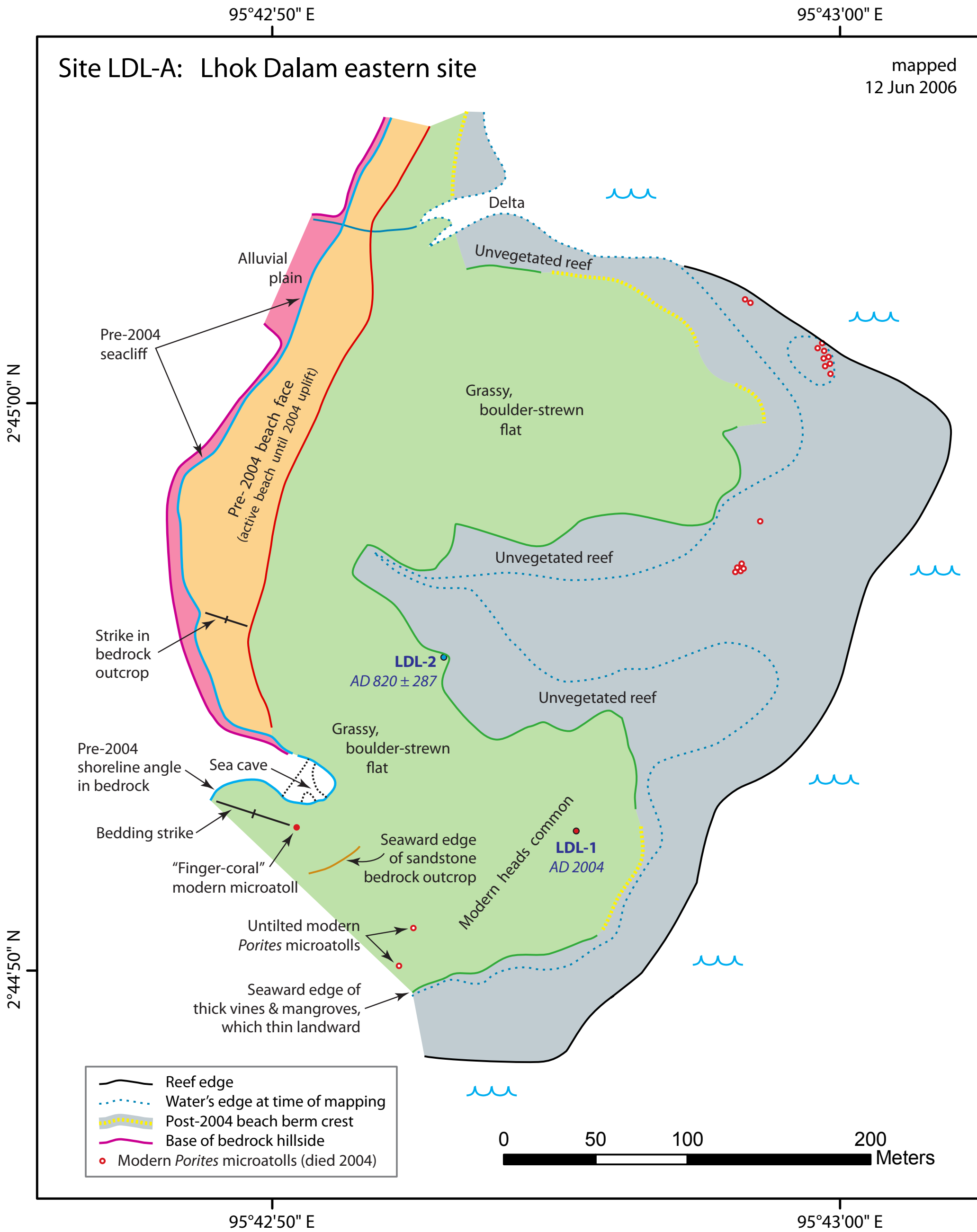

Figure S3a. Map of site LDL-A, near the western tip of Simeulue, showing sampled microatolls and their dates of death.

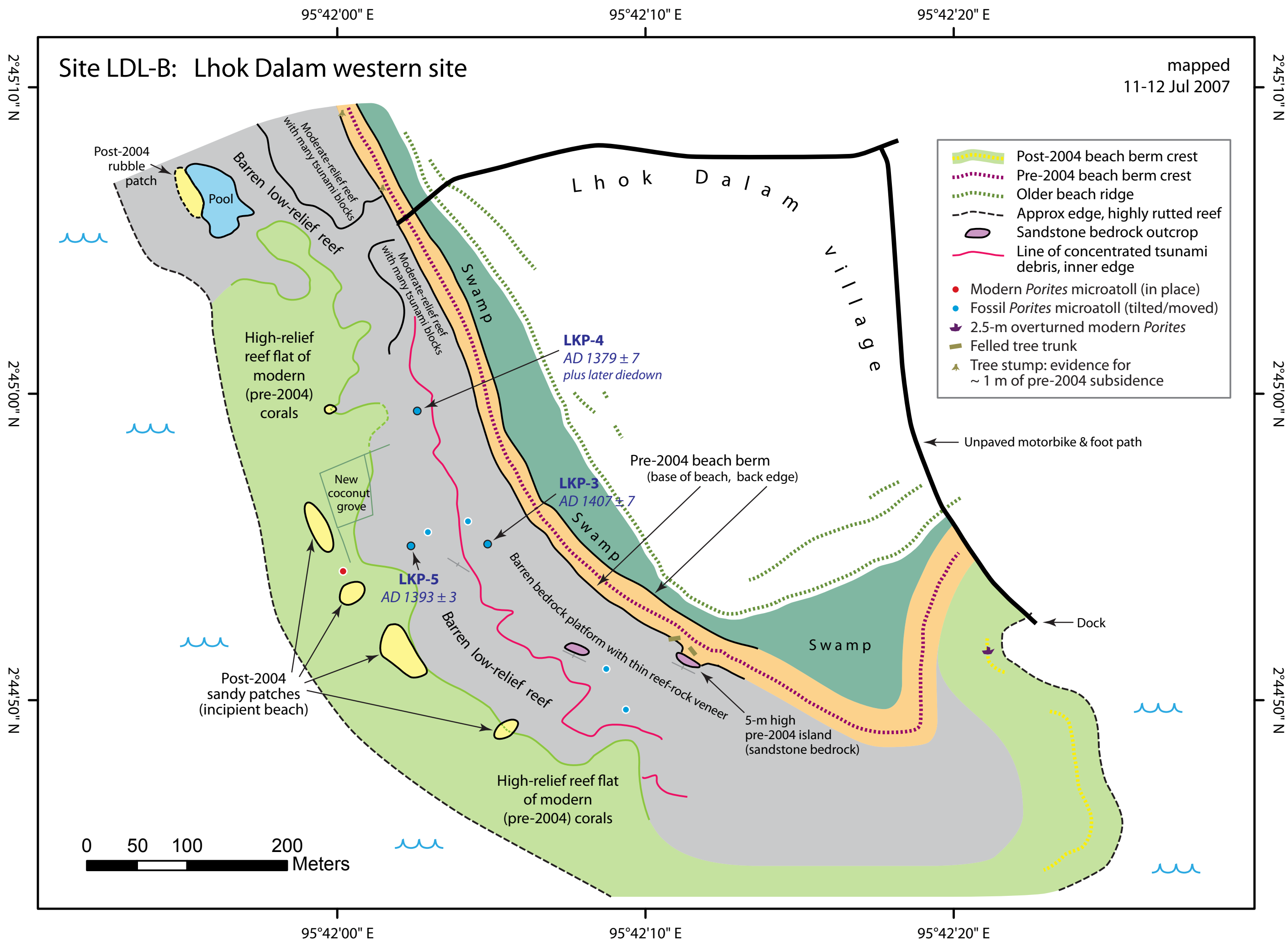

Figure S3b. Map of site LDL-B, near the western tip of Simeulue, showing sampled microatolls and their dates of death.

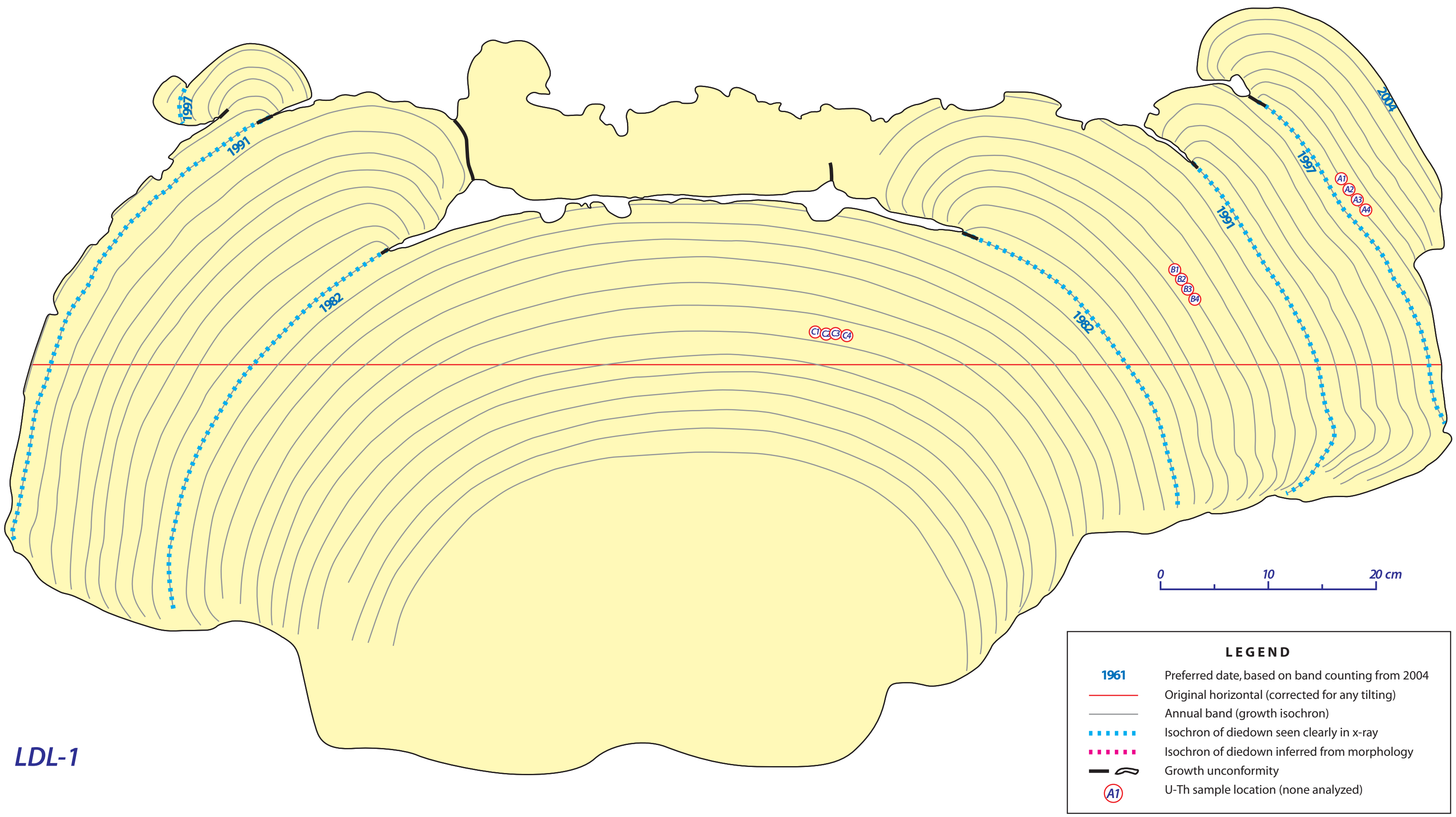

Figure S4a. Cross-section of slab LDL-1, from site LDL-A.

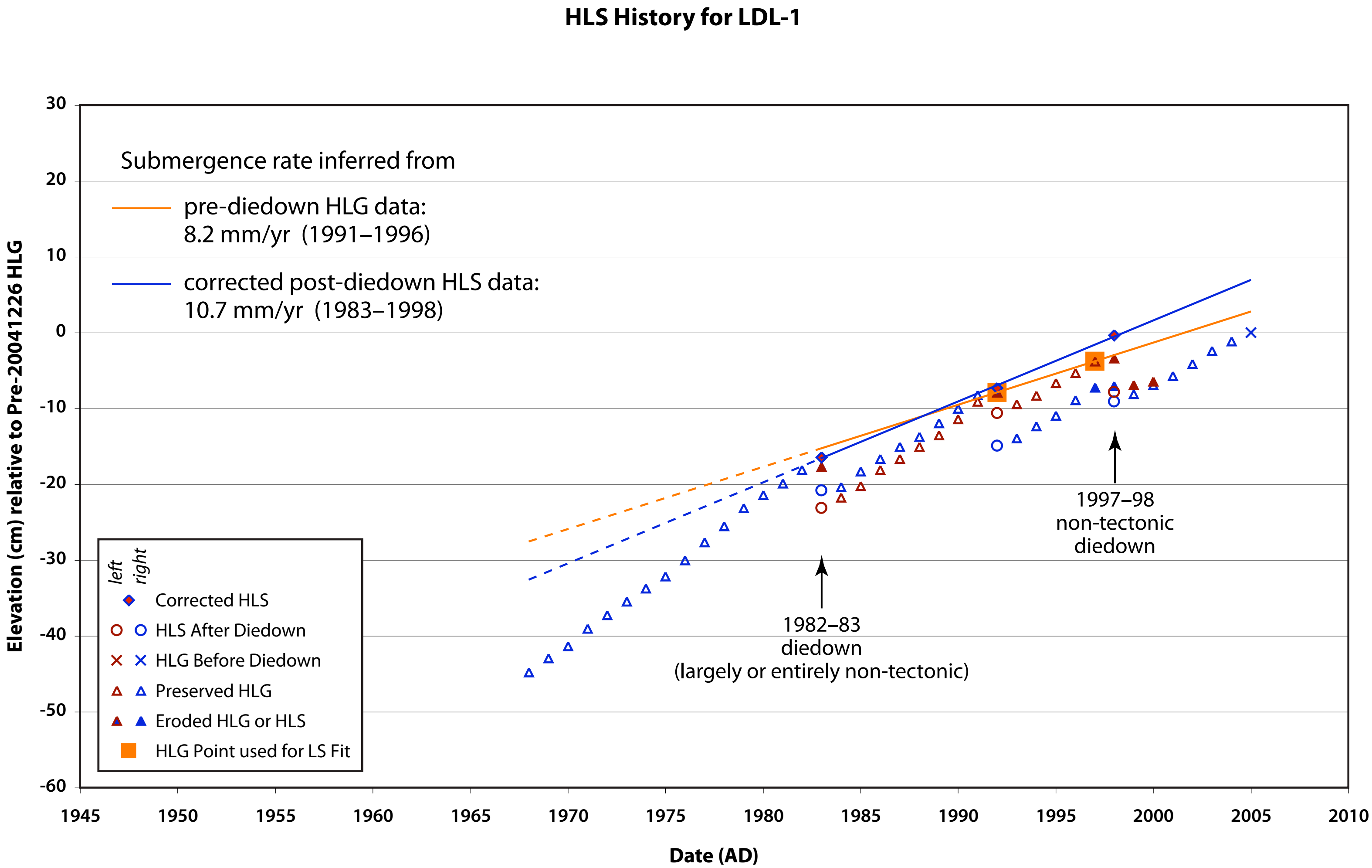

Figure S4b. Graph of relative sea level history derived from slab LDL-1.

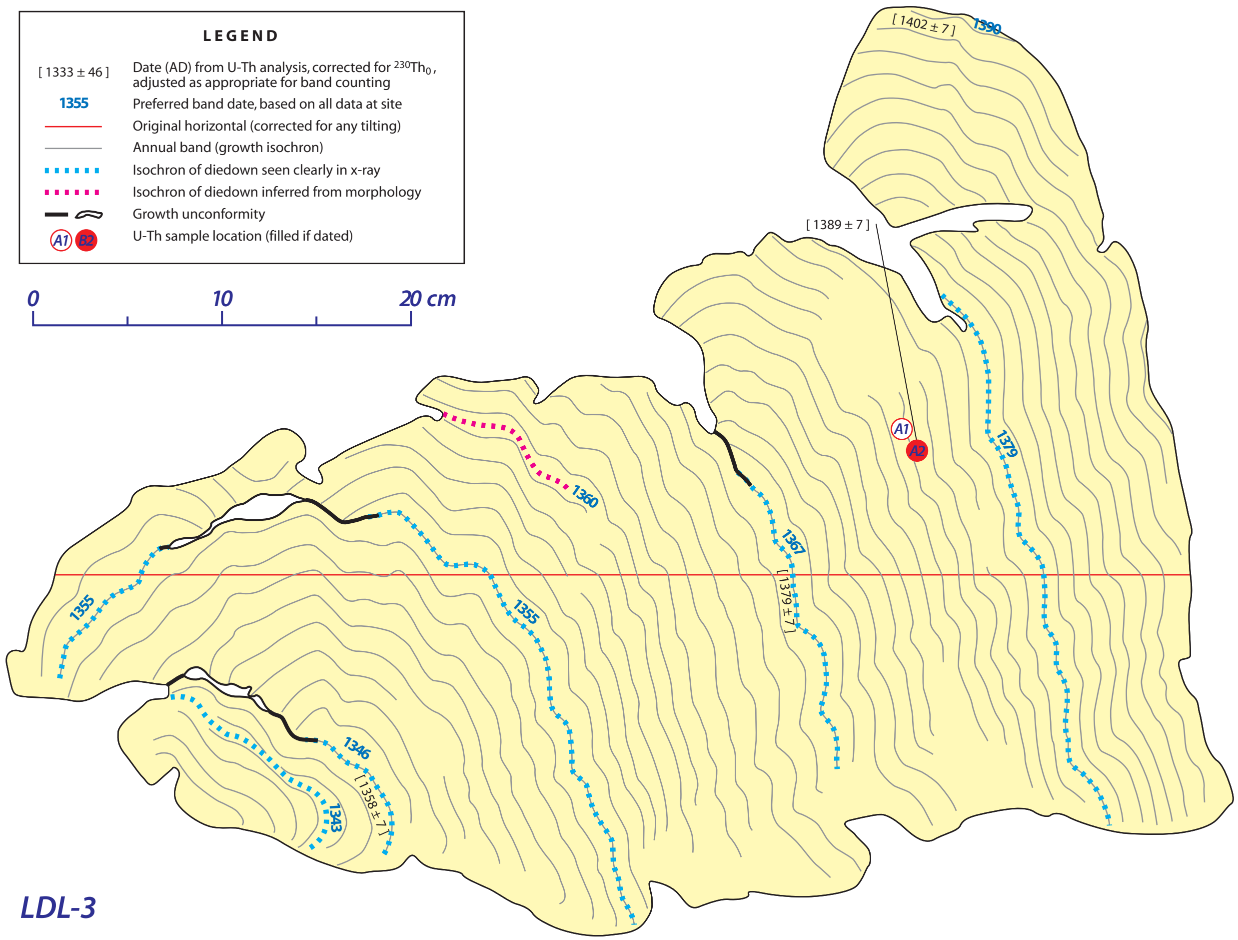

Figure S5a. Cross-section of slab LDL-3, from site LDL-B.

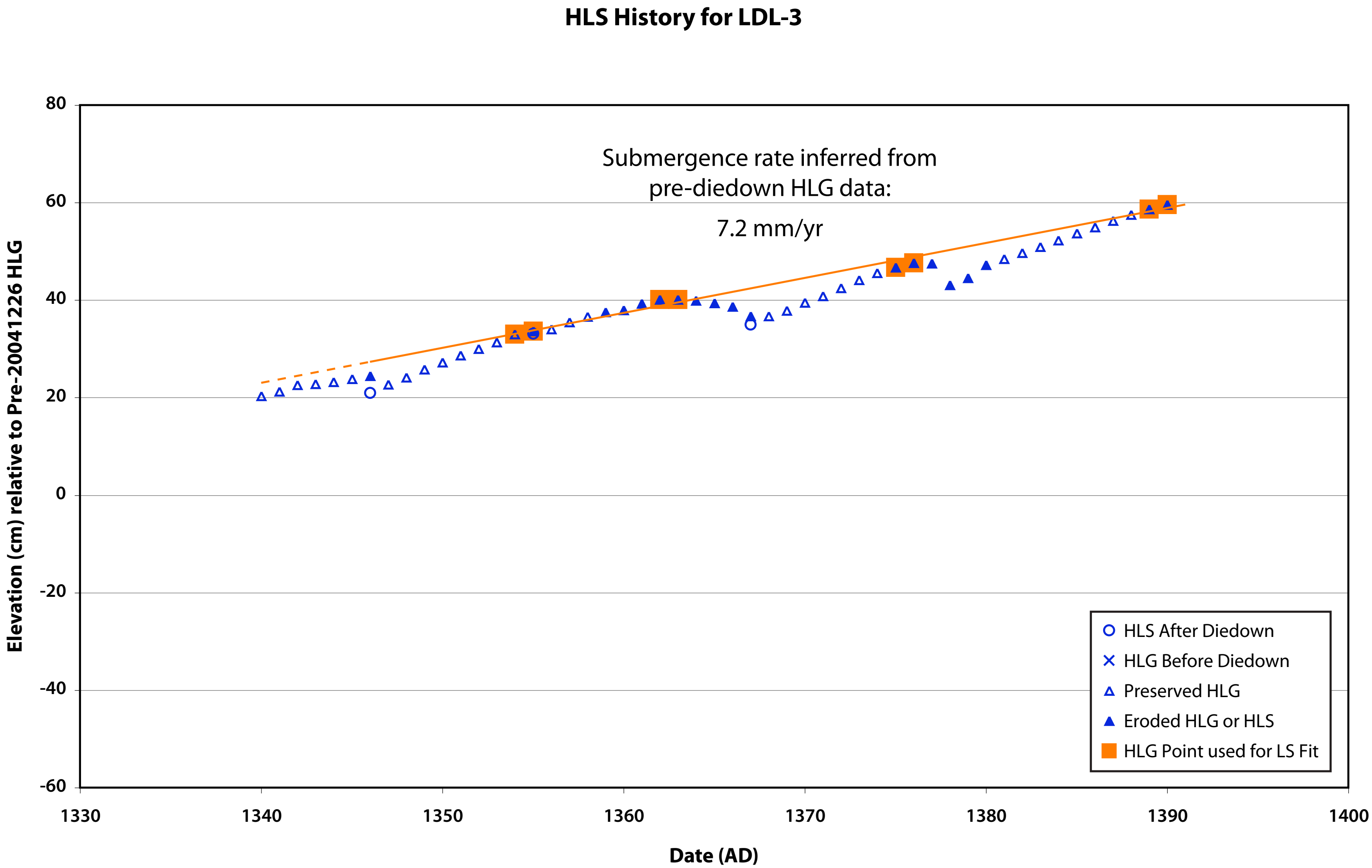

Figure S5b. Graph of relative sea level history derived from slab LDL-3.

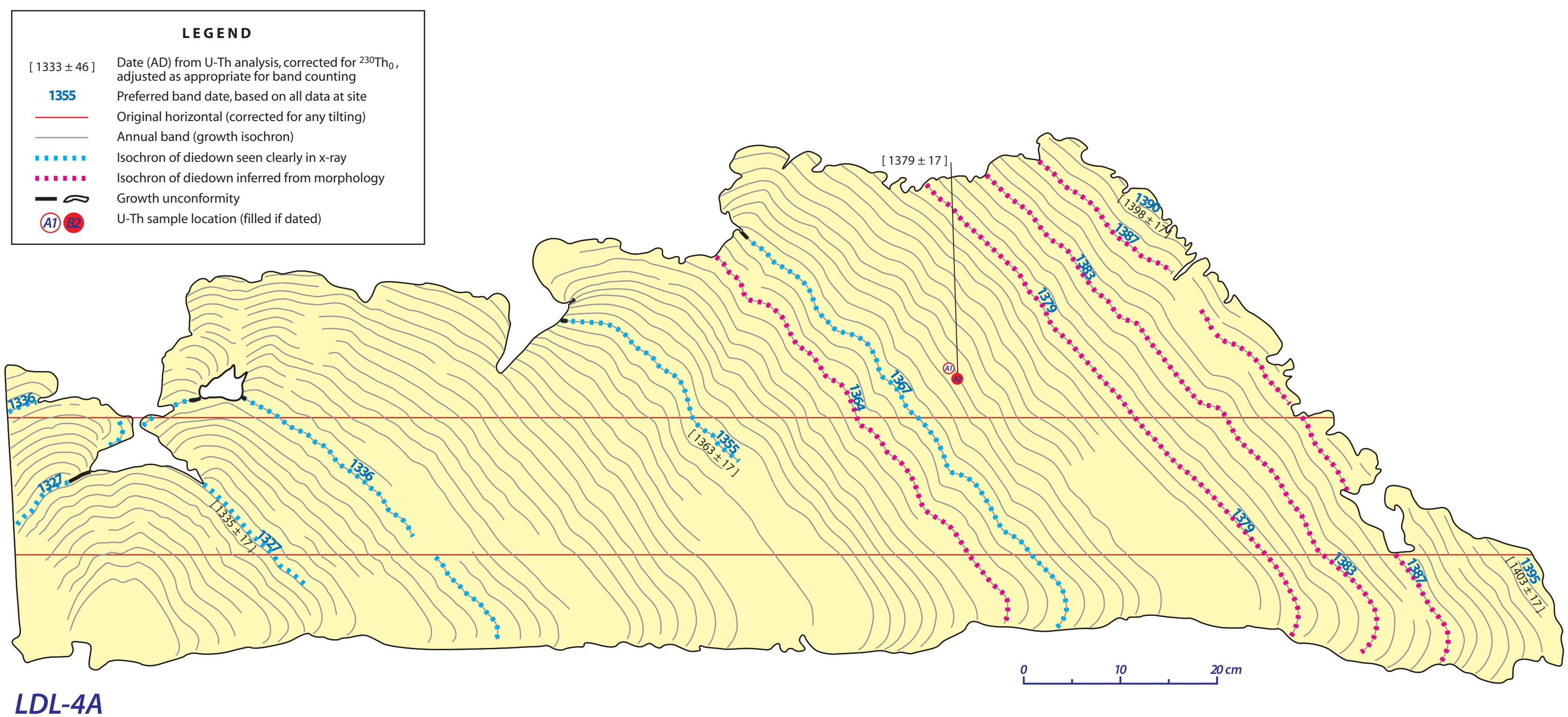

Figure S6a. Cross-section of slab LDL-4A, from site LDL-B.

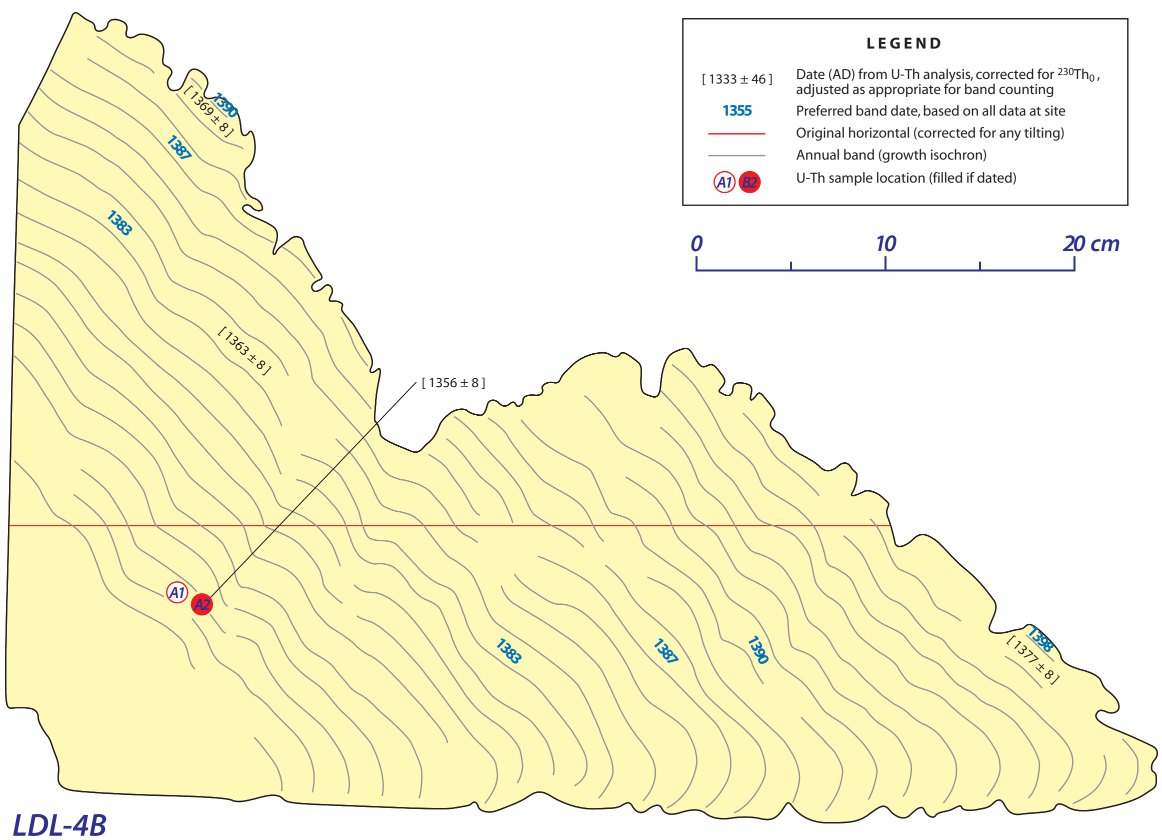

Figure S6b. Cross-section of slab LDL-4B, from site LDL-B.

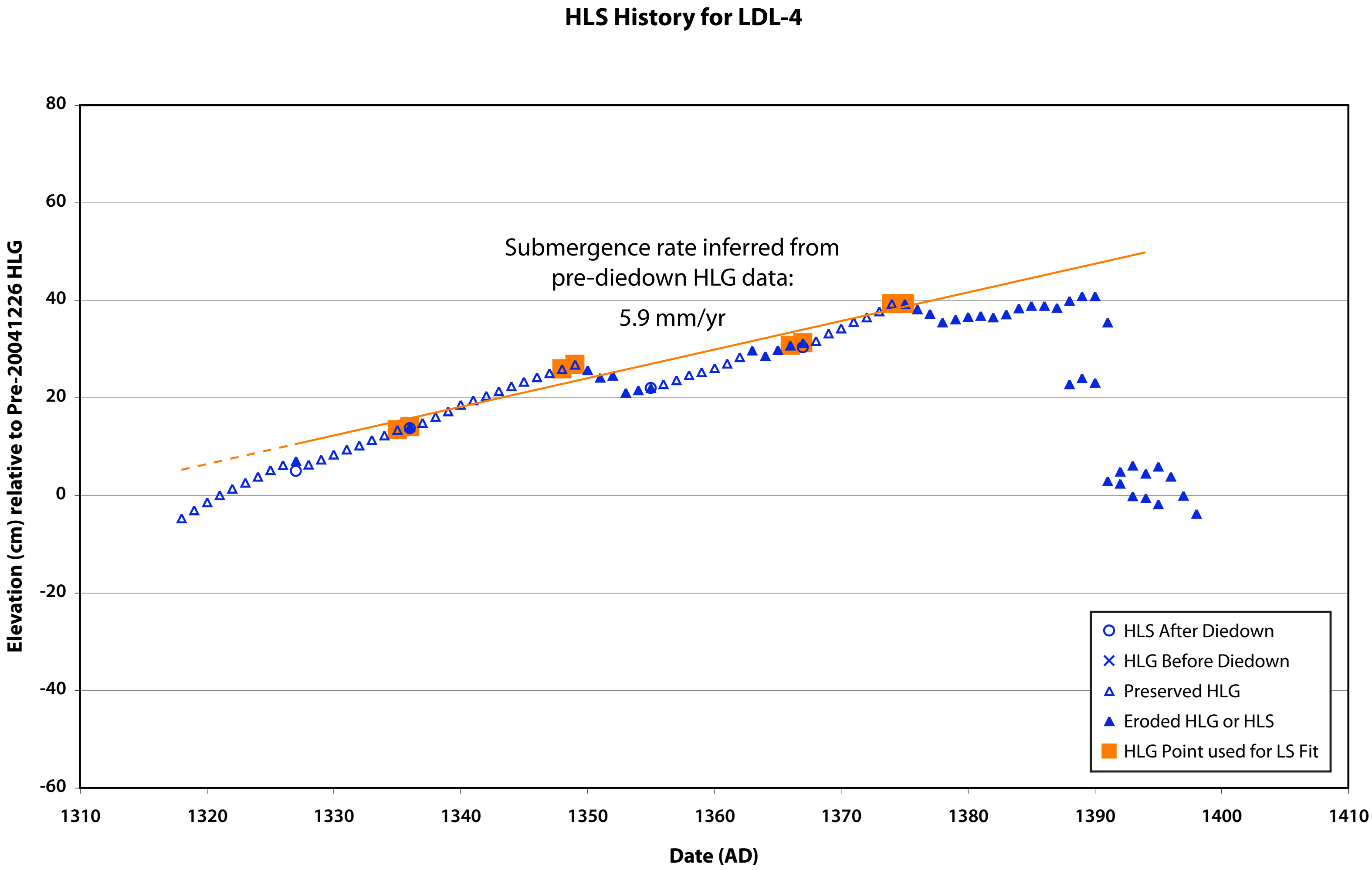

Figure S6c. Graph of relative sea level history derived from slabs LDL-4A and LDL-4B.

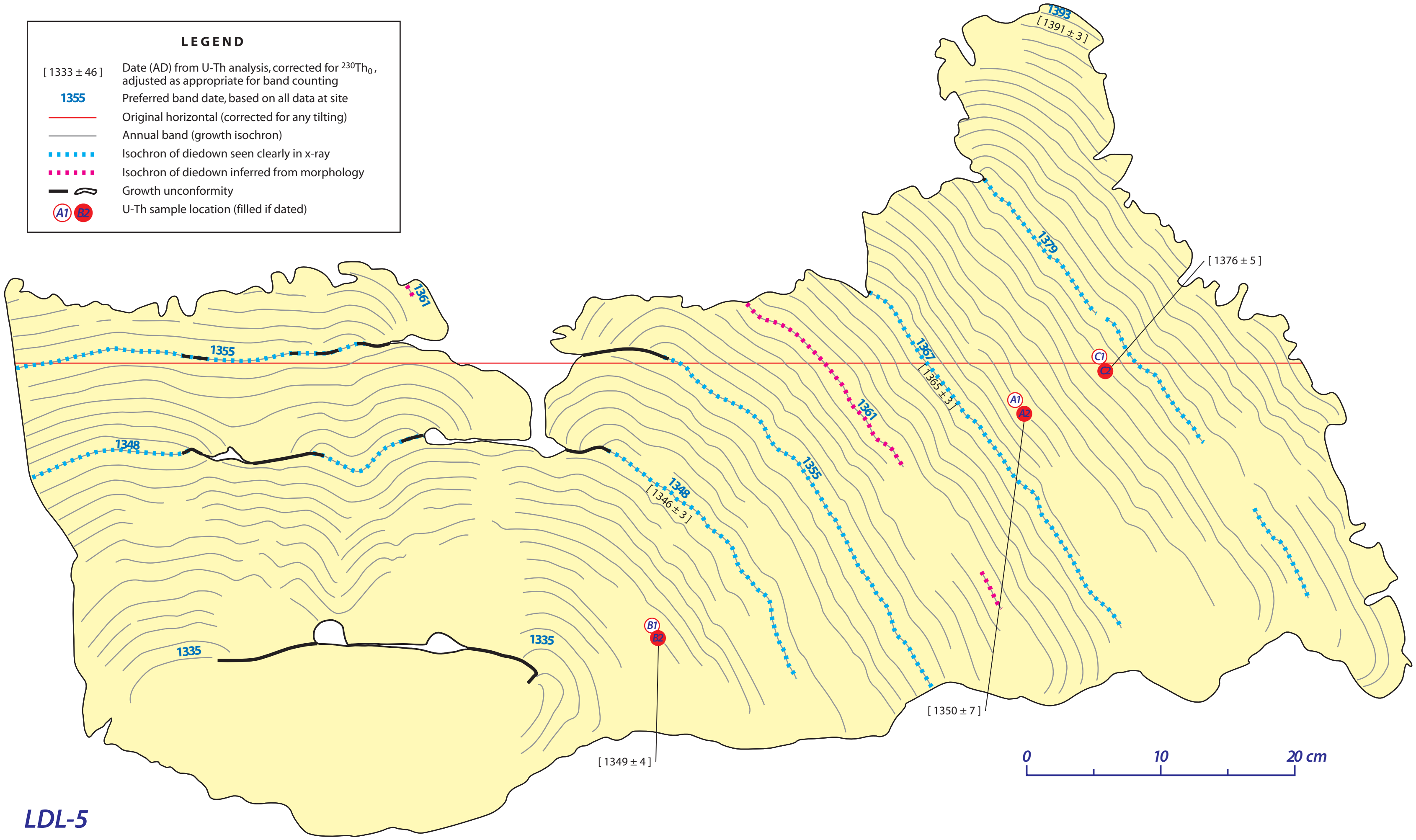

Figure S7a. Cross-section of slab LDL-5, from site LDL-B.

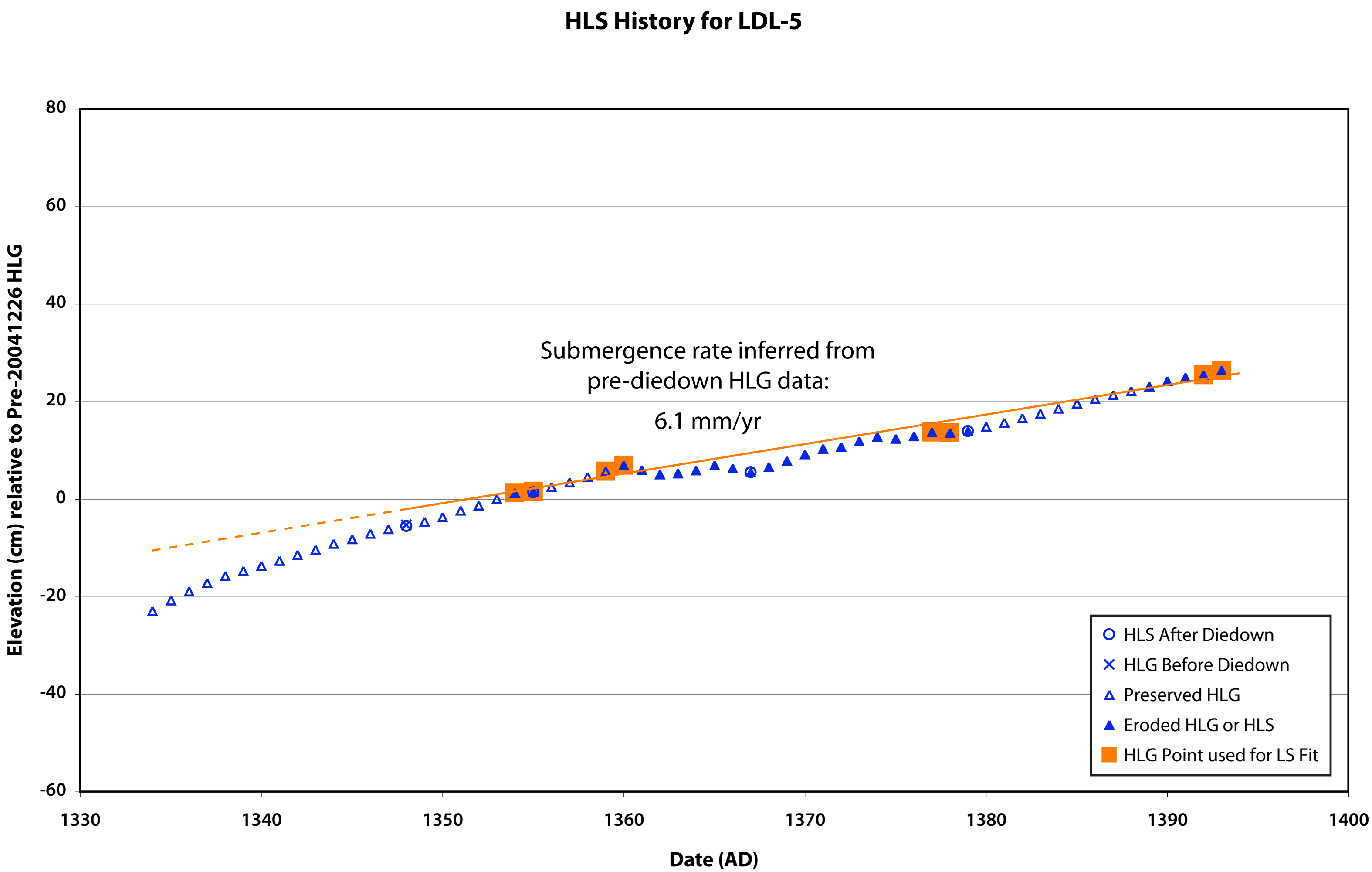

Figure S7b. Graph of relative sea level history derived from slab LDL-5.

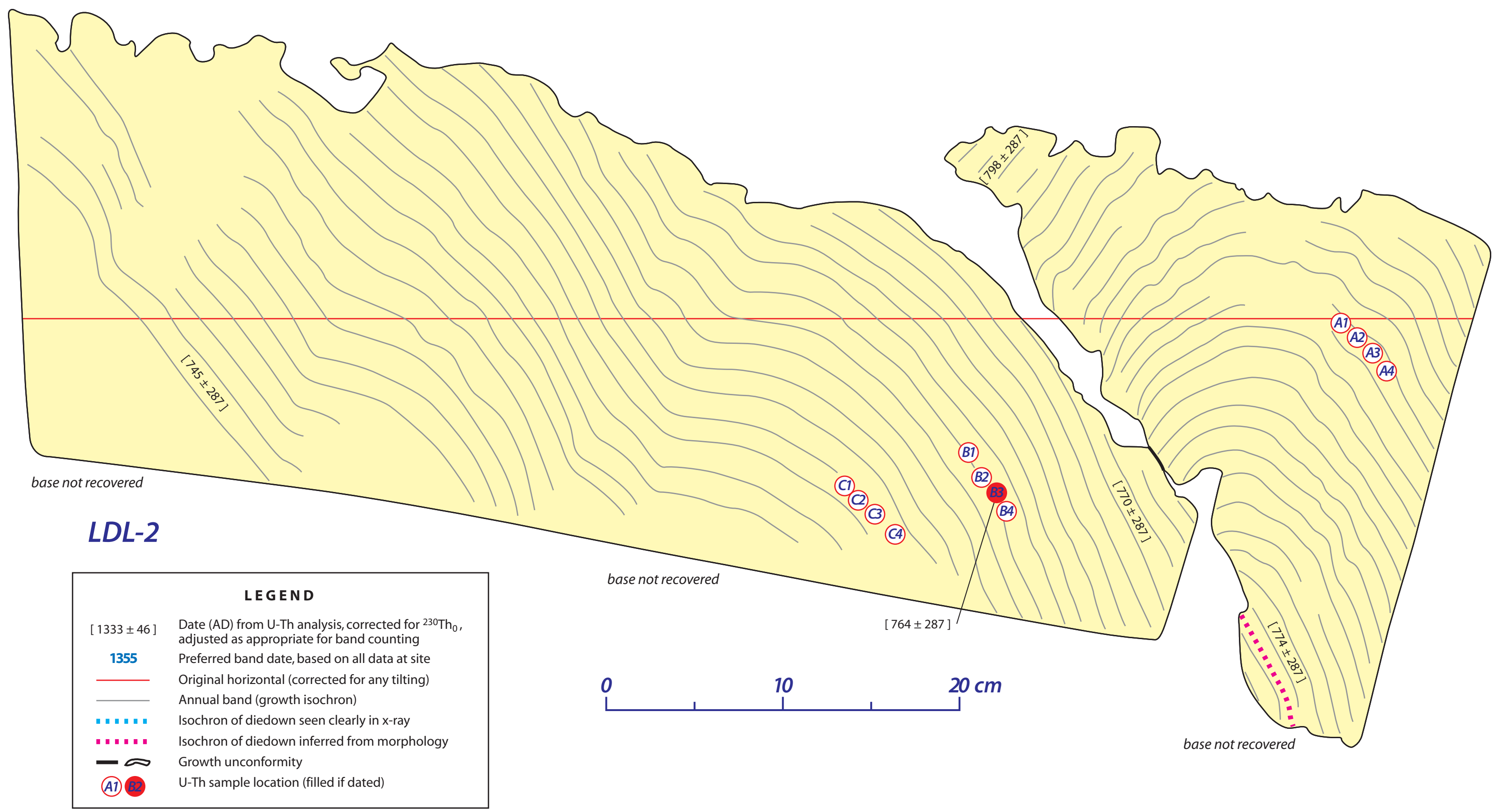

Figure S8. Cross-section of slab LDL-2, from site LDL-A.

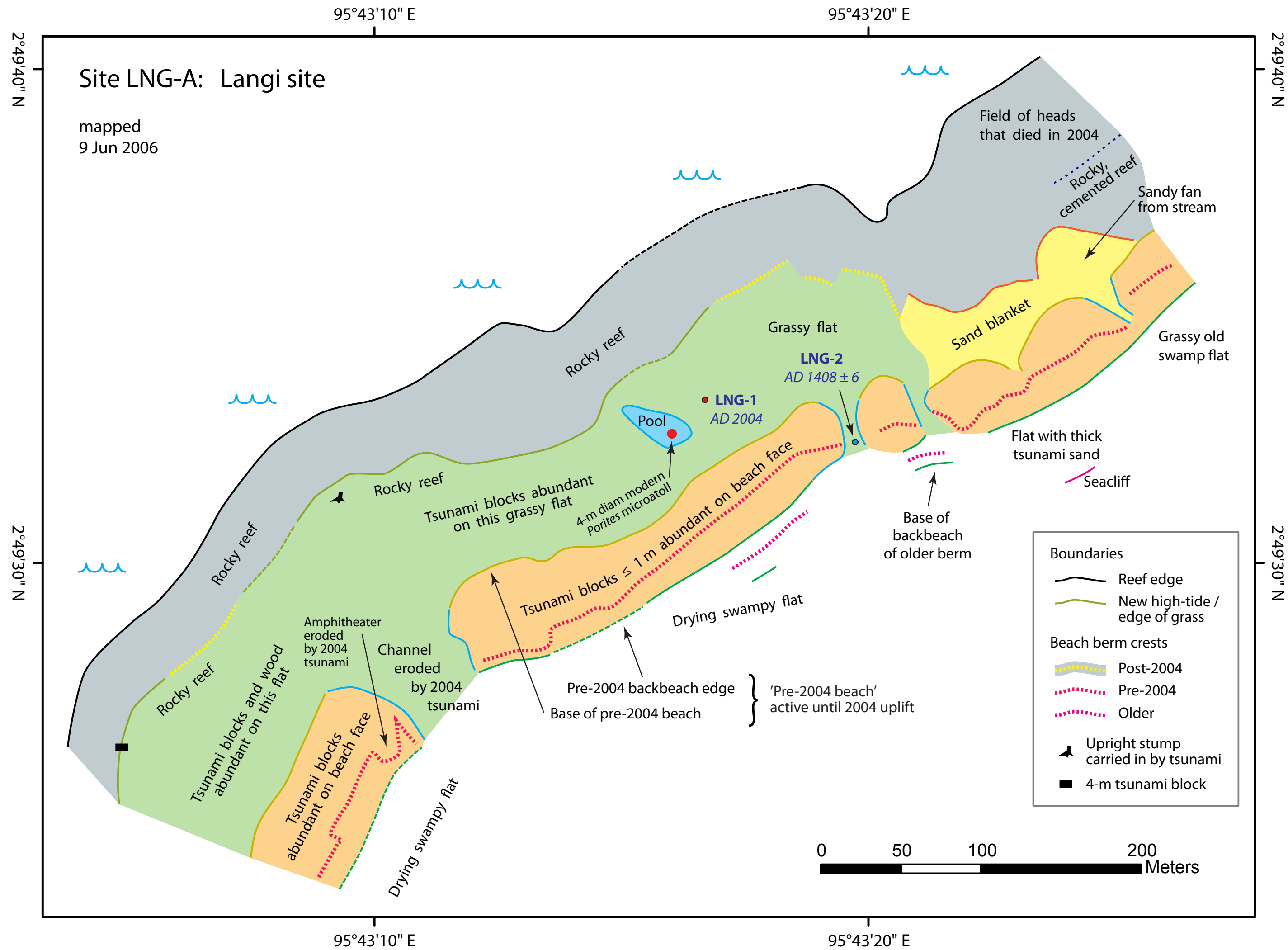

Figure S9. Map of site LNG-A, northwest coast of Simeulue, showing sampled microatolls and their dates of death.

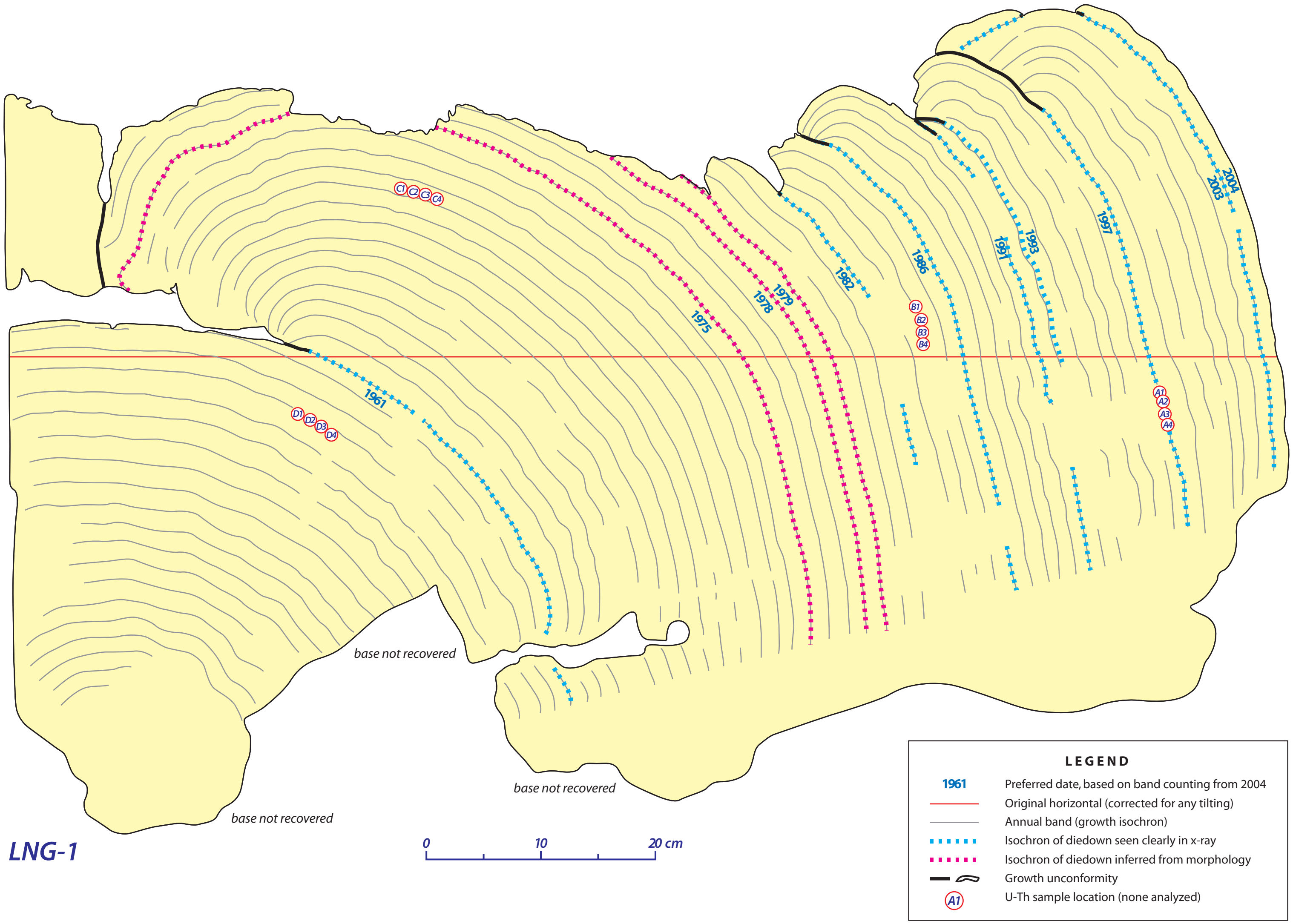

Figure S10a. Cross-section of slab LNG-1, from site LNG-A.

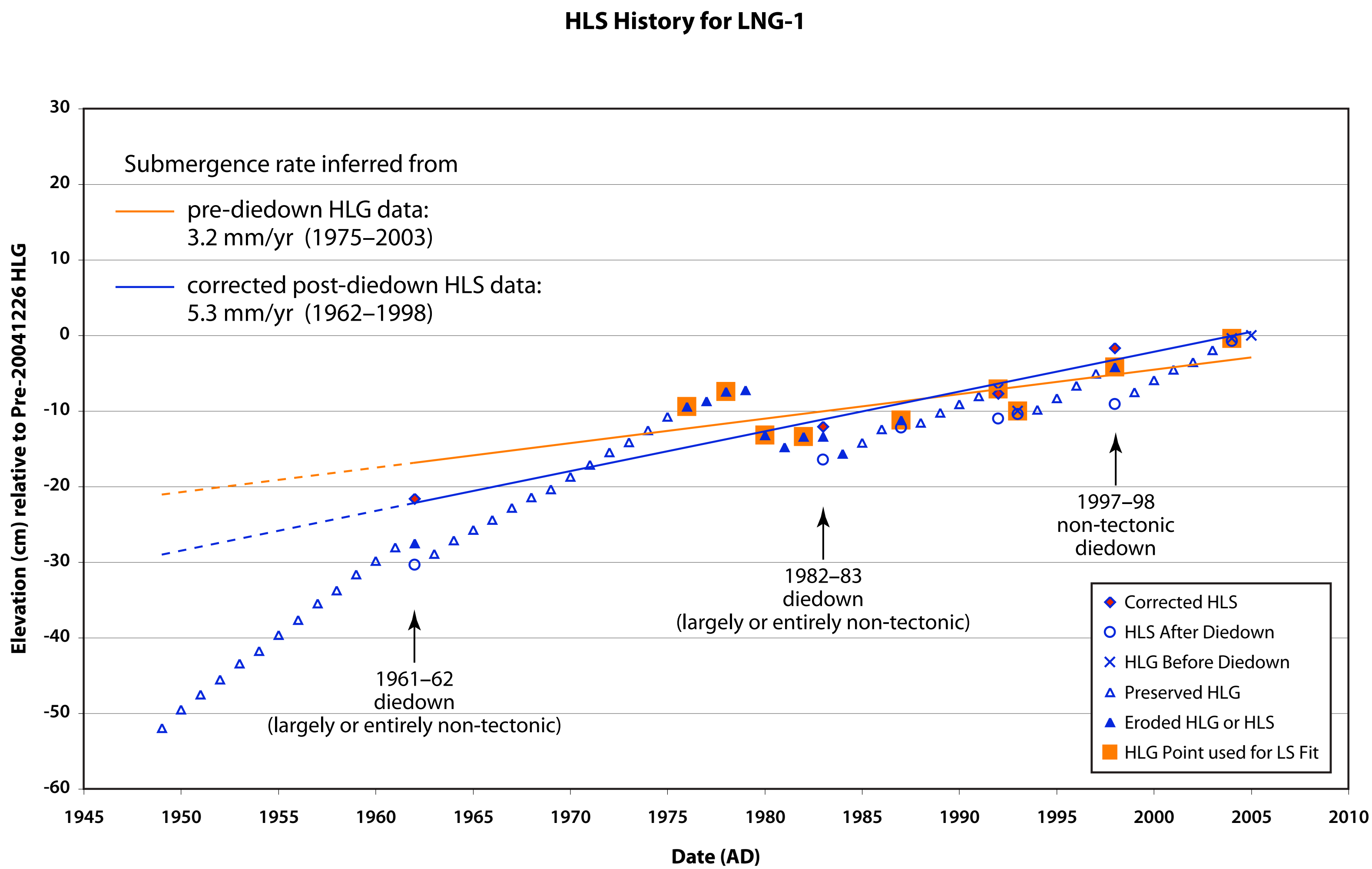

Figure S10b. Graph of relative sea level history derived from slab LNG-1.

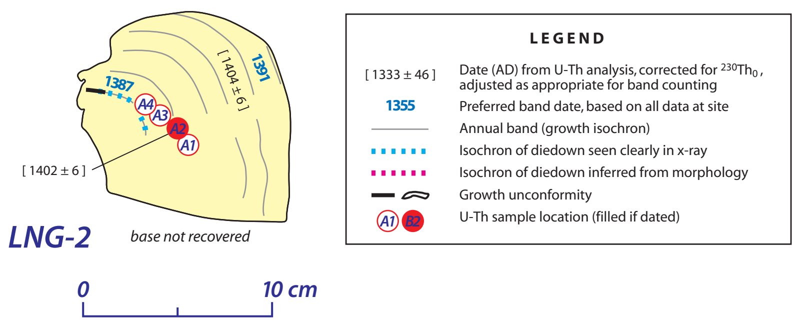

Figure S11. Cross-section of slab LNG-2, from site LNG-A.

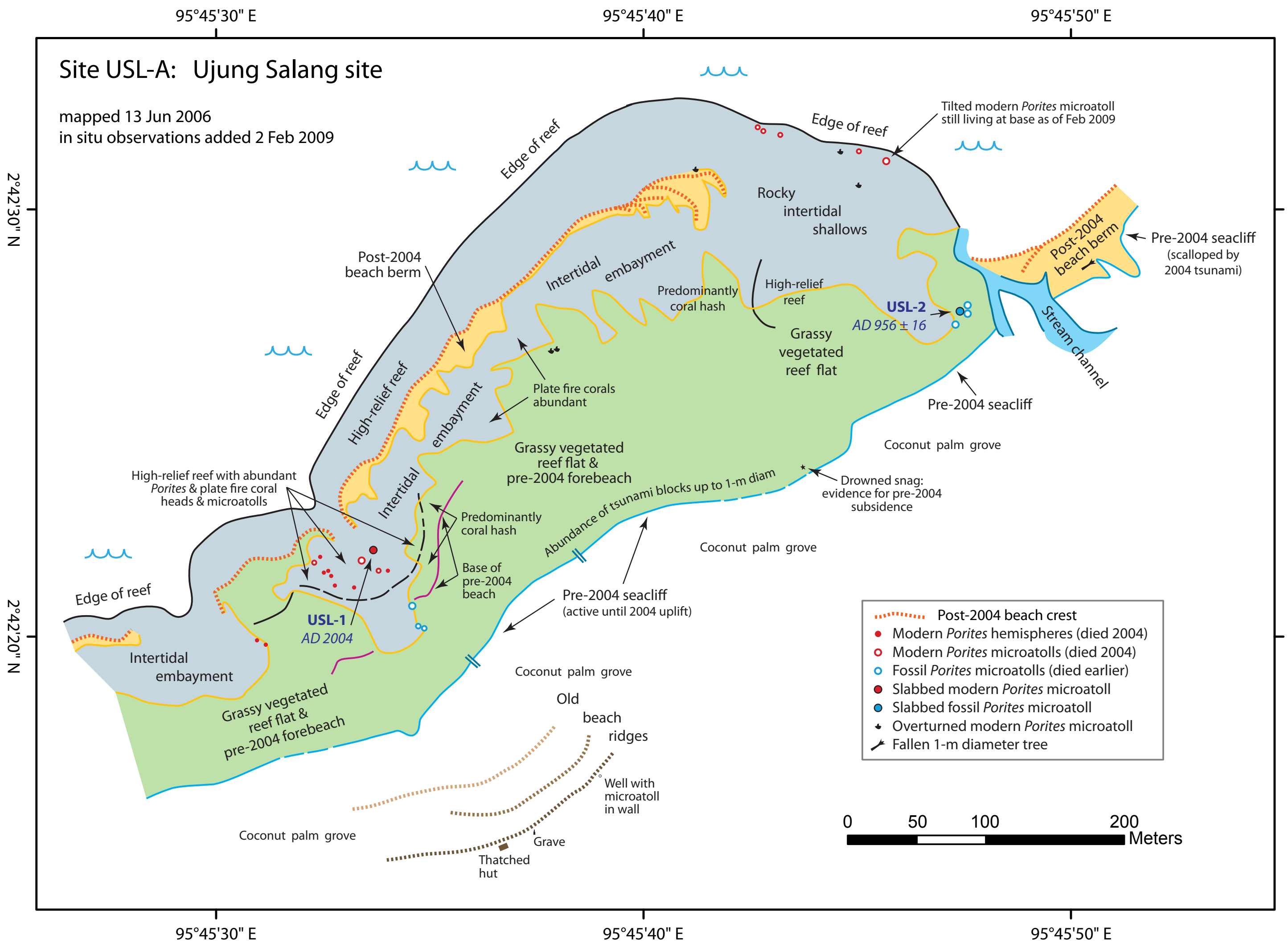

Figure S12. Map of site USL-A, southwest coast of Simeulue, showing sampled microatolls and their dates of death.

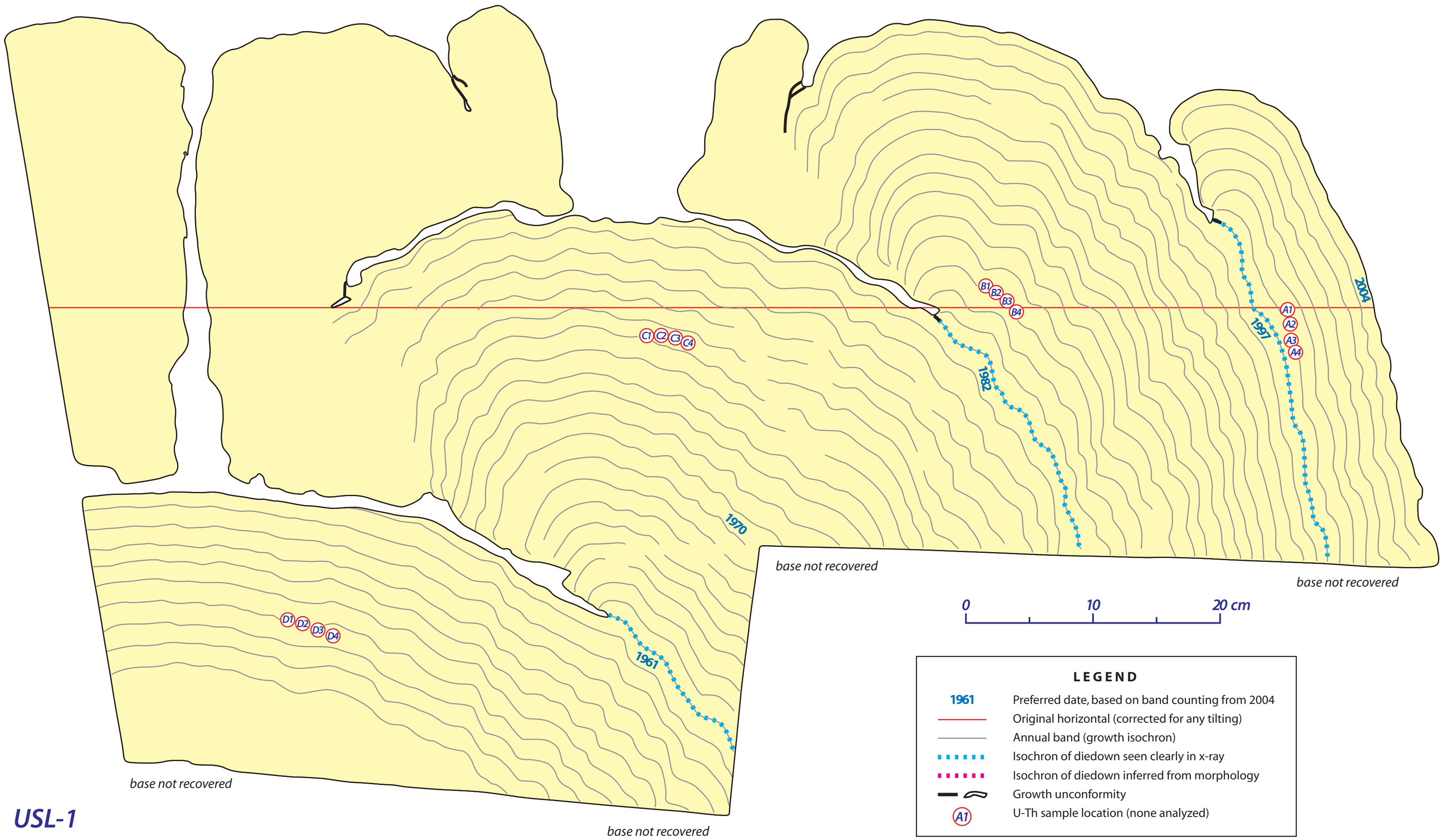

Figure S13a. Cross-section of slab USL-1, from site USL-A.

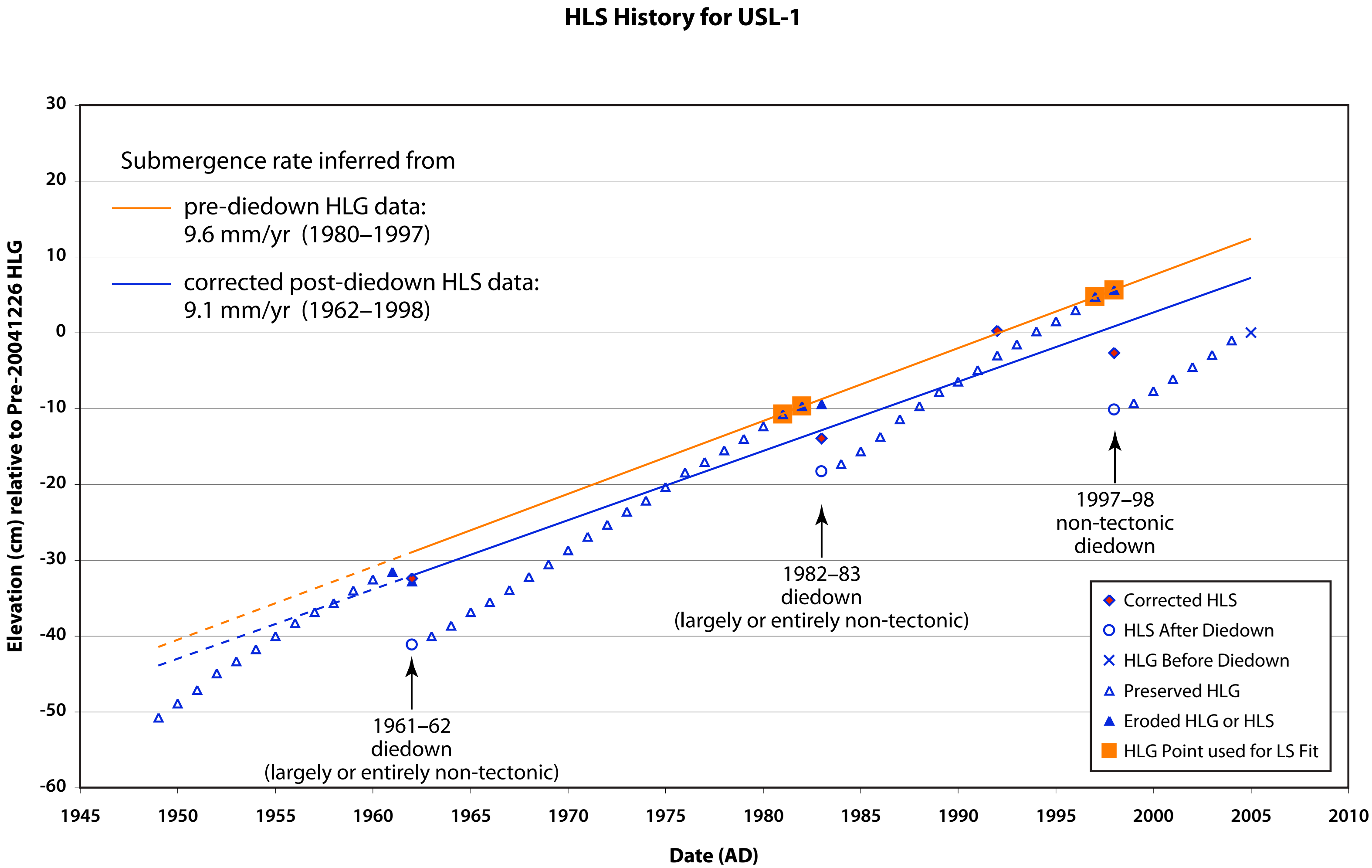

Figure S13b. Graph of relative sea level history derived from slab USL-1.

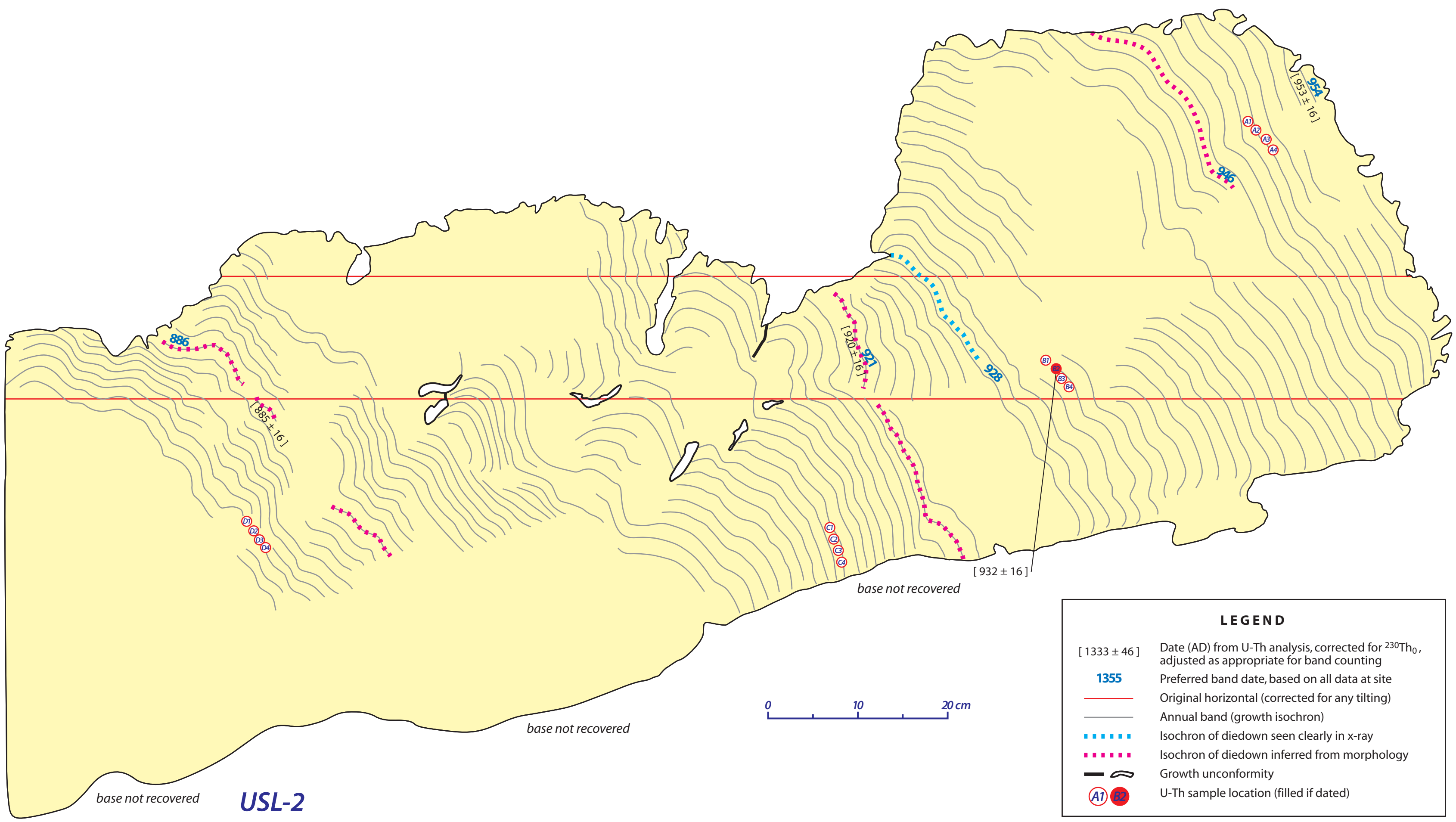

Figure S14a. Cross-section of slab USL-2, from site USL-A.

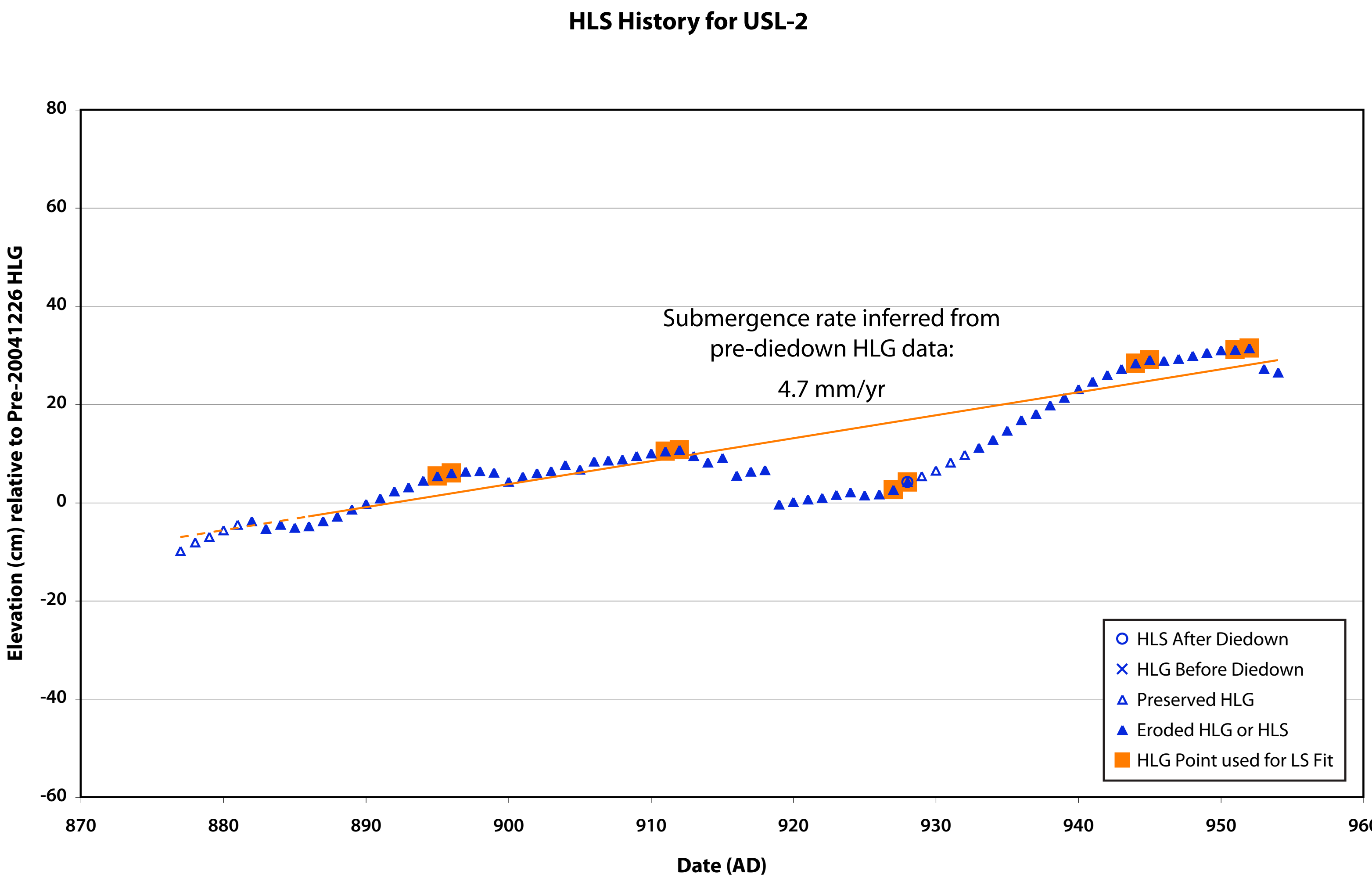

Figure S14b. Graph of relative sea level history derived from slab USL-2.

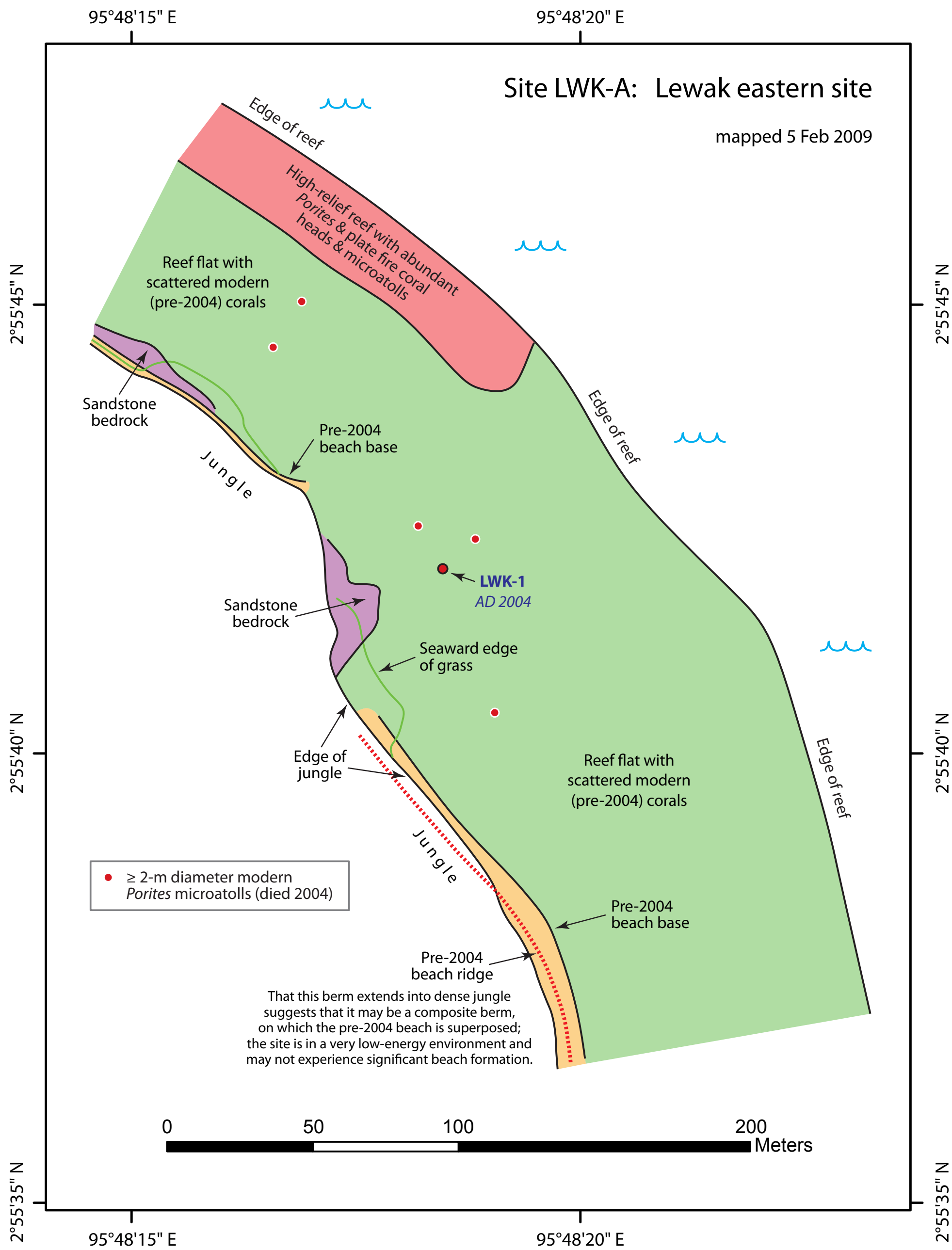

Figure S15a. Map of site LWK-A, near the northern tip of Simeulue, showing the sampled microatoll and its date of death.

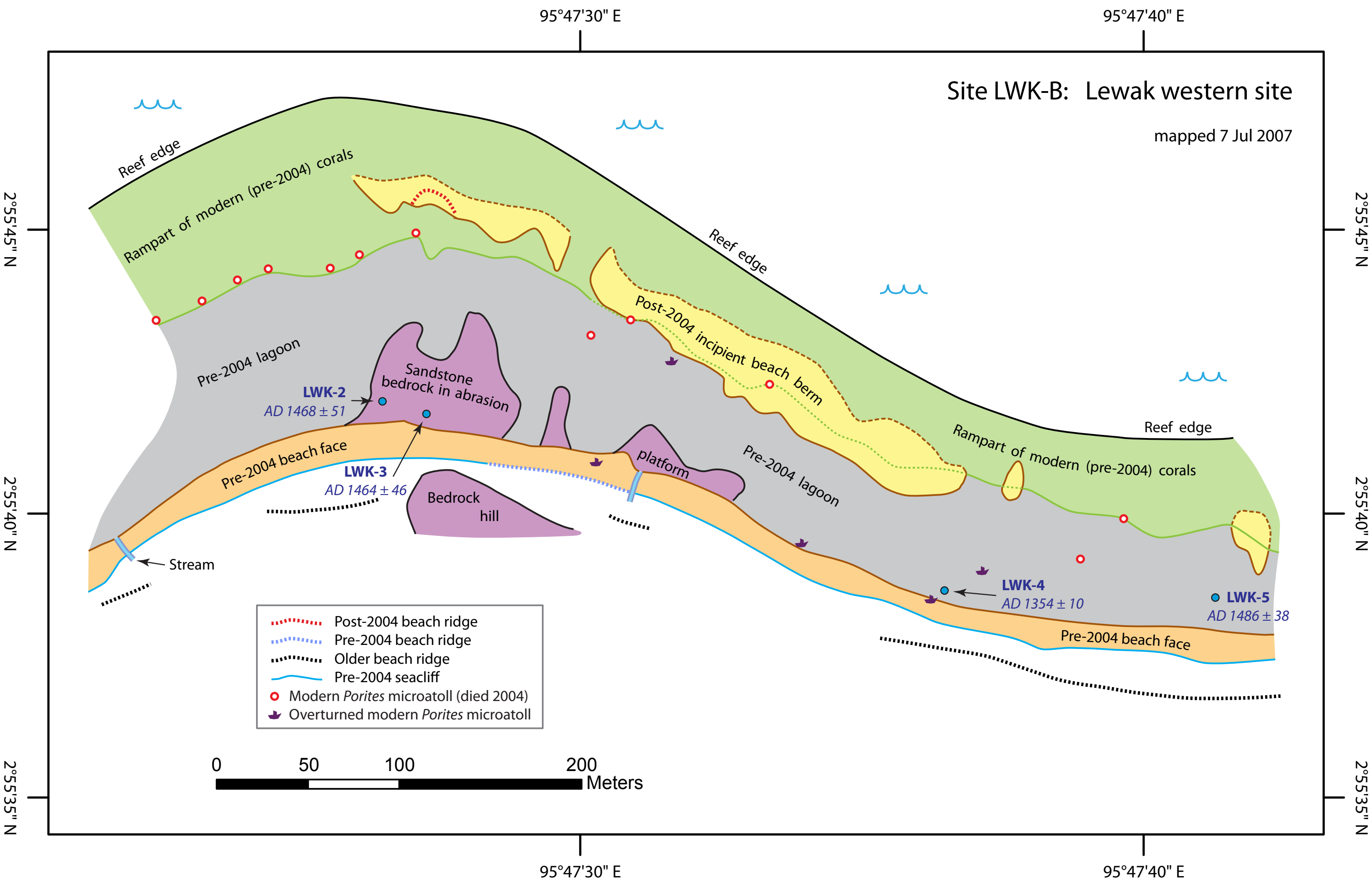

Figure S15b. Map of site LWK-B, near the northern tip of Simeulue, showing sampled microatolls and their dates of death.

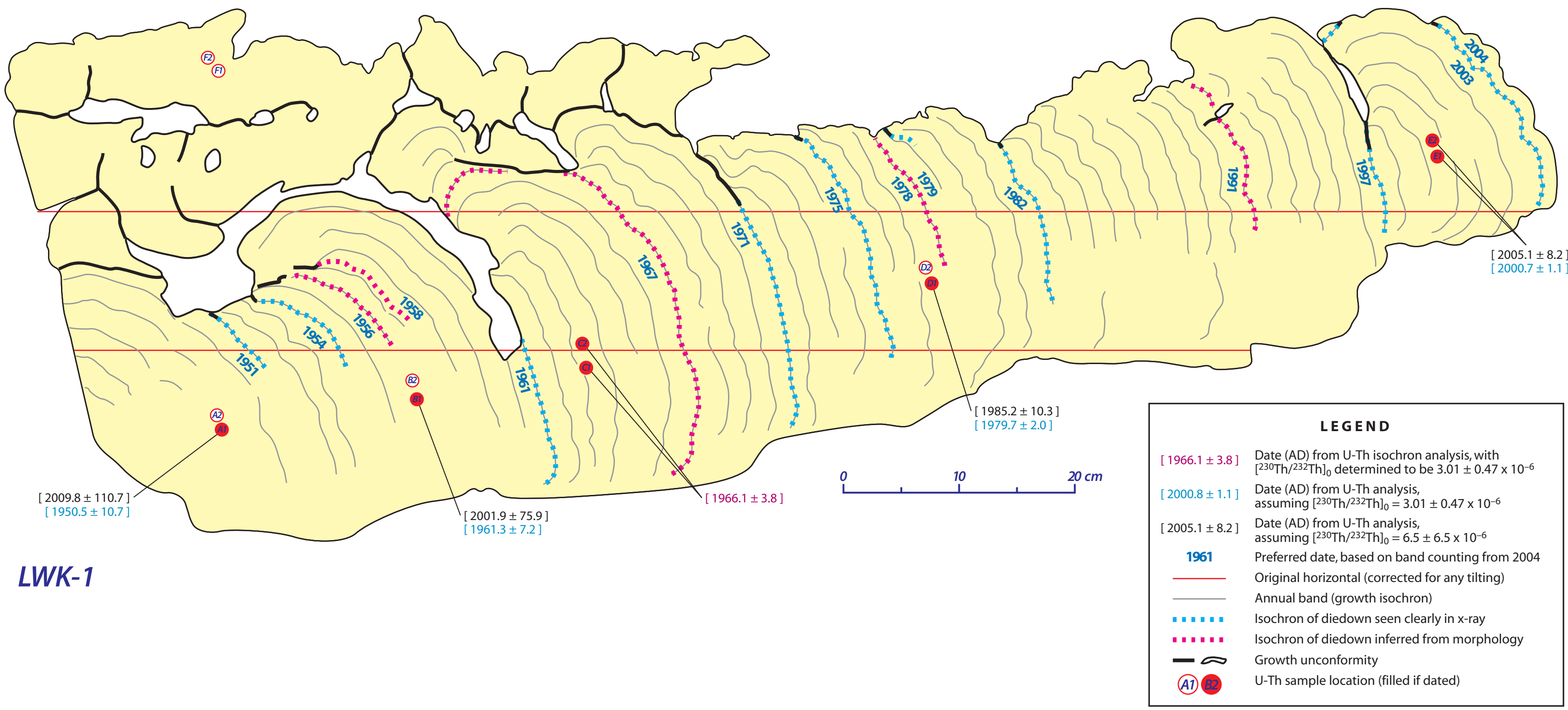

Figure S16a. Cross-section of slab LWK-1, from site LWK-A.

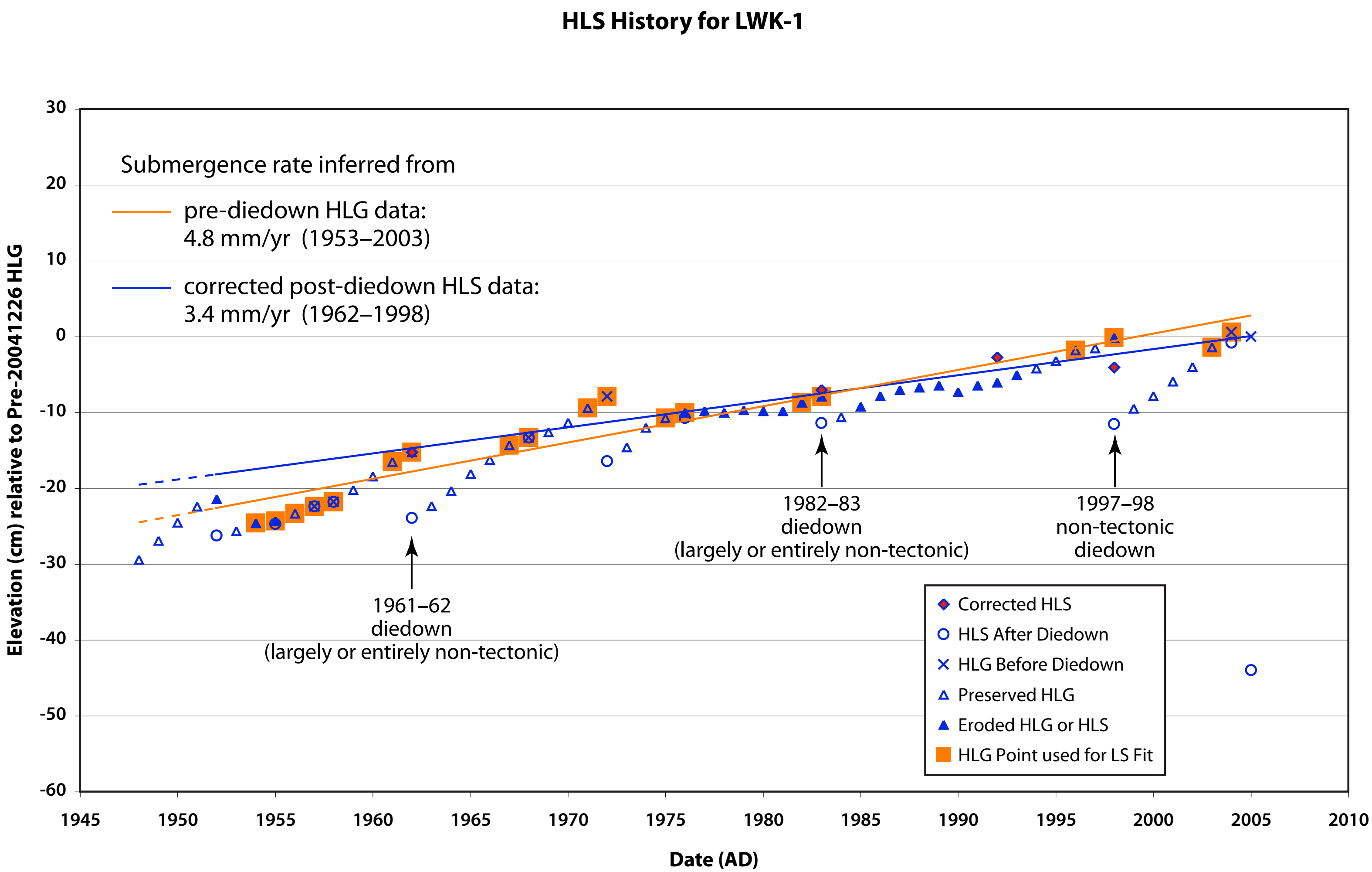

Figure S16b. Graph of relative sea level history derived from slab LWK-1.

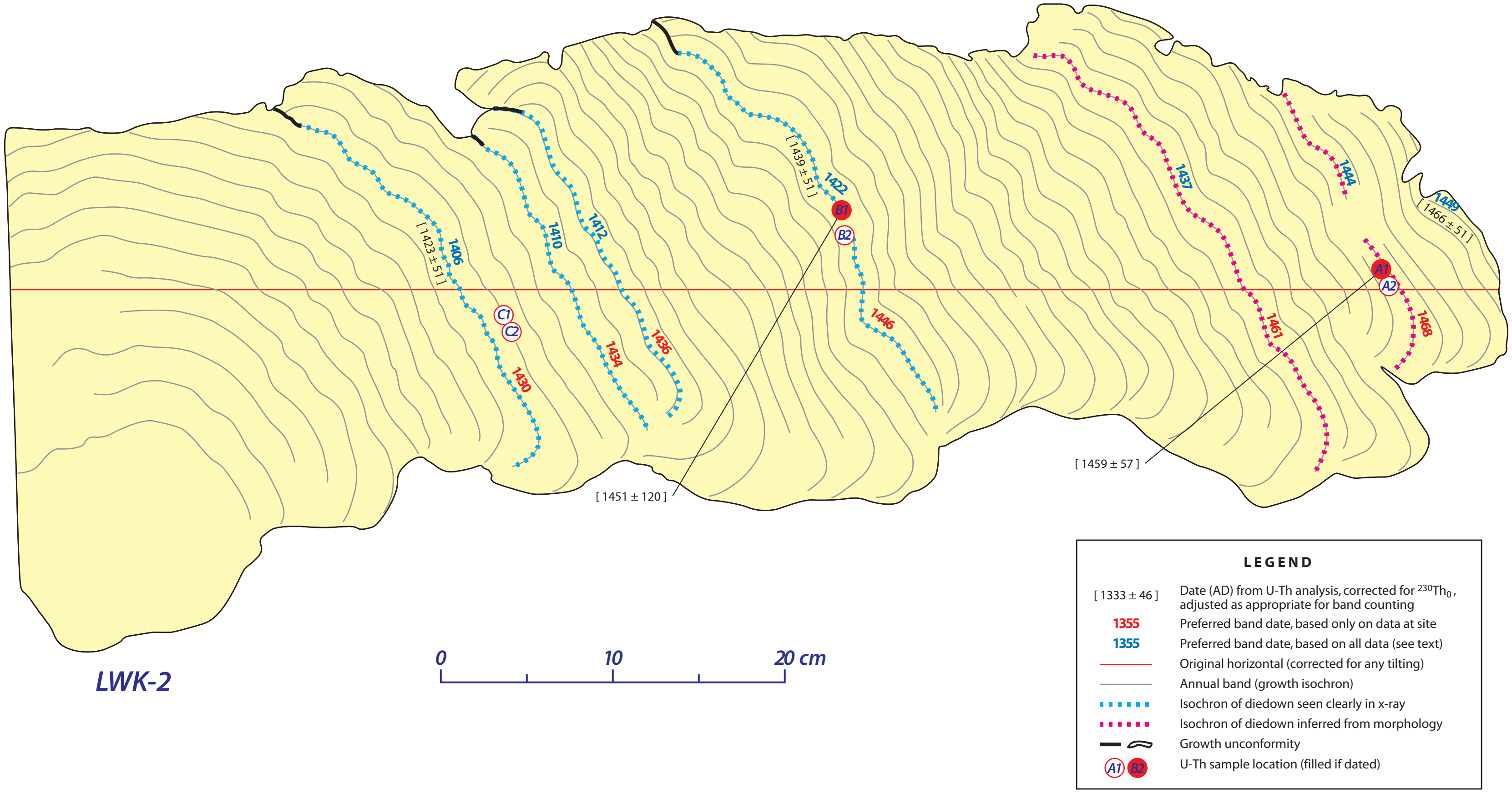

Figure S17a. Cross-section of slab LWK-2, from site LWK-B.
Red banding dates assume the head died in AD 1474; blue banding dates assume the head died in AD 1450. See text.

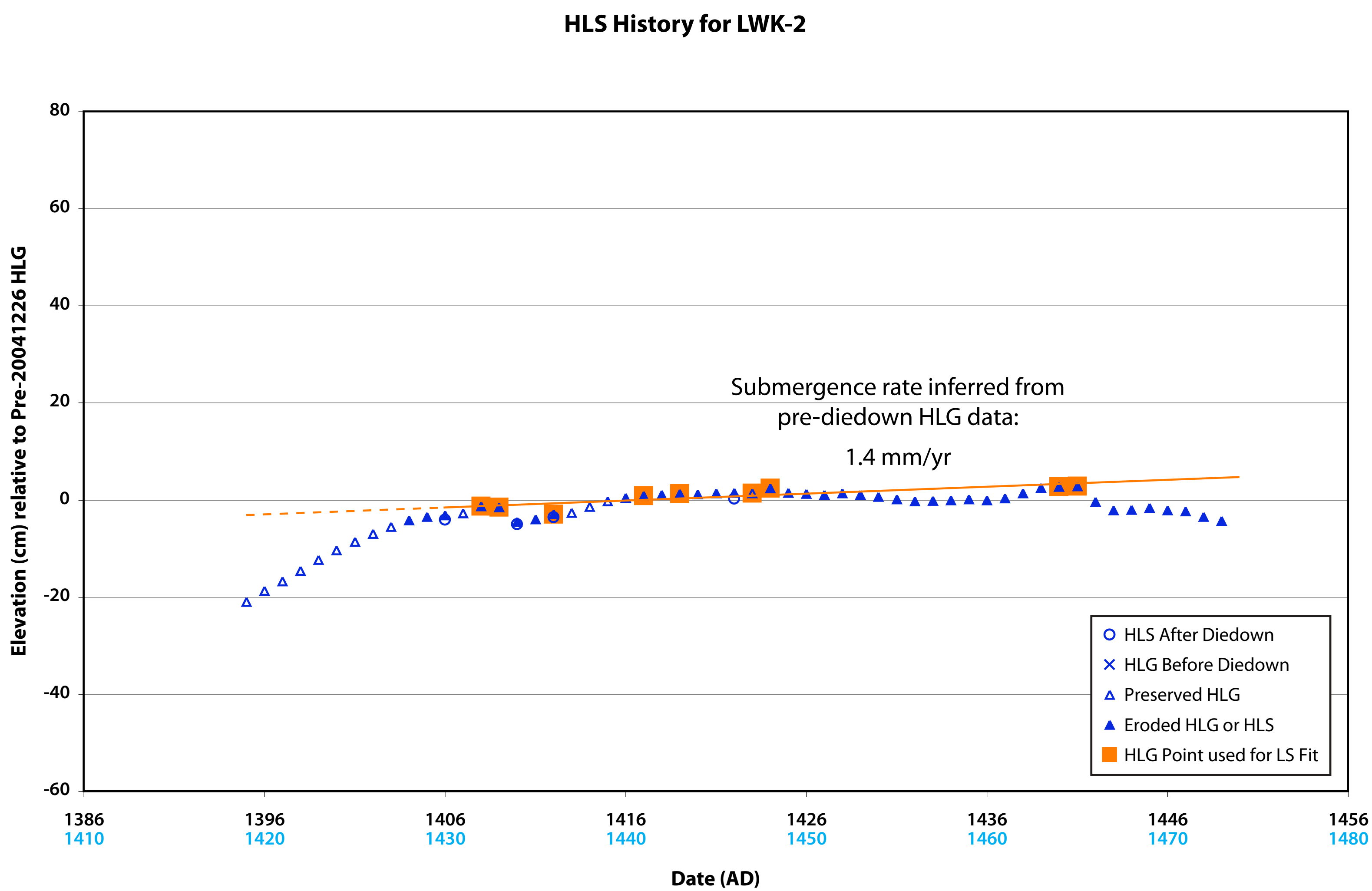

Figure S17b. Graph of relative sea level history derived from slab LWK-2.
Blue years on the horizontal axis assume the head died in AD 1474; black years assume the head died in AD 1450.

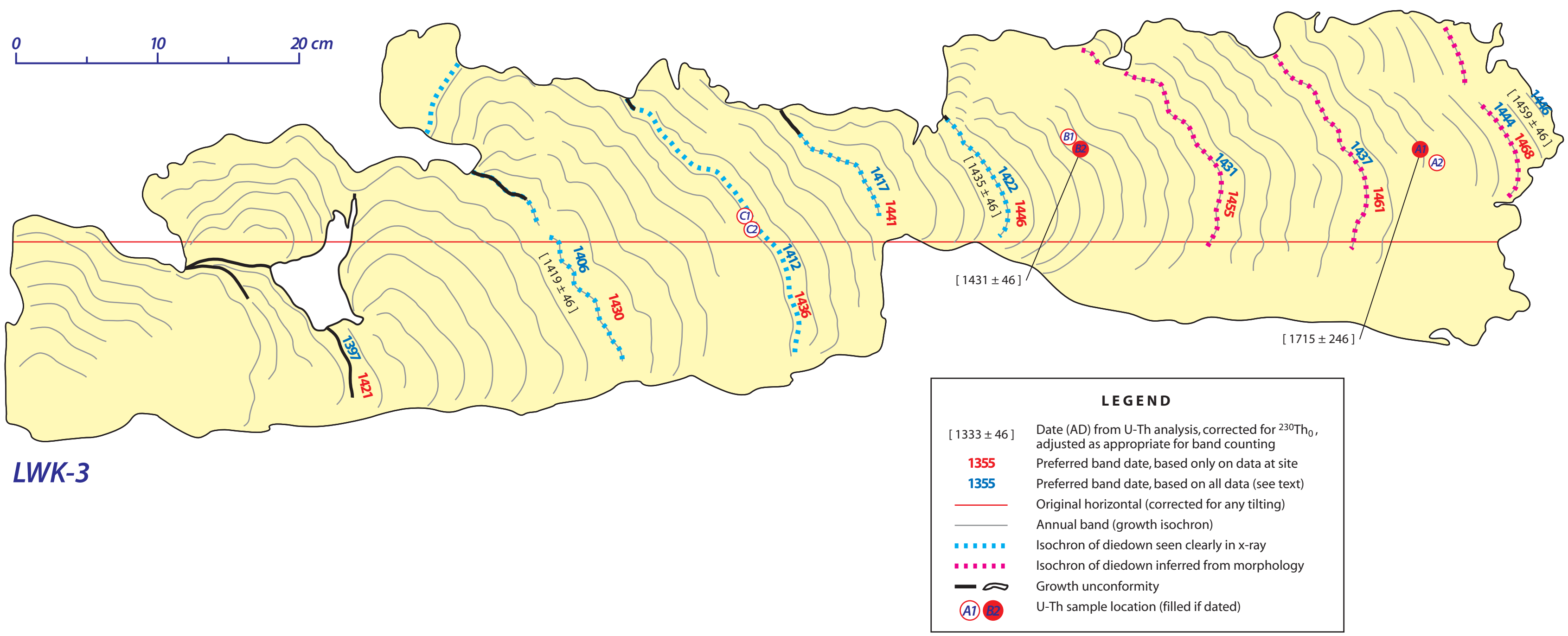

Figure S18a. Cross-section of slab LWK-3, from site LWK-B.
Red banding dates assume the head died in AD 1474; blue banding dates assume the head died in AD 1450. See text.

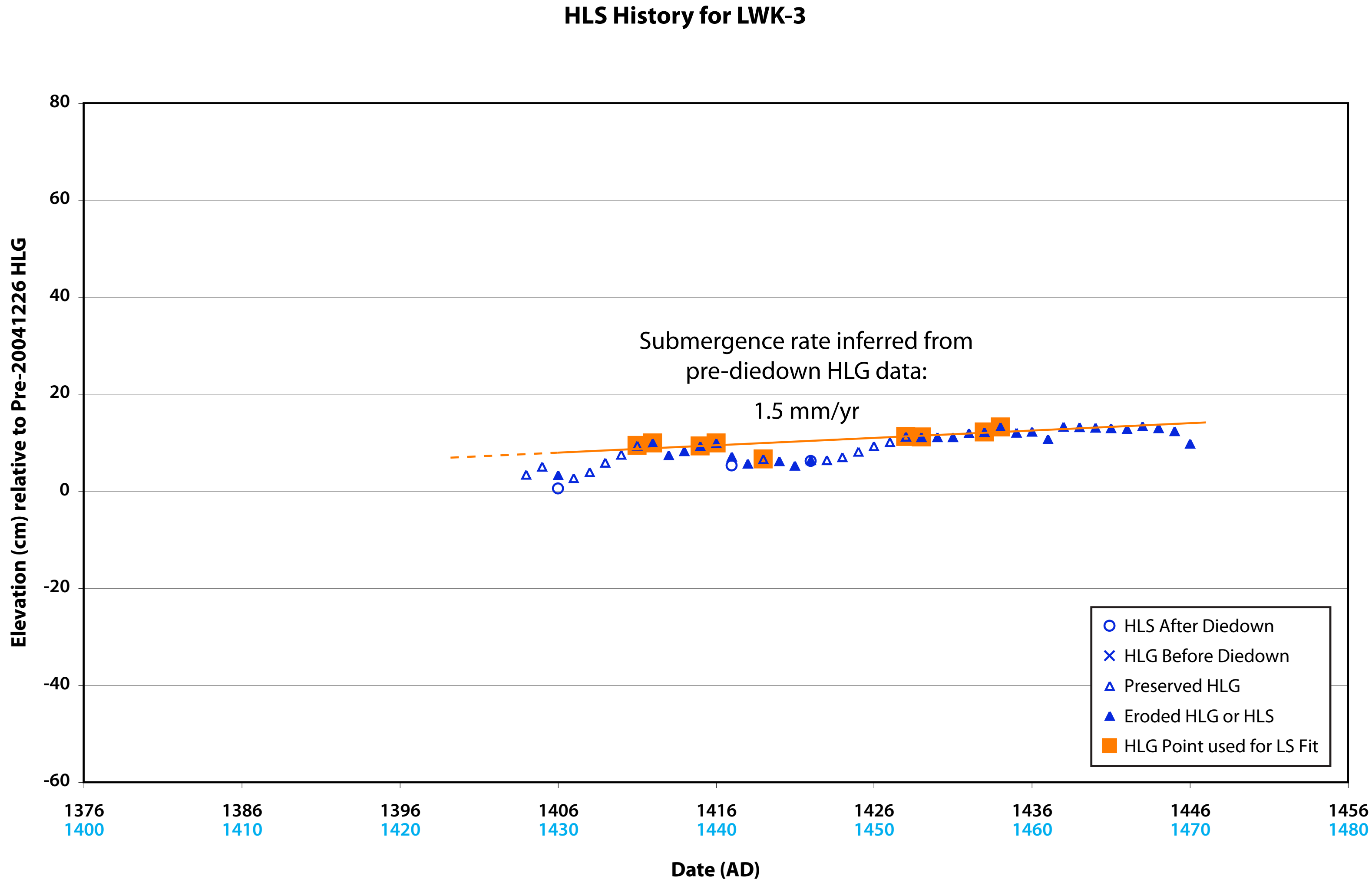

Figure S18b. Graph of relative sea level history derived from slab LWK-3.
Blue years on the horizontal axis assume the head died in AD 1474; black years assume the head died in AD 1450.

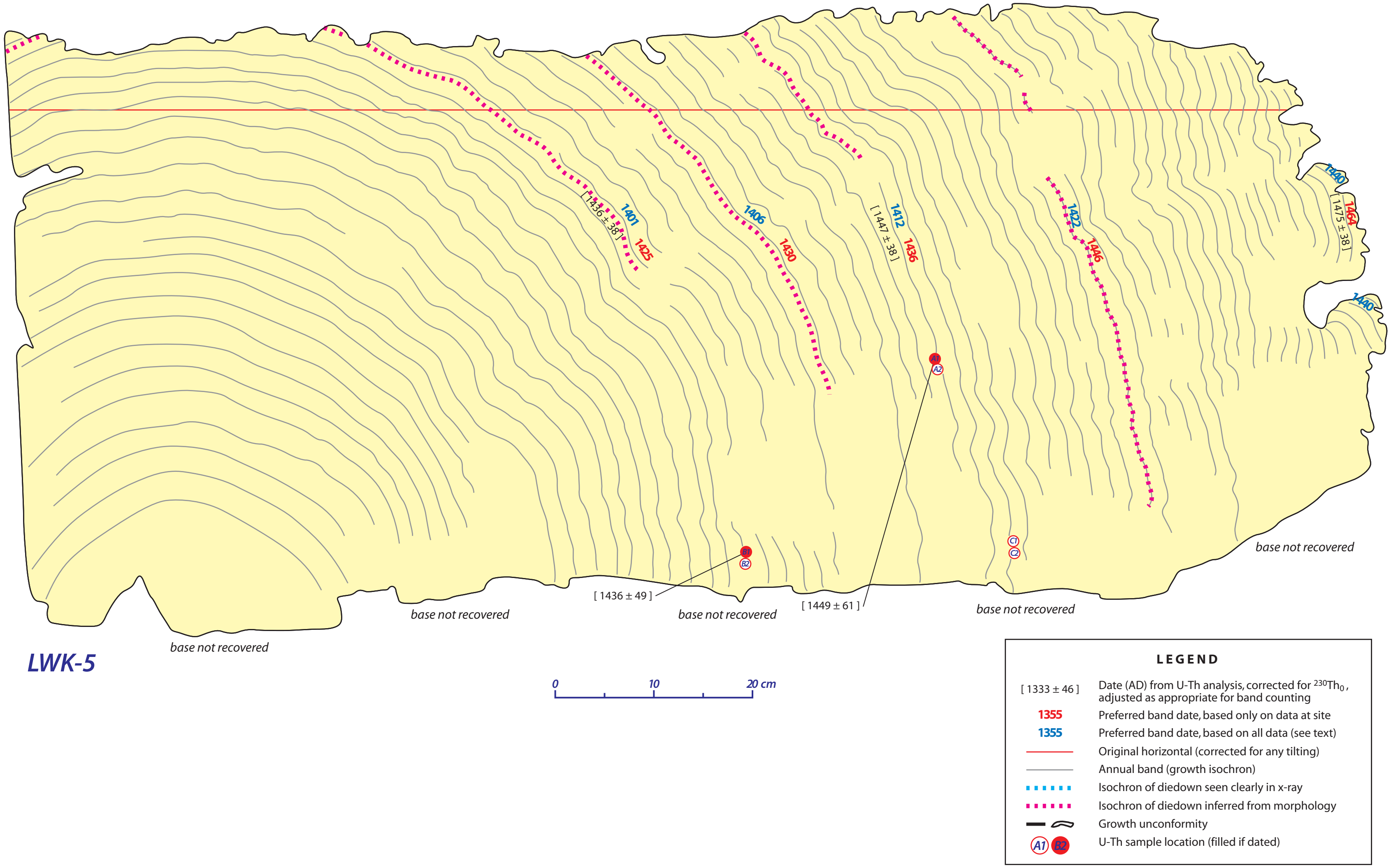

Figure S19a. Cross-section of slab LWK-5, from site LWK-B.
Red banding dates assume the head died in AD 1474; blue banding dates assume the head died in AD 1450. See text.

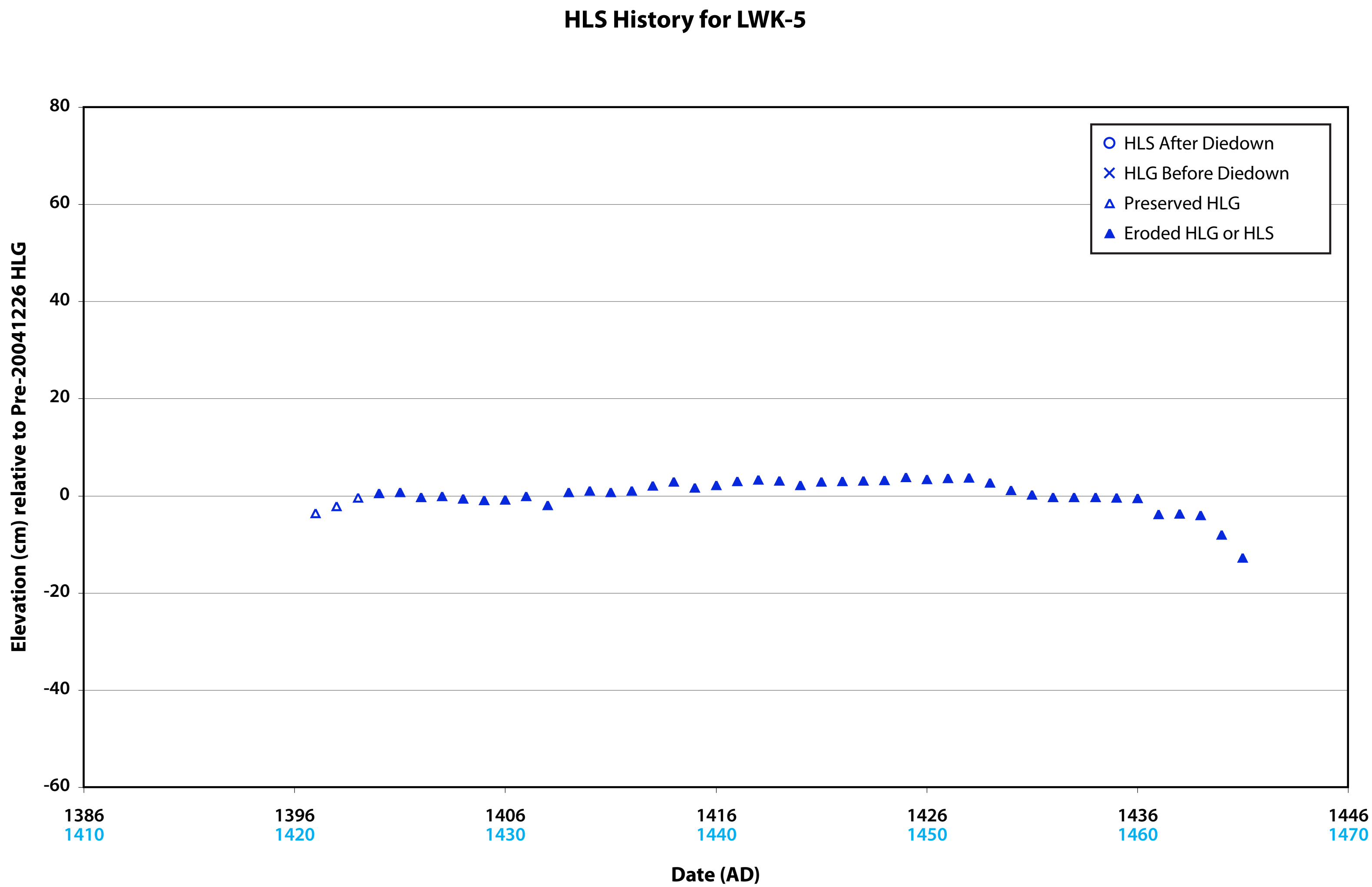

Figure S19b. Graph of relative sea level history derived from slab LWK-5.
Blue years on the horizontal axis assume the head died in AD 1474; black years assume the head died in AD 1450.

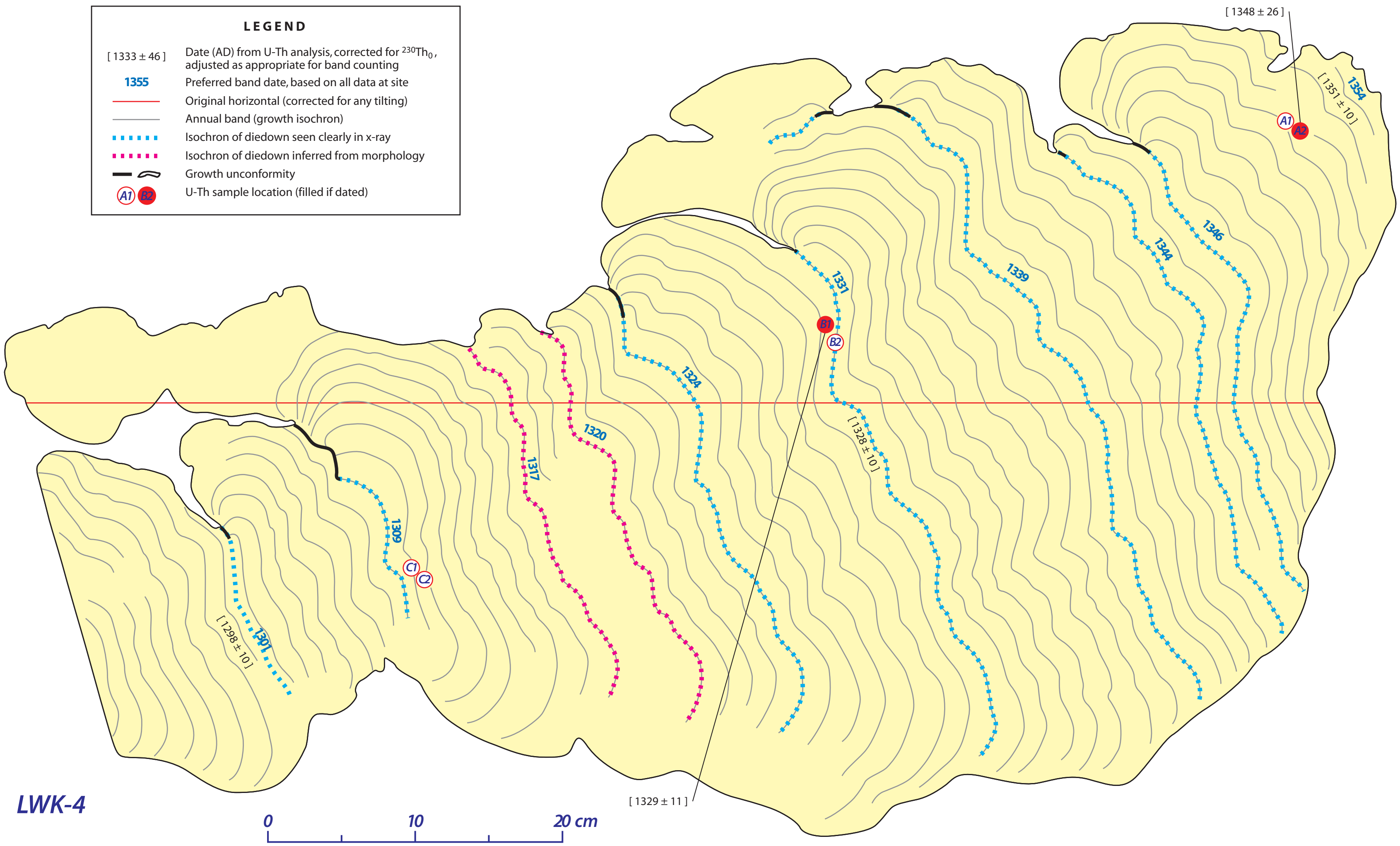

Figure S20a. Cross-section of slab LWK-4, from site LWK-B.

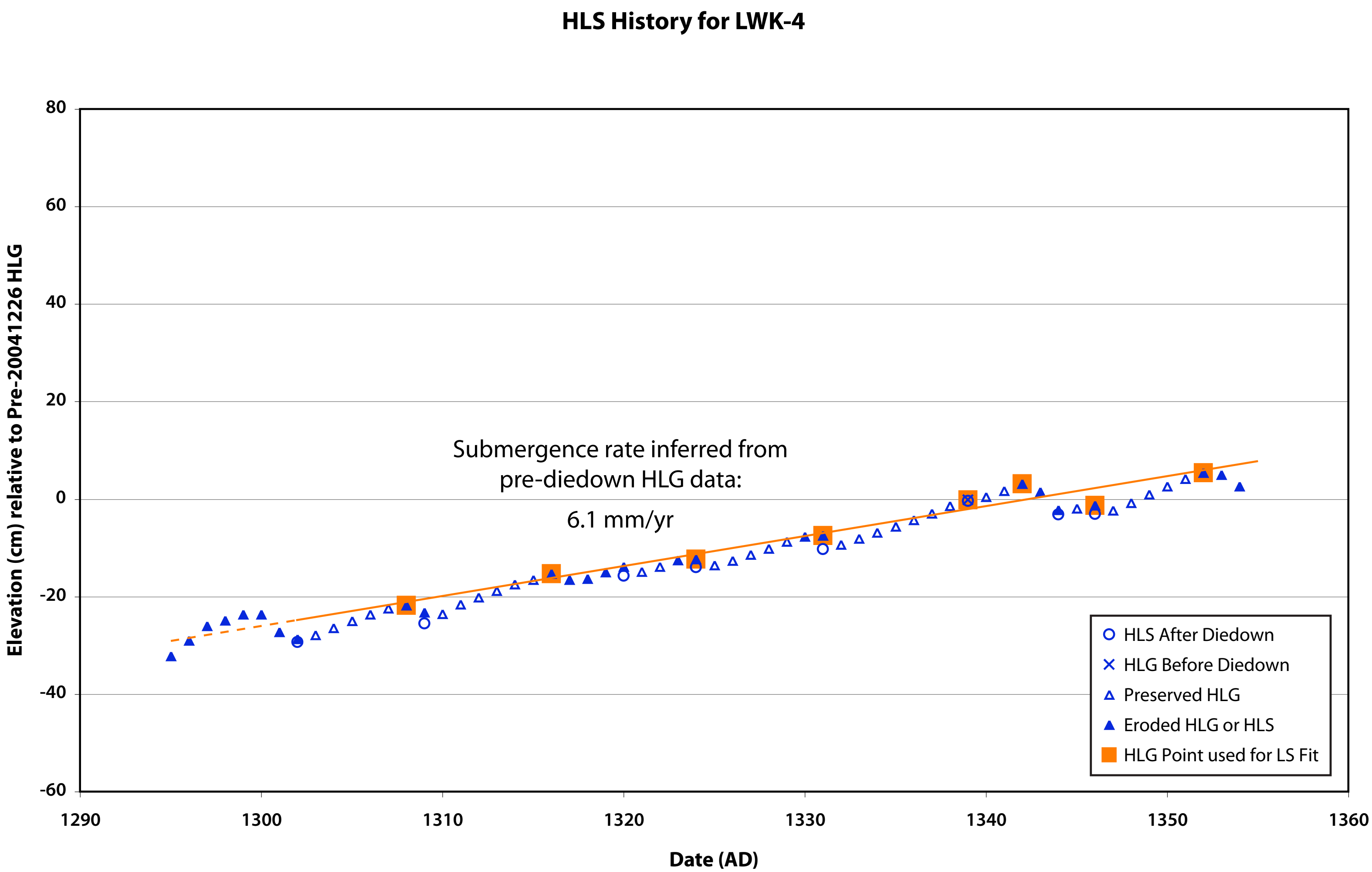

Figure S20b. Graph of relative sea level history derived from slab LWK-4.

Figure S21. Relative sea level history for the 14th–15th centuries at site LWK-B, assuming LWK-2, LWK-3, and LWK-5 died together in AD 1474. An alternate interpretation—that these three heads died in the AD 1450 event seen elsewhere—is depicted in Figures 15–16. For the 15th century, the interseismic submergence rates determined separately from LWK-2 and LWK-3 agree (after each head was corrected for any possible tilting), but LWK-3 was higher than LWK-2 and LWK-5. See auxiliary material for further discussion.

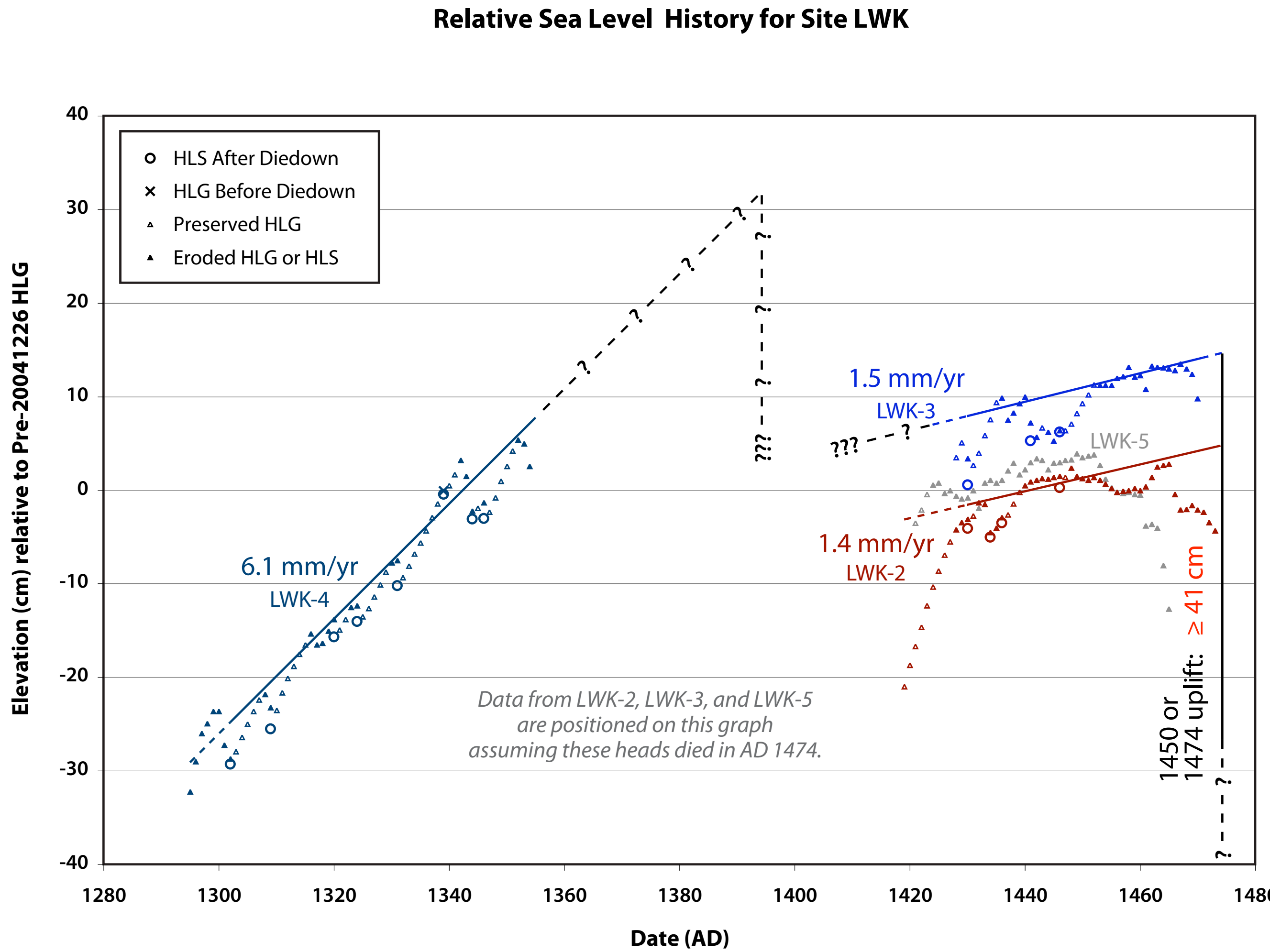
Relative Sea Level History for Site LWK
HLS After Diedown
HLG Before Diedown
Preserved HLG
Eroded HLG or HLS
6.1 mm/yr
LWK-4
1.5 mm/yr
LWK-3
LWK-5
1.4 mm/yr
LWK-2
Data from LWK-2, LWK-3, and LWK-5 are positioned on this graph assuming these heads died in AD 1474.
1450 or 1474 uplift: ≥ 41 cm
Elevation (cm) relative to Pre-20041226 HLG
Date (AD)

Figure S21.

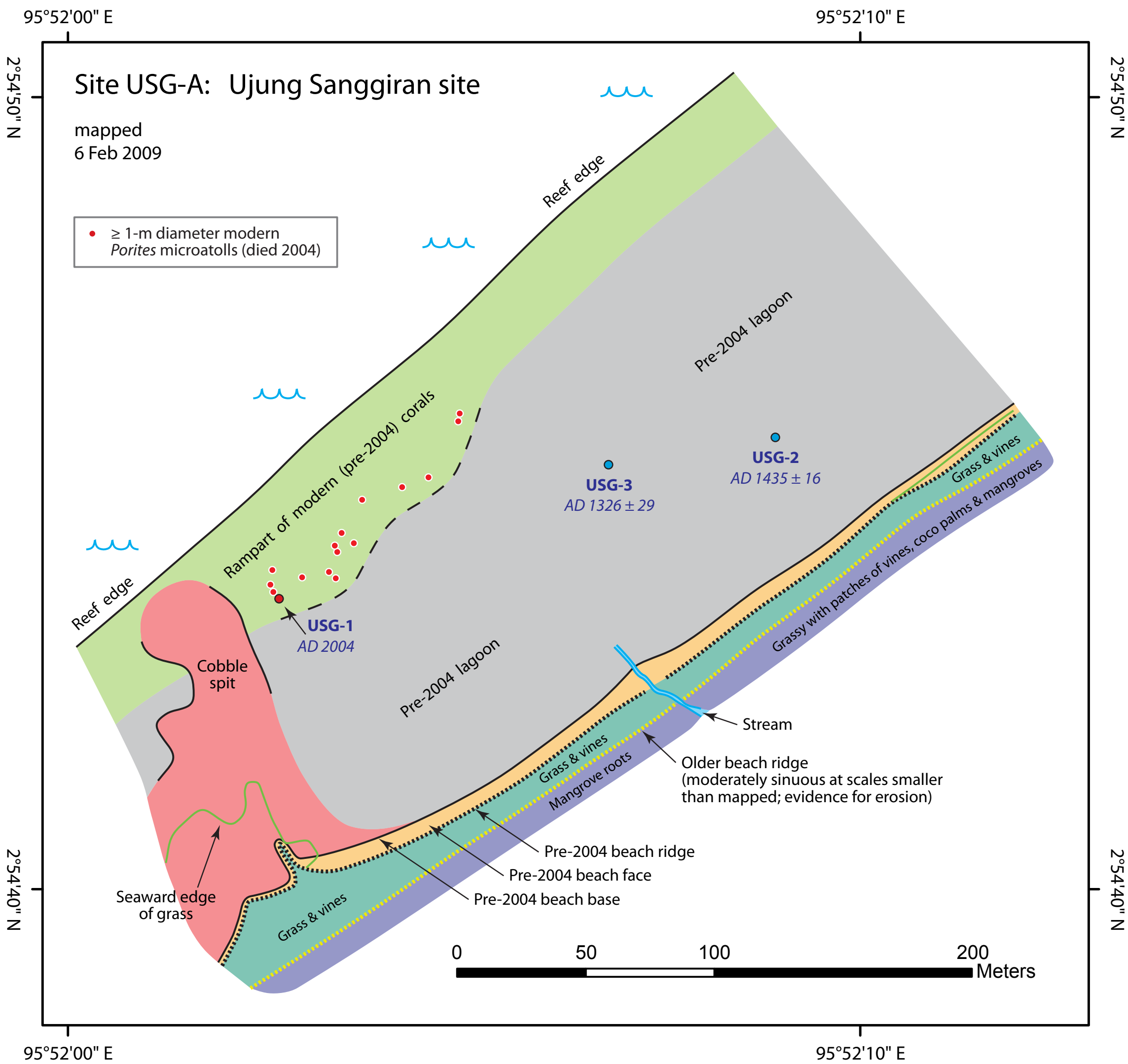

Figure S22. Map of site USG-A, northeast coast of Simeulue, showing sampled microatolls and their dates of death.

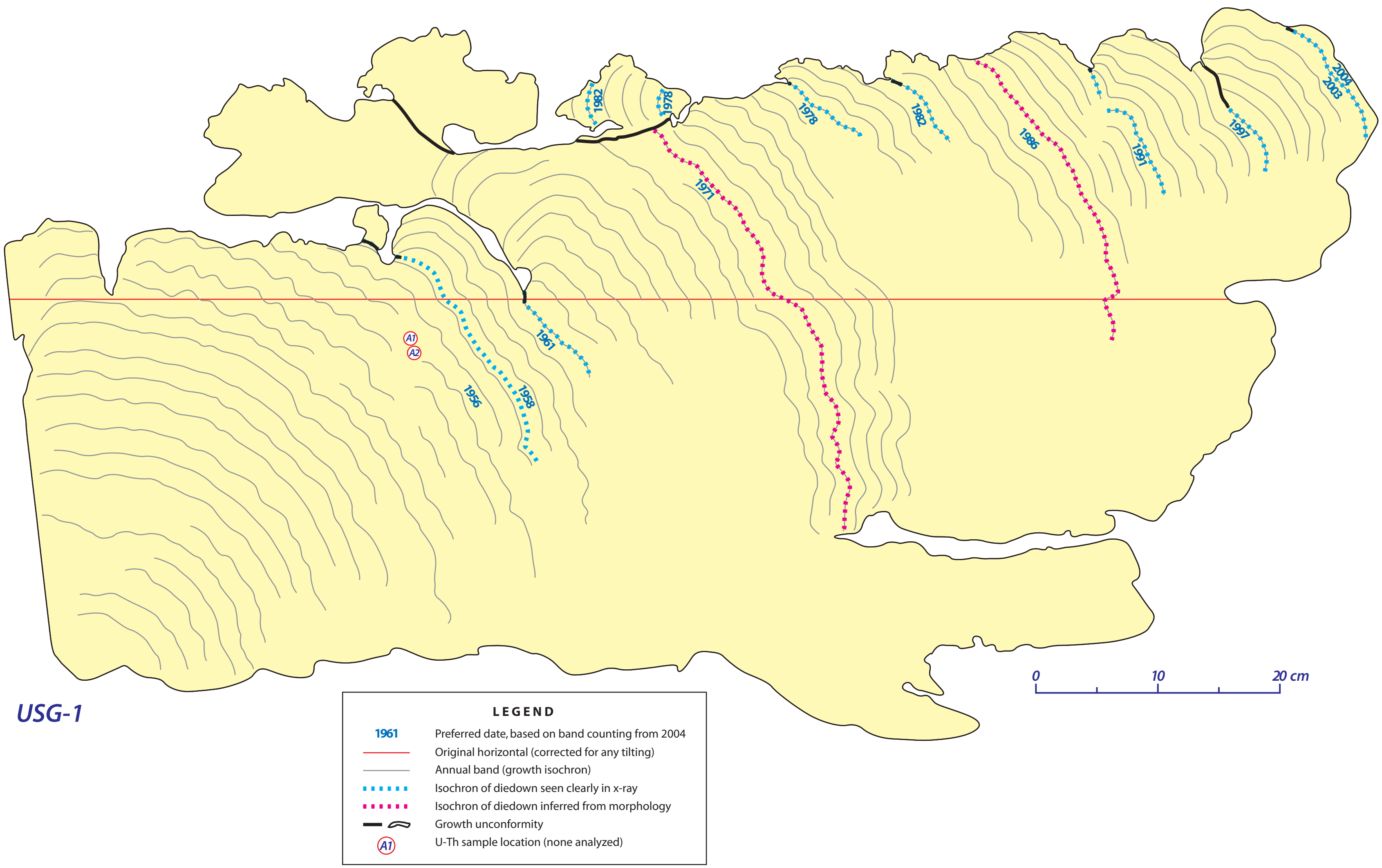

Figure S23a. Cross-section of slab USG-1, from site USG-A.

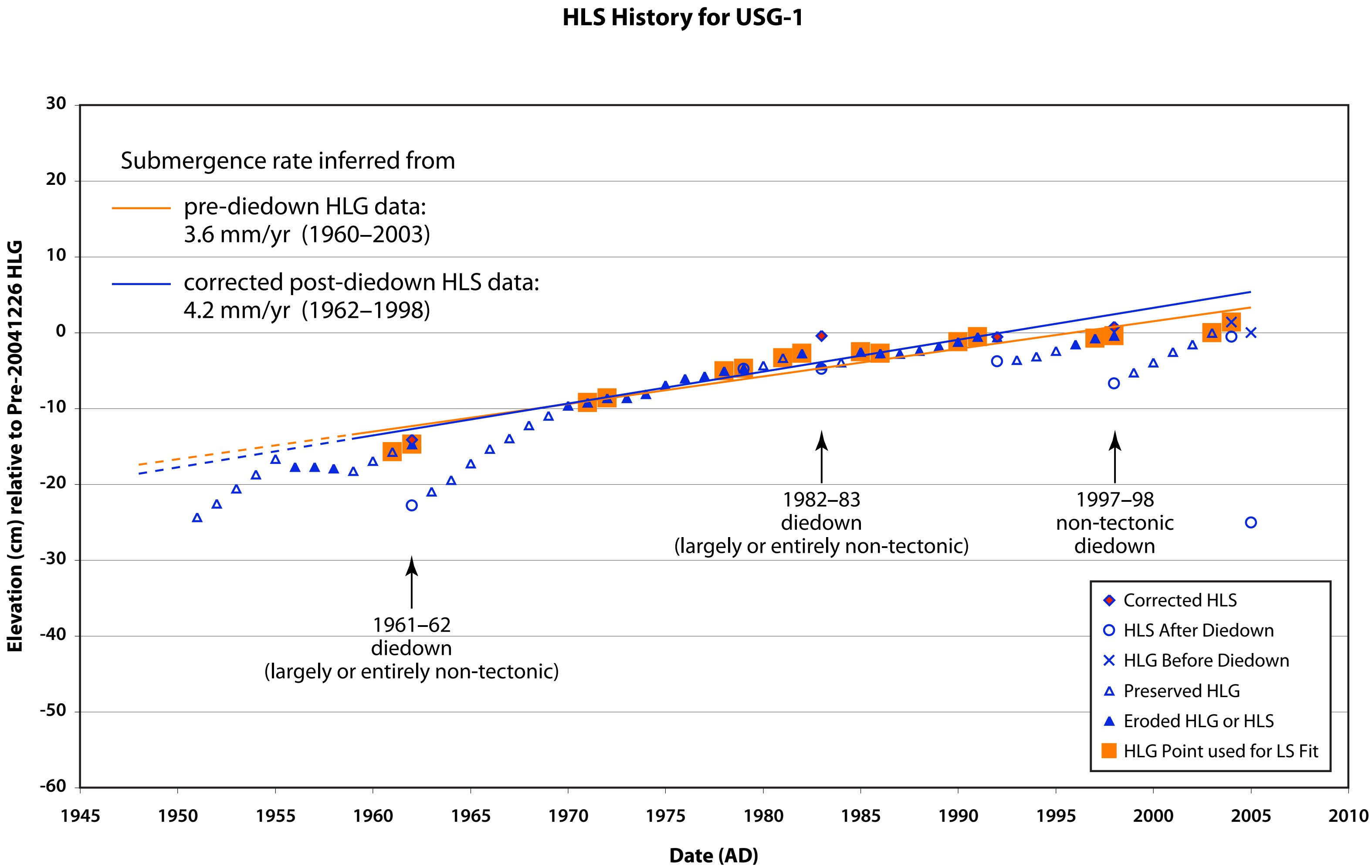

Figure S23b. Graph of relative sea level history derived from slab USG-1.

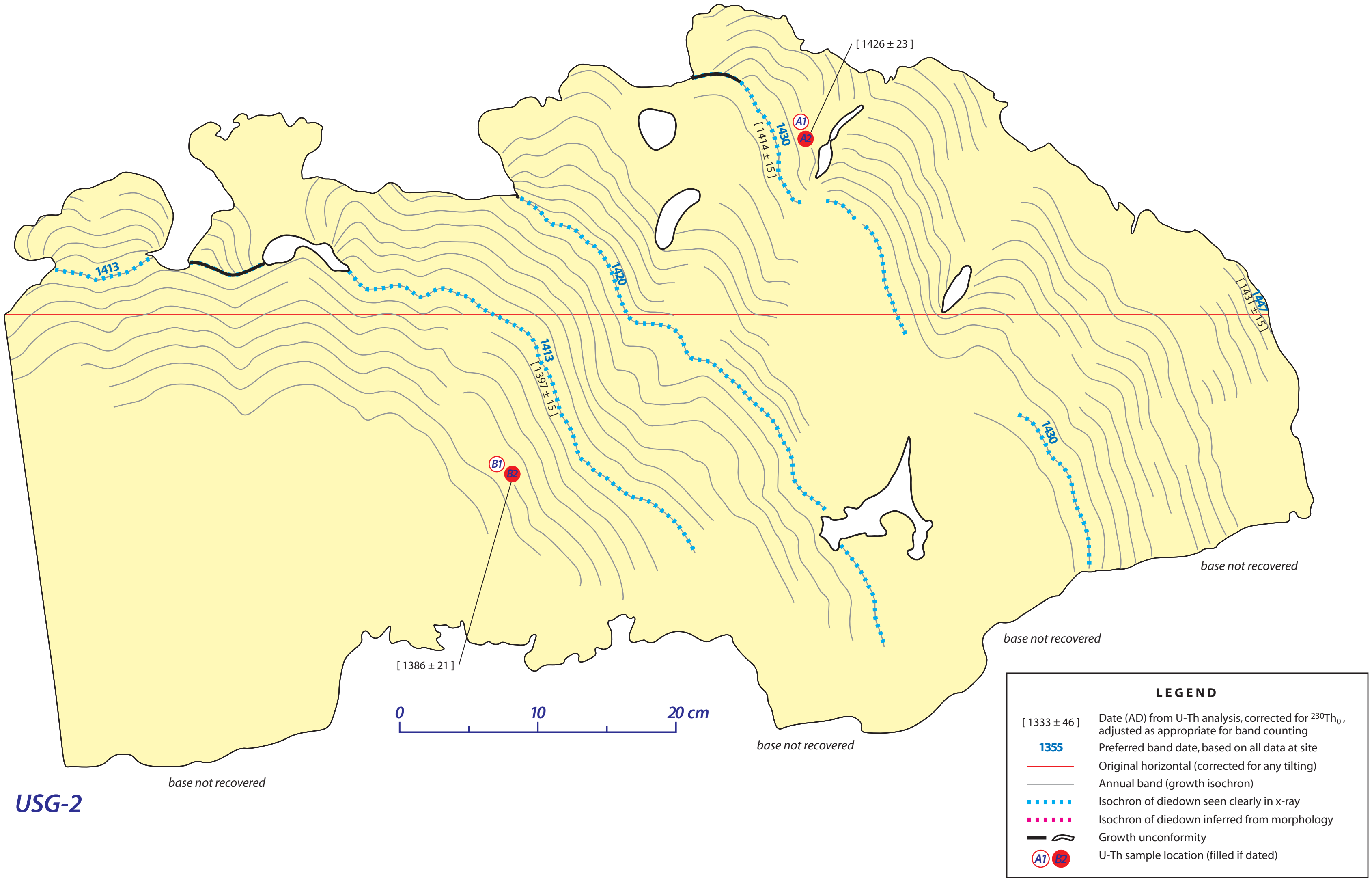

Figure S24a. Cross-section of slab USG-2, from site USG-A.

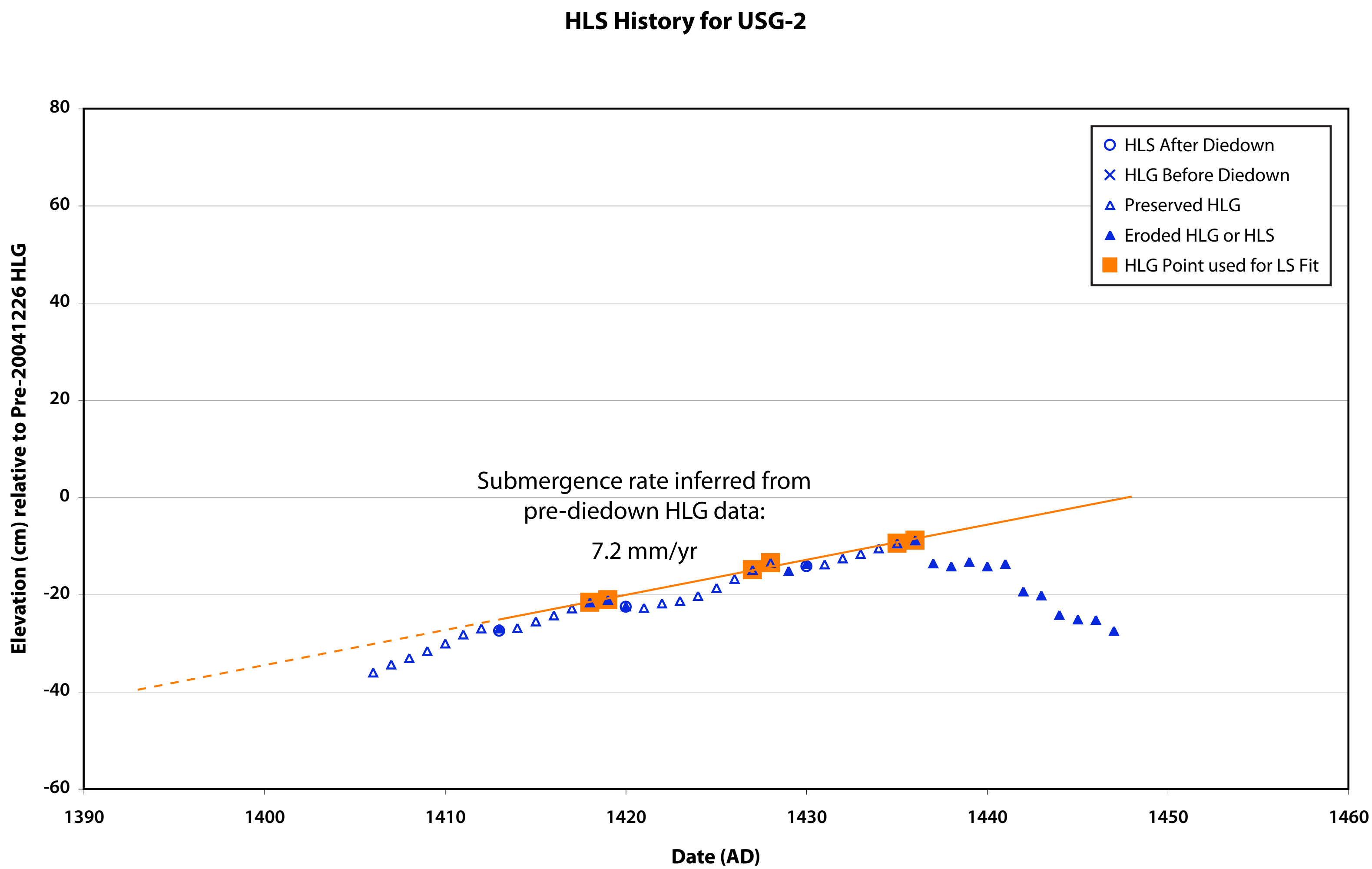

Figure S24b. Graph of relative sea level history derived from slab USG-2.

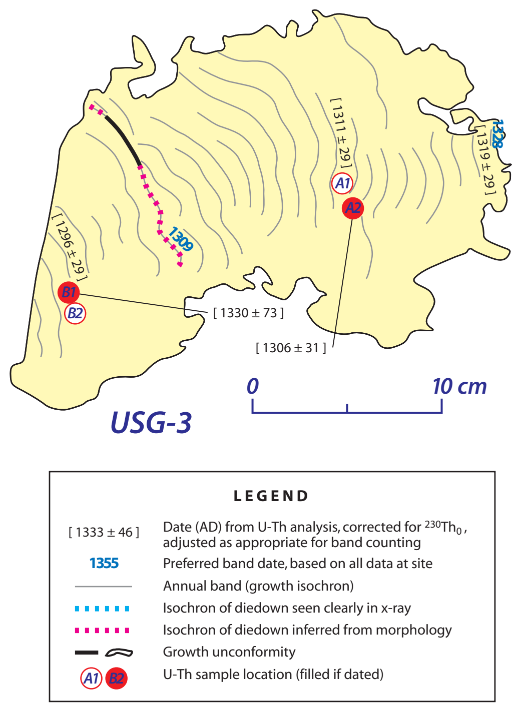

Figure S25. Cross-section of slab USG-3, from site USG-A.

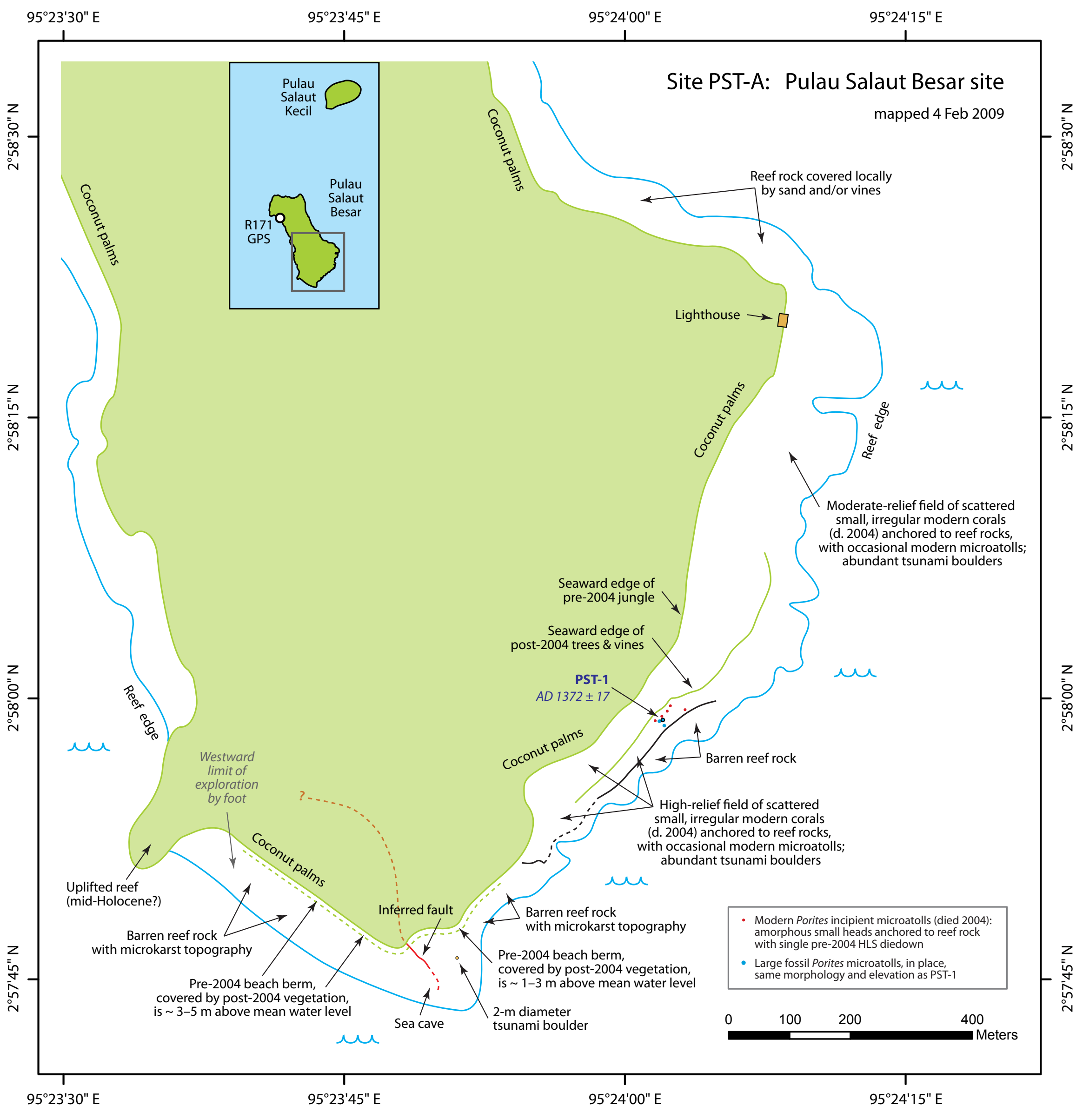

Figure S26. Map of site PST-A, southern Pulau Salaut Besar, showing the sampled microatoll and its date of death, as well as the location of the inferred fault. Inset shows the location relative to all of Salaut Besar and Salaut Kecil. Also shown on the inset is the location of campaign GPS monument R171, discussed in the auxiliary material.

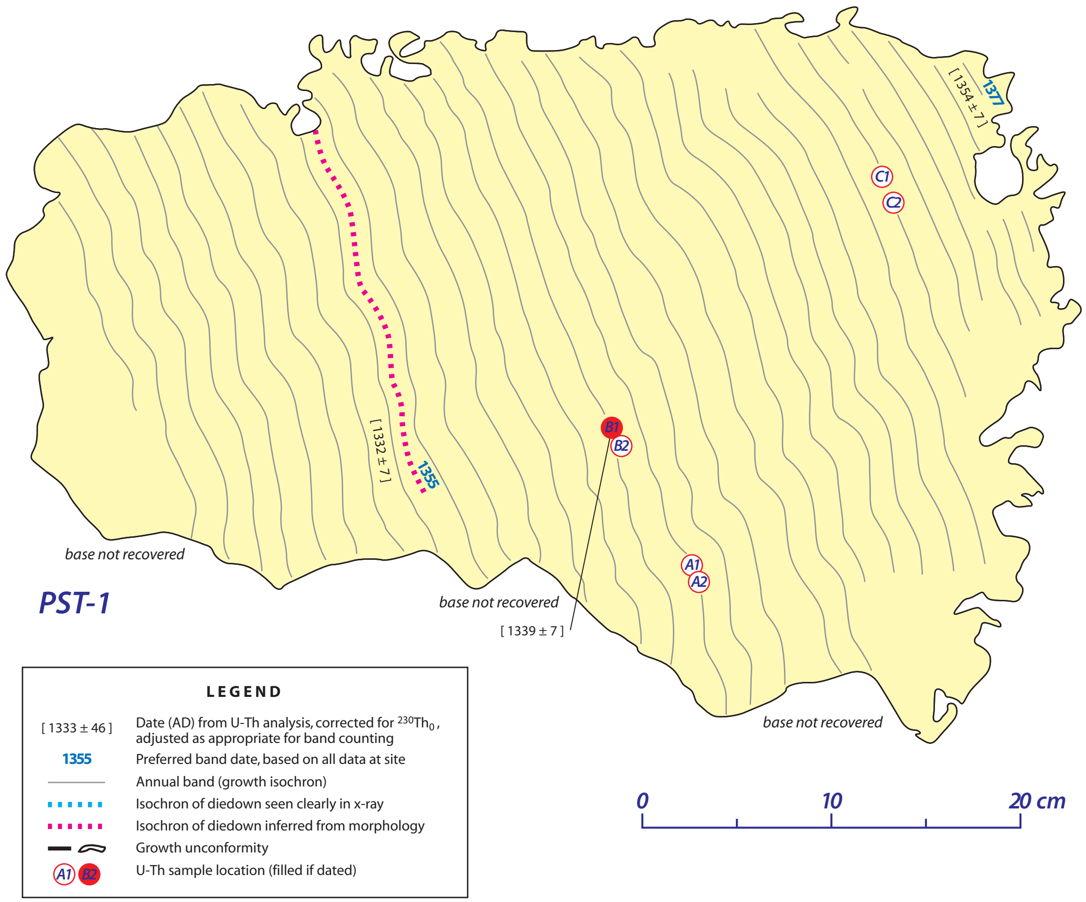

Figure S27. Cross-section of slab PST-1, from site PST-A.

Sampled Coral Microatolls: Location and Information **Table S1**

Head Name	Site Name	Collected	Latitude	Longitude	Mod/Fsl	Genus	2004 Uplift (cm)
USL-1	USL-A	Jun 2006	2.70612	95.75935	Modern	*Porites*	125 ± 15
USL-2	USL-A	Jun 2006	2.70767	95.76317	Fossil	*Porites*	125 ± 15
LDL-1	LDL-A	Jun 2006	2.74791	95.71538	Modern	*Porites*	153 ± 10
LDL-2	LDL-A	Jun 2006	2.74876	95.71473	Fossil	*Porites*	153 ± 10
LDL-3	LDL-B	Jul 2007	2.74864	95.70136	Fossil	*Porites*	
LDL-4	LDL-B	Jul 2007	2.74984	95.70072	Fossil	*Porites*	
LDL-5	LDL-B	Jul 2007	2.74862	95.70066	Fossil	*Porites*	
LNG-1	LNG-A	Jun 2006	2.82592	95.72130	Modern	*Porites*	142 ± 10
LNG-2	LNG-A	Jun 2006	2.82571	95.72211	Fossil	*Porites*	142 ± 10
LKP-1	LKP-A	Jun 2006	2.86160	95.76324	Modern	*Porites*	123 ± 15
LKP-2	LKP-A	Jun 2006	2.85848	95.76419	Fossil	*Porites*	123 ± 15
LKP-3	LKP-B	Jul 2007	2.87715	95.76522	Fossil	*Porites*	~ 100
LKP-4	LKP-B	Jul 2007	2.87585	95.76546	Fossil	*Porites*	~ 100
LKP-5	LKP-B	Jul 2007	2.87596	95.76525	Fossil	*Porites*	~ 100
LKP-6	LKP-B	Jul 2007	2.87749	95.76500	Fossil	*Goniastrea*	~ 100
LKP-7	LKP-B	Jul 2007	2.87722	95.76493	Fossil	*Goniastrea*	~ 100
LKP-8	LKP-B	Jul 2007	2.87656	95.76526	Fossil	*Porites*	~ 100
LKP-9	LKP-B	Jul 2007	2.87568	95.76475	Modern	*Porites*	~ 100
LKP-10	LKP-C	Feb 2009	2.86960	95.76646	Fossil	*Porites*	105 ± 6
LWK-1	LWK-A	Jun 2005	2.92835	95.80513	Modern	*Porites*	44 ± 12
LWK-2	LWK-B	Jul 2007	2.92833	95.79069	Fossil	*Porites*	
LWK-3	LWK-B	Jul 2007	2.92827	95.79091	Fossil	*Porites*	
LWK-4	LWK-B	Jul 2007	2.92740	95.79346	Fossil	*Porites*	
LWK-5	LWK-B	Jul 2007	2.92737	95.79480	Fossil	*Porites*	
USG-1	USG-A	Jul 2007	2.91213	95.86741	Modern	*Porites*	~ 25
USG-2	USG-A	Jul 2007	2.91270	95.86915	Fossil	*Porites*	~ 25
USG-3	USG-A	Jul 2007	2.91260	95.86856	Fossil	*Porites*	~ 25
PST-1	PST-A	Feb 2009	2.96635	95.40056	Fossil	*Porites*	

Uranium and Thorium isotopic compositions and ^{230}Th ages for Sumatran coral samples by ICP-MS **Table S2**

Sample ID	Weight g	^{238}U ppb	^{232}Th ppt	δ^{234}U measured [a]	[^{230}Th/^{238}U] activity [c]	[^{230}Th/^{232}Th] (x 10^{-6}) [d]	$\delta^{234}U_{initial}$ corrected [b]	^{230}Th Age uncorrected	^{230}Th Age corrected [c,e]	Chemistry Date (AD)	Chemistry Date (AD)	Date (AD) of Sample Growth	[^{230}Th/^{232}Th]$_0$ (x 10^{-6}) [e]
PST-1-B1	0.107	2095 ± 1	136 ± 6	144.5 ± 1.1	0.00703 ± 0.00007	1,782 ± 87	144.7 ± 1.1	672.8 ± 6.5	670.4 ± 7.0	2009/04/29	2009.3	**1338.9 ± 7.0**	6.5 ± 6.5
USL-2-B2 (1)	0.446	2326 ± 3	3600 ± 10	146.2 ± 2.1	0.01163 ± 0.00014	124.0 ± 1.5	146.6 ± 2.1	1,113 ± 14	1,075 ± 16	2006/12/21	2007.0	**932.0 ± 15.5**	4.6 ± 1.4
USL-2-B2 (2)	0.723	2280 ± 3	2041 ± 5	145.9 ± 2.0	0.01145 ± 0.00014	211.2 ± 2.5	146.4 ± 2.0	1,097 ± 13	*sample age and initial thorium ratio determined by 3-D isochron method*				
USL-2-B2 (3)	0.455	2266 ± 7	1518 ± 9	146.9 ± 3.4	0.01146 ± 0.00024	282.3 ± 6.1	147.3 ± 3.4	1,096 ± 24					
USL-2-B2 (4)	0.412	2236 ± 3	7220 ± 21	150.3 ± 2.1	0.01212 ± 0.00016	62.0 ± 0.9	150.7 ± 2.1	1,157 ± 16					
LDL-2-B3 (1)	0.859	2508 ± 8	23737 ± 156	143.9 ± 3.4	0.01711 ± 0.00040	29.8 ± 0.7	144.4 ± 3.4	1,645 ± 39	1,289 ± 359	2006/08/20	2006.6	717.5 ± 358.8	6.5 ± 6.5
LDL-2-B3 (2)	0.345	2553 ± 4	32069 ± 160	146.5 ± 2.0	0.01701 ± 0.00057	22.4 ± 0.8	147.0 ± 2.0	1,632 ± 55	1,160 ± 476	2006/08/20	2006.6	846.6 ± 476.0	6.5 ± 6.5
										weight-averaged age		***764.3 ± 286.5***	
LDL-3-A2	0.110	2360 ± 4	256 ± 6	143.1 ± 2.4	0.00651 ± 0.00006	989 ± 26	143.4 ± 2.4	623.3 ± 5.5	619.2 ± 6.8	2007/11/19	2007.9	**1388.7 ± 6.8**	6.5 ± 6.5
LDL-4A-A2	0.127	2300 ± 4	1000 ± 6	143.7 ± 2.6	0.00674 ± 0.00005	255.7 ± 2.4	143.9 ± 2.6	644.9 ± 5.3	629 ± 17	2007/11/19	2007.9	**1379.3 ± 17.2**	6.5 ± 6.5
LDL-4B-A2 (1)	0.102	1864 ± 3	399 ± 7	145.8 ± 2.3	0.00693 ± 0.00007	534 ± 11	146.1 ± 2.3	662.1 ± 6.8	654 ± 11	2008/05/16	2008.4	1354.3 ± 10.5	6.5 ± 6.5
LDL-4B-A2 (2)	0.098	2121 ± 4	516 ± 7	144.1 ± 2.6	0.00690 ± 0.00006	468.7 ± 7.8	144.4 ± 2.6	660.4 ± 6.2	651 ± 11	2008/05/18	2008.4	1357.1 ± 11.1	6.5 ± 6.5
										weight-averaged age		***1355.7 ± 7.6***	
LDL-5-A2	0.120	2352 ± 4	221 ± 6	144.0 ± 2.7	0.00691 ± 0.00006	1,216 ± 34	144.3 ± 2.7	661.8 ± 5.8	658.3 ± 6.8	2007/11/19	2007.9	**1349.6 ± 6.8**	6.5 ± 6.5
LDL-5-B2 (1)	0.116	2378 ± 4	257 ± 6	148.0 ± 2.8	0.00696 ± 0.00005	1,063 ± 26	148.3 ± 2.8	664.2 ± 5.1	660.1 ± 6.5	2008/05/16	2008.4	1348.2 ± 6.5	6.5 ± 6.5
LDL-5-B2 (2)	0.107	2540 ± 5	245 ± 7	148.0 ± 2.4	0.00695 ± 0.00005	1,189 ± 33	148.3 ± 2.4	663.2 ± 5.0	659.6 ± 6.2	2008/05/18	2008.4	1348.8 ± 6.2	6.5 ± 6.5
										weight-averaged age		***1348.5 ± 4.5***	
LDL-5-C2 (1)	0.097	2343 ± 4	289 ± 7	151.3 ± 2.6	0.00673 ± 0.00006	900 ± 24	151.6 ± 2.6	640.4 ± 5.8	635.8 ± 7.4	2008/05/16	2008.4	1372.6 ± 7.4	6.5 ± 6.5
LDL-5-C2 (2)	0.102	2433 ± 5	375 ± 7	147.1 ± 2.7	0.00663 ± 0.00006	711 ± 14	147.4 ± 2.7	633.1 ± 5.6	627.3 ± 8.1	2008/05/18	2008.4	1381.1 ± 8.1	6.5 ± 6.5
										weight-averaged age		***1376.5 ± 5.5***	
LNG-2-A2	0.533	2760 ± 3	164 ± 1	145.6 ± 1.7	0.00636 ± 0.00005	1,768 ± 21	145.8 ± 1.7	607.7 ± 5.2	605.4 ± 5.7	2007/03/16	2007.2	**1401.8 ± 5.7**	6.5 ± 6.5
LKP-2-B2 (1)	0.407	2497 ± 4	3715 ± 9	148.8 ± 2.2	0.00717 ± 0.00010	79.6 ± 1.1	149.1 ± 2.2	683.5 ± 9.8	674 ± 46	2007/01/19	2007.1	**1333.1 ± 46.0**	1.9 ± 4.8
LKP-2-B2 (2)	0.600	2521 ± 7	2272 ± 9	143.6 ± 3.0	0.00713 ± 0.00014	130.7 ± 2.6	143.9 ± 3.0	683 ± 14	*sample age and initial thorium ratio determined by 3-D isochron method*				
LKP-2-B2 (3)	0.506	2505 ± 3	3671 ± 8	145.8 ± 2.0	0.00732 ± 0.00010	82.5 ± 1.1	146.0 ± 2.0	700.0 ± 9.3					
LKP-2-B2 (4)	0.792	2513 ± 3	5187 ± 10	145.2 ± 1.8	0.00729 ± 0.00011	58.4 ± 0.8	145.5 ± 1.8	698 ± 10					
LKP-2-B2 (5)	0.299	2475 ± 2	4707 ± 16	144.3 ± 1.5	0.00727 ± 0.00014	63.1 ± 1.2	144.6 ± 1.5	696 ± 13					
LKP-3-A1 (1)	0.199	2464 ± 2	1776 ± 5	144.8 ± 1.3	0.00668 ± 0.00005	153.1 ± 1.3	145.1 ± 1.3	639.3 ± 5.1	612 ± 28	2007/10/23	2007.8	1395.5 ± 27.5	6.5 ± 6.5
LKP-3-A1 (2)	0.108	2462 ± 1	825 ± 2	147.2 ± 1.0	0.00672 ± 0.00003	330.9 ± 1.8	147.5 ± 1.0	641.0 ± 3.4	628 ± 13	2008/06/26	2008.5	1380.1 ± 13.0	6.5 ± 6.5
LKP-3-A1 (3)	0.107	2471 ± 2	880 ± 2	145.7 ± 1.4	0.00670 ± 0.00004	310.5 ± 1.7	146.0 ± 1.5	639.9 ± 3.5	627 ± 14	2008/06/26	2008.5	1381.9 ± 13.8	6.5 ± 6.5
LKP-3-A1 (4)	0.119	2466 ± 2	779 ± 1	145.3 ± 1.5	0.00668 ± 0.00003	349.5 ± 1.7	145.5 ± 1.5	639.1 ± 3.1	627 ± 12	2008/06/26	2008.5	1381.2 ± 12.2	6.5 ± 6.5
										weight-averaged age		***1382.0 ± 7.2***	
LKP-3-C2 (1)	0.098	2312 ± 2	1786 ± 3	146.4 ± 1.5	0.00664 ± 0.00005	142.0 ± 1.0	146.7 ± 1.5	634.6 ± 4.7	613 ± 33	2008/05/18	2008.4	**1395.4 ± 33.0**	4.9 ± 5.9
LKP-3-C2 (2)	0.106	2455 ± 2	2429 ± 3	145.5 ± 1.3	0.00673 ± 0.00005	112.2 ± 0.8	145.8 ± 1.3	643.0 ± 4.6	*sample age and initial thorium ratio determined by 3-D isochron method*				
LKP-3-C2 (3)	0.100	2381 ± 2	2923 ± 5	147.9 ± 1.4	0.00675 ± 0.00005	90.8 ± 0.7	148.1 ± 1.4	644.3 ± 5.3					
LKP-3-C2 (4)	0.097	2476 ± 4	1991 ± 8	148.6 ± 2.5	0.00660 ± 0.00007	135.5 ± 1.5	148.9 ± 2.5	629.1 ± 6.7					
LKP-4-A2 (1)	0.220	2531 ± 2	5688 ± 23	143.9 ± 1.3	0.00687 ± 0.00013	50.4 ± 0.9	144.1 ± 1.3	657 ± 12	573 ± 85	2007/10/23	2007.8	1435.0 ± 85.4	6.5 ± 6.5
LKP-4-A2 (2)	0.109	2465 ± 2	5133 ± 17	146.4 ± 1.4	0.00702 ± 0.00009	55.7 ± 0.8	146.6 ± 1.4	670.6 ± 9.1	592 ± 79	2007/12/27	2008.0	1415.5 ± 78.7	6.5 ± 6.5
LKP-4-A2 (3)	0.097	2303 ± 3	4158 ± 13	146.2 ± 1.7	0.00708 ± 0.00010	64.7 ± 0.9	146.5 ± 1.7	676.5 ± 9.3	609 ± 68	2007/12/27	2008.0	1399.2 ± 68.4	6.5 ± 6.5
LKP-4-A2 (4)	0.153	2321 ± 4	3630 ± 12	139.0 ± 2.5	0.00713 ± 0.00009	75.3 ± 1.0	139.2 ± 2.5	686.0 ± 8.9	627 ± 60	2007/12/20	2008.0	1381.0 ± 59.7	6.5 ± 6.5
										weight-averaged age [f]		***1413.9 ± 44.2***	
LKP-4-B1 (1)	0.102	2133 ± 4	4713 ± 11	144.2 ± 2.2	0.00740 ± 0.00008	55.3 ± 0.6	144.4 ± 2.2	708.3 ± 8.1	625 ± 83	2008/05/16	2008.4	1383.1 ± 83.4	6.5 ± 6.5
LKP-4-B1 (2)	0.131	2387 ± 4	5577 ± 13	145.8 ± 2.0	0.00725 ± 0.00008	51.3 ± 0.6	146.1 ± 2.1	693.3 ± 7.9	606 ± 88	2008/05/18	2008.4	1402.7 ± 88.1	6.5 ± 6.5
										weight-averaged age		***1392.4 ± 60.6***	
LKP-4-C1 (1)	0.098	2381 ± 4	9405 ± 21	149.7 ± 2.2	0.00731 ± 0.00009	30.6 ± 0.4	149.9 ± 2.2	696.6 ± 8.8	549 ± 148	2008/05/16	2008.4	1459.5 ± 148.1	6.5 ± 6.5
LKP-4-C1 (2)	0.104	2727 ± 4	10322 ± 26	148.8 ± 2.3	0.00702 ± 0.00010	30.6 ± 0.4	149.1 ± 2.3	642.3 ± 7.1	577 ± 66	2008/05/18	2008.4	1431.7 ± 66.0	6.5 ± 6.5
										weight-averaged age		***1436.3 ± 60.3***	

Uranium and Thorium isotopic compositions and ^{230}Th ages for Sumatran coral samples by ICP-MS **Table S2**

Sample ID	Weight g	^{238}U ppb	^{232}Th ppt	δ^{234}U measured [a]	[^{230}Th/^{238}U] activity [c]	[^{230}Th/^{232}Th] (x 10^{-6}) [d]	δ^{234}U$_{initial}$ corrected [b]	^{230}Th Age uncorrected	^{230}Th Age corrected [c,e]	Chemistry Date (AD)	Chemistry Date (AD)	Date (AD) of Sample Growth	[^{230}Th/^{232}Th]$_0$ (x 10^{-6}) [e]
LKP-5-A1 (1)	0.187	2701 ± 2	11417 ± 41	146.0 ± 1.3	0.00784 ± 0.00012	30.6 ± 0.5	146.3 ± 1.3	750 ± 12	591 ± 159	2007/10/23	2007.8	1416.8 ± 159.2	6.5 ± 6.5
LKP-5-A1 (2)	0.093	2667 ± 3	11258 ± 43	147.8 ± 1.9	0.00766 ± 0.00016	30.0 ± 0.6	148.0 ± 2.0	732 ± 15	573 ± 159	2007/12/20	2008.0	1434.6 ± 159.0	6.5 ± 6.5
LKP-5-A1 (3)	0.097	2697 ± 3	10762 ± 40	144.3 ± 2.0	0.00746 ± 0.00015	30.9 ± 0.6	144.5 ± 2.0	714 ± 14	564 ± 151	2007/12/20	2008.0	1443.5 ± 150.8	6.5 ± 6.5
LKP-5-A1 (4)	0.095	2501 ± 6	11588 ± 61	136.9 ± 3.2	0.00759 ± 0.00024	27.0 ± 0.9	137.1 ± 3.2	731 ± 23	556 ± 177	2007/12/27	2008.0	1451.9 ± 176.9	6.5 ± 6.5
										weight-averaged age [f]		***1432.1 ± 90.2***	
LKP-5-B1 (1)	0.192	2803 ± 2	5398 ± 15	146.4 ± 1.1	0.00785 ± 0.00007	67.3 ± 0.7	146.7 ± 1.1	750.5 ± 7.0	664 ± 33	2007/12/20	2008.0	**1344.0 ± 32.5**	7.7 ± 3.3
LKP-5-B1 (2)	0.151	2956 ± 3	4424 ± 13	146.5 ± 2.0	0.00760 ± 0.00007	83.9 ± 0.9	146.8 ± 2.0	726.1 ± 7.3	*sample age and initial thorium ratio determined by 3-D isochron method*				
LKP-5-B1 (3)	0.099	2871 ± 3	4197 ± 12	146.7 ± 1.9	0.00769 ± 0.00008	86.9 ± 0.9	147.0 ± 1.9	735.0 ± 7.9					
LKP-5-B1 (4)	0.092	2811 ± 3	4416 ± 12	145.1 ± 2.1	0.00768 ± 0.00008	80.7 ± 0.9	145.3 ± 2.1	734.8 ± 8.1					
LKP-5-C2 (1)	0.197	2747 ± 2	6424 ± 17	143.1 ± 1.3	0.00802 ± 0.00009	56.7 ± 0.6	143.3 ± 1.3	769.0 ± 8.4	681 ± 88	2007/10/23	2007.8	1326.7 ± 88.4	6.5 ± 6.5
LKP-5-C2 (2)	0.106	2819 ± 3	5886 ± 14	143.8 ± 1.9	0.00802 ± 0.00008	63.4 ± 0.7	144.1 ± 1.9	767.9 ± 7.9	689 ± 79	2008/05/07	2008.3	1319.0 ± 78.9	6.5 ± 6.5
LKP-5-C2 (3)	0.101	2718 ± 3	6715 ± 16	147.5 ± 1.5	0.00810 ± 0.00009	54.1 ± 0.6	147.7 ± 1.5	773.4 ± 8.3	681 ± 93	2008/05/07	2008.3	1327.5 ± 93.0	6.5 ± 6.5
										weight-averaged age		***1323.9 ± 49.7***	
LKP-5-D1 (1)	0.099	2606 ± 4	6558 ± 15	145.5 ± 2.3	0.00773 ± 0.00009	50.7 ± 0.6	145.8 ± 2.3	738.9 ± 8.8	644 ± 95	2008/05/16	2008.4	1363.9 ± 94.9	6.5 ± 6.5
LKP-5-D1 (2)	0.099	2831 ± 5	7203 ± 18	145.1 ± 2.3	0.00770 ± 0.00009	50.0 ± 0.6	145.4 ± 2.3	737.0 ± 8.4	642 ± 96	2008/05/18	2008.4	1366.8 ± 95.9	6.5 ± 6.5
										weight-averaged age		***1365.3 ± 67.5***	
LKP-5-F2 (1)	0.110	2512 ± 4	5641 ± 14	149.4 ± 2.5	0.00822 ± 0.00008	60.5 ± 0.6	149.7 ± 2.5	783.8 ± 7.7	700 ± 84	2008/05/16	2008.4	1308.6 ± 84.4	6.5 ± 6.5
LKP-5-F2 (2)	0.107	2874 ± 4	8186 ± 19	148.6 ± 2.3	0.00821 ± 0.00009	47.6 ± 0.5	148.9 ± 2.3	782.9 ± 8.8	676 ± 107	2008/05/18	2008.4	1332.1 ± 107.0	6.5 ± 6.5
										weight-averaged age		***1317.6 ± 66.3***	
LKP-6-A2	0.266	2721 ± 2	40 ± 3	145.7 ± 1.3	0.00645 ± 0.00003	7,216 ± 472	145.9 ± 1.3	616.6 ± 3.3	616.0 ± 3.3	2007/10/23	2007.8	**1391.8 ± 3.3**	6.5 ± 6.5
LKP-7-A2	0.163	2869 ± 2	83 ± 4	145.1 ± 1.4	0.00648 ± 0.00004	3,691 ± 191	145.4 ± 1.4	619.5 ± 3.6	618.4 ± 3.8	2007/10/23	2007.8	**1389.4 ± 3.8**	6.5 ± 6.5
LKP-8-A1 (1)	0.143	2485 ± 1	11272 ± 32	146.7 ± 1.0	0.00749 ± 0.00011	27.3 ± 0.4	146.9 ± 1.0	716 ± 11	653 ± 45	2008/05/07	2008.3	**1355.3 ± 45.0**	2.4 ± 2.1
LKP-8-A1 (2)	0.104	2485 ± 3	8493 ± 21	147.6 ± 1.7	0.00733 ± 0.00009	35.4 ± 0.4	147.9 ± 1.7	699.4 ± 8.4	*sample age and initial thorium ratio determined by 3-D isochron method*				
LKP-8-A1 (3)	0.099	2465 ± 3	9397 ± 23	146.6 ± 1.8	0.00746 ± 0.00010	32.3 ± 0.4	146.8 ± 1.8	712.7 ± 9.9					
LKP-10-A1	0.096	2845 ± 1	2890 ± 8	144.7 ± 1.0	0.00666 ± 0.00007	108.1 ± 1.2	145.0 ± 1.0	636.6 ± 6.7	598 ± 39	2009/04/29	2009.3	**1410.8 ± 38.7**	6.5 ± 6.5
LKP-10-B2	0.094	2702 ± 1	1670 ± 8	143.7 ± 1.0	0.00680 ± 0.00007	181.7 ± 2.0	143.9 ± 1.0	651.3 ± 6.6	628 ± 24	2009/04/29	2009.3	**1381.2 ± 24.2**	6.5 ± 6.5
LWK-2-A1 (1)	0.134	2565 ± 2	7974 ± 27	146.3 ± 1.5	0.00695 ± 0.00011	36.9 ± 0.6	146.6 ± 1.5	664 ± 11	547 ± 117	2007/10/24	2007.8	1460.6 ± 117.2	6.5 ± 6.5
LWK-2-A1 (2)	0.096	2453 ± 2	7399 ± 26	146.7 ± 1.7	0.00694 ± 0.00013	38.0 ± 0.7	146.9 ± 1.7	663 ± 12	550 ± 114	2007/12/20	2008.0	1458.2 ± 113.8	6.5 ± 6.5
LWK-2-A1 (3)	0.091	2454 ± 2	7634 ± 24	146.9 ± 1.8	0.00691 ± 0.00012	36.7 ± 0.7	147.1 ± 1.8	659 ± 12	543 ± 117	2007/12/20	2008.0	1465.2 ± 117.3	6.5 ± 6.5
LWK-2-A1 (4)	0.121	2519 ± 2	7203 ± 24	143.3 ± 1.5	0.00693 ± 0.00011	40.0 ± 0.7	143.6 ± 1.5	663 ± 11	556 ± 108	2008/01/01	2008.0	1452.1 ± 108.2	6.5 ± 6.5
										weight-averaged age		***1458.8 ± 57.0***	
LWK-2-B1 (1)	0.095	2510 ± 5	11085 ± 26	148.9 ± 2.8	0.00762 ± 0.00011	28.5 ± 0.4	149.1 ± 2.8	726 ± 10	561 ± 166	2008/05/16	2008.4	1447.4 ± 165.8	6.5 ± 6.5
LWK-2-B1 (2)	0.097	2385 ± 4	10963 ± 52	144.8 ± 2.8	0.00759 ± 0.00023	27.3 ± 0.8	145.0 ± 2.8	726 ± 22	554 ± 174	2008/05/18	2008.4	1454.6 ± 174.2	6.5 ± 6.5
										weight-averaged age		***1450.8 ± 120.1***	
LWK-3-A1 (1)	0.084	2508 ± 2	36332 ± 192	145.8 ± 1.4	0.00726 ± 0.00022	8.3 ± 0.3	145.9 ± 1.4	694 ± 21	149 ± 547	2007/10/24	2007.8	1858.8 ± 546.6	6.5 ± 6.5
LWK-3-A1 (2)	0.099	2355 ± 3	22234 ± 72	144.9 ± 1.7	0.00739 ± 0.00013	12.9 ± 0.2	145.1 ± 1.7	707 ± 13	352 ± 356	2008/05/07	2008.3	1656.1 ± 355.9	6.5 ± 6.5
LWK-3-A1 (3)	0.119	2367 ± 3	27401 ± 109	146.6 ± 1.8	0.00766 ± 0.00016	10.9 ± 0.2	146.8 ± 1.8	732 ± 15	297 ± 436	2008/05/07	2008.3	1711.1 ± 435.9	6.5 ± 6.5
										weight-averaged age		***1714.7 ± 246.1***	
LWK-3-B2 (1)	0.096	2390 ± 5	4093 ± 13	146.4 ± 2.7	0.00675 ± 0.00008	65.1 ± 0.8	146.6 ± 2.7	644.8 ± 7.7	581 ± 65	2008/05/16	2008.4	1427.8 ± 64.7	6.5 ± 6.5
LWK-3-B2 (2)	0.121	2389 ± 5	4186 ± 11	145.0 ± 3.0	0.00669 ± 0.00007	63.1 ± 0.7	145.3 ± 3.0	640.1 ± 7.0	574 ± 66	2008/05/18	2008.4	1434.1 ± 66.2	6.5 ± 6.5
										weight-averaged age		***1430.9 ± 46.3***	
LWK-4-A2 (1)	0.119	2501 ± 3	18532 ± 70	145.3 ± 1.9	0.00769 ± 0.00015	17.1 ± 0.3	145.5 ± 1.9	736 ± 14	660 ± 26	2007/12/20	2008.0	**1348.0 ± 26.0**	1.8 ± 3.2
LWK-4-A2 (2)	0.100	2465 ± 3	10289 ± 33	148.1 ± 1.8	0.00743 ± 0.00013	29.4 ± 0.5	148.4 ± 1.8	709 ± 12	*sample age and initial thorium ratio determined by 3-D isochron method*				
LWK-4-A2 (3)	0.101	2526 ± 2	10267 ± 31	146.1 ± 1.7	0.00726 ± 0.00013	29.5 ± 0.5	146.3 ± 1.7	694 ± 12					
LWK-4-B1 (1)	0.100	2466 ± 5	940 ± 7	144.7 ± 3.0	0.00726 ± 0.00006	314.4 ± 3.3	145.0 ± 3.0	694.8 ± 5.6	681 ± 15	2008/05/16	2008.4	1327.9 ± 15.4	6.5 ± 6.5
LWK-4-B1 (2)	0.096	2680 ± 5	1048 ± 7	145.0 ± 2.8	0.00725 ± 0.00006	305.9 ± 3.2	145.3 ± 2.8	693.3 ± 5.6	679 ± 16	2008/05/18	2008.4	1329.8 ± 15.7	6.5 ± 6.5
										weight-averaged age		***1328.8 ± 11.0***	

Uranium and Thorium isotopic compositions and ^{230}Th ages for Sumatran coral samples by ICP-MS **Table S2**

Sample ID	Weight g	^{238}U ppb	^{232}Th ppt	δ^{234}U measured [a]	[^{230}Th/^{238}U] activity [c]	[^{230}Th/^{232}Th] (x 10^{-6}) [d]	$\delta^{234}U_{initial}$ corrected [b]	^{230}Th Age uncorrected	^{230}Th Age corrected [c,e]	Chemistry Date (AD)	Chemistry Date (AD)	Date (AD) of Sample Growth	[^{230}Th/^{232}Th]$_0$ (x 10^{-6}) [e]
LWK-5-A1	0.093	2338 ± 2	3771 ± 13	146.3 ± 1.3	0.00649 ± 0.00009	66.4 ± 0.9	146.5 ± 1.3	619.6 ± 8.2	559 ± 61	2007/10/24	2007.8	**1448.7 ± 61.1**	6.5 ± 6.5
LWK-5-B1 (1)	0.106	2354 ± 4	4133 ± 11	150.9 ± 2.6	0.00675 ± 0.00007	63.5 ± 0.7	151.1 ± 2.6	642.3 ± 7.1	577 ± 66	2008/05/16	2008.4	1431.7 ± 66.0	6.5 ± 6.5
LWK-5-B1 (2)	0.106	2193 ± 3	4253 ± 11	140.1 ± 3.6	0.00667 ± 0.00009	56.8 ± 0.8	140.3 ± 3.6	640.6 ± 8.7	567 ± 74	2008/05/18	2008.4	1440.9 ± 73.7	6.5 ± 6.5
										weight-averaged age		***1435.8 ± 49.2***	
USG-2-A2 (1)	0.204	2323 ± 2	2770 ± 9	147.4 ± 1.6	0.00644 ± 0.00008	89.1 ± 1.2	147.6 ± 1.6	614.2 ± 8.0	570 ± 45	2007/10/22	2007.8	1438.3 ± 45.4	6.5 ± 6.5
USG-2-A2 (2)	0.097	2301 ± 3	2161 ± 8	147.5 ± 2.1	0.00651 ± 0.00006	114.4 ± 1.2	147.7 ± 2.1	620.8 ± 6.2	586 ± 36	2008/05/05	2008.3	1422.7 ± 35.7	6.5 ± 6.5
USG-2-A2 (3)	0.097	2255 ± 2	2408 ± 9	144.9 ± 1.7	0.00657 ± 0.00007	101.6 ± 1.1	145.2 ± 1.7	628.4 ± 6.6	588 ± 41	2008/05/07	2008.3	1420.0 ± 40.6	6.5 ± 6.5
										weight-averaged age		***1425.9 ± 23.1***	
USG-2-B2 (1)	0.103	2274 ± 4	1577 ± 8	149.0 ± 2.8	0.00682 ± 0.00006	162.3 ± 1.7	149.2 ± 2.9	650.0 ± 6.4	624 ± 27	2008/05/16	2008.4	1384.3 ± 26.7	6.5 ± 6.5
USG-2-B2 (2)	0.100	2258 ± 4	1890 ± 8	146.8 ± 2.9	0.00682 ± 0.00007	134.5 ± 1.4	147.1 ± 2.9	650.9 ± 6.7	620 ± 32	2008/05/18	2008.4	1388.8 ± 32.1	6.5 ± 6.5
										weight-averaged age		***1386.2 ± 20.5***	
USG-3-A2 (1)	0.206	2903 ± 3	6929 ± 23	148.0 ± 1.6	0.00802 ± 0.00010	55.5 ± 0.7	153.0 ± 1.6	765.5 ± 9.7	702 ± 31	2008/05/05	2008.3	**1306.3 ± 31.0**	4.4 ± 2.1
USG-3-A2 (2)	0.112	2934 ± 5	5964 ± 16	149.9 ± 2.2	0.00793 ± 0.00008	64.4 ± 0.7	150.1 ± 2.2	755.4 ± 7.7	*sample age and initial thorium ratio determined by 3-D isochron method*				
USG-3-A2 (3)	0.095	3011 ± 4	8862 ± 27	148.3 ± 2.5	0.00817 ± 0.00009	45.8 ± 0.5	148.6 ± 2.5	779.8 ± 8.8					
USG-3-B1 (1)	0.104	2539 ± 5	7663 ± 20	145.2 ± 2.8	0.00811 ± 0.00009	44.4 ± 0.5	145.5 ± 2.8	776.2 ± 9.0	663 ± 114	2008/05/16	2008.4	1345.5 ± 113.7	6.5 ± 6.5
USG-3-B1 (2)	0.101	2584 ± 3	6572 ± 15	145.2 ± 1.7	0.00820 ± 0.00009	53.2 ± 0.6	145.5 ± 1.7	784.7 ± 9.0	689 ± 96	2008/05/18	2008.4	1319.2 ± 96.0	6.5 ± 6.5
										weight-averaged age		***1330.1 ± 73.3***	

For a discussion of the ICP-MS method, see *Shen et al.* [2002]. Analytical errors are 2σ of the mean.

[a] $\delta^{234}U = ([^{234}U/^{238}U]_{activity} - 1) \times 1000$.

[b] $\delta^{234}U_{initial}$ corrected was calculated based on ^{230}Th age (T), i.e., $\delta^{234}U_{initial} = \delta^{234}U_{measured}\ X\ e^{\lambda 234 * T}$, and T is corrected age.

[c] $[^{230}Th/^{238}U]_{activity} = 1 - e^{-\lambda 230\, T} + (\delta^{234}U_{measured}/1000)[\lambda_{230}/(\lambda_{230} - \lambda_{234})](1 - e^{-(\lambda 230 - \lambda 234)\, T})$, where T is the age.

Decay constants are 9.1577×10^{-6} yr^{-1} for ^{230}Th, 2.8263×10^{-6} yr^{-1} for ^{234}U, and 1.55125×10^{-10} yr^{-1} for ^{238}U [*Cheng et al.*, 2000].

[d] The degree of detrital ^{230}Th contamination is indicated by the [^{230}Th/^{232}Th] atomic ratio instead of the activity ratio.

[e] Except where isochron techniques were used to determine the ages and initial ^{230}Th/^{232}Th atomic ratios, the initial ^{230}Th/^{232}Th atomic ratio is assumed to be $6.5 \pm 6.5 \times 10^{-6}$ [*Zachariasen et al.*, 1999].

[f] Dates with $\delta^{234}U_{initial}$ corrected beyond 146 ± 4, which show apparent diagenesis, are excluded from the weighted-average age calculations.

Dates of Presumed Uplift of Individual Coral Heads **Table S3**

Sample ID	Date of Sample (AD)	Preserved Bands after Sample	Date of Outer Band (AD)	Slab Weighted Mean Date of Outer Band	Inferred Number of Missing Bands	Slab Weighted Mean Date of Coral Death	Outer Rim Elevation (cm) above Pre-20041226 HLG	
PST-1-B1	1338.9 ± 7.0	17.0 ± 0.5	1355.9 ± 7.0	**1355.9 ± 7.0**	16.0 ± 16.0	**1371.9 ± 17.5**	71.8	
USL-2-B2	932.0 ± 15.5	22.5 ± 0.5	954.5 ± 15.5	**954.5 ± 15.5**	2.0 ± 2.0	**956.5 ± 15.6**	31.6	tilted
LDL-2-B3	764.3 ± 286.5	36.0 ± 1.0	800.3 ± 286.5	**800.3 ± 286.5**	20.0 ± 20.0	**820.3 ± 287.2**	-64.3	tilted, eroded
LDL-3-A2	1388.7 ± 6.8	15.0 ± 0.5	1403.7 ± 6.8	**1403.7 ± 6.8**	3.5 ± 0.5	**1407.2 ± 6.9**	59.7	
LDL-4A-A2	1379.3 ± 17.2	20.0 ± 0.5	1399.3 ± 17.2	**1399.3 ± 17.2**	3.5 ± 0.5	**1402.8 ± 17.2**	41.3	inner die-down
LDL-4A-A2	1379.3 ± 17.2	25.0 ± 0.5	1404.3 ± 17.2	**1404.3 ± 17.2**	54.0 ± 40.0	**1458.3 ± 43.5**	4.3	final death of head
LDL-4B-A2	1355.7 ± 7.6	14.5 ± 0.5	1370.2 ± 7.6	**1370.2 ± 7.6**	3.0 ± 3.0	**1373.2 ± 8.2**	41.3	inner die-down
LDL-4B-A2	1355.7 ± 7.6	22.5 ± 0.5	1378.2 ± 7.6	**1378.2 ± 7.6**	51.0 ± 40.0	**1429.2 ± 40.7**	4.3	final death of head
LDL-5-A2	1349.6 ± 6.8	23.0 ± 0.5	1372.6 ± 6.8					
LDL-5-B2	1348.5 ± 4.5	53.0 ± 0.5	1401.5 ± 4.5	**1392.9 ± 3.1**	0.5 ± 0.5	**1393.4 ± 3.1**	27.0	
LDL-5-C2	1376.5 ± 5.5	17.0 ± 0.5	1393.5 ± 5.5					
LNG-2-A2	1401.8 ± 5.7	4.0 ± 1.0	1405.8 ± 5.8	**1405.8 ± 5.8**	2.0 ± 2.0	**1407.8 ± 6.1**		elevation uncertain
LKP-2-B2	1333.1 ± 46.0	14.0 ± 1.0	1347.1 ± 46.0	**1347.1 ± 46.0**	0.5 ± 0.5	**1347.6 ± 46.0**	39.2	elevation uncertain
LKP-3-A1	1382.0 ± 7.2	18.0 ± 1.0	1400.0 ± 7.3	**1400.3 ± 7.1**	0.5 ± 0.5	**1400.8 ± 7.1**	38.4	
LKP-3-C2	1395.4 ± 33.0	10.0 ± 1.0	1405.4 ± 33.0					
LKP-4-A2	1413.9 ± 44.2	33.5 ± 0.5	1447.4 ± 44.2					
LKP-4-B1	1392.4 ± 60.6	40.5 ± 0.5	1432.9 ± 60.6	**1443.1 ± 30.7**	0.5 ± 0.5	**1443.6 ± 30.7**	24.2	
LKP-4-C1	1436.3 ± 60.3	9.0 ± 0.5	1445.3 ± 60.3					
LKP-5-A1	1432.1 ± 90.2	13.0 ± 1.0	1445.1 ± 90.2					
LKP-5-B1	1344.0 ± 32.5	35.5 ± 6.0	1379.5 ± 33.0					
LKP-5-C2	1323.9 ± 49.7	49.5 ± 8.0	1373.4 ± 50.4	**1381.1 ± 23.1**	22.5 ± 1.0	**1403.6 ± 23.1**	6.0	tilted & settled ?
LKP-5-D1	1365.3 ± 67.5	13.0 ± 1.0	1378.3 ± 67.5					
LKP-5-F2	1317.6 ± 66.3	51.0 ± 8.0	1368.6 ± 66.7					
LKP-6-A2	1391.8 ± 3.3	3.5 ± 0.5	1395.3 ± 3.3	**1395.3 ± 3.3**	0.0 ± 0.0	**1395.3 ± 3.3**		Goni; for date only
LKP-7-A2	1389.4 ± 3.8	1.0 ± 0.5	1390.4 ± 3.8	**1390.4 ± 3.8**	0.5 ± 0.5	**1390.9 ± 3.8**	35.9	Goni; not good HLS
LKP-8-A1	1355.3 ± 45.0	18.5 ± 2.5	1373.8 ± 45.1	**1373.8 ± 45.1**	2.0 ± 2.0	**1375.8 ± 45.1**	14.5	moved ?
LKP-10-A1	1410.8 ± 38.7	28.0 ± 0.5	1438.8 ± 38.7	**1435.2 ± 20.5**	1.5 ± 0.5	**1436.7 ± 20.5**	10.8	tilted & settled ~20 yrs before ultimate death
LKP-10-B2	1381.2 ± 24.2	52.5 ± 0.5	1433.7 ± 24.2					
LWK-2-A1	1458.8 ± 57.0	6.0 ± 2.0	1464.8 ± 57.0	**1467.3 ± 51.5**	0.5 ± 0.5	**1467.8 ± 51.5**	3.1	
LWK-2-B1	1450.8 ± 120.1	27.5 ± 2.0	1478.3 ± 120.1					
LWK-3-A1	1714.7 ± 246.1	6.5 ± 2.0	1721.2 ± 246.2	**1460.2 ± 45.6**	3.5 ± 0.5	**1463.7 ± 45.6**	13.9	where not tilted
LWK-3-B2	1430.9 ± 46.3	20.0 ± 4.0	1450.9 ± 46.4					
LWK-4-A2	1348.0 ± 26.0	3.5 ± 0.5	1351.5 ± 26.0	**1353.0 ± 10.1**	0.5 ± 0.5	**1353.5 ± 10.1**	5.6	
LWK-4-B1	1328.8 ± 11.0	24.5 ± 0.5	1353.3 ± 11.0					
LWK-5-A1	1448.7 ± 61.1	29.5 ± 2.0	1478.2 ± 61.1	**1477.3 ± 38.4**	8.5 ± 2.0	**1485.8 ± 38.4**	4.2	farily eroded
LWK-5-B1	1435.8 ± 49.2	41.0 ± 4.0	1476.8 ± 49.3					
USG-2-A2	1425.9 ± 23.1	16.0 ± 0.5	1441.9 ± 23.1	**1432.8 ± 15.4**	2.0 ± 2.0	**1434.8 ± 15.5**	-8.6	fairly eroded
USG-2-B2	1386.2 ± 20.5	39.5 ± 2.0	1425.7 ± 20.6					
USG-3-A2	1306.3 ± 31.0	8.0 ± 1.0	1314.3 ± 31.0	**1320.5 ± 28.6**	5.0 ± 5.0	**1325.5 ± 29.0**	-2.3	fairly eroded
USG-3-B1	1330.1 ± 73.3	25.0 ± 3.0	1355.1 ± 73.4					

Weighted Average Dates of Presumed Uplift Events **Table S4**

Pre-Historical Event	Site	Head	Date of Death/Event (AD) Per Head	Site Avg	All-Site Avg
Northern Simeulue – AD 1390s	LDL	LDL-3	1407.2 ± 6.9		
	LDL	LDL-4 †	1378.7 ± 7.4	1393.6 ± 2.7	
	LDL	LDL-5	1393.4 ± 3.1		**1393.9 ± 1.8** *(LDL, LKP)*
	LNG	LNG-2	1407.8 ± 6.1	1407.8 ± 6.1	
	LKP	LKP-3	1400.8 ± 7.1		**1395.0 ± 1.7** *(LDL, LNG, LKP)*
	LKP	LKP-6	1395.3 ± 3.3	1394.2 ± 2.4	
	LKP	LKP-7	1390.9 ± 3.8		
Northern Simeulue – AD 1450-1475	LKP	LKP-4	1443.6 ± 30.7 *	1438.8 ± 17.1	
	LKP	LKP-10	1436.7 ± 20.5		**1449.8 ± 14.2** *(LKP, LWK)*
	LWK	LWK-2	1467.8 ± 51.5		
	LWK	LWK-3	1463.7 ± 45.6	1474.4 ± 25.5	
	LWK	LWK-5	1485.8 ± 38.4		**1443.0 ± 10.5** *(LKP, LWK, USG)*
	USG	USG-2	1434.8 ± 15.5	1434.8 ± 15.5	

† *The 'Per Head' Date of Death for head LDL-4 is the weighted mean of the dates of the inner diedown, as determined on the two slabs from that head (LDL-4A and LDL-4B; see Table S3).*

* *Joint analysis of the dates and morphologies of LKP-3 and LKP-4 suggests that the most appropriate date of death for LKP-4 is 1450 ± 3 (see text).*

Uranium and Thorium isotopic compositions and ^{230}Th ages for modern Sumatran coral samples by ICP-MS **Table S5**

a) Data for modern head LWK-1, assuming an initial ratio of [6.5 ± 6.5 x 10^{-6}] [e]

Sample ID	*Shen et al.* [2008] ID	Weight g	^{238}U ppb	^{232}Th ppt	δ^{234}U measured [a]	[^{230}Th/^{238}U] activity [c]	[^{230}Th/^{232}Th] (x 10^{-6}) [d]	$\delta^{234}U_{initial}$ corrected [b]	^{230}Th Age uncorrected	^{230}Th Age corrected [c,e]	Chemistry Date (AD)	Chemistry Date (AD)	Date (AD) of Sample Growth	[^{230}Th/^{232}Th]$_0$ (x 10^{-6}) [e]
LWK-1-A1	LWK05 6a	1.598	2302 ± 5	6769 ± 49	145.4 ± 2.5	0.00112 ± 0.00007	6.3 ± 0.4	145.4 ± 2.5	106.5 ± 7.1	-4 ± 111	2005/12/14	2006.0	2009.8 ± 110.7	6.5 ± 6.5
LWK-1-B1	LWK05 5a	1.403	2319 ± 5	4671 ± 33	144.0 ± 2.5	0.00084 ± 0.00005	6.8 ± 0.4	144.0 ± 2.5	79.7 ± 4.6	4 ± 76	2005/12/14	2006.0	2001.9 ± 75.9	6.5 ± 6.5
LWK-1-C1 (1)	LWK05 4a#1	1.438	2340 ± 4	2354 ± 8	146.0 ± 2.1	0.00061 ± 0.00003	10.0 ± 0.5	146.0 ± 2.1	58.4 ± 2.7	39.9 ± 3.8	2005/12/14	2006.0	1966.1 ± 3.8	3.01 ± 0.47
LWK-1-C1 (2)	LWK05 4a#2	1.170	2300 ± 5	7005 ± 33	143.4 ± 2.9	0.00101 ± 0.00011	5.5 ± 0.6	143.4 ± 2.9	96 ± 10	*sample age and initial thorium ratio determined by 3-D isochron method*				
LWK-1-C2 (1)	LWK05 4b#1	1.792	2292 ± 5	2685 ± 10	146.8 ± 2.3	0.00063 ± 0.00002	8.8 ± 0.3	146.8 ± 2.3	59.5 ± 2.2					
LWK-1-C2 (2)	LWK05 4b#2	1.063	2292 ± 4	8246 ± 55	145.6 ± 2.1	0.00107 ± 0.00008	4.9 ± 0.4	145.6 ± 2.1	101.6 ± 7.8					
LWK-1-D1	LWK05 3a	1.819	2138 ± 3	577 ± 2	142.9 ± 1.7	0.00032 ± 0.00002	19.8 ± 1.2	142.9 ± 1.7	30.9 ± 1.9	21 ± 10	2005/12/14	2006.0	1985.2 ± 10.3	6.5 ± 6.5
LWK-1-E1&E2	LWK05 2a+2b	2.074	2275 ± 5	497 ± 2	149.3 ± 2.3	0.00009 ± 0.00001	7.1 ± 0.7	149.3 ± 2.3	9.0 ± 0.9	0.8 ± 8.2	2005/12/14	2006.0	2005.1 ± 8.2	6.5 ± 6.5

For a discussion of the ICP-MS method, see *Shen et al.* [2002]. Analytical errors are 2σ of the mean.

[a] $\delta^{234}U = ([^{234}U/^{238}U]_{activity} - 1) \times 1000$.

[b] $\delta^{234}U_{initial}$ corrected was calculated based on ^{230}Th age (T), i.e., $\delta^{234}U_{initial} = \delta^{234}U_{measured} \, X \, e^{\lambda 234 * T}$, and T is corrected age.

[c] $[^{230}Th/^{238}U]_{activity} = 1 - e^{-\lambda 230\,T} + (\delta^{234}U_{measured}/1000)[\lambda_{230}/(\lambda_{230} - \lambda_{234})](1 - e^{-(\lambda 230 - \lambda 234)\,T})$, where T is the age.

Decay constants are 9.1577 x 10^{-6} yr^{-1} for ^{230}Th, 2.8263 x 10^{-6} yr^{-1} for ^{234}U, and 1.55125 x 10^{-10} yr^{-1} for ^{238}U [*Cheng et al.*, 2000].

[d] The degree of detrital ^{230}Th contamination is indicated by the [^{230}Th/^{232}Th] atomic ratio instead of the activity ratio.

[e] Except where isochron techniques were used to determine the ages and initial ^{230}Th/^{232}Th atomic ratios, the initial ^{230}Th/^{232}Th atomic ratio is assumed to be 6.5 ± 6.5 x10^{-6}, as suggested generally by *Zachariasen et al.* [1999].

b) Data for modern head LWK-1, assuming an initial ratio of [3.01 ± 0.47 x 10^{-6}] [e]

Subsample ID	*Shen et al.* [2008] ID	Weight g	^{238}U ppb	^{232}Th ppt	δ^{234}U measured [a]	[^{230}Th/^{238}U] activity [c]	[^{230}Th/^{232}Th] (x 10^{-6}) [d]	$\delta^{234}U_{initial}$ corrected [b]	^{230}Th Age uncorrected	^{230}Th Age corrected [c,e]	Chemistry Date (AD)	Chemistry Date (AD)	Date (AD) of Sample Growth	[^{230}Th/^{232}Th]$_0$ (x 10^{-6}) [e]
LWK-1-A1	LWK05 6a	1.598	2302 ± 5	6769 ± 49	145.4 ± 2.5	0.00112 ± 0.00007	6.3 ± 0.4	145.5 ± 2.5	106.5 ± 7.1	55 ± 11	2005/12/14	2006.0	1950.5 ± 10.7	3.01 ± 0.47
LWK-1-B1	LWK05 5a	1.403	2319 ± 5	4671 ± 33	144.0 ± 2.5	0.00084 ± 0.00005	6.8 ± 0.4	144.0 ± 2.5	79.7 ± 4.6	44.7 ± 7.2	2005/12/14	2006.0	1961.3 ± 7.2	3.01 ± 0.47
LWK-1-C1 (1)	LWK05 4a#1	1.438	2340 ± 4	2354 ± 8	146.0 ± 2.1	0.00061 ± 0.00003	10.0 ± 0.5	146.0 ± 2.1	58.4 ± 2.7	39.9 ± 3.8	2005/12/14	2006.0	1966.1 ± 3.8	3.01 ± 0.47
LWK-1-C1 (2)	LWK05 4a#2	1.170	2300 ± 5	7005 ± 33	143.4 ± 2.9	0.00101 ± 0.00011	5.5 ± 0.6	143.4 ± 2.9	96 ± 10	*sample age and initial thorium ratio determined by 3-D isochron method*				
LWK-1-C2 (1)	LWK05 4b#1	1.792	2292 ± 5	2685 ± 10	146.8 ± 2.3	0.00063 ± 0.00002	8.8 ± 0.3	146.8 ± 2.3	59.5 ± 2.2					
LWK-1-C2 (2)	LWK05 4b#2	1.063	2292 ± 4	8246 ± 55	145.6 ± 2.1	0.00107 ± 0.00008	4.9 ± 0.4	145.6 ± 2.1	101.6 ± 7.8					
LWK-1-D1	LWK05 3a	1.819	2138 ± 3	577 ± 2	142.9 ± 1.7	0.00032 ± 0.00002	19.8 ± 1.2	142.9 ± 1.7	30.9 ± 1.9	26.2 ± 2.0	2005/12/14	2006.0	1979.7 ± 2.0	3.01 ± 0.47
LWK-1-E1&E2	LWK05 2a+2b	2.074	2275 ± 5	497 ± 2	149.3 ± 2.3	0.00009 ± 0.00001	7.1 ± 0.7	149.3 ± 2.3	9.0 ± 0.9	5.2 ± 1.1	2005/12/14	2006.0	2000.7 ± 1.1	3.01 ± 0.47

For a discussion of the ICP-MS method, see *Shen et al.* [2002]. Analytical errors are 2σ of the mean.

[a] $\delta^{234}U = ([^{234}U/^{238}U]_{activity} - 1) \times 1000$.

[b] $\delta^{234}U_{initial}$ corrected was calculated based on ^{230}Th age (T), i.e., $\delta^{234}U_{initial} = \delta^{234}U_{measured} \, X \, e^{\lambda 234 * T}$, and T is corrected age.

[c] $[^{230}Th/^{238}U]_{activity} = 1 - e^{-\lambda 230\,T} + (\delta^{234}U_{measured}/1000)[\lambda_{230}/(\lambda_{230} - \lambda_{234})](1 - e^{-(\lambda 230 - \lambda 234)\,T})$, where T is the age.

Decay constants are 9.1577 x 10^{-6} yr^{-1} for ^{230}Th, 2.8263 x 10^{-6} yr^{-1} for ^{234}U, and 1.55125 x 10^{-10} yr^{-1} for ^{238}U [*Cheng et al.*, 2000].

[d] The degree of detrital ^{230}Th contamination is indicated by the [^{230}Th/^{232}Th] atomic ratio instead of the activity ratio.

[e] Except where isochron techniques were used to determine the ages and initial ^{230}Th/^{232}Th atomic ratios, the initial ^{230}Th/^{232}Th atomic ratio is assumed to be 3.01 ± 0.47 x10^{-6}, as suggested specifically for this head by *Shen et al.* [2008].

References

Banerjee, P., F. Pollitz, B. Nagarajan, and R. Bürgmann (2007), Coseismic slip distributions of the 26 December 2004 Sumatra–Andaman and 28 March 2005 Nias earthquakes from GPS static offsets, *Bull. Seismol. Soc. Am.*, 97, S86-S102, doi:10.1785/0120050609.

Briggs, R. W., K. Sieh, A. J. Meltzner, D. Natawidjaja, J. Galetzka, B. Suwargadi, Y.-j. Hsu, M. Simons, N. Hananto, I. Suprihanto, D. Prayudi, J.-P. Avouac, L. Prawirodirdjo, and Y. Bock (2006), Deformation and slip along the Sunda megathrust in the great 2005 Nias–Simeulue earthquake, *Science*, 311, 1897-1901, doi:10.1126/science.1122602.

Cheng, H., R. L. Edwards, J. Hoff, C. D. Gallup, D. A. Richards, and Y. Asmerom (2000), The half-lives of uranium-234 and thorium-230, *Chem. Geol.*, 169, 17-33, doi:10.1016/S0009-2541(99)00157-6.

Chlieh, M., J.-P. Avouac, V. Hjorleifsdottir, T.-R. A. Song, C. Ji, K. Sieh, A. Sladen, H. Hebert, L. Prawirodirdjo, Y. Bock, and J. Galetzka (2007), Coseismic slip and afterslip of the great M_W 9.15 Sumatra–Andaman earthquake of 2004, *Bull. Seismol. Soc. Am.*, 97, S152-S173, doi:10.1785/0120050631.

Engdahl, E. R., A. Villaseñor, H. R. DeShon, and C. H. Thurber (2007), Teleseismic relocation and assessment of seismicity (1918–2005) in the region of the 2004 M_W 9.0 Sumatra–Andaman and 2005 M_W 8.6 Nias Island great earthquakes, *Bull. Seismol. Soc. Am.*, 97, S43-S61, doi:10.1785/0120050614.

Jaffe, B. E., et al. (2006), Northwest Sumatra and offshore islands field survey after the December 2004 Indian Ocean tsunami, *Earthq. Spectra*, 22, S105-S135, doi:10.1193/1.2207724.

Jevrejeva, S., A. Grinsted, J. C. Moore, and S. Holgate (2006), Nonlinear trends and multiyear cycles in sea level records, *J. Geophys. Res.*, 111, C09012, doi:10.1029/2005JC003229.

Klingelhoefer, F., M.-A. Gutscher, S. Ladage, J.-X. Dessa, D. Graindorge, D. Franke, C. André, H. Permana, T. Yudistira, and A. Chauhan (2010), Limits of the seismogenic zone in the epicentral region of the 26 December 2004 great Sumatra–Andaman earthquake: results from seismic refraction and wide-angle reflection surveys and thermal modeling, *J. Geophys. Res.*, 115, B01304, doi:10.1029/2009JB006569.

Meltzner, A. J., K. Sieh, M. Abrams, D. C. Agnew, K. W. Hudnut, J.-P. Avouac, and D. H. Natawidjaja (2006), Uplift and subsidence associated with the great Aceh–Andaman earthquake of 2004, *J. Geophys. Res.*, 111, B02407, doi:10.1029/2005JB003891.

Plafker, G. (1972), Alaskan earthquake of 1964 and Chilean earthquake of 1960: implications for arc tectonics, *J. Geophys. Res.*, 77, 901-925, doi:10.1029/JB077i005p00901.

Plafker, G., and J. C. Savage (1970), Mechanism of the Chilean earthquakes of May 21 and 22, 1960, *Geol. Soc. Am. Bull.*, 81, 1001-1030, doi:10.1130/0016-7606(1970)81[1001:MOTCEO]2.0.CO;2.

Rhie, J., D. Dreger, R. Bürgmann, and B. Romanowicz (2007), Slip of the 2004 Sumatra–Andaman earthquake from joint inversion of long-period global seismic waveforms and GPS static offsets, *Bull. Seismol. Soc. Am.*, 97, S115-S127, doi:10.1785/0120050620.

Scoffin, T. P., and D. R. Stoddart (1978), The nature and significance of microatolls, *Philos. Trans. R. Soc. London Ser. B*, 284, 99-122, doi:10.1098/rstb.1978.0055.

Shen, C.-C., R. L. Edwards, H. Cheng, J. A. Dorale, R. B. Thomas, S. B. Moran, S. E. Weinstein, and H. N. Edmonds (2002), Uranium and thorium isotopic and concentration measurements by magnetic sector inductively coupled plasma mass spectrometry, *Chem. Geol.*, 185, 165-178, doi:10.1016/S0009-2541(01)00404-1.

Shen, C.-C., K.-S. Li, K. Sieh, D. Natawidjaja, H. Cheng, X. Wang, R. L. Edwards, D. D. Lam, Y.-T. Hsieh, T.-Y. Fan, A. J. Meltzner, F. W. Taylor, T. M. Quinn, H.-W. Chiang, and K. H. Kilbourne (2008), Variation of initial ^{230}Th/^{232}Th and limits of high precision U-Th dating of shallow-water corals, *Geochim. Cosmochim. Acta*, 72, 4201-4223, doi:10.1016/j.gca.2008.06.011.

Singh, S. C., H. Carton, P. Tapponnier, N. D. Hananto, A. P. S. Chauhan, D. Hartoyo, M. Bayly, S. Moeljopranoto, T. Bunting, P. Christie, H. Lubis, and J. Martin (2008), Seismic evidence for broken oceanic crust in the 2004 Sumatra earthquake epicentral region, *Nature Geosci.*, 1, 777-781, doi:10.1038/ngeo336.

Smithers, S. G., and C. D. Woodroffe (2000), Microatolls as sea-level indicators on a mid-ocean atoll, *Mar. Geol.*, 168, 61-78, doi:10.1016/S0025-3227(00)00043-8.

Subarya, C., M. Chlieh, L. Prawirodirdjo, J.-P. Avouac, Y. Bock, K. Sieh, A. J. Meltzner, D. H. Natawidjaja, and R. McCaffrey (2006), Plate-boundary deformation associated with the great Sumatra–Andaman earthquake, *Nature*, 440, 46-51, doi:10.1038/nature04522.

Zachariasen, J., K. Sieh, F. W. Taylor, R. L. Edwards, and W. S. Hantoro (1999), Submergence and uplift associated with the giant 1833 Sumatran subduction earthquake: evidence from coral microatolls, *J. Geophys. Res.*, 104, 895-919, doi:10.1029/1998JB900050.

Chapter 5

Persistent segmentation at the boundary of the 2004 and 2005 Sunda megathrust ruptures

1. Introduction

Simeulue island, off the west coast of northern Sumatra, straddles the boundary of the 2004 (M_W 9.2) and 2005 (M_W 8.6) Sunda megathrust ruptures. The 26 December 2004 earthquake nucleated north of the northern tip of Simeulue island and propagated bilaterally into the 100-km-long island. Three months later, the 28 March 2005 event began southeast of Simeulue and also propagated bilaterally into the island. Both ruptures were arrested under central Simeulue, and only small amounts of slip occurred there: cumulative uplift was 1.5 m at both the northwestern and southeastern tips of the island but diminished toward the island's center, where uplift was 0.5 m or less [*Briggs et al.*, 2006] (Fig. S1). Hence, although the 2004 and 2005 uplifts overlapped, there was an uplift deficit on central Simeulue. Contours of 2004–2005 cumulative uplift on Simeulue resemble a saddle, which led *Briggs et al.* [2006] to refer to central Simeulue as the Simeulue Saddle.

The question arises as to whether the 2004–2005 rupture boundary is a transient or persistent feature. Elsewhere along strike on the Sunda megathrust, studies have documented evidence for both: the Batu Islands patch at the southern end of the 2005 rupture has repeatedly behaved as a barrier to rupture [*Natawidjaja et al.*, 2006; *Sieh*, 2007], whereas along the Mentawai patch farther south, the boundaries of the 2007 sequence appear to be transient features that do not coincide with rupture boundaries during the previous sequence [*Konca et al.*, 2008].

In this study, we present observations and analysis from the Bunon site on southern central Simeulue, above the northern limit of the March 2005 rupture. In conjunction with our results from northern Simeulue sites above the southern end of the 2004 rupture (see previous chapters), our findings provide evidence that the 2004–2005 rupture boundary—the "Simeulue Saddle" of Briggs et al.—has been a persistent barrier to rupture in past megathrust earthquakes.

2. Description of the Bunon (BUN) Site

The Bunon site sits along the southwest coast of Simeulue, ~10 km south of the center of the island, near Bunon village (Fig. S1). As we will discuss, the site was uplifted 60–70 cm in the 2005 earthquake but experienced little vertical change in 2004. Thus, at least for the 2004–2005 sequence, Bunon has acted as part of the southern Simeulue patch and has been independent of northern Simeulue. In addition, Bunon rose 15–20 cm in the M_W 7.2 earthquake of 2 November 2002, which had a locus of deformation centered ~15 km to the west-northwest in central Simeulue.

The Bunon site consists of two subsites: BUN-A is the primary site, and BUN-B is a subsidiary site ~ 1.8 km to the west-northwest. Both subsites have abundant modern heads (i.e., coral heads that were living at the time of the 2004 and 2005 earthquakes), although none of the modern heads had records of relative sea level extending back more than ~25 years. In addition, the BUN-A site has multiple generations of large fossil microatolls (i.e., microatolls that died long before 2004, possibly in prior uplift events) from the 9th–11th and 14th–17th centuries AD. A total of three modern and seven fossil corals were sampled from the BUN sites; all but one modern head originated from site BUN-A (Table S1).

Of the sampled fossil microatolls from Bunon, six are from overlapping generations that combine to provide a continuous history of relative sea level at the site from the early 14th to the early 17th century. This time period encompasses the 14th–15th century continuous record from sites on northern Simeulue (see earlier chapters), allowing us to compare the behavior of the two sections of the megathrust for the duration of the overlap. The seventh fossil head from Bunon provides a discrete, older record that ends in the early 11th century. This, too, overlaps with observations on northern Simeulue, providing another window to examine the simultaneous behavior of the two portions of the fault. The joint analysis of the Bunon and northern Simeulue records reveals strikingly disparate relative sea level histories for the two parts of the island:

during those parts of the record that overlap, all ruptures observed as significant uplifts at one end of the island had little effect at the other end.

The two modern microatolls and the six 14th–17th century fossil heads from BUN-A will be described in detail in this chapter. The older fossil head will be discussed briefly, but a detailed description will be deferred to a subsequent publication. In addition, the modern head from BUN-B confirms certain ambiguous interpretations on the modern heads at BUN-A but does not otherwise add unique information; discussion of this head will also be deferred to a subsequent publication.

3. Changes since 2004 at the Bunon (BUN) Sites

Field observations by K. Sieh in mid-January 2005, observations by R. Briggs of freshly uplifted microatolls in early June 2005, and conversations with local villagers and fishermen in 2005 and 2006 all suggest there was little if any vertical change at Bunon in the 2004 earthquake. Perhaps as much as a decimeter or two of coseismic subsidence in December 2004 might have gone unrecognized, but our own coral microatoll cross-sections (e.g., Figs. S2–S3) preclude uplift in late 2004.

Briggs et al. [2006] reported 47 ± 16 cm (2σ) of uplift in 2005 at their site RDD05-L, which corresponds to our site BUN-B. This value was determined by comparing the pre-uplift HLS on several consistent *Porites* microatolls with ELW, but (as discussed in previous chapters) the calculation did not consider SLAs. Redoing the calculation with the original field measurements, an updated tide model, documented SLAs, the revised correction for the difference between HLS and ELW, and an appropriate inverted barometer correction results in a higher estimate of 60 ± 9 cm. This value represents the net vertical change that occurred between late 2004 and 2 June 2005.

In June 2006, we measured the net uplift at site BUN-A by surveying the water level relative to pre-uplift HLS and tying the water level to ELW. The net uplift as of June 2006 at that more southeasterly site was 68 ± 9 cm. The slightly larger value at BUN-A in June 2006 than at BUN-B in June 2005 was probably mostly or entirely due to the difference in location, although we cannot preclude additional minor postseismic uplift between June 2005 and June 2006; in any case, the two values are statistically indistinguishable.

In July 2007, we re-measured the net uplift at site BUN-A in a similar manner and obtained a result of 78 ± 9 cm. The difference between this value and that measured in 2006 suggests a small amount of uplift (10 ± 13 cm) between June 2006 and July 2007, although we note that this difference is not statistically significant.

In January 2009, nearly a year after the 20 February 2008 M_W 7.3 Simeulue earthquake, we independently re-measured the net uplift (since 2004) at both BUN-A and BUN-B, again by comparing the pre-uplift HLS with ELW at both sites. At BUN-A, we estimated the net uplift to be 75 ± 9 cm, indistinguishable from the July 2007 estimate; this suggests there was little if any change there during the 2008 earthquake. At BUN-B, we estimated the net uplift to be 66 ± 9 cm, consistent with the spatial trend of decreasing uplift to the northwest, and slightly larger than but statistically indistinguishable from the uplift measured there in June 2005.

4. Modern Paleogeodetic Record at BUN-A

At the BUN-A site, the BUN-1 *Porites* microatoll was selected for slabbing because of its nearly perfect radial symmetry and pristine condition, and the BUN-2 *Porites* microatoll was selected because it appeared to have a longer record. As with other heads in this study, we followed the methodology for slab extraction and analysis described in earlier chapters. Figures S2 and S3 show the interpreted x-ray mosaics of slabs BUN-1 and BUN-2, respectively.

BUN-1 began growing in the early 1980s and first recorded an HLS "hit" in late 1997. BUN-2 probably began growing in the 1960s and recorded its first "hit" in late 1982. BUN-2 recorded additional HLS diedowns in late 1986, late 1989, and late 1991. Both heads recorded the late 1997 diedown, as well as subsequent diedowns in late 2002, late 2003, and ultimately early 2005, when the diedown was sufficient that the entirety of both corals died. Except for the diedowns in late 1989, late 2002, and early 2005, all of these are seen repeatedly on northern Simeulue. The 2002 and 2005 diedowns are attributed to tectonic uplifts that were spatially restricted to areas south of northern Simeulue. At both BUN-A and BUN-B, the 2002 diedown was in the range 15–20 cm. The cause of the 1989 diedown on BUN-2 is unclear, but it was very minor, affecting only the uppermost few millimeters of the head.

We can also use the coral microatoll cross-sections to constrain interseismic subsidence rates. A time series of HLG and HLS is plotted on Figures S2 and S3 for BUN-1 and BUN-2, respectively. As outlined in previous chapters, we attempt a linear fit to the data, using the head's HLG in the years prior to each diedown, and omitting data prior to the head's initial diedown. For all sites, we treat post-1997 elevations with caution, because it is not always clear whether heads had grown up to near their theoretical HLS prior to tectonic uplift; for sites in central Simeulue, we explicitly exclude data following the November 2002 earthquake, because we know those elevations are affected by coseismic uplift, and we are interested in the longer-term interseismic signal averaged over the years to decades prior to that uplift.

The linear least squares fit for BUN-2 suggests an average interseismic submergence rate of 5.6 mm/yr over the period 1986–2002 (Fig. S3). Considering only 1986–1995, the average submergence rate is 7.3 mm/yr (not shown). Correcting for eustatic sea level rise as discussed in previous chapters, these correspond to tectonic subsidence rates of 3.6 and 5.3 mm/yr, respectively, for 1986–2002 and 1986–1995. It is noteworthy that these rates are lower than at Lhok Dalam and Ujung Salang (see sites LDL-A and USL-A, Chapter 3, figure 19), sites approximately equidistant from the trench along the southwest coast of northern Simeulue. Unfortunately, the limitations on this method preclude a fit to the data from BUN-1, which has only a single usable datum prior to the 2002 uplift.

5. Fossil Paleogeodetic Record at BUN-A

Not including the oldest sampled microatoll at the site (BUN-9) and several severely eroded microatolls that may be even older, most of the fossil microatolls at BUN-A can be divided into two populations based on their morphologies. One sizable population consists of large cowboy hat or sombrero-shaped microatolls (e.g., Figs. S4–S7). The centers of these heads are either hemispheres or cup-shaped microatolls in their own right, with upper surfaces rising toward the outer rims of the inner heads. As these heads grew, their HLS suddenly dropped to lower levels: the inner heads are surrounded by much lower brims, which themselves rise very gradually (with gradients lower than on the inner parts of these heads) toward their outer perimeters. For clarity, we will refer to the initial large diedown as the inner diedown, and the final death of these sombrero-shaped heads as the outer diedown. The second population of fossil microatolls at BUN-A has more conventional cup-shaped morphologies, except for an exceptionally pronounced upward step in their outward growth (e.g., Figs. S8–S9), suggesting a burst of rapid interseismic subsidence or sea level rise amidst a longer period of steady, slower relative sea level rise.

5.1. 14th–15th century record at BUN-A

5.1.1. Sampled heads

In the field, we decided to take slabs from three of the sombrero-shaped microatolls. We chose to sample BUN-7 (Fig. S4) because it had a beautifully preserved inner head with stairstepping concentric rings that record a century of steady relative sea level rise. The uppermost part of the crown of this inner head had sustained significant erosion, and in places it appeared as though parts of the upper crown had been chiseled off prior to our visit, but this head was still in better condition than most in the population. The main problem with BUN-7 was that its outer brim had broken off and settled relative to the inner head. It was not clear in the field how the broken-off outer brim fit back onto the inner part of the head, and we feared it would have been impossible to confidently reconstruct the elevation of points on the outer brim.

Fortunately, the outer brim of a nearby head with a similar morphology had remained intact. The inner part of this nearby head (BUN-8) and its uppermost crown were much more extensively eroded than the corresponding portions of BUN-7, but the similarity of the two heads suggested that the outer brim of head BUN-8 could serve as a proxy for the broken-off outer brim of BUN-7. The slab of BUN-7 is an entire radius through the inner head of microatoll BUN-7 (including what remains of its uppermost crown), and the slab of BUN-8 (Fig. S5) is a radius through the outer edge of its uppermost crown and the low brim outboard of its upper crown. Even prior to confirmation by U-Th dating analyses, we anticipated that these two slabs could be combined to form a single continuous record of relative sea level.

The third sombrero microatoll (BUN-6; Fig. S6) had a hemispherical center and was much more eroded than BUN-7 or BUN-8, but its outer brim was considerably wider (and taller) than those of BUN-7, BUN-8, and most other heads in the population. The taller nature of the BUN-6 outer brim is consistent with a deeper substrate in that vicinity, and it could have allowed BUN-6 to survive a small diedown that completely killed shallower heads, including BUN-7 and BUN-8. This interpretation implied to us in the field that BUN-6 contains a part of the sea level record beyond that recorded by BUN-7 or BUN-8.

A fourth head, BUN-5 (Fig. S7), also belongs to the sombrero generation, although this association was not evident until revealed by U-Th dating analyses. BUN-5, which was mostly buried in the pre-2005 beach berm until we dug it out, captures the last few decades of growth of the inner, higher parts of the sombrero heads, just prior to the inner diedown. BUN-5 started growing decades (to nearly a century) after the more recognizable sombrero-shaped microatolls in the population, so its record is much more brief; furthermore, it was not tall enough to survive the inner diedown, so BUN-5 has no outer brim. BUN-5 is very well preserved, however, and its record spans the time period of the eroded crowns of BUN-7, BUN-8, and the other sombrero heads; BUN-5 thus adds critical data to that portion of the HLS record.

5.1.2. Dating results and preferred interpretation

One sample from BUN-5, two from BUN-6, three from BUN-7, and two from BUN-8 were dated by U-Th analysis (Tables S2–S3). Most of the dates agree and indicate these four heads span the 14th–15th centuries AD. The weighted-mean dates for the inner diedown (assuming it was a single diedown; see also Section 5.1.4) on the sombrero heads are late 1437 ± 23, early 1425 ± 11, and late 1434 ± 13, from BUN-5, BUN-7, and BUN-8, respectively (Table S4), which combine to yield an overall weighted average of AD 1430.4 ± 7.9. This date is indistinguishable from and may be correlative with the AD 1430 ± 3 minor diedown seen on northern Simeulue; we adopt AD 1430 as our preferred timing of the sombrero heads' inner diedown (again assuming it was a single diedown). Counting outward from the inferred 1430 diedown on BUN-8, the date of that head's outer preserved band is AD 1474.

Interpretation of the two dates from BUN-6 is less straightforward. The two dates are mutually exclusive, as they are only compatible when the error of each is simultaneously considered at 4σ (Table S3; Fig. S6). Indeed, the morphology of BUN-6 is incompatible with any of the other sombrero heads at the site if the date from BUN-6-A1 is valid. If the date obtained on BUN-6-A1 is thrown out and we instead rely on only BUN-6-B1, the apparent age of head BUN-6 makes much more sense: in that case, the inner diedown on BUN-6 would date to within a few years of AD 1430 (the date estimated from BUN-5, BUN-7, and BUN-8), well within the stated 2σ uncertainty of ±21 years on BUN-6-B1. Using the preferred date of AD 1430 for the inner diedown on BUN-6 and counting outward, we estimate the date of the outer preserved band on BUN-6 to be AD 1511.

As we had interpreted in the field, BUN-6 appears to contain a part of the sea level record beyond that recorded by BUN-7 or BUN-8. Possible explanations for this are (*a*) that the thin outer brims of BUN-7 and BUN-8 were killed entirely by a very small diedown shortly after AD 1474, but the taller nature of the BUN-6 outer brim, and the deeper substrate nearby, allowed BUN-6 to continue growing after this small diedown; or (*b*) that BUN-7 and BUN-8 originally had much wider brims, but the outermost parts of those brims subsequently broke off and were transported away. Unfortunately, because of extensive erosion of BUN-6, that head is not useful for distinguishing among these possible explanations. Indeed, we cannot preclude the possibility that BUN-6 is also missing many outer bands: as wide as the preserved outer brim is on BUN-6, it may have originally been much wider. The apparent outer diedown on BUN-6 might not signal an event at that time, especially given the lack of corroborating heads with morphologically similar outer perimeters.

Time series of relative sea level determined from the 14th–15th century microatolls are plotted individually on Figures S4–S7 and together on Figure S10a. From Figure S10a, it is evident how BUN-5 fills in the part of the BUN-7 record lost by erosion of its upper crown. Although BUN-7 provides an excellent record of relative sea level from AD 1311 to 1411, BUN-5 provides the best record from 1412 until shortly before the 1430 uplift.

5.1.3. ~1430 uplift (preferred interpretation)

To quantify the 1430 uplift (assuming it was a single event; see also Section 5.1.4), we measure down from the HLG on BUN-5 in the years before 1430 to the post-diedown HLS in 1430 on BUN-8. We estimate that uplift to be 82–86 cm (Fig. S10a). After the 1430 diedown, BUN-8 experienced unrestricted upward growth of at least 11 cm in ~11 years, suggesting the coseismic uplift was followed by a decimeter of postseismic subsidence.

5.1.4. Dating results and ~1430 uplift (alternative interpretation)

Although the observations at site BUN-A are for the most part consistent with the interpretation presented in Sections 5.1.2 and 5.1.3, the morphology of BUN-8 suggests an alternative interpretation: that there were two diedowns less than 10 years apart around 1430. The simpler interpretation—that there was a single diedown around that time—requires that 10 bands have been completely eroded from the upper part of BUN-8, as shown on Figure S5a. While such erosion is possible, it would be a little surprising, given the comparatively good preservation of the head's outer brim. Moreover, the upper part of the head appeared in the field to be radially symmetric, requiring any inward erosion to have been uniform from all directions and hence suggesting (by Occam's razor) that the total inward erosion was not substantial. These concerns lead us to consider an alternative (dual diedown) hypothesis.

In this alternative scenario, the majority of the diedown on BUN-8 would have occurred about 7–9 years prior to the band labeled "1430" on Figure S5a; following this first diedown, HLS would have been about 10–15 cm higher than after the second diedown (labeled "1430"). In this scenario, although the second diedown is the more obvious of the two on the slab, it would have been the smaller one. The slabs from BUN-7, BUN-5, and BUN-6 are not inconsistent with dual diedowns around 1430, but in that case BUN-7 and BUN-5 record only the first, and BUN-6 is sufficiently eroded that the two diedowns are indistinguishable.

In the alternative interpretation, the weighted-mean ages are calculated differently. The dates for the first (and larger) of the successive inner diedowns are still late 1437 ± 23 and early 1425 ± 11 from BUN-5 and BUN-7 (Table S4), but the appropriate date from BUN-8 is ~8 years earlier, or late 1426 ± 13; these combine to yield an overall weighted average of AD 1427.2 ± 8.0. The second (smaller) diedown would have occurred 8 ± 2 years later.

While this alternative hypothesis proposes two diedowns in rapid succession and the first diedown is so large that it must reflect uplift, the second diedown is not necessarily tectonic. If the alternative hypothesis is taken to be true, we still consider it equally plausible for (*a*) the first diedown to have been followed by a second uplift of 10–15 cm and then ~11 cm of postseismic subsidence, or (*b*) the first tectonic diedown to have been followed by a non-tectonic diedown similar to the 1997–98 IOD event. If two uplifts occurred around 1430, the uplift calculated in Section 5.1.3 (82–86 cm) represents the cumulative uplift in those events. From the morphology of BUN-8, we estimate the uplift in the first event to be roughly 70–75 cm, with 10–15 cm of uplift in the second. If in this scenario only the first diedown was tectonic, then only 70–75 cm of uplift occurred.

5.1.5. Maximum uplift at Bunon in 1394 and 1450

Two large uplift events on northern Simeulue dated to AD 1394 ± 2 and 1450 ± 3 do not show up as significant events at Bunon. A small diedown is seen on BUN-7 some time around 1394, but even if it corresponds to the northern Simeulue uplift, that diedown on BUN-7 was not more than ~4 cm. No diedown is evident around 1450 on BUN-8, although evidence for a small diedown (a few centimeters or less) could have been eroded away. Even if the alternative hypothesis discussed in Section 5.1.4 is correct, no large diedowns (of more than a few centimeters) appear on BUN-5, BUN-7, or BUN-8 that could date to around AD 1394 or 1450.

5.1.6. Interseismic submergence

We estimate the average interseismic submergence rate for AD 1311–1430 from BUN-7 and BUN-5 to be 5.5 mm/yr, although a closer examination of BUN-7 reveals the rate was faster than that average prior to 1319, slowed to ~2.2 mm/yr between 1319 and 1348, was interrupted by rapid submergence for an unknown duration at some time between 1348 and 1360, and ultimately settled to ~6.6 mm/yr from 1361 possibly until 1430 (Fig. S10a). We estimate the rate for 1441–1474 to be a much lower 0.3 mm/yr, based on BUN-8. Based on the limited evidence discussed in earlier chapters, we assume that eustatic sea level change was negligible in the millennium preceding the 20th century AD, which would imply that tectonic subsidence rates prior to the 20th century roughly equal the submergence rates determined from our fossil microatolls.

5.1.7. Settling of BUN-6

It is evident from Figure S10a that head BUN-6 has settled relative to coeval heads at the site, by as much as 10 cm. This is not surprising, as BUN-6 is farther out on the reef than any of the coeval heads (Fig. S1), and observations at other sites have suggested that the outer parts of the reef tend to be more susceptible to settling and slumping. If any of the settling of BUN-6 occurred during the recent earthquakes, it would imply that the modern heads at the site—all of which are located nearby (Fig. S1)—may have settled by several centimeters as well.

5.2. 16th–17th century record at BUN-A

5.2.1. Sampled heads

We collected two slabs from the population of cup-shaped fossil microatolls with a pronounced upward step. BUN-3 (Fig. S8) was the most well preserved of a cluster of similar tilted heads growing ~200 m northeast of the other slabbed heads at the site. BUN-4 (Fig. S9) grew apart from the main BUN-3 population and was mostly buried in the pre-2005 beach berm (along with BUN-5) when we found it. The morphology of BUN-4 was similar but not identical to that of BUN-3, so it was not obvious in the field that they belonged to the same generation.

5.2.2. Dating results and preferred interpretation

One sample was dated from each head (Tables S2–S3). The dates are close enough, and the records on each head are long enough and similar enough, that they must overlap. Indeed, starting with the diedown labeled "1511" on both BUN-3 and BUN-4 (Figs. S8–S9), both heads experienced additional diedowns 23, 26, 33, 43, and ~55 years later—and both heads experienced faster-than-average upward growth beginning ~26 years later—strongly suggesting those portions of the two heads are coeval. If that is the case, however, BUN-4 must be missing 36.5 outer bands that are preserved on BUN-3. That so many bands are missing from BUN-4 is surprising, considering that the head appears to be in good condition with minimal erosion, but we find the similarities in BUN-3 and BUN-4 to be compelling evidence that is difficult to refute.

Assuming BUN-3 is missing 2.0 ± 2.0 bands and BUN-4 is missing exactly 36.5 bands more (38.5 ± 2.0), the U-Th analyses for these heads yield dates of death of mid-1570 ± 42 and mid-1613 ± 38 for BUN-3 and BUN-4, respectively (Table S3); the weighted average of these two dates is early 1594 ± 28 (Table S4). If we were to use this date as the actual date of the event that killed BUN-3 and BUN-4, then the earliest diedown recorded on BUN-3, 106 years prior to its outer preserved edge, would have occurred in 1486 ± 28.

BUN-6 also bears on this matter. Comparing the records of BUN-3 and BUN-4 to that of BUN-6, with the assumption that BUN-6 is dated correctly, suggests that the earliest possible date of the initial diedown on BUN-3 is AD 1500. We assume 1500 as our preferred date for that initial diedown, which corresponds to a preferred date of 1605 for the outer preserved band on BUN-3. The estimated date of the diedown that killed BUN-3 and BUN-4 would then be AD 1607, but the true date of that final diedown could be later, if either (*a*) the date of the initial diedown is later than assumed, or (*b*) we are underestimating the number of missing bands.

5.2.3. Dating results: alternative interpretation

Unfortunately, the considerable erosion of BUN-6 and the problematic dates from that head make interpretation of its history challenging. If we discard all information from BUN-6 based on the contention that this information is less reliable, then the dates from BUN-3 and BUN-4 alone suggest those heads may be slightly older than indicated on Figure S10.

5.2.4. BUN-3: original elevation

BUN-3, and all the other heads within tens of meters, were clearly tilted and had settled relative to one another. By carefully surveying the most well preserved concentric ring of BUN-3, we were able to restore the head's original horizontality, but its original elevation was still unknown. Assuming BUN-4 was in place and that the HLS following each diedown was the same on the two heads (to within a small error), we determined the original elevation of BUN-3 by comparing the 1511, 1537, 1544, and 1554 post-diedown HLS on the two heads. The calculated original elevation of BUN-3 is reflected in the time series plots in Figures S8 and S10.

5.2.5. Interseismic submergence

The long-term (AD 1509–1604) average submergence (and subsidence) rate recorded by BUN-3 is 6.0 mm/yr. As suggested by the morphology of the head, however, this rate does not appear to be constant over time. The average rate was 5.8 mm/yr from 1509 to 1544, increased to 11.7 mm/yr from 1544 to at least 1555, was below the long-term average (but is poorly resolved) until ~ 1573, and then returned to 5.6 mm/yr from 1573 until at least 1604. Similarly, BUN-4 records an average rate of 5.9 mm/yr from 1508 to 1544, followed by an average rate of 10.1 mm/yr from 1544 until at least 1566. The faster submergence rate beginning around or just prior to 1544 probably reflects a period of faster interseismic subsidence, but we should not preclude an extended period (2-3 decades) of persistently higher-than-average sea levels, as the early and late parts of the HLS record on BUN-3 can essentially be fit by a single straight line. The cause of the exceptionally pronounced upward step in the morphology of the BUN-3 and BUN-4 microatolls was clearly not a sudden (effectively instantaneous) subsidence "event"; during the decades of rapid upward growth, both BUN-3 and BUN-4 repeatedly experienced HLS "hits," an indication that the corals' HLG was close to their theoretical HLS for most, if not all, of that time.

5.3. 9th–11th century record at BUN-A

In addition to the abundant fossil microatolls at the BUN-A site belonging to the 14th–17th century populations described above, a solitary 7-m diameter pancake-shaped microatoll was observed at the site (BUN-9; Figs. S1, S11). Four discontinuous slabs were cut from this head: BUN-9A through the outer edge, BUN-9B through the outer ring, BUN-9C through the second ring, and BUN-9D in the center. The number of bands between each slab can be estimated only based on the average thickness of bands in this head and the spacing between the slabs. Nonetheless, U-Th analyses provide a precise estimate for the age of the head's outer preserved band: AD 1017 ± 14 (Table S3). Incidentally, this is ~60 years after the estimated AD 956 ± 16 date for the death of a fossil coral microatoll at the Ujung Salang site of northern Simeulue. Although this head has yet to be fully analyzed, it experienced <20 cm of net upward growth over an estimated ~140 years, suggesting an average submergence rate of <1.4 mm/yr, and more importantly yielded no evidence for any large uplift or subsidence events in the century prior to its outer preserved band. Thus, although information regarding the 10th-century tectonic histories of northern and southern Simeulue is still sketchy, the evidence collectively hints at yet another northern Simeulue uplift that is not seen at the Bunon site.

6. Summary and Implications of Paleogeodetic Observations at Bunon

We have obtained three discrete continuous histories of relative sea level at the BUN-A site, spanning the mid-9th to early 11th centuries AD, the early 14th to early 17th centuries, and AD 1982 to present. A summary of observations and potential inferences of relative sea level at Bunon since AD 1300 is presented in Figure S10b.

The mid-9th to early 11th century record is one of remarkably steady relative sea level, with any tectonic change in land level offset by a similar change in absolute sea level; presumably both were small or zero. The inferred death of BUN-9 around AD 1022 suggests a modest uplift event at around that time.

The record picks up again three centuries later around AD 1311 as the site was rapidly accumulating strain, with an average subsidence rate of 5.5 mm/yr. This subsidence continued until the site rose suddenly around AD 1430, with 70–86 cm of coseismic uplift, possibly followed by postseismic subsidence of ~10 cm. Then, from ~1441 to ~1474, there was little vertical change. By AD 1509, the site was subsiding again at ~6 mm/yr, and that subsidence continued until the early 17th century. Significant and robust variability in the rates, at scales of 15–70 years, are superimposed on the century-scale averages. Another uplift event is inferred in the early part of the 17th century.

Finally, the modern record reveals an interseismic subsidence rate of 5.3 mm/yr from 1986 to 1995, followed by 15–20 cm of coseismic uplift in 2002 and 60–70 cm of coseismic uplift in 2005, with little vertical change in 2004. We infer from observations elsewhere on southern Simeulue [*Meltzner et al.*, 2009] that Bunon was uplifted during the 1861 southern Simeulue–Nias earthquake, but no evidence was documented at Bunon to either confirm or refute such a proposition.

The records from the BUN-A site provide robust positive evidence that none of the major uplifts known or inferred on northern Simeulue in the past 1100 years involved significant uplift or subsidence at Bunon. Specifically, significant land-level changes did not occur at Bunon in AD 956 ± 16, AD 1394 ± 2, AD 1450 ± 3, or AD 2004. In addition, the largest uplifts at Bunon in the modern or paleogeodetic record—the 70–86-cm uplift around AD 1430 and the 60–70-cm uplift in 2005—had little or no effect on northern Simeulue. Around 1430, there was ~12 cm of uplift at Lhok Pauh on northern Simeulue (Fig. S12); even if this and the similarly dated uplift at Bunon correspond to the same event, the uplift at Lhok Pauh is small compared to the 100 cm of uplift there in 2004 and could be consistent with a megathrust rupture petering out to the north.

Alternatively, it is entirely possible that the 12-cm uplift at Lhok Pauh in 1430 ± 3 did not coincide with the 70–86 cm of uplift at Bunon—those two uplifts could have been separated by months, as in 2004 and 2005, or even a few years—and if that were the case, the argument would be even stronger for strict segmentation of the megathrust between Bunon and northern Simeulue. Regardless of the details of the ~1430 event or events, central Simeulue—somewhere between Bunon and Lhok Pauh—has behaved as a persistent barrier to rupture over at least the past 1100 years.

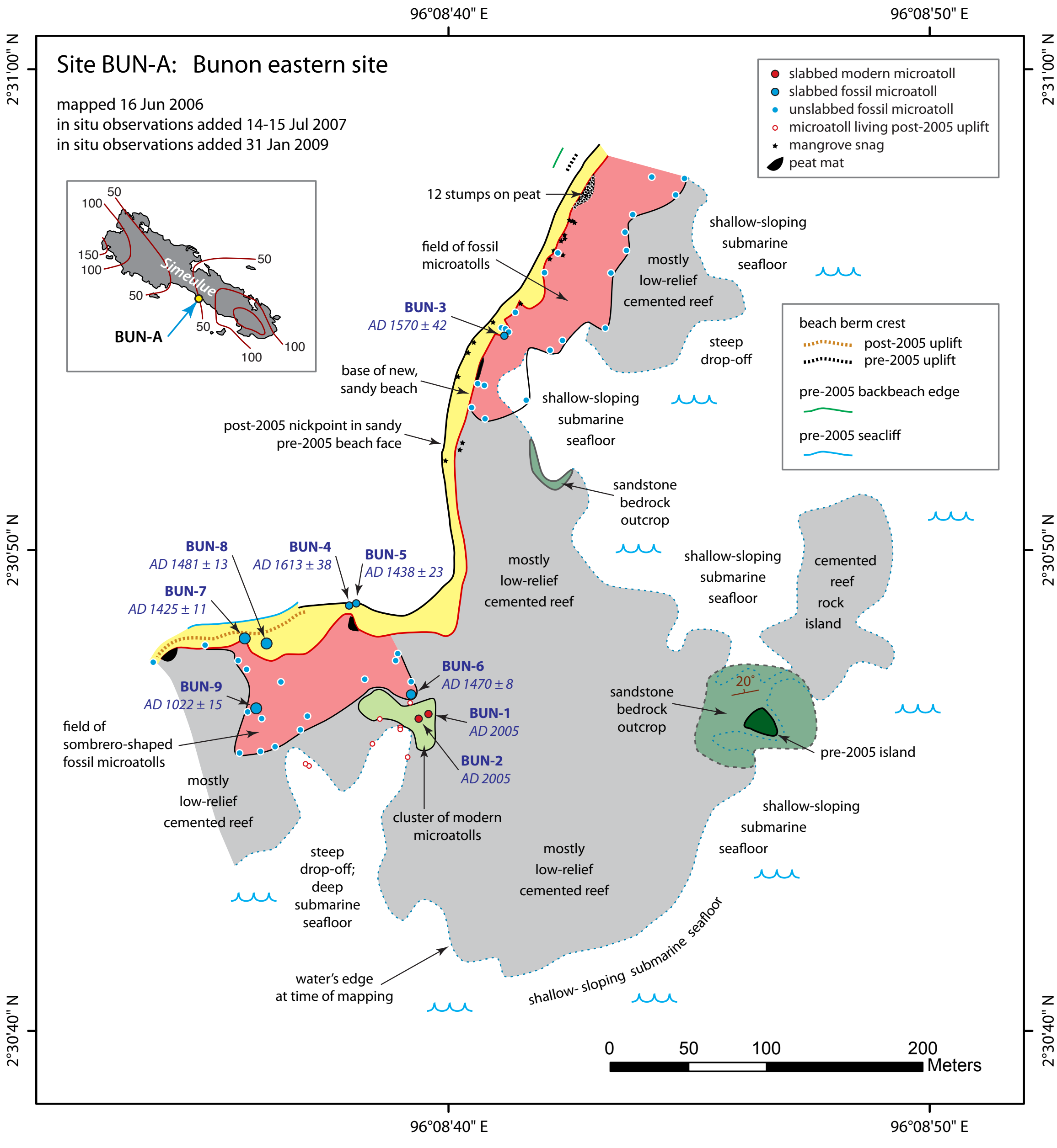

Figure S1. Map of site BUN-A, southwest coast of Simeulue, showing sampled microatolls and their dates of death. Inset shows the relative location of the BUN-A site on Simeulue, along with contours of cumulative uplift (in centimeters) in 2004 and 2005, modified from *Briggs et al.* [2006]. The locus of uplift on the northwestern part of the island is attributed to the 2004 earthquake, while the southeastern locus of uplift occurred in 2005.

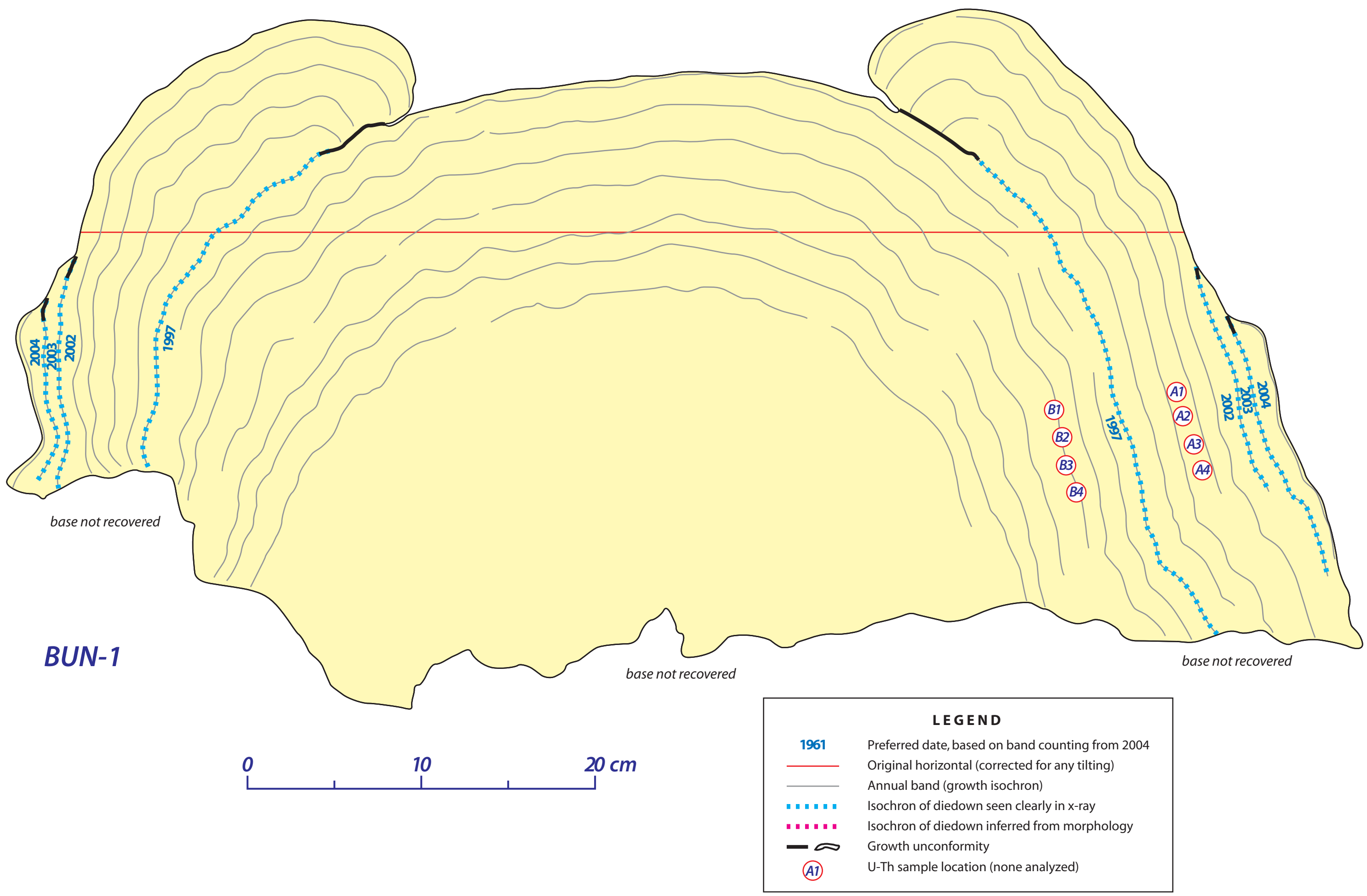

Figure S2a. Cross-section of slab BUN-1, from site BUN-A.

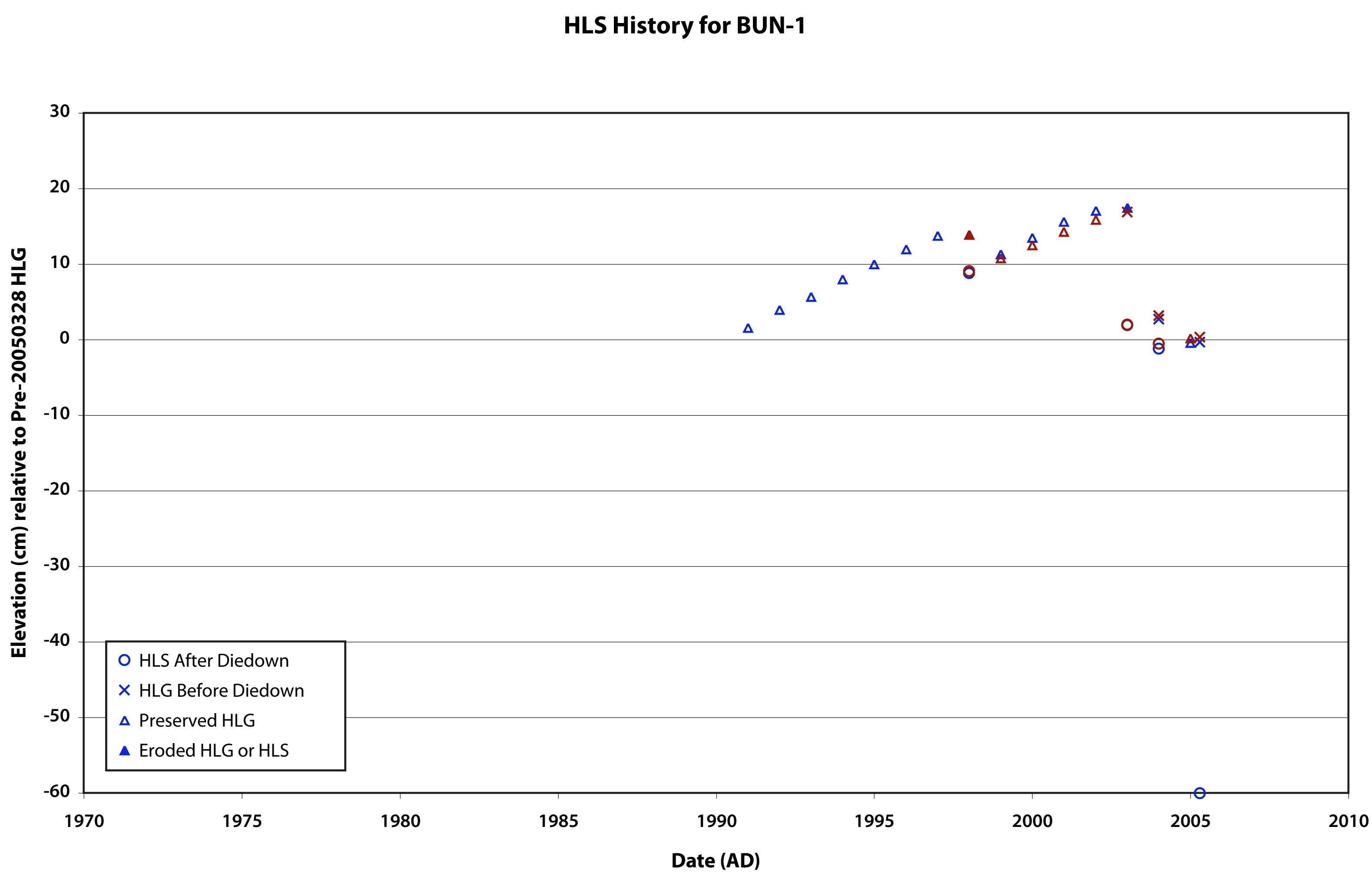

Figure S2b. Graph of relative sea level history derived from slab BUN-1.

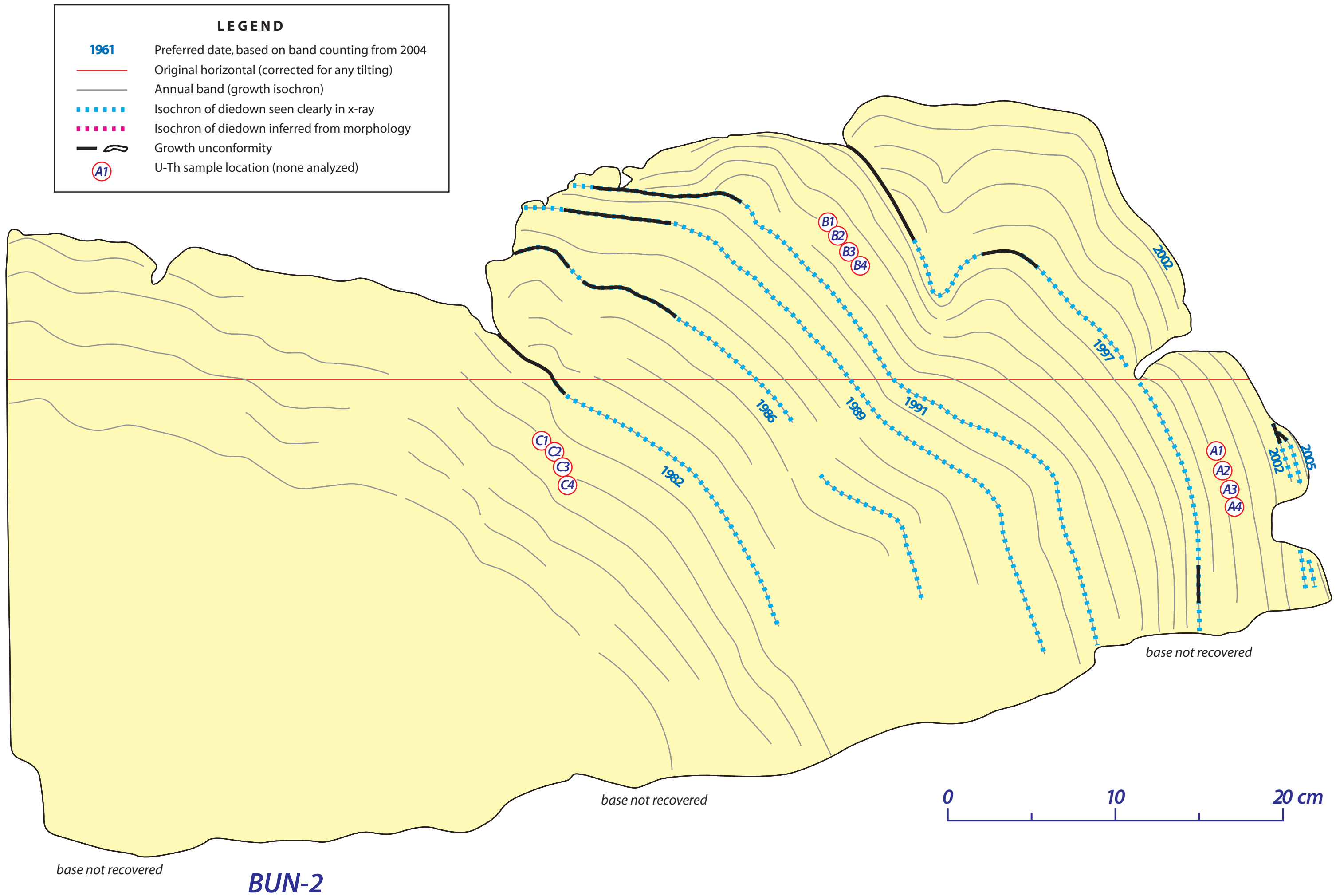

Figure S3a. Cross-section of slab BUN-2, from site BUN-A.

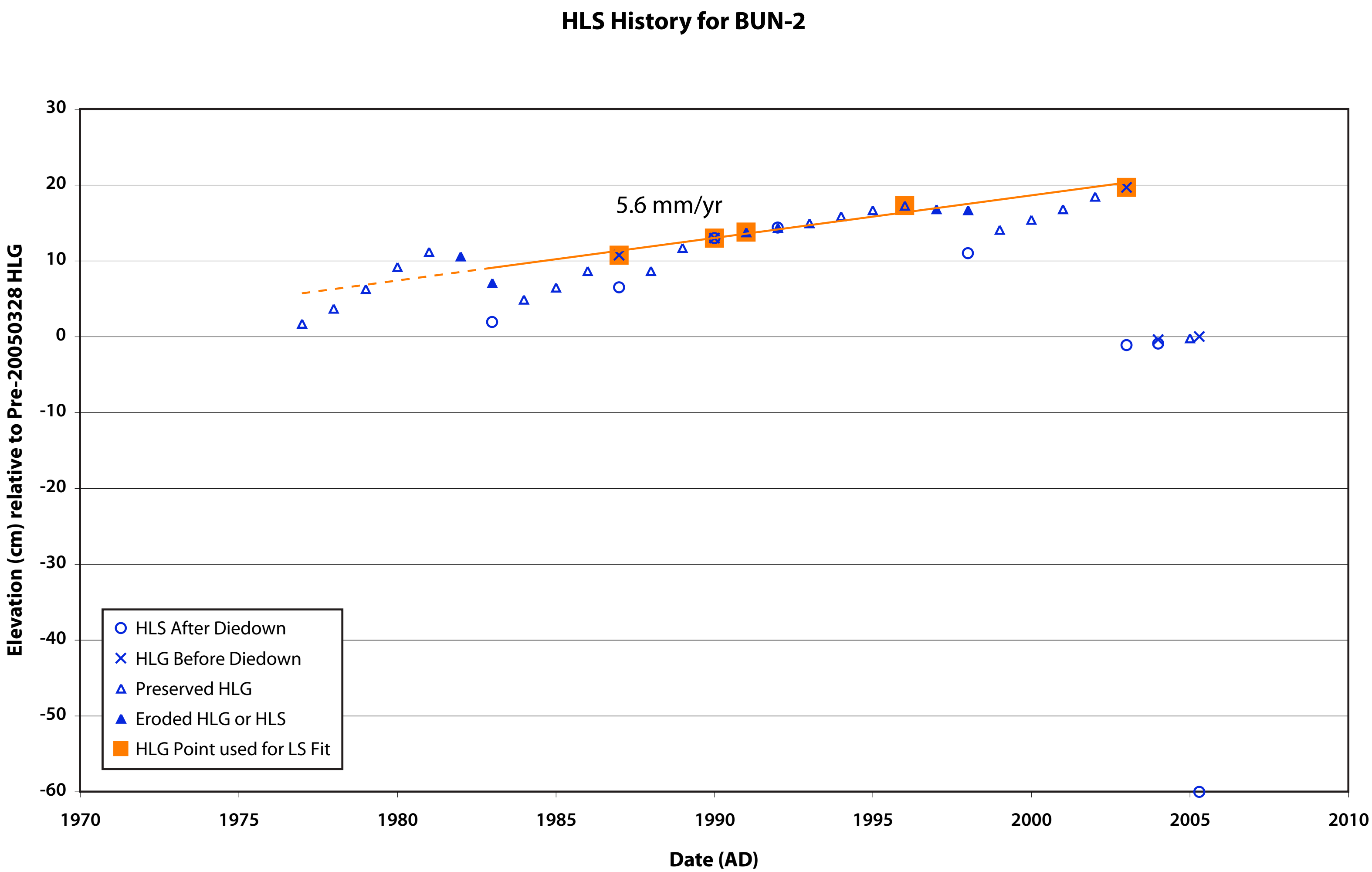

Figure S3b. Graph of relative sea level history derived from slab BUN-2.

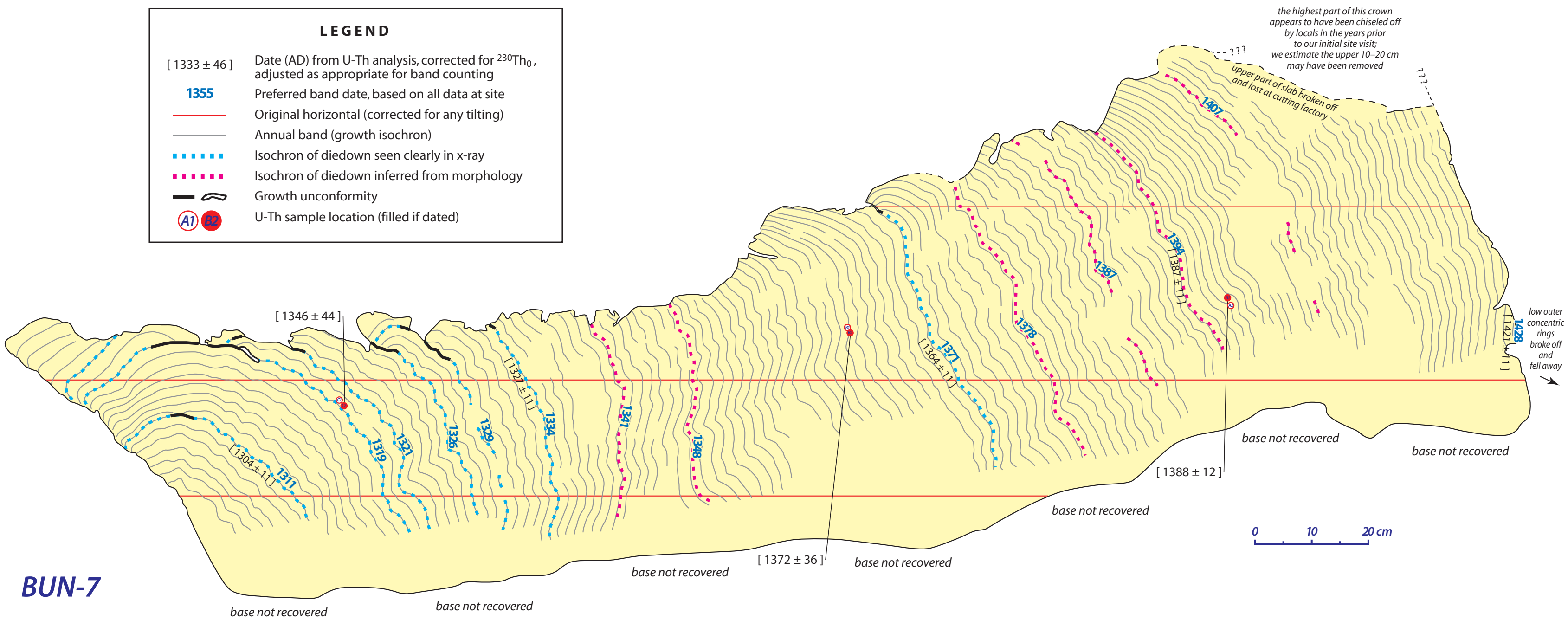

Figure S4a. Cross-section of slab BUN-7, from site BUN-A.

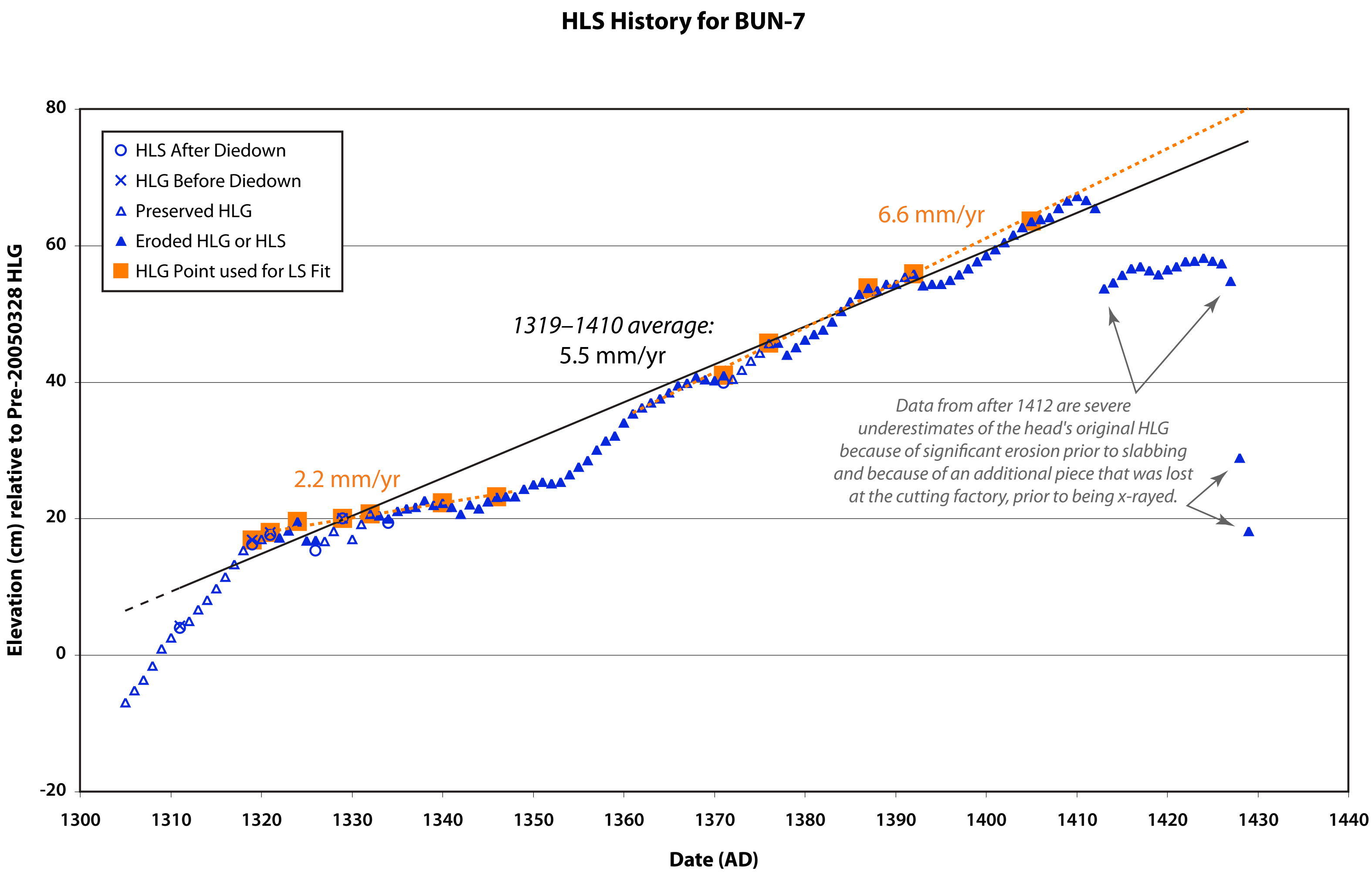

Figure S4b. Graph of relative sea level history derived from slab BUN-7.

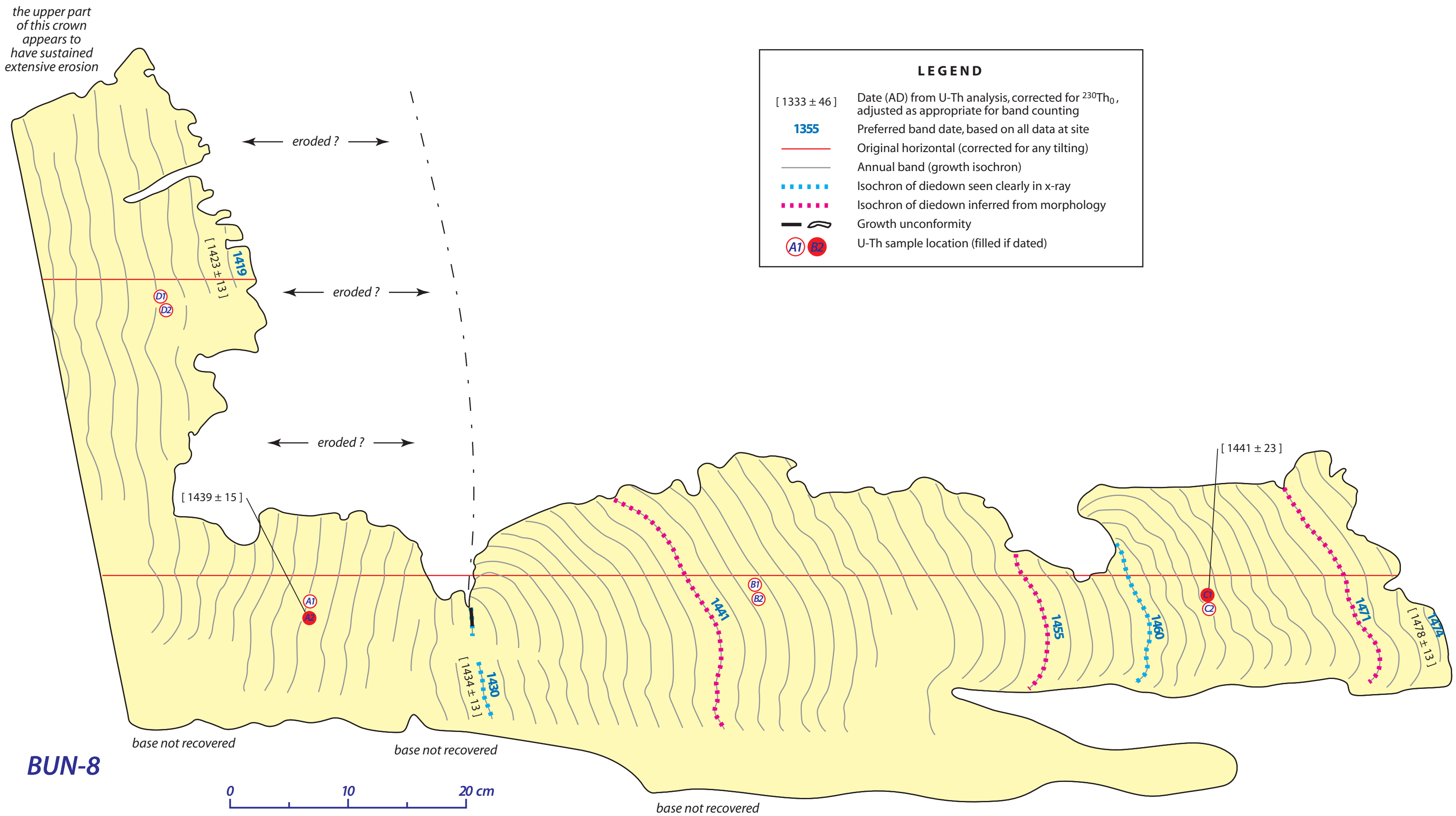

Figure S5a. Cross-section of slab BUN-8, from site BUN-A.

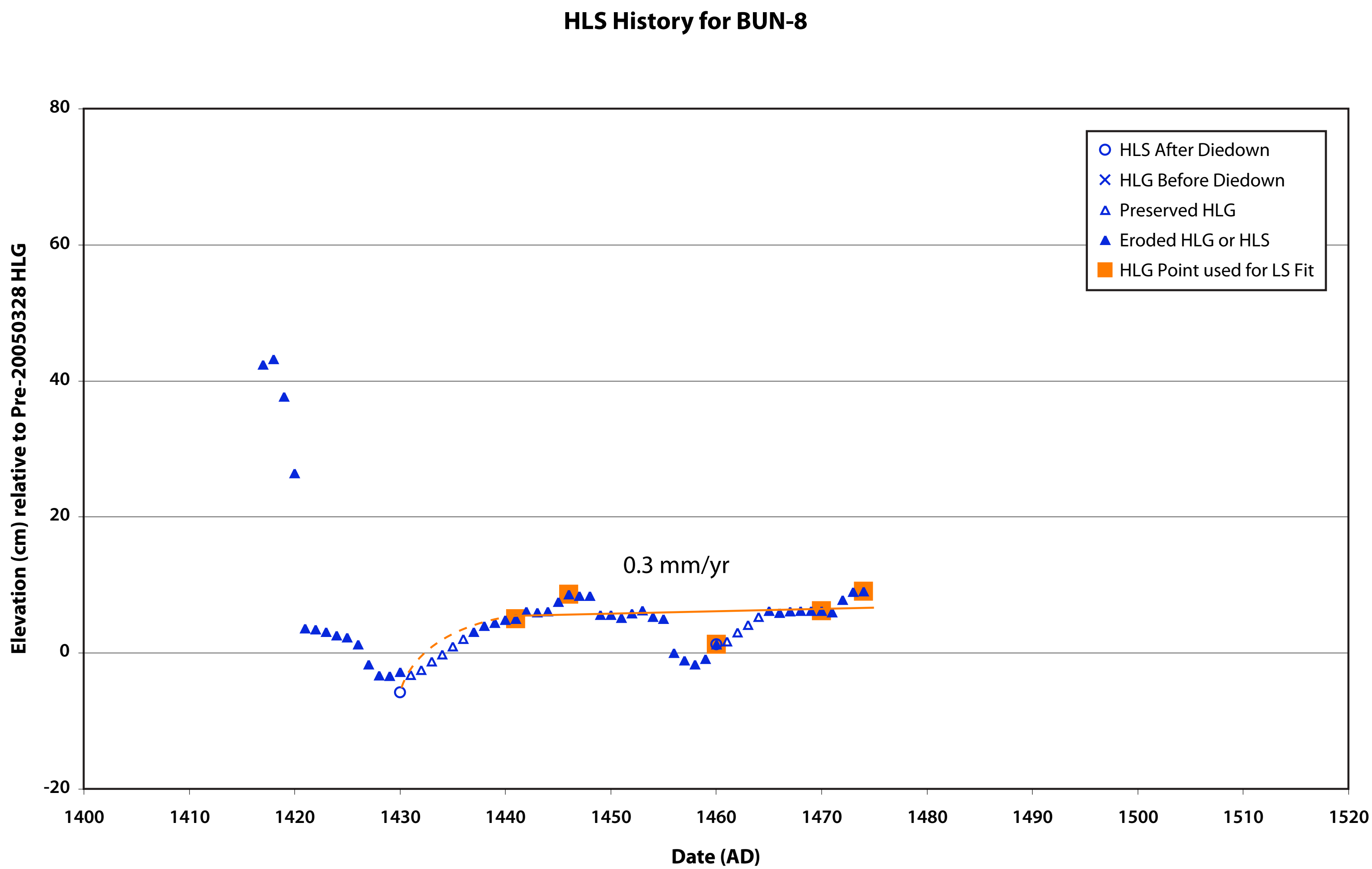

Figure S5b. Graph of relative sea level history derived from slab BUN-8.

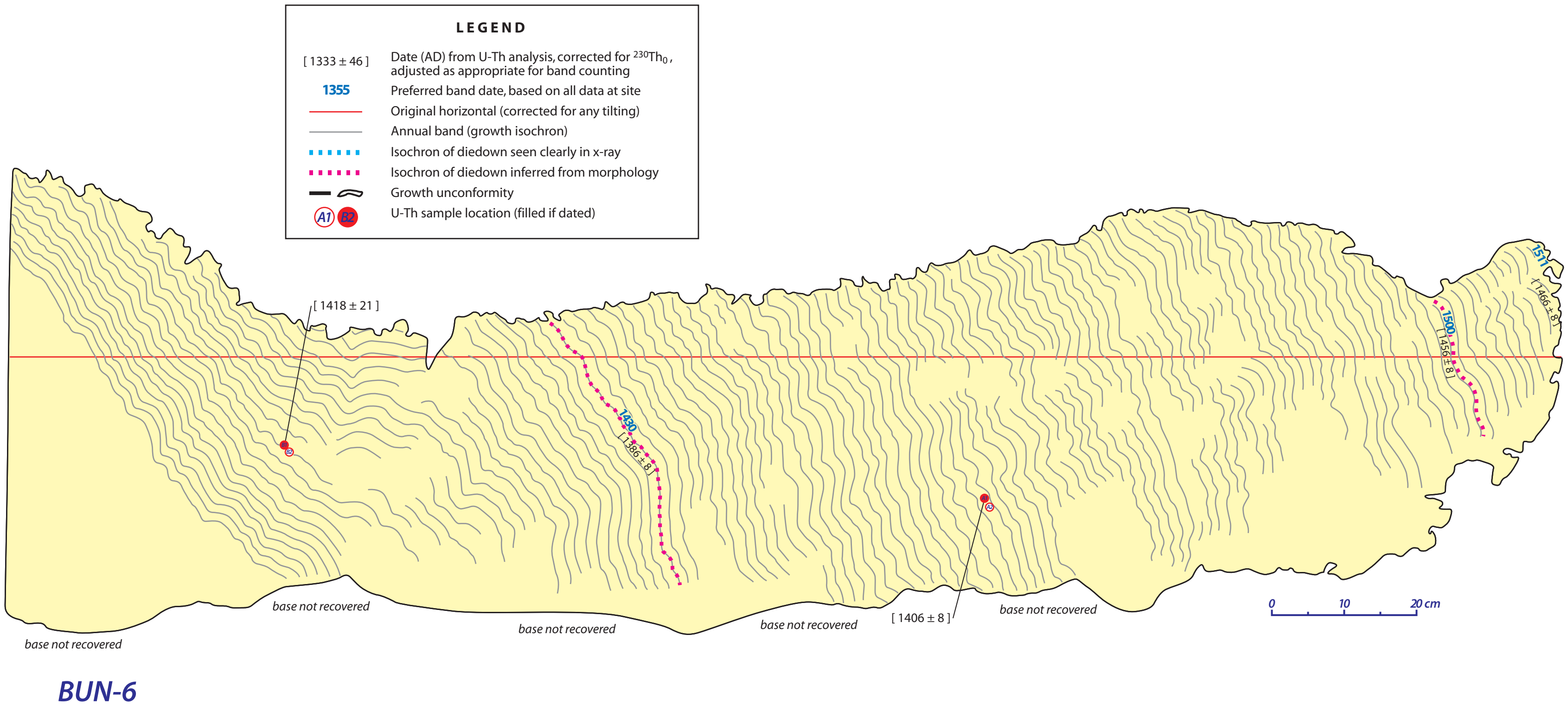

Figure S6a. Cross-section of slab BUN-6, from site BUN-A.

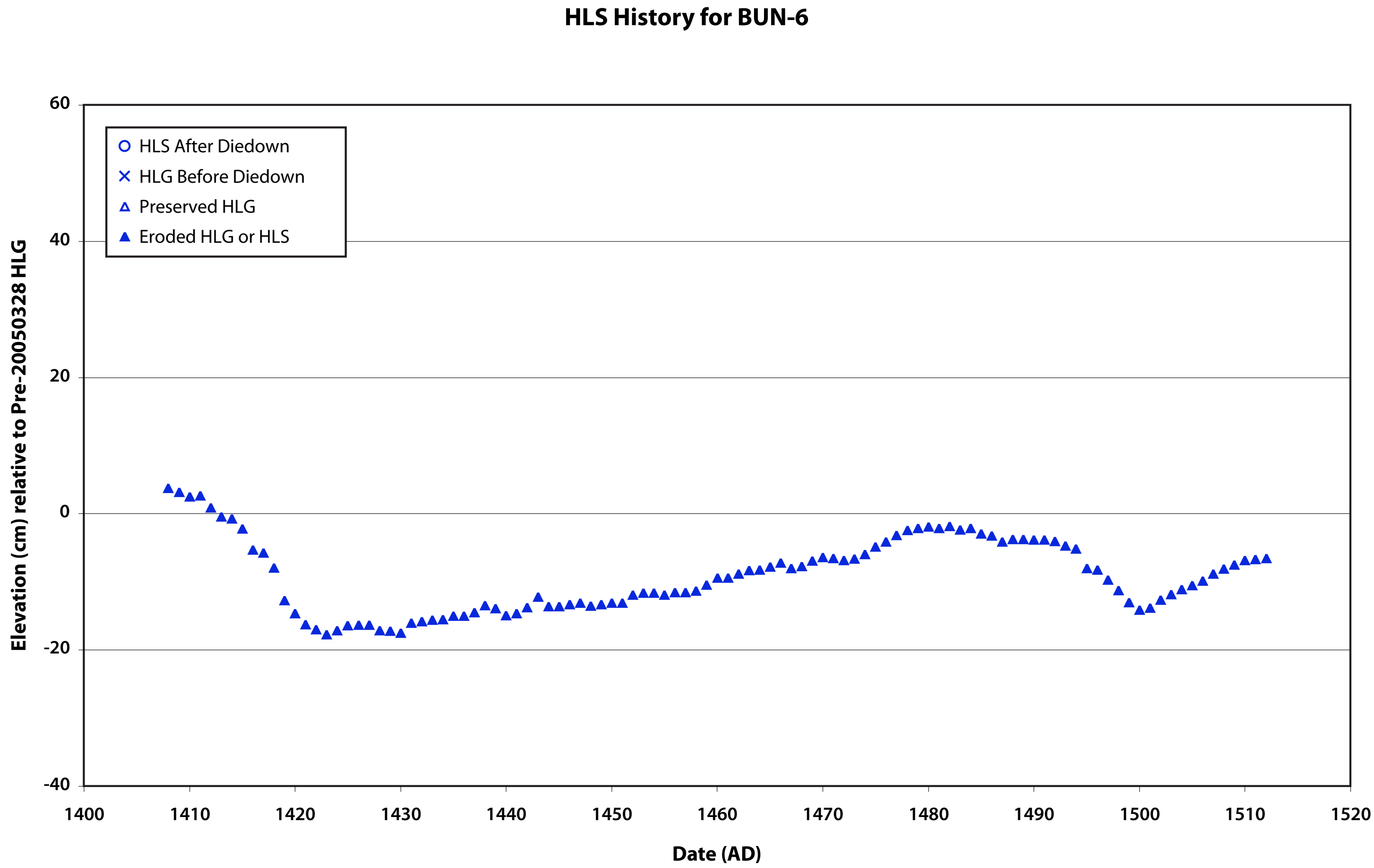

Figure S6b. Graph of relative sea level history derived from slab BUN-6.

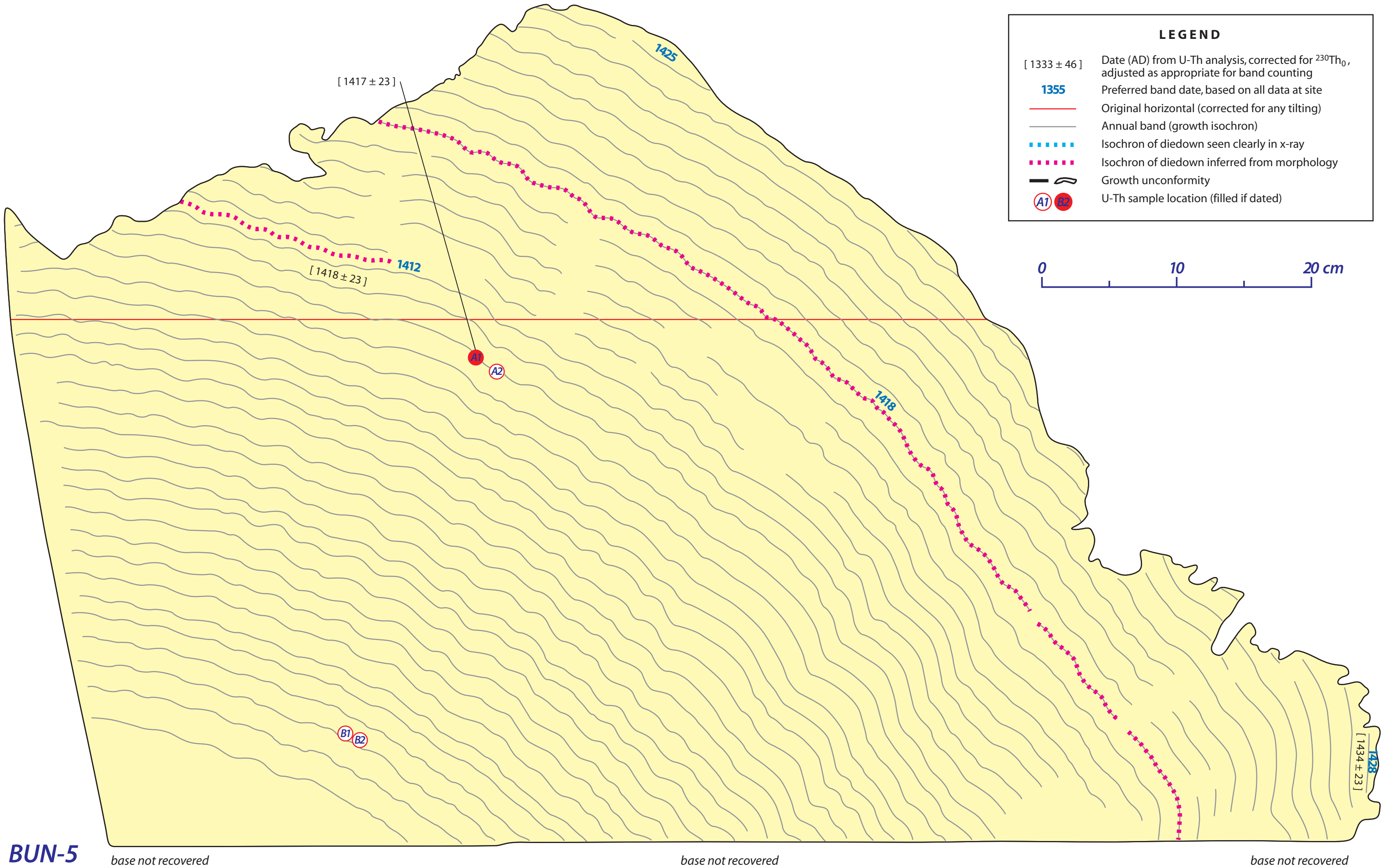

Figure S7a. Cross-section of slab BUN-5, from site BUN-A.

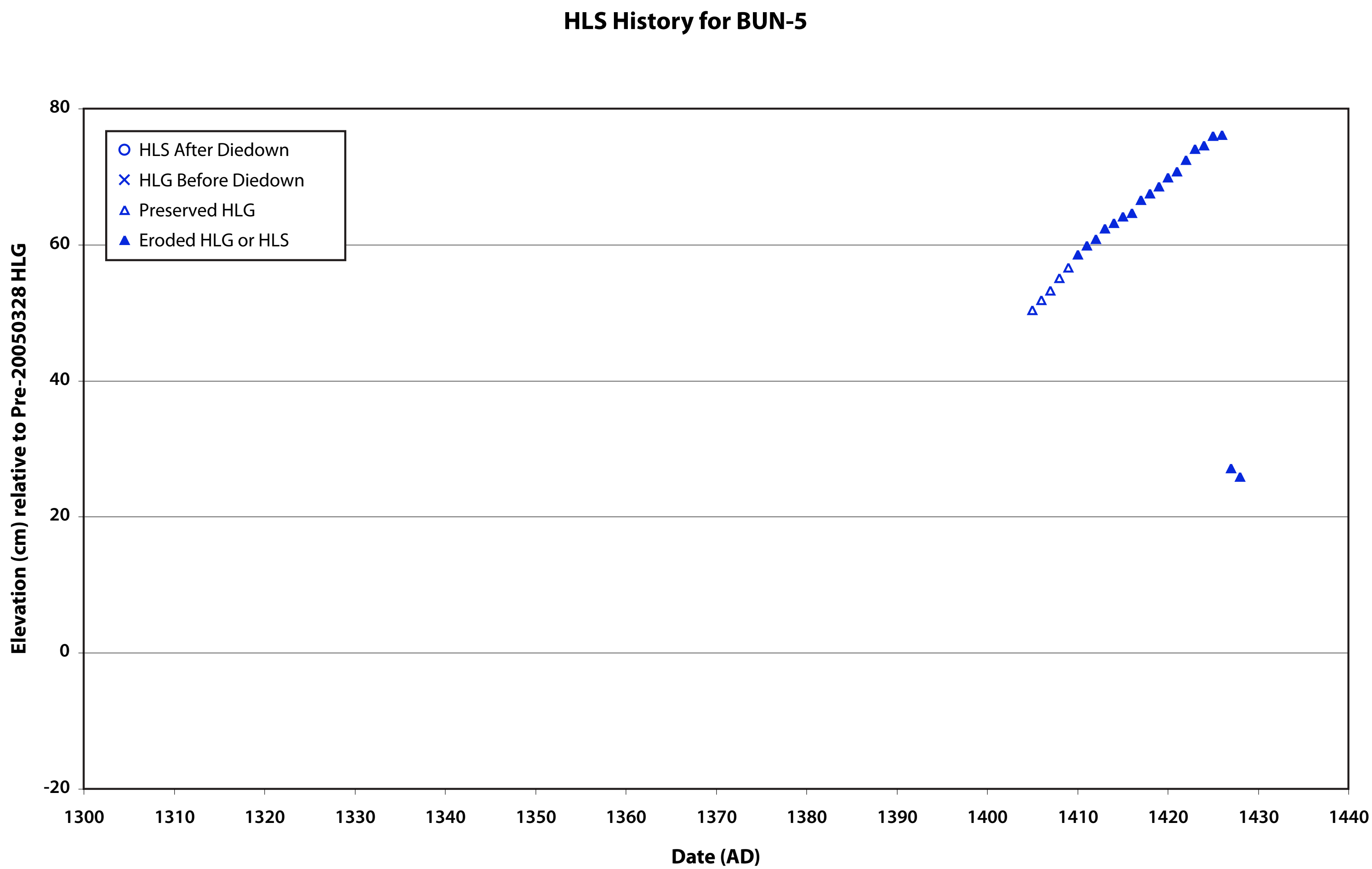

Figure S7b. Graph of relative sea level history derived from slab BUN-5.

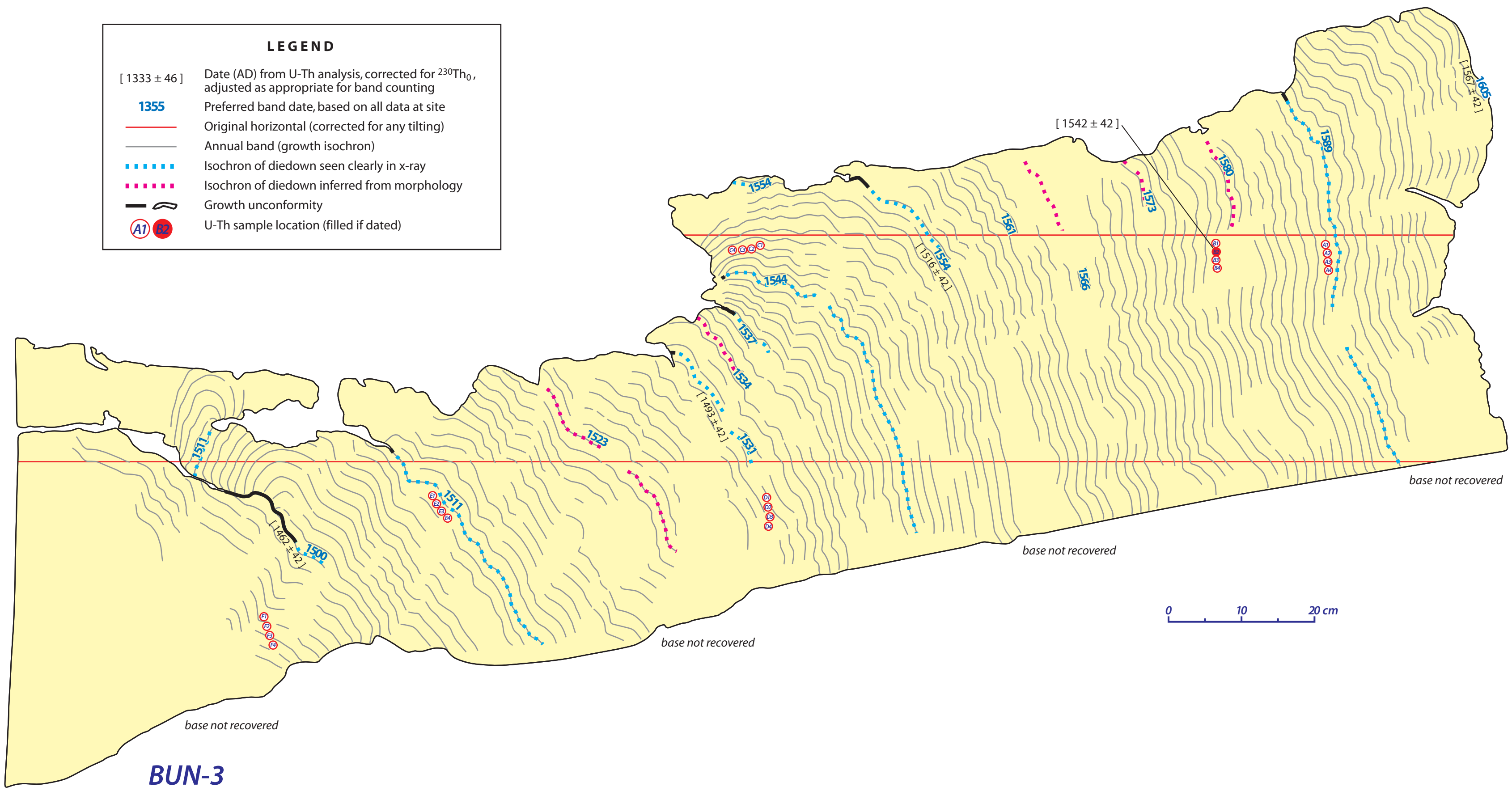

Figure S8a. Cross-section of slab BUN-3, from site BUN-A.

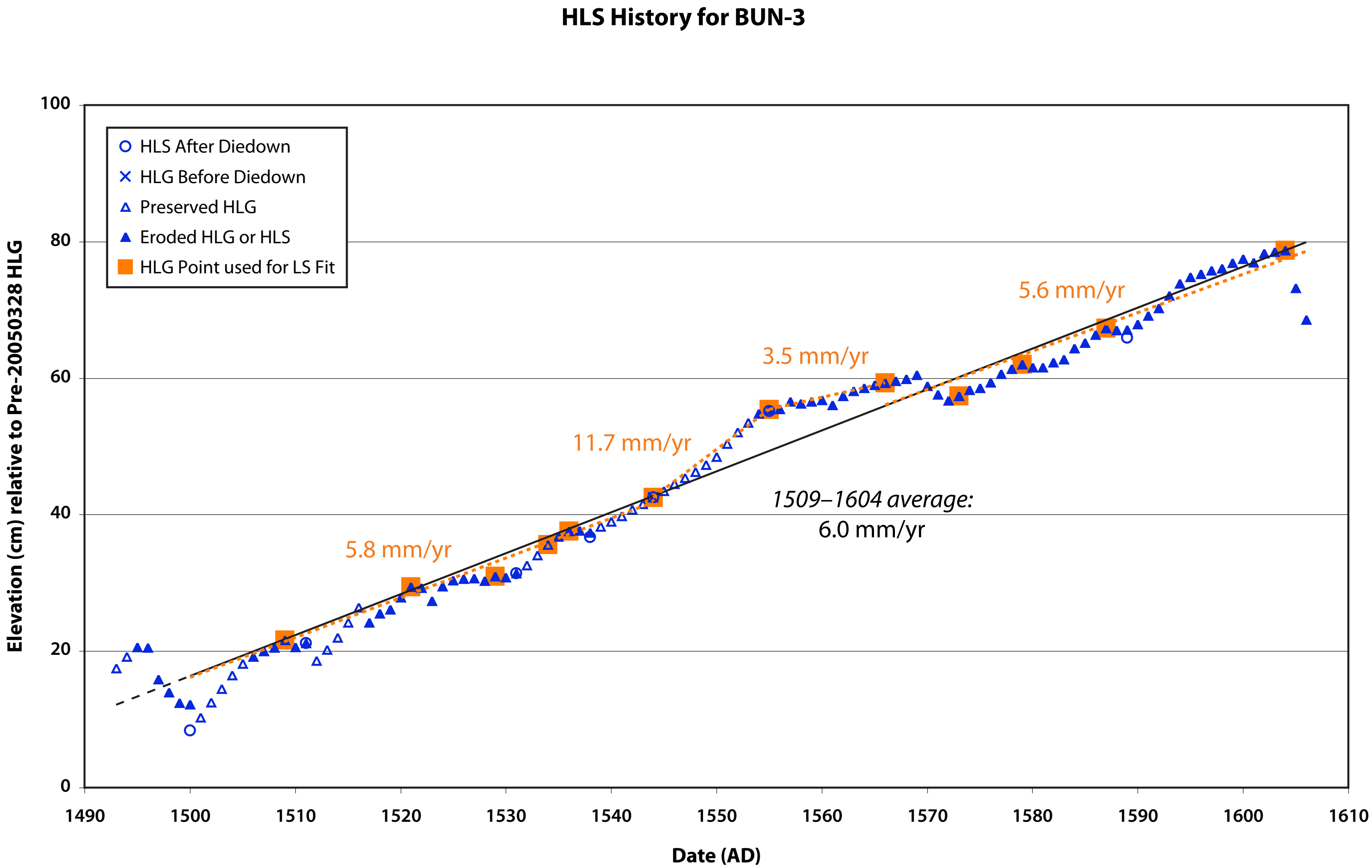

Figure S8b. Graph of relative sea level history derived from slab BUN-3.

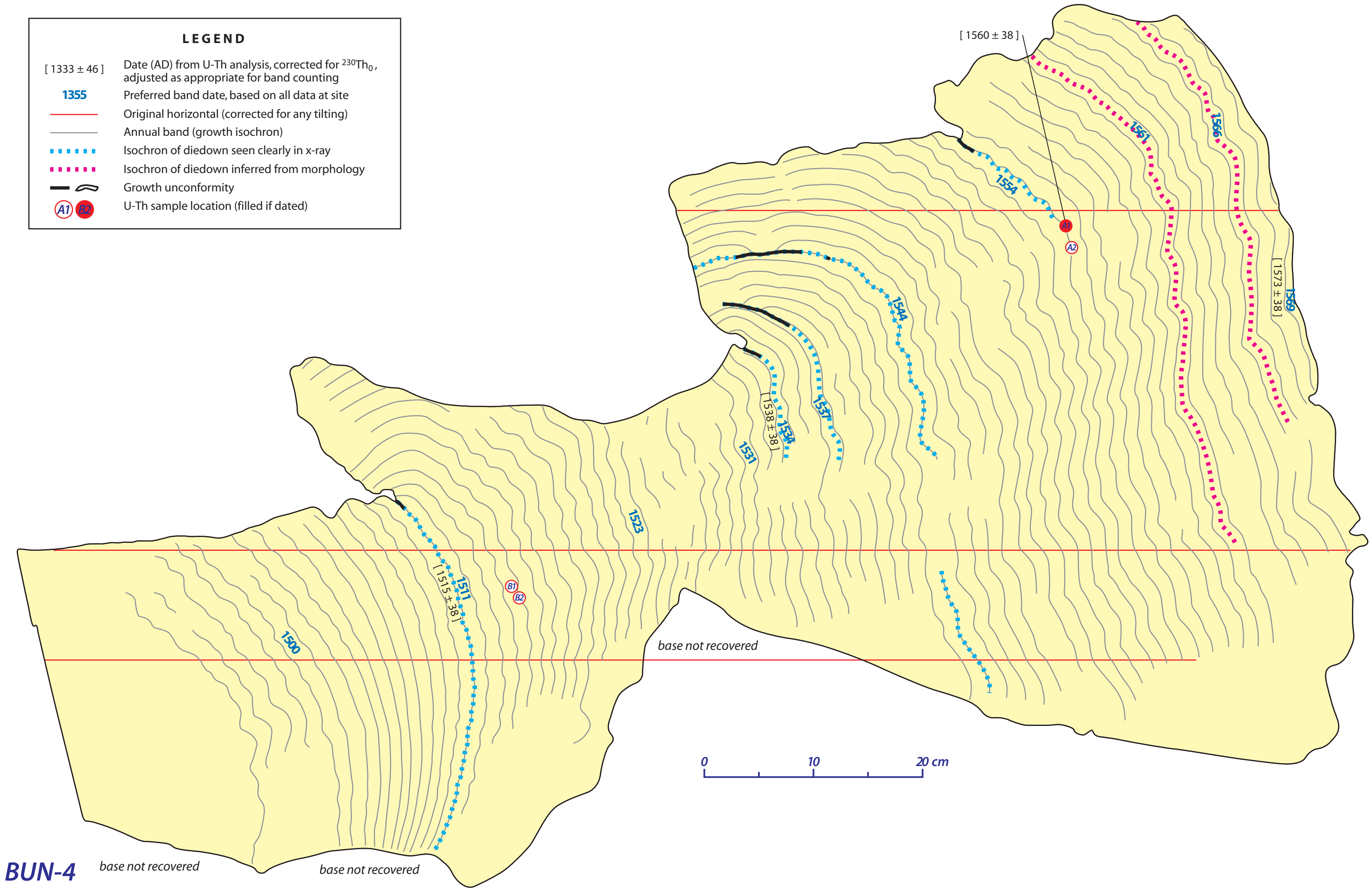

Figure S9a. Cross-section of slab BUN-4, from site BUN-A.

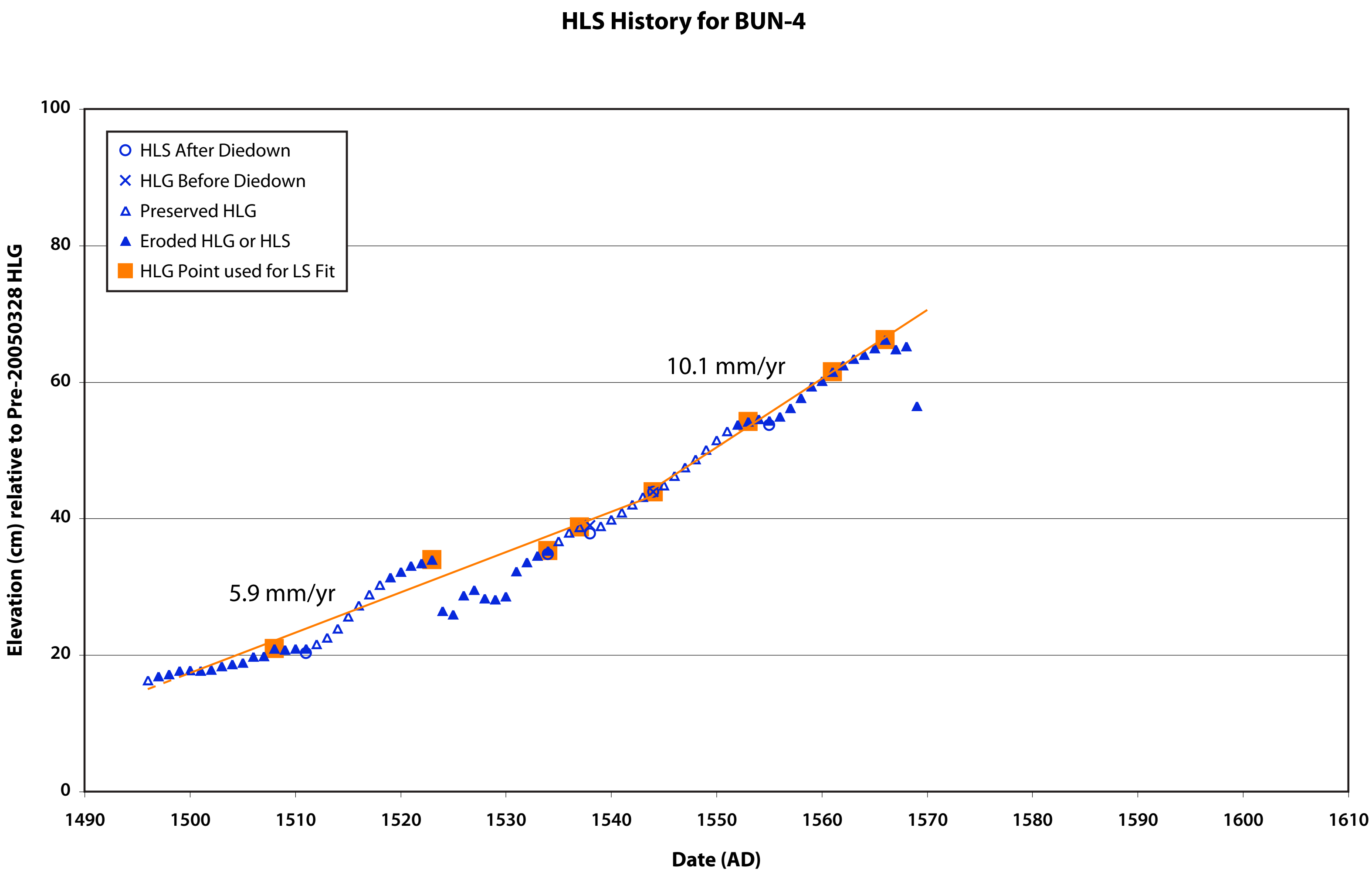

Figure S9b. Graph of relative sea level history derived from slab BUN-4.

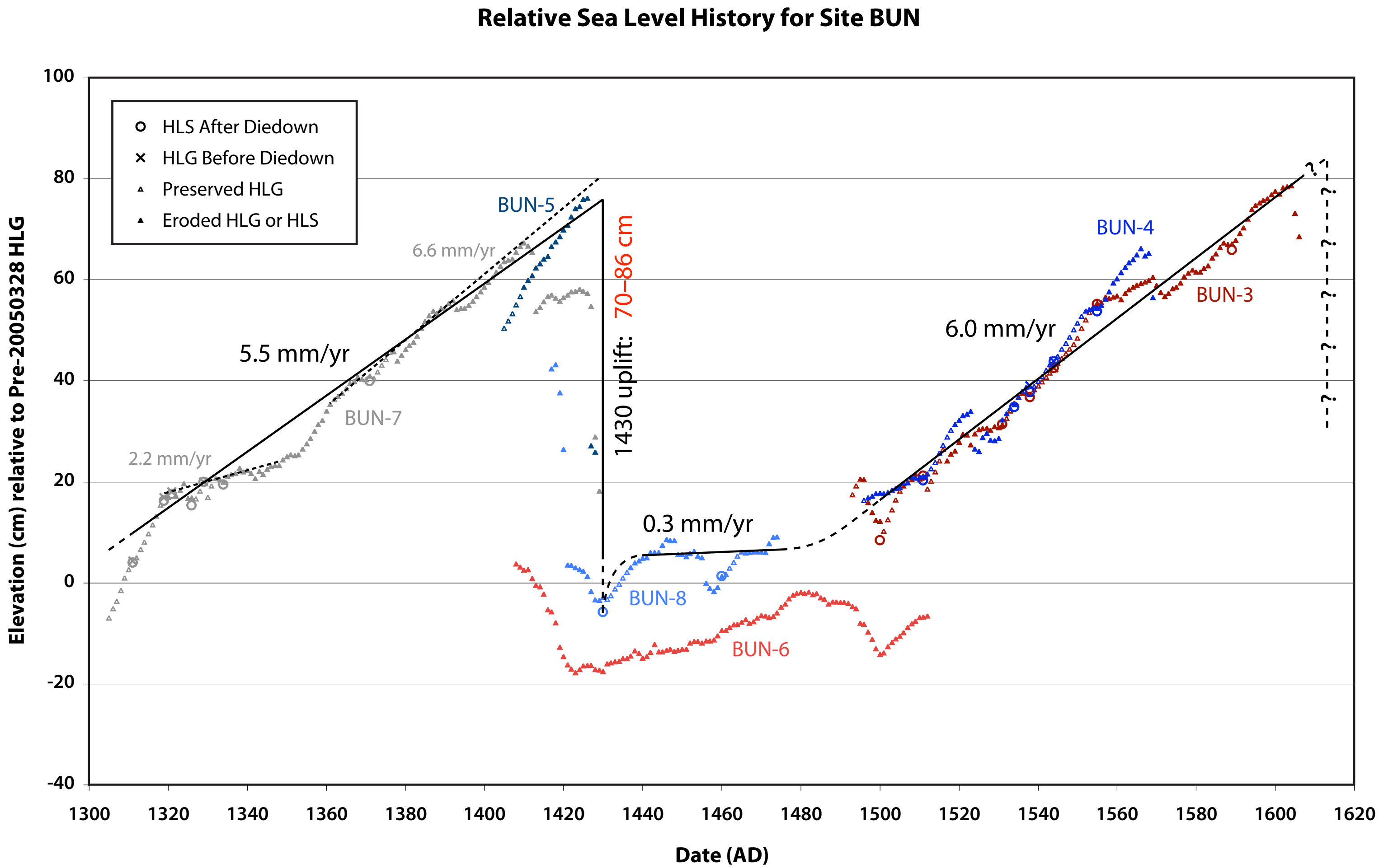

Figure S10a. Relative sea level history for the 14th–17th centuries at site BUN-A. The sea level curve (black) is solid where well constrained by data, dashed where inferred, and queried where conjectural; dotted lines depict short-term deviations of the interseismic rates.

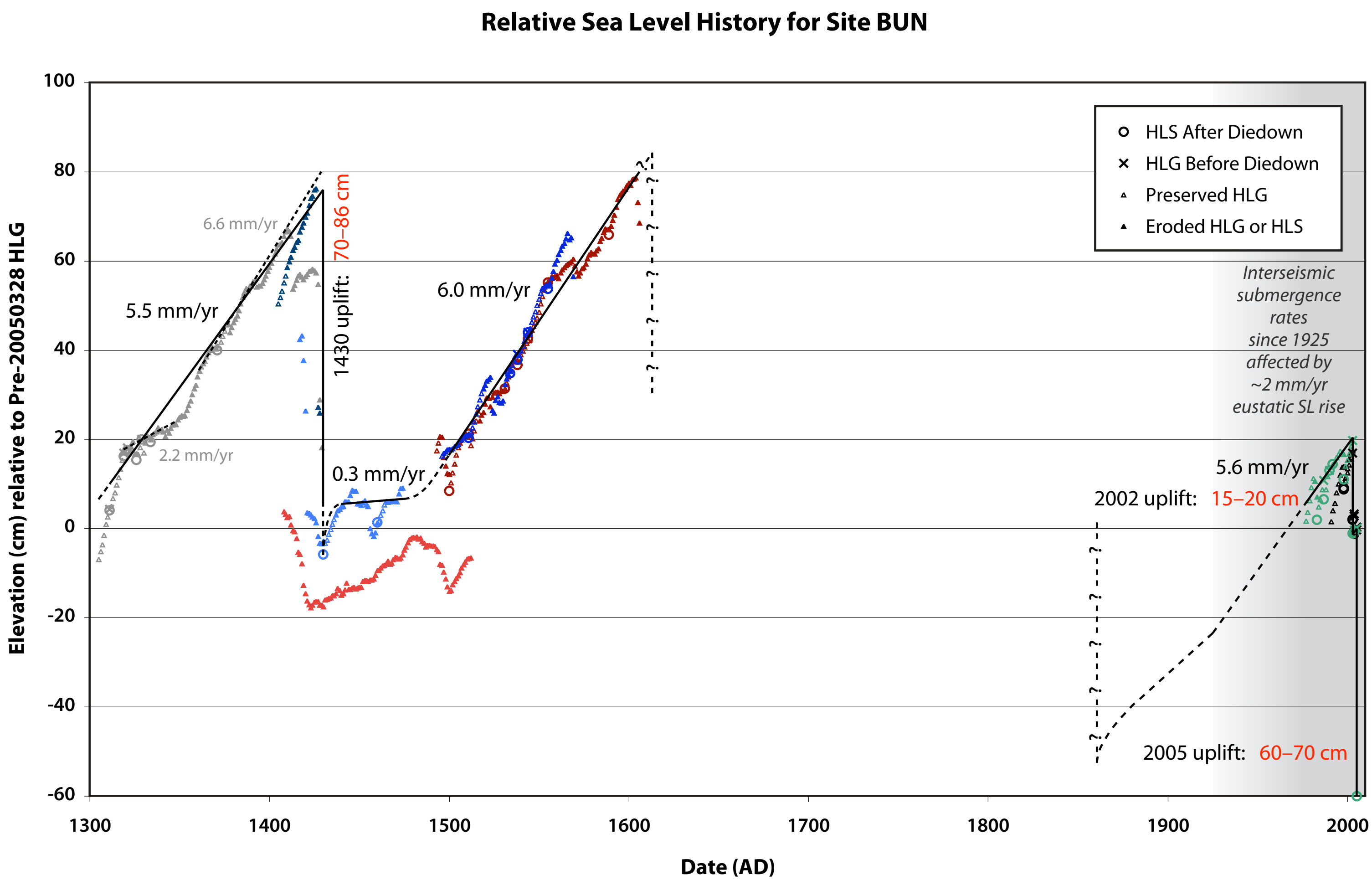

Figure S10b. BUN-A relative sea level history from the 14th century through the present. Note that the rates and elevations measured are influenced by time-varying eustatic sea level change and hydroisostasy; such signals must be removed before long-term tectonic uplift and subsidence are determined.

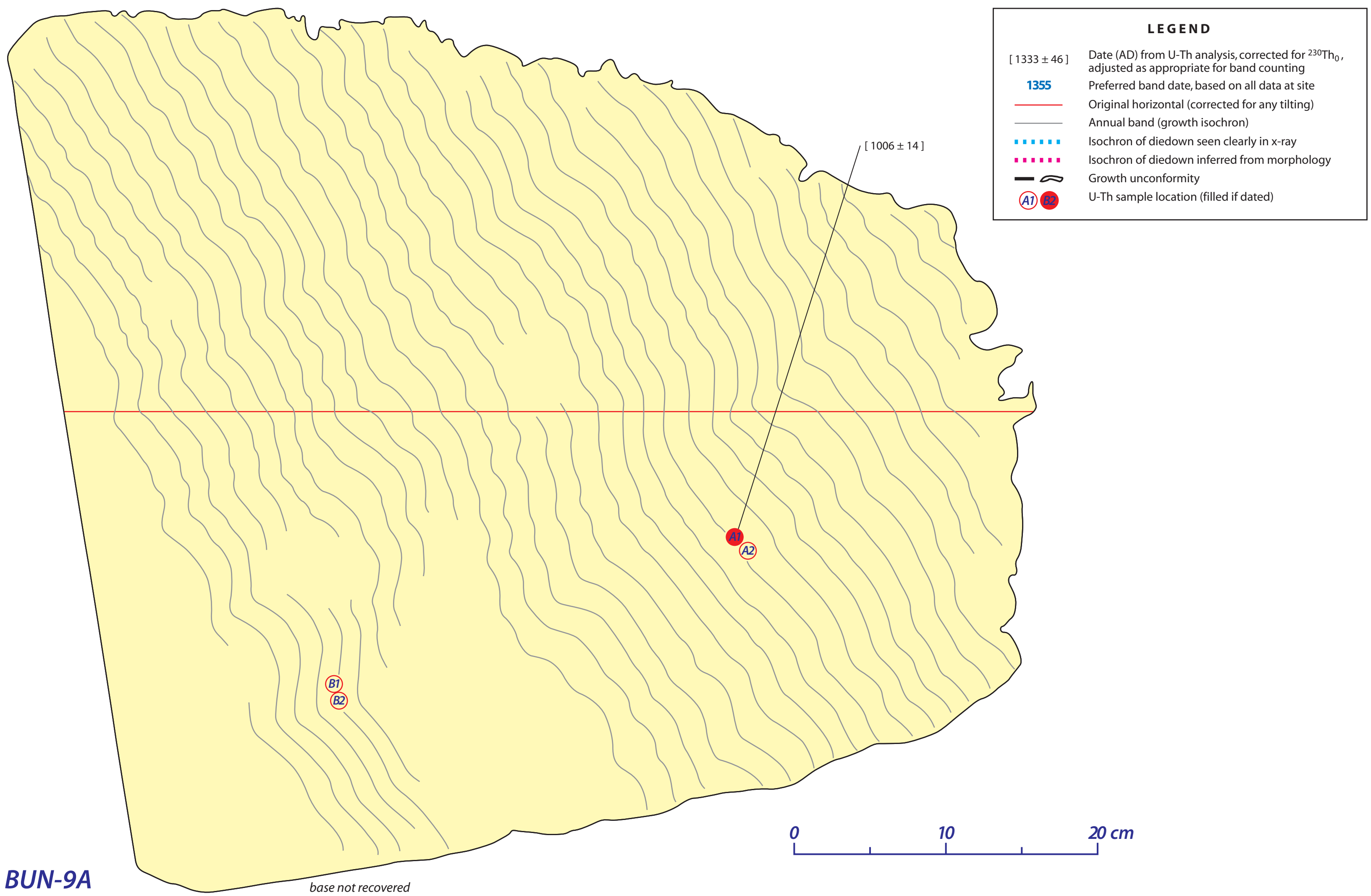

Figure S11a. Cross-section of slab BUN-9A, from site BUN-A.

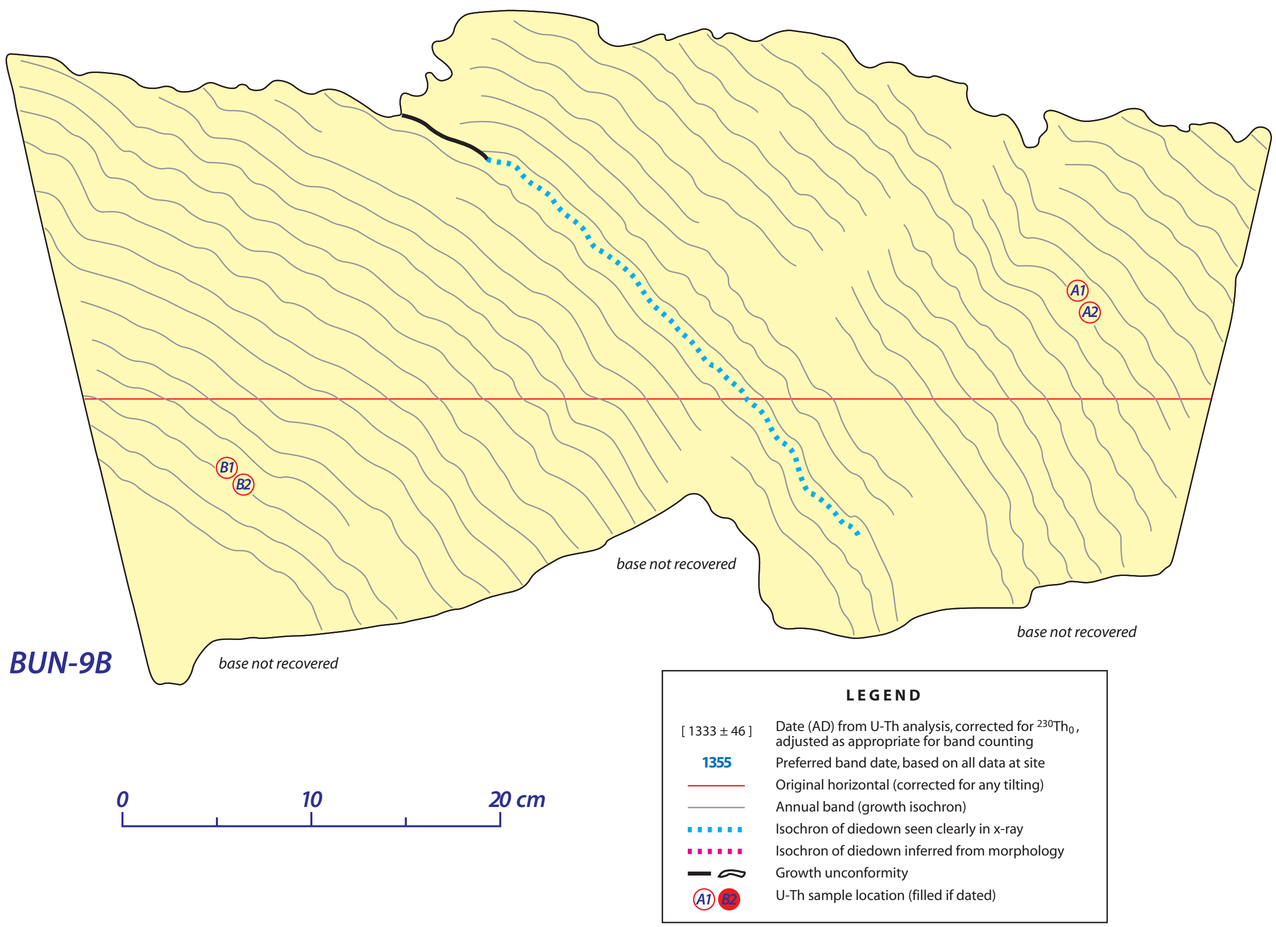

Figure S11b. Cross-section of slab BUN-9B, from site BUN-A.

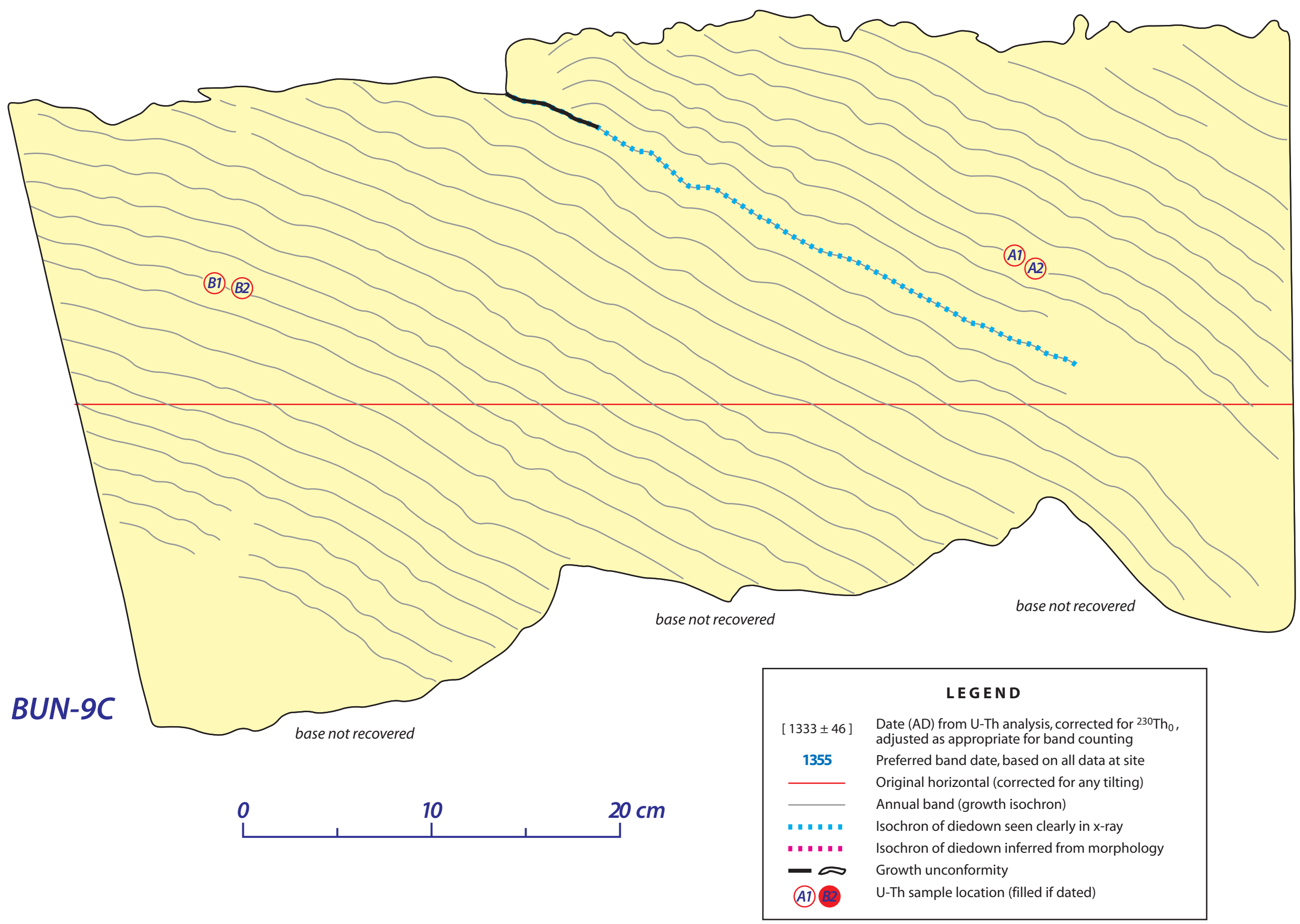

Figure S11c. Cross-section of slab BUN-9C, from site BUN-A.

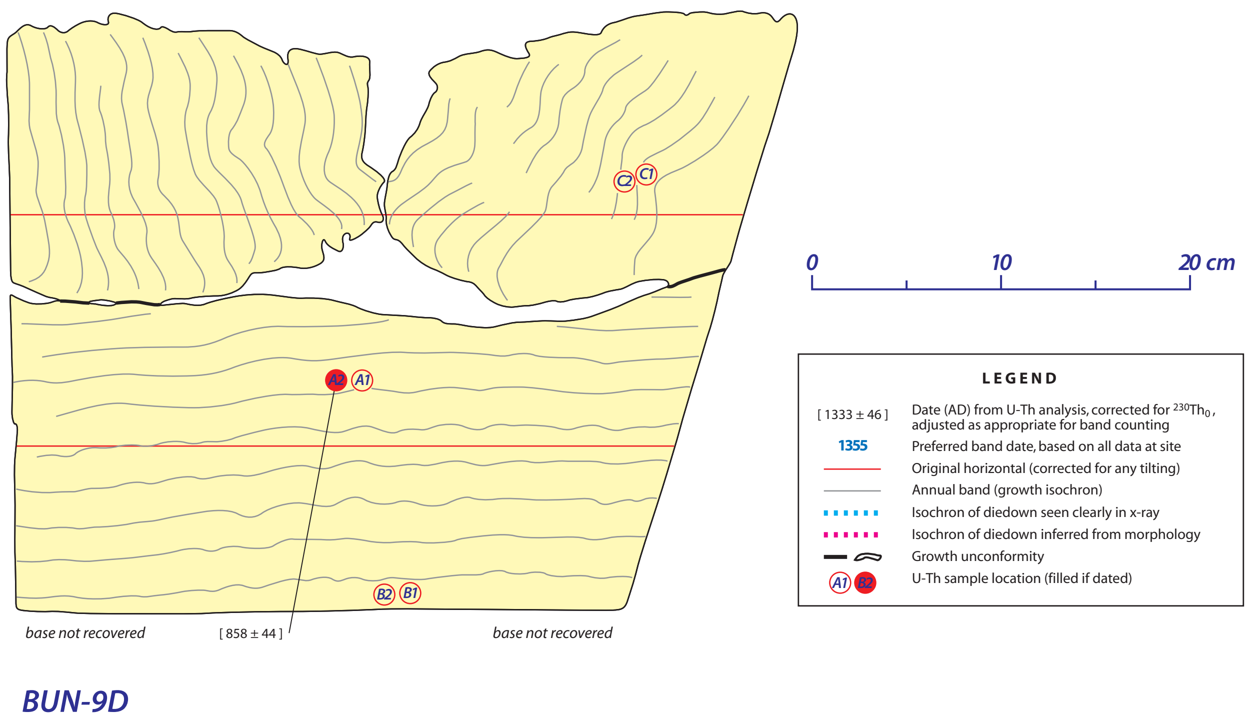

Figure S11d. Cross-section of slab BUN-9D, from site BUN-A.

Figure S12. Histories of interseismic subsidence and coseismic uplift through the 14th–15th centuries at Lewak, Lhok Pauh, and Lhok Dalam on northern Simeulue, compared to the 14th–17th century history at the southern Simeulue site of Bunon. Data constrain solid parts of the curves well; dashed portions are inferred, and queried portions are conjectural. Dotted black lines depict significant short-term deviations of the interseismic rates from longer-term averages. Uplift amounts (in centimeters) are red. Interseismic subsidence rates (in millimeters per year) are blue. Vertical dotted white lines mark dates of uplifts. The zero elevation datum at each site is the site's elevation immediately prior to the 2004 uplift (Lewak and Lhok Pauh) or immediately prior to the 2005 uplift (Bunon), corrected as described in previous chapters for eustatic sea level rise since the 20th century. 14th-century elevations at Lhok Dalam are not known relative to 2004 elevations because none of the 14th-century heads at the site were in place.

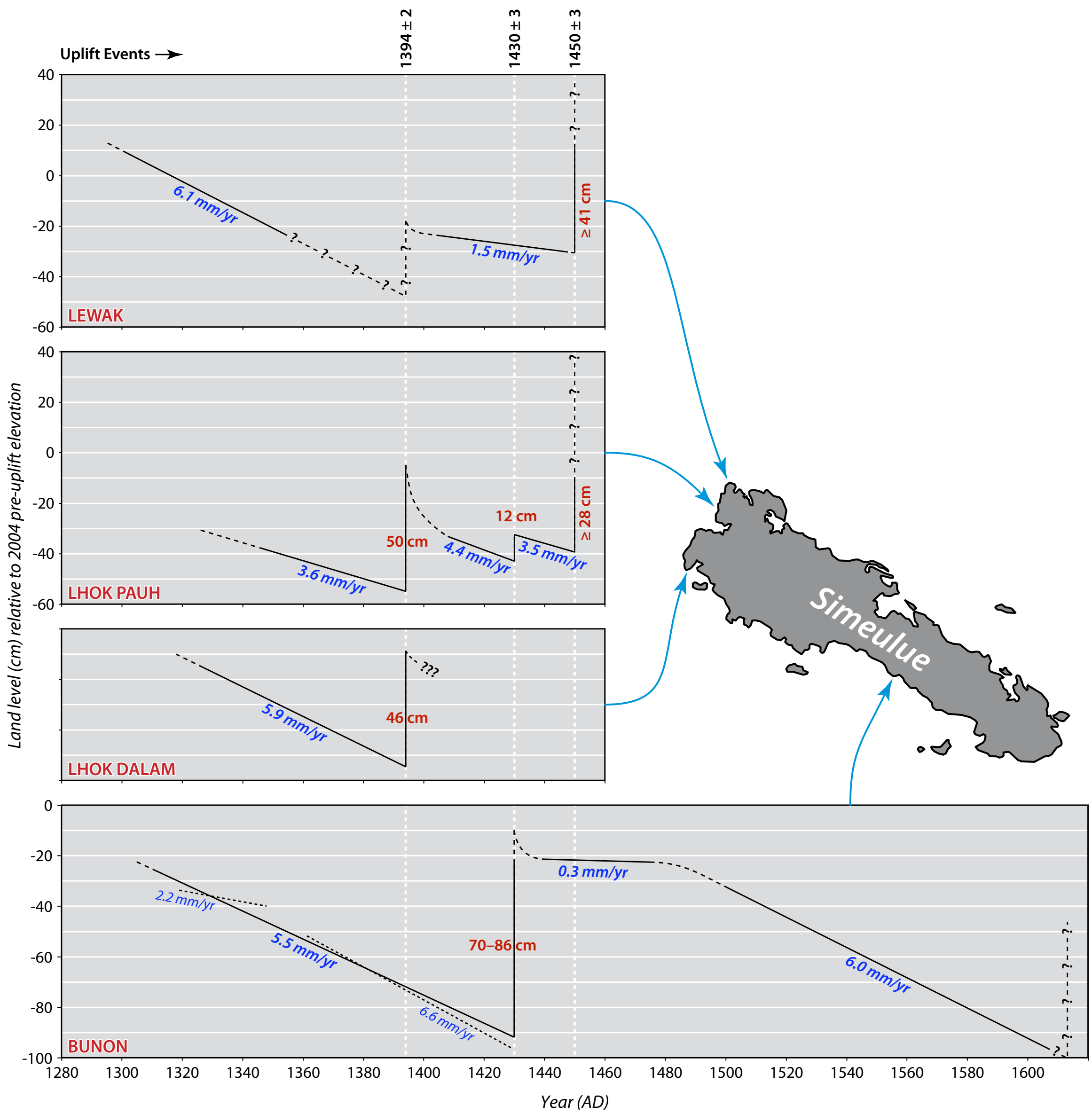
Uplift Events
1394 ± 2
1430 ± 3
1450 ± 3
LEWAK
6.1 mm/yr
1.5 mm/yr
≥ 41 cm
LHOK PAUH
3.6 mm/yr
50 cm
4.4 mm/yr
12 cm
3.5 mm/yr
≥ 28 cm
LHOK DALAM
5.9 mm/yr
46 cm
???
BUNON
2.2 mm/yr
5.5 mm/yr
6.6 mm/yr
70–86 cm
0.3 mm/yr
6.0 mm/yr
Land level (cm) relative to 2004 pre-uplift elevation
Year (AD)
Simeulue

Figure S12.

Sampled Coral Microatolls: Location and Information **Table S1**

Head Name	Site Name	Collected	Latitude	Longitude	Mod/Fsl	Genus
BUN-1	BUN-A	Jun 2006	2.51294	96.14433	Modern	*Porites*
BUN-2	BUN-A	Jun 2006	2.51291	96.14427	Modern	*Porites*
BUN-3	BUN-A	Jun 2006	2.51513	96.14477	Fossil	*Porites*
BUN-4	BUN-A	Jul 2007	2.51357	96.14387	Fossil	*Porites*
BUN-5	BUN-A	Jul 2007	2.51358	96.14391	Fossil	*Porites*
BUN-6	BUN-A	Jul 2007	2.51305	96.14423	Fossil	*Porites*
BUN-7	BUN-A	Jul 2007	2.51338	96.14327	Fossil	*Porites*
BUN-8	BUN-A	Jul 2007	2.51335	96.14339	Fossil	*Porites*
BUN-9	BUN-A	Jul 2007	2.51297	96.14333	Fossil	*Porites*
BUN-10	BUN-B	Jan 2009	2.51870	96.12891	Modern	*Porites*

Uranium and Thorium isotopic compositions and ^{230}Th ages for Sumatran coral samples by ICP-MS **Table S2**

Sample ID	Weight g	^{238}U ppb	^{232}Th ppt	δ^{234}U measured [a]	[^{230}Th/^{238}U] activity [c]	[^{230}Th/^{232}Th] (x 10^{-6}) [d]	δ^{234}U$_{initial}$ corrected [b]	^{230}Th Age uncorrected	^{230}Th Age corrected [c,e]	Chemistry Date (AD)	Chemistry Date (AD)	Date (AD) of Sample Growth	[^{230}Th/^{232}Th]$_0$ (x 10^{-6}) [e]
BUN-3-B2 (1)	0.641	1821 ± 3	1529 ± 3	142.9 ± 2.1	0.00547 ± 0.00008	107.7 ± 1.6	143.1 ± 2.1	524.2 ± 7.8	465 ± 42	2006/12/21	2007.0	**1542.0 ± 42.0**	10.8 ± 11.9
BUN-3-B2 (2)	0.810	2075 ± 5	813 ± 3	142.1 ± 2.9	0.00525 ± 0.00010	221.3 ± 4.4	142.3 ± 2.9	503 ± 10	*sample age and initial thorium ratio determined by 3-D isochron method*				
BUN-3-B2 (3)	0.571	1999 ± 3	912 ± 2	145.8 ± 1.9	0.00517 ± 0.00008	186.9 ± 2.9	146.0 ± 1.9	493.3 ± 7.7					
BUN-3-B2 (4)	0.434	2179 ± 3	1241 ± 3	145.8 ± 2.0	0.00519 ± 0.00007	150.3 ± 1.9	146.0 ± 2.0	495.3 ± 6.4					
BUN-4-A1	0.102	1857 ± 2	1842 ± 8	144.8 ± 1.5	0.00507 ± 0.00008	84.4 ± 1.4	145.0 ± 1.5	484.6 ± 7.8	447 ± 38	2007/10/24	2007.8	**1560.5 ± 38.1**	6.5 ± 6.5
BUN-5-A1	0.101	2513 ± 2	1511 ± 8	145.4 ± 1.5	0.00641 ± 0.00006	176.2 ± 1.9	145.7 ± 1.5	613.1 ± 5.9	591 ± 23	2007/10/24	2007.8	**1417.2 ± 23.3**	6.5 ± 6.5
BUN-6-A1	0.119	2183 ± 2	359 ± 6	144.4 ± 1.5	0.00636 ± 0.00006	638 ± 12	144.6 ± 1.5	608.2 ± 5.5	602.0 ± 8.3	2007/10/24	2007.8	**1405.8 ± 8.3**	6.5 ± 6.5
BUN-6-B1	0.100	2352 ± 4	1301 ± 4	145.5 ± 2.6	0.00640 ± 0.00005	190.8 ± 1.4	145.7 ± 2.6	611.3 ± 4.6	591 ± 21	2008/10/13	2008.8	**1418.2 ± 21.3**	6.5 ± 6.5
BUN-7-A1	0.100	2418 ± 2	664 ± 7	143.9 ± 1.2	0.00658 ± 0.00007	395.7 ± 5.9	144.1 ± 1.2	630.1 ± 6.4	620 ± 12	2007/10/24	2007.8	**1388.0 ± 12.1**	6.5 ± 6.5
BUN-7-B2	0.115	2090 ± 3	1962 ± 5	145.4 ± 2.2	0.00703 ± 0.00006	123.7 ± 1.1	145.7 ± 2.2	672.3 ± 5.9	637 ± 36	2008/10/13	2008.8	**1371.7 ± 35.7**	6.5 ± 6.5
BUN-7-C2 (1)	0.094	2460 ± 4	5328 ± 14	147.0 ± 2.2	0.00779 ± 0.00009	59.4 ± 0.7	147.3 ± 2.2	744.5 ± 8.7	663 ± 82	2008/10/13	2008.8	1345.5 ± 81.7	6.5 ± 6.5
BUN-7-C2 (2)	0.101	2406 ± 4	5625 ± 15	143.1 ± 2.3	0.00784 ± 0.00009	55.4 ± 0.7	143.3 ± 2.3	751.2 ± 9.1	663 ± 88	2008/10/13	2008.8	1345.5 ± 88.4	6.5 ± 6.5
BUN-7-C2 (3)	0.102	2469 ± 3	5925 ± 14	143.1 ± 2.3	0.00789 ± 0.00009	54.3 ± 0.6	143.3 ± 2.3	756.2 ± 8.7	666 ± 91	2008/10/13	2008.8	1342.9 ± 90.7	6.5 ± 6.5
BUN-7-C2 (4)	0.125	2512 ± 6	6154 ± 14	150.5 ± 2.9	0.00786 ± 0.00009	53.0 ± 0.6	150.7 ± 2.9	748.6 ± 8.7	657 ± 92	2008/10/13	2008.8	1351.8 ± 92.0	6.5 ± 6.5
										weight-averaged age		***1346.3 ± 44.0***	
BUN-8-A2 (1)	0.092	3049 ± 3	4082 ± 12	144.9 ± 1.5	0.00629 ± 0.00007	77.6 ± 0.9	145.1 ± 1.5	601.9 ± 7.0	569 ± 15	2007/10/24	2007.8	**1438.8 ± 15.0**	4.2 ± 1.5
BUN-8-A2 (2)	0.090	2925 ± 5	4316 ± 13	144.2 ± 2.5	0.00633 ± 0.00007	70.8 ± 0.8	144.4 ± 2.5	605.7 ± 6.8	*sample age and initial thorium ratio determined by 3-D isochron method*				
BUN-8-A2 (3)	0.102	3098 ± 5	7373 ± 21	144.1 ± 2.4	0.00656 ± 0.00008	45.5 ± 0.5	144.3 ± 2.4	627.7 ± 7.4					
BUN-8-A2 (4)	0.118	2890 ± 5	4742 ± 12	144.7 ± 2.6	0.00638 ± 0.00007	64.2 ± 0.7	145.0 ± 2.6	610.5 ± 6.5					
BUN-8-C1 (1)	0.097	2925 ± 4	10245 ± 26	146.5 ± 2.2	0.00618 ± 0.00010	29.1 ± 0.5	146.7 ± 2.2	589.8 ± 9.4	568 ± 23	2008/10/13	2008.8	**1440.8 ± 23.0**	1.2 ± 1.0
BUN-8-C1 (2)	0.094	2966 ± 3	16767 ± 48	146.5 ± 1.7	0.00634 ± 0.00013	18.5 ± 0.4	146.8 ± 1.7	606 ± 12	*sample age and initial thorium ratio determined by 3-D isochron method*				
BUN-8-C1 (3)	0.123	2850 ± 3	9016 ± 22	147.2 ± 1.7	0.00617 ± 0.00009	32.2 ± 0.5	147.4 ± 1.7	589.0 ± 8.9					
BUN-8-C1 (4)	0.106	2848 ± 4	10800 ± 28	147.9 ± 2.1	0.00625 ± 0.00009	27.2 ± 0.4	148.1 ± 2.1	596.0 ± 8.6					
BUN-9A-A1	0.111	2476 ± 3	833 ± 7	146.2 ± 1.6	0.01060 ± 0.00007	519.7 ± 5.2	146.6 ± 1.6	1,014.2 ± 6.4	1,002 ± 14	2007/10/24	2007.8	**1006.2 ± 14.2**	6.5 ± 6.5
BUN-9D-A2 (1)	0.099	2677 ± 2	22731 ± 93	145.0 ± 1.4	0.01263 ± 0.00024	24.6 ± 0.5	145.3 ± 1.4	1,211 ± 23	1,150 ± 44	2007/10/24	2007.8	**857.8 ± 44.0**	1.6 ± 1.4
BUN-9D-A2 (2)	0.083	2567 ± 4	21109 ± 66	145.9 ± 2.5	0.01292 ± 0.00018	25.9 ± 0.4	146.3 ± 2.6	1,238 ± 17	*sample age and initial thorium ratio determined by 3-D isochron method*				
BUN-9D-A2 (3)	0.097	2449 ± 5	32700 ± 134	147.0 ± 2.7	0.01331 ± 0.00025	16.5 ± 0.3	147.4 ± 2.7	1,274 ± 24					
BUN-9D-A2 (4)	0.126	2636 ± 5	37697 ± 188	144.2 ± 2.5	0.01344 ± 0.00028	15.5 ± 0.3	144.5 ± 2.5	1,290 ± 27					

For a discussion of the ICP-MS method, see *Shen et al.* [2002]. Analytical errors are 2σ of the mean.

[a] $\delta^{234}U = ([^{234}U/^{238}U]_{activity} - 1) \times 1000$.

[b] $\delta^{234}U_{initial}$ corrected was calculated based on ^{230}Th age (T), i.e., $\delta^{234}U_{initial} = \delta^{234}U_{measured}\ X\ e^{\lambda 234 * T}$, and T is corrected age.

[c] $[^{230}Th/^{238}U]_{activity} = 1 - e^{-\lambda 230\, T} + (\delta^{234}U_{measured}/1000)[\lambda_{230}/(\lambda_{230} - \lambda_{234})](1 - e^{-(\lambda 230 - \lambda 234)\, T})$, where T is the age.

Decay constants are $9.1577 \times 10^{-6}\ yr^{-1}$ for ^{230}Th, $2.8263 \times 10^{-6}\ yr^{-1}$ for ^{234}U, and $1.55125 \times 10^{-10}\ yr^{-1}$ for ^{238}U [*Cheng et al.*, 2000].

[d] The degree of detrital ^{230}Th contamination is indicated by the [^{230}Th/^{232}Th] atomic ratio instead of the activity ratio.

[e] Except where isochron techniques were used to determine the ages and initial ^{230}Th/^{232}Th atomic ratios, the initial ^{230}Th/^{232}Th atomic ratio is assumed to be $6.5 \pm 6.5 \times 10^{-6}$ [*Zachariasen et al.*, 1999].

Dates of Presumed Uplift of Individual Coral Heads **Table S3**

Sample ID	Date of Sample (AD)	Preserved Bands after Sample	Date of Outer Band (AD)	Slab Weighted Mean Date of Outer Band	Inferred Number of Missing Bands	Slab Weighted Mean Date of Coral Death	Outer Rim Elevation (cm) above Pre-20050328 HLG	
BUN-3-B2	1542.0 ± 42.0	26.5 ± 0.5	1568.5 ± 42.0	**1568.5 ± 42.0**	2.0 ± 2.0	**1570.5 ± 42.1**	56.7	tilted and settled **
BUN-4-A1	1560.5 ± 38.1	14.5 ± 0.5	1575.0 ± 38.1	**1575.0 ± 38.1**	38.5 ± 2.0	**1613.5 ± 38.1**	66.4	inner of double rim
BUN-5-A1	1417.2 ± 23.3	18.5 ± 0.5	1435.7 ± 23.3	**1435.7 ± 23.3**	2.0 ± 2.0	**1437.7 ± 23.4**	76.3	where less eroded
BUN-6-A1	1405.8 ± 8.3	55.0 ± 0.5	1460.8 ± 8.3	**1468.3 ± 7.7**	2.0 ± 2.0 *	**1470.3 ± 8.0 ***	-5.8	fairly eroded
BUN-6-B1	1418.2 ± 21.3	99.5 ± 0.5	1517.7 ± 21.3					
BUN-7-A1	1388.0 ± 12.1	31.0 ± 0.5	1419.0 ± 12.2	**1423.0 ± 11.1**	2.0 ± 2.0	**1425.0 ± 11.3**	76.0	crown of outer rim has sustained substantial erosion, esp. near slab
BUN-7-B2	1371.7 ± 35.7	64.5 ± 0.5	1436.2 ± 35.7					
BUN-7-C2	1346.3 ± 44.0	109.0 ± 0.5	1455.3 ± 44.0					
BUN-8-A2	1438.8 ± 15.0	52.5 ± 0.5	1491.3 ± 15.0	**1479.4 ± 12.6**	2.0 ± 2.0 *	**1481.4 ± 12.7 ***	9.1	outer preserved rim
BUN-8-C1	1440.8 ± 23.0	10.5 ± 0.5	1451.3 ± 23.0					
BUN-9A-A1	1006.2 ± 14.2	12.0 ± 0.5	1018.2 ± 14.2	**1017.0 ± 13.7**	5.0 ± 5.0	**1022.0 ± 14.6**	-11.6	fairly eroded
BUN-9D-A2	857.8 ± 44.0	140.0 ± 35.0	997.8 ± 56.2					

* *Although BUN-6 and BUN-8 are each listed as missing 2 ± 2 outer bands, the real number may be much higher. The outer part of each of those heads was very thin; it is possible that tens of bands or even >100 additional bands originally grew, but broke off and were subsequently transported away. Also, either of those heads may have plausibly died for reasons other than a tectonic diedown, considering their thin perimeters.*

** *The original pre-tilting elevation of BUN-3 can be determined by comparison with BUN-4; see text for details.*

Weighted Average Dates of Presumed Uplift Events **Table S4**

Pre-Historical Event	Site	Head	Date of Tectonic Diedown (AD)		
			Per Head	Site Avg	All-Site Avg
Central Simeulue: AD 1420s–1430s *(assuming a single diedown)*	BUN BUN BUN	BUN-5 BUN-7 BUN-8	1437.7 ± 23.4 1425.0 ± 11.3 1434.9 ± 12.6 *	1430.4 ± 7.9	**1430.4 ± 7.9**
Central Simeulue: AD 1420s–1430s *(assuming dual diedowns; this is the date of the first and larger of the two)*	BUN BUN BUN	BUN-5 BUN-7 BUN-8	1437.7 ± 23.4 1425.0 ± 11.3 1426.9 ± 12.7 º	1427.2 ± 8.0	**1427.2 ± 8.0**
Central Simeulue: early AD 1600s	BUN BUN	BUN-3 BUN-4	1570.5 ± 42.1 1613.5 ± 38.1	1594.1 ± 28.2	**1594.1 ± 28.2**

* *This date is 44.5 ± 0.5 years prior to the date of the outer edge of slab BUN-8.*
º *This date is 52.5 ± 2.0 years prior to the date of the outer edge of slab BUN-8.*

References

Briggs, R. W., K. Sieh, A. J. Meltzner, D. Natawidjaja, J. Galetzka, B. Suwargadi, Y.-j. Hsu, M. Simons, N. Hananto, I. Suprihanto, D. Prayudi, J.-P. Avouac, L. Prawirodirdjo, and Y. Bock (2006), Deformation and slip along the Sunda megathrust in the great 2005 Nias–Simeulue earthquake, *Science*, 311, 1897-1901, doi:10.1126/science.1122602.

Cheng, H., R. L. Edwards, J. Hoff, C. D. Gallup, D. A. Richards, and Y. Asmerom (2000), The half-lives of uranium-234 and thorium-230, *Chem. Geol.*, 169, 17-33, doi:10.1016/S0009-2541(99)00157-6.

Konca, A. O., J.-P. Avouac, A. Sladen, A. J. Meltzner, K. Sieh, P. Fang, Z. Li, J. Galetzka, J. Genrich, M. Chlieh, D. H. Natawidjaja, Y. Bock, E. J. Fielding, C. Ji, and D. V. Helmberger (2008), Partial rupture of a locked patch of the Sumatra megathrust during the 2007 earthquake sequence, *Nature*, 456, 631-635, doi:10.1038/nature07572.

Meltzner, A. J., K. E. Sieh, H. Chiang, C. Shen, B. Philibosian, B. W. Suwargadi, and D. H. Natawidjaja (2009), Earthquake clusters and persistent segmentation near the boundary of the 2004 and 2005 Sunda megathrust ruptures, *Eos Trans. AGU*, 90, Fall Meet. Suppl., Abstract T11D-07.

Natawidjaja, D. H., K. Sieh, M. Chlieh, J. Galetzka, B. W. Suwargadi, H. Cheng, R. L. Edwards, J.-P. Avouac, and S. N. Ward (2006), Source parameters of the great Sumatran megathrust earthquakes of 1797 and 1833 inferred from coral microatolls, *J. Geophys. Res.*, 111, B06403, doi:10.1029/2005JB004025.

Shen, C.-C., R. L. Edwards, H. Cheng, J. A. Dorale, R. B. Thomas, S. B. Moran, S. E. Weinstein, and H. N. Edmonds (2002), Uranium and thorium isotopic and concentration measurements by magnetic sector inductively coupled plasma mass spectrometry, *Chem. Geol.*, 185, 165-178, doi:10.1016/S0009-2541(01)00404-1.

Sieh, K. (2007), Persistent behaviors of the Sunda megathrust in Sumatra: opportunities to forecast destructive earthquakes, *Eos Trans. AGU*, 88, Fall Meet. Suppl., Abstract S22A-01.

Zachariasen, J., K. Sieh, F. W. Taylor, R. L. Edwards, and W. S. Hantoro (1999), Submergence and uplift associated with the giant 1833 Sumatran subduction earthquake: evidence from coral microatolls, *J. Geophys. Res.*, 104, 895-919, doi:10.1029/1998JB900050.